

## Data Base for Dynamic Soil Properties of Seismic Active Zones in Iraq

**Qassun Sa'ad Al-Deen Mohammed Shafiqu**

Assistant Professor

Department of Civil Engineering

College of Engineering, Al-Nahrain University

[qassun@yahoo.com](mailto:qassun@yahoo.com)

**Ruba Hanna Sa'ur**

Engineer

Department of Civil Engineering

College of Engineering, Al-Nahrain University

[rubasaur@yahoo.co.uk](mailto:rubasaur@yahoo.co.uk)

### ABSTRACT

Iraq is located near the northern tip of the Arabian plate, which is advancing northwards relative to the Eurasian plate, and is predictably, a tectonically active country. Seismic activity in Iraq increased significantly during the last decade. So structural and geotechnical engineers have been giving increasing attention to the design of buildings for earthquake resistance. Dynamic properties play a vital role in the design of structures subjected to seismic load. The main objective of this study is to prepare a data base for the dynamic properties of different soils in seismic active zones in Iraq using the results of cross hole and down hole tests. From the data base collected it has been observed that the average vertical compressional wave velocities were ranged from (1125-2500) m/s in the North, (306-1544) m/s in the Middle, (805-1812) m/s in the western south, (377-1326) m/s in the eastern south and (334-1404) m/s in the South of Iraq. And the average vertical shear wave velocities were ranged from (225-476) m/s in the North, (111-408) m/s in the Middle, (268-659) m/s in the western south, (131-380)m/s in the eastern south and (102-365) m/s in the South of Iraq.

**Key words:** data base, soil, dynamic properties, seismic zones, Iraq

### قاعدة بيانات لخواص التربة الديناميكية لمناطق العراق ذات النشاط الزلزالي

ربي حنا ساعور

مهندس

قسم الهندسة المدنية

كلية الهندسة - جامعة النهرين

قاسيون سعد الدين محمد شفيق

أستاذ مساعد

قسم الهندسة المدنية

كلية الهندسة - جامعة النهرين

### الخلاصة

يقع العراق بالقرب من الطرف الشمالي من الصفيفة العربية التي لها علاقة بالصفيفة الأوراسية عند التقدم شمالاً، ومن المتوقع ان يكون العراق من البلدان النشطة تكتونيا ونتيجة للزيادة الملحوظة للنشاط الزلزالي في العالم خلال العقود الأخيرة خاصة في منطقة الشرق الأوسط فقد أولى المهندسون اهتمام كبير في تصاميم الأبنية المقاومة للزلازل. ان الخواص الديناميكية تلعب دوراً مهماً في تصميم المنشآت المعرضة للقوى الزلزالية. الهدف الرئيسي من هذه الدراسة هو اعداد قاعدة بيانات للخصائص الديناميكية لأنواع مختلفة من التربة للمناطق النشطة زلزالياً في العراق وذلك بالاعتماد على نتائج فحصي cross hole و down hole ، حيث لوحظ من قاعدة البيانات التي تم جمعها أن معدل سرعة الموجة الانضغاطية تتراوح بين (2500-1125) م/ثا في المنطقة الشمالية و (1544-306) م/ثا في المنطقة الوسطى و (1812-805) م/ثا في الجنوب الغربي و (1326-377) م/ثا في الجنوب الشرقي و (1404-334) م/ثا في المنطقة الجنوبية من العراق. وكان معدل سرعة موجة القص تتراوح بين (476-225) م/ثا في المنطقة الشمالية و (408-111) م/ثا في المنطقة الوسطى و (659-268) م/ثا في الجنوب الغربي و (380-131) م/ثا في الجنوب الشرقي و (365-102) م/ثا في المنطقة الجنوبية من العراق.

**الكلمات الرئيسية:** قاعدة بيانات ، تربة ، الخصائص الديناميكية ، المناطق الزلزالية ، العراق

## 1. INTRODUCTION

Tectonically Iraq is located in a relatively active seismic zone at the northeastern boundaries of the Arabian Plate. The corresponding Zagros - Tauros Belts manifest the subduction of the Arabian plate into the Iranian and Anatolian Plates. The seismic history reveals annual seismic activity of different strength. The north and northeastern zones depicts the highest seismic activity with strong diminution in the south and southwestern parts of the country.

The territory of Iraq, although not directly located on a dense cluster of recent earthquake epicenters; but the geodynamic configurations show a medium to high seismic risk. This will be coupled with the increasing vulnerability of the major highly populated cities. The state of seismological research, seismic monitoring, and seismic hazard awareness have seen better times during the last two decades, **Alsinawi and Al-Qasrani, 2003**.

Determination of dynamic soil properties is an utmost critical and important aspect of geotechnical earthquake engineering problems.. Evaluation of dynamic soil properties by field tests has a number of advantages, as these tests do not require sampling that can alter the stress and structural conditions in soil specimens. Further. the tests measure the response of relatively large volumes of soil. However, these field tests can be again classified based on the range of magnitude of strain as low-strain and high-strain tests. Low-strain tests are based on the theory of wave propagation in the materials. Some of the low-strain field tests are seismic reflection test, seismic refraction test, suspension logging test, steady-state vibration or Rayleigh wave test, spectral analysis of surface wave test (SASW), seismic cross-hole test, seismic down-hole test and seismic cone test, **Sitharam et al., 2004**. The field tests which are generally used in Iraq for determining the dynamic properties of soils used in designing purposes is the seismic cross-hole and down-hole tests. So it became necessary to study the dynamic parameters of soils in different regions of Iraq.

In this study, a data base for the dynamic properties of Iraqi different soils using cross hole and down hole test results will be prepared. This will require getting information for dynamic soil properties of different zones in Iraq from varying geophysical and geotechnical investigation tests reports.

## 2. THEORETICAL WORK

### 2.1 Resource of Data and Presentation

The current study based on experimental results for underground conditions and the engineering properties of the various strata of many geophysical and soil investigation reports for projects in Iraq which is collected from engineering consulting bureaus of Baghdad, Al-Nahrain and Technology universities, also from National Center of Construction Laboratories and Research (NCCLR), and from other sources. Geophysical and soil investigation reports were for projects of water treatment plants and pumping stations, multi-story buildings, electrical substations, stadiums, oil refinery and other projects located at north, middle, western south, eastern south and south regions of Iraq as shown in **Table. 1** and **Fig. 1**.

### 2.2 Geotechnical and Geophysical Parameters Investigated for Iraq Soils

The geotechnical and geophysical parameters for Iraq soils are collected from different projects reports as mentioned before, the collection of data was performed depending up on reports containing both soil investigation and geophysical investigation data, borehole logs of each report are examined well so as the data of the geotechnical and geophysical investigations for each project are collected either from the same borehole or two adjacent ones which have the same soil layers profile. These parameters with their standard units are listed below:

$\gamma_{\text{wet}}$ : unit weight	[kN/m <sup>3</sup> ]
$\gamma_{\text{dry}}$ : dry unit weight	[kN/m <sup>3</sup> ]
$\phi$ : friction angle	[°]
$c$ : cohesion	[kN/m <sup>2</sup> ]
$V_s$ : shear wave velocity	[m/s]
$V_p$ : compression wave velocity	[m/s]
$E_d$ : dynamic modulus of elasticity	[kN/m <sup>2</sup> ]
$G_d$ : dynamic shear modulus	[kN/m <sup>2</sup> ]
$\nu$ : poisson's ratio	[-]

If there is some unavailable strength soil parameters ( $c$  or  $\phi$ ) for particular layers within the reports they would be either evaluated from N value (SPT) or estimated according to type of soil.

### 3. SOIL PARAMETERS EVALUATION

Soil parameters such as;  $\gamma_{\text{wet}}$ ,  $\gamma_{\text{dry}}$ ,  $c$ ,  $\phi$  are evaluated from field tests or laboratory tests, other dynamic parameters such as;  $V_s$  and  $V_p$  are evaluated by geophysical investigations in which other parameters like;  $E_d$ ,  $G_d$  and  $\nu$  are given by, **Doyle, 1995**:

$$G_d = \rho V_s^2 \quad (1)$$

$$E_d = 2 G_d (1 + \nu) \quad (2)$$

$$\nu = \left[ \frac{1/2(V_p/V_s)^2 - 1}{(V_p/V_s)^2 - 1} \right] \quad (3)$$

#### 3.1 Field Testing

##### 3.1.1 Standard penetration test (S.P.T)

The Standard Penetration Test, or SPT, is the most widely used in-situ test, in a great variety of geotechnical exploration projects, in Iraq and throughout the world, as an indicator of the density and compressibility of granular soils. It is also commonly used to check the consistency of stiff or stony cohesive soils and weak rocks. Estimation of the liquefaction potential of saturated granular soils for earthquake design is often based on these tests. This test method provides a soil sample for identification purposes and for laboratory tests appropriate for soil obtained from a sampler that may produce large shear strain disturbance in the sample, **ASTM D 1586 – 99**.

Many local correlations and widely published correlations which relate SPT blow count, or N-value, and the engineering behavior of earthworks and foundations are available, **Fig. 2** shows a useful relationship between N - values and shear wave velocities. **Table 2** and **Table 3** shows the relationships between N-value and friction angle  $\phi$  and unconfined compressive strength  $q_u$ , respectively. The test is performed using a barrel split spoon sampler which is driven into the cased borehole by means of a 65 kg hammer falling freely through a height of 760mm onto the top of the boring rods as shown in **Fig. 3**, different methods of releasing the hammer are used in different countries. The borehole must be cleaned out to the required depth, care being taken to ensure that the material to be tested is not disturbed. Initially the sampler is driven 150mm into the sand to seat the device and to bypass any disturbed sand at the bottom of the borehole. The number of blows required to drive the sampler a further 300mm is then recorded: this number is called the standard penetration resistance (N). The number of blows required for each 75mm of penetration (including the initial drive) should be recorded separately. If 50 blows

are reached before a penetration of 300 mm, no further blows should be applied but the actual penetration should be recorded. At the conclusion of a test the sampler is withdrawn and the sand extracted. Tests are normally carried out at intervals of between 0.75 and 1.50m to a depth below foundation level at least equal to the width (B) of the foundation, **Craig, 2004**. The SPT has been used for many purposes. At its simplest, it is a low quality sampler. At its most useful it is a rapid, inexpensive, qualitative test which can provide data even when other techniques of sampling or testing are not viable or cannot be justified financially. Due to the collected reports the SPT was performed for each test boring at different intervals depending on the stratification of the soil.

### 3.1.2 Field density (Core Cutter Test)

This method provides the determination of bulk field density  $\gamma_{\text{wet}}$  of the surface layers of soil or at the base of test pit; it is suitable for soft fine grained soils. A steel cylinder (core cutter) is driven into the ground, dug out and the soil shaved off level. The mass of soil is found by weighing and deducting the mass of the cylinder. Determining the water content of small samples taken from both ends of the cylinder, **BS 1377:1999**. Then the dry density  $\gamma_{\text{dry}}$  can be determined easily after obtaining the water content w% of the soil.

## 3.2 Laboratory Testing

### 3.2.1 Soil classification ( Sieve analysis and hydrometer )

According to **ASTM D 422-36** this test method covers the quantitative determination of the distribution of particle sizes in soils. The distribution of particle sizes larger than 75  $\mu\text{m}$  (retained on the No. 200 sieve) is determined by sieving, while the distribution of particle sizes smaller than 75  $\mu\text{m}$  is determined by a sedimentation process, using a hydrometer to secure the necessary data.

### 3.2.2 Direct shear test

This test method covers the determination of the consolidated drained shear strength of a soil material in direct shear it is suitable for cohesionless soils. The test is performed by inserting deformation to a specimen at a controlled strain rate on or near a single shear plane determined by the configuration of the apparatus. Generally, three or more specimens are tested, each under a different normal load, to determine the effects upon shear resistance and displacement, and strength properties such as Mohr strength envelopes, **ASTM D 3080 / D3080M-98**.

### 3.2.3 Unconfined compression test

This test method covers the determination of the unconfined compressive strength of cohesive soil in the undisturbed, remolded, or compacted condition, using strain-controlled application of the axial load. This test method provides an approximate value of the strength of cohesive soils in terms of total stresses. This test method is applicable only to cohesive materials which will not expel or bleed water (water expelled from the soil due to deformation or compaction) during the loading portion of the test and which will retain intrinsic strength after removal of confining pressures, such as clays or cemented soils, **ASTM D 2166-00**.

### 3.2.4 Unconsolidated undrained triaxial compression test (UU test)

This test method covers determination of the strength and stress-strain relationships of a cylindrical specimen of either undisturbed or remolded cohesive soil. Specimens are subjected to a confining fluid pressure in a triaxial chamber. No drainage of the specimen is permitted during the test. The specimen is sheared in compression without drainage at a constant rate of axial



deformation (strain controlled). According to **ASTM D 2850-95** this test method provides data for determining undrained strength properties and stress-strain relations for soils.

### 3.2.5 Consolidated undrained triaxial compression test (CU test)

This test method covers the determination of strength and stress-strain relationships of a cylindrical specimen of either an undisturbed or remolded saturated cohesive soil. Specimens are isotropically consolidated and sheared in compression without drainage at a constant rate of axial deformation (strain controlled). The provided calculations are of total and effective stresses, and axial compression by measurement of axial load, axial deformation, and pore-water pressure. This test method provides data useful in determining strength and deformation properties of cohesive soils such as Mohr strength envelopes and Young's modulus. According to **ASTM D4767-04** three specimens are tested at different effective consolidation stresses to define a strength envelope. The determination of strength envelopes and the development of relationships to aid in interpreting and evaluating test results are beyond the scope of this test method and must be performed by a qualified, experienced professional.

### 3.2.6 Consolidated drained triaxial compression test (CD test)

This test method covers the determination of strength and stress-strain relationships of a cylindrical specimen of either intact or reconstituted soil. Specimens are consolidated and sheared in compression with drainage at a constant rate of axial deformation (strain controlled). This test method provides for the calculation of principal stresses and axial compression by measurement of axial load, axial deformation, and volumetric changes. This test method provides data useful in determining strength and deformation properties such as Mohr strength envelopes. According to **ASTM D7181-11** three specimens are tested at different effective consolidation stresses to define a strength envelope. If this test method is used on cohesive soil, a test may take weeks to complete. The determination of strength envelopes and the development of relationships to aid in interpreting and evaluating test results are beyond the scope of this test method and must be performed by a qualified, experienced professional.

## 3.3 Geophysical Investigation

### 3.3.1 Cross hole test

This technique consists of drilling two to three boreholes to depths below the proposed foundation and requires the generation of elastic waves at certain depth down a borehole. For this purpose SPT test hammer was used and the energy is transferred to the base of the borehole by means of drill rods, **Davis and Schultheiss, 1980**. Vertical shear and compressional waves propagating in a horizontal layer were detected by two receivers placed in adjacent boreholes at the same depth as the energy source, as shown in **Fig. 4**. Galvanized pipes 7.5cm diameter were used for casing the boreholes. The space between the pipe and borehole wall was filled by a soil material to make firm contact between the Galvanized pipes and the borehole shaft.

The measurements were taken using a probe (consists of three geophones, two horizontal, and one vertical), which get down on casing holes. The results of shear wave velocity  $V_s$  and compressional wave velocity  $V_p$  were printed on seismic record using (Terraloc ABEM), **ASTM D 4428/D 4428M – 00**.

### 3.3.2 down-hole test

The basic seismic down-hole test consists of measuring the time of arrival of wave from a source to a detector which occupies successive positions down a borehole, as shown in **Fig. 5**, a three component geophone lowered down and fixed against the soil wall using a clamping

device so that a good coupling could be made between the instrument and the medium, **Davis and Schultheiss, 1980**. The source used for generating elastic wave (compressional and shear waves) is placed at the surface some distance from the hole and testing is carried out at 3m interval by striking a plate with impact hammer. The detecting and recording equipment consists of three component geophones (two are horizontal and one is vertical) (borehole picks) with a packer to fix the probe at the required depth, coupled to the ABEM Teraloc seismograph which record the results of shear wave velocity  $V_s$  and compressional wave velocity  $V_p$ , **ASTM D 7400 – 08**.

#### 4. RESULTS AND DATA BASE PREPARED

Soil shear strength and dynamic parameters for soils in seismic active zones of Iraq from different locations (North, Middle and South) are collected. They are collected from geotechnical and geophysical reports of important projects in these zones and are given as database finally arranged in **Table 4**.

#### 5. SITE SOIL SEISMIC CLASSIFICATION

Site soil is classified according to **the Preliminary draft of Iraqi Seismic Code** submitted to Central Organization for Standardization and Quality Control COSQC, **2013** and Federal Emergency Management Agency, **FEMA, 2010**, as shown in **Table 5** and **Table 6** respectively, while according to the European Standard, **Eurocode 8, 2004**, site soil is classified to type (A,B,C,D,E  $S_1$  or  $S_2$ ) as shown in **Table 7**, depending on one of the three methods:

1.  $V_s$  value method, the site soil should be classified according to the value of the average shear wave velocity,  $V_{s,30}$ , which represents a measurement or estimation of average shear wave velocity in the upper 30 m of soil and could be computed in accordance with the following expression:

$$V_{s,30} = \frac{H}{\sum_{i=1,N} \frac{h_i}{v_i}} \quad (4)$$

where  $H$  is the total depth of soil less than or equal to 30m,  $h_i$  and  $v_i$  denote the thickness (in metres) and shear-wave velocity of the  $i$ -th formation or layer, in a total of  $N$ , existing in the top 30 m.

2. N value method, another method used for site soil classification by N value of SPT (Standard Penetration Test).

3.  $S_u$  value method, using the undrained shear strength value  $s_u$  or  $c_u$  in the classification of site soil.

##### 5.1 Site Soil Seismic Classification of Iraq Soils

According to **the Preliminary draft of Iraqi Seismic Code**, submitted to Central Organization for Standardization and Quality Control COSQC, **2013**, **FEMA, 2010** and **Eurocode 8, 2004** Iraq site soils can be classified depending on the average shear velocity  $V_s$  as shown in **Table 7**. The available geophysical investigations in Iraq provides  $V_s$  values for depths from 10 m to 22m.

## 6. CONCLUSIONS

The following conclusions from the collected database may be drawn :

1. The average vertical compressional and shear wave velocities, as well as, the corresponding average dynamic moduli for soil layers are shown in **Table 4**, together with the soil parameters  $\gamma_{wet}$ ,  $\gamma_{dry}$ ,  $c$ ,  $\phi$  evaluated. Thus, database of the soil and dynamic parameters for seismic active zones in Iraq are prepared to be used as input data for simulation of different geotechnical problems under earthquake effects using FEM softwares.
2. The compressional wave velocities were ranged from (1125-2500) m/s in the North, (306-1544) m/s in the Middle, (805-1812) m/s in the Western south , (377-1326) m/s in the Eastern south and (334-1404) m/s in the South of Iraq.
3. The shear wave velocities were ranged from (225-476) m/s in the North, (111-408) m/s in the Middle, (268-659) m/s in the Western south , (131-380)m/s in the Eastern south and (102-365) m/s in the South of Iraq.
4. Modulus of Elasticity was ranged from ( 290.15-1409.8 ) MN/m<sup>2</sup> in the North, (57.9-1107.4) MN/ m<sup>2</sup> in the Middle, (457-2472.2) MN/ m<sup>2</sup> in the Western south , (90.15-1082.8) MN/ m<sup>2</sup> in the Eastern south and (61.8-682.52) MN/ m<sup>2</sup> in the South of Iraq.
5. Shear modulus of Elasticity was ranged from ( 98.09-475.98 ) MN/ m<sup>2</sup> in the North, (20.33-378.73) MN/ m<sup>2</sup> in the Middle, (154.6-868.03) MN/ m<sup>2</sup> in the Western south , (31.5-374.17) MN/ m<sup>2</sup> in the Eastern south and (21.23-233.14) MN/ m<sup>2</sup> in the South of Iraq.
6. Iraq site soils are classified according to different seismic codes depending on  $V_{s,30}$  value as shown in **Table 8** , according to the Preliminary draft of Iraqi Seismic Code and FEMA, 2010 the sites soils are classified as types (E,D and C) while according to Eurocode 8, 2004 sites soils are classified as types (D, C and B) and concluding that Iraq soils are ranging between;
  - a) Very dense soil , soft rock or gravel for WS<sub>1</sub> and WS<sub>3</sub> sites of the Western south region in Iraq.
  - b) Soft clayey soil or loose-to-medium cohesionless soil for M<sub>3</sub> site of the Middle region in Iraq , also S<sub>3</sub> and S<sub>4</sub> sites of South region in Iraq.

## REFERENCES

- Alsinawi S.A., Al-Qasrani Z.O. 2003, *Earthquake Hazards Considerations for Iraq*, Fourth International Conference of Earthquake Engineering and Seismology,12-14 May, Tehran, Islamic Republic of Iran.
- ASTM D 1586 – 99, *Penetration Test and Split-Barrel Sampling of Soils*.
- ASTM D 2166-00, *Unconfined Compressive Strength of Cohesive Soil*.
- ASTM D 2850-95, *Unconsolidated-Undrained Triaxial Compression Test on Cohesive Soils*.
- ASTM D 3080/D3080M- 98, *Direct Shear Test of Soils Under Consolidated Drained Conditions*.
- ASTM D 422-36 (1998), *Particle-Size Analysis of Soils*.
- ASTM D 4428/D 4428M – 00, *Standard Test Methods for Crosshole Seismic Testing*.

- ASTM D 7400 – 08 , *Standard Test Methods for Downhole Seismic Testing*.
- ASTM D4767-04, *Consolidated Undrained Triaxial Compression Test*.
- ASTM D7181-11, *Method for Consolidated Drained Triaxial Compression Test for Soils*.
- Bowles, J. E. 1997, *Foundation Analysis and Design*, 5<sup>th</sup> Edition, McGraw-Hill, New York.
- BS 1377 : 1999 ,*Core Cutter Insitu Density Test*, Part 9.
- Clayton, C.R.I. 1995. *The Standard Penetration test (SPT): Methods and use*, CIRIA Report 143, London.
- Craig R.F. , 2004, *Craig's Soil Mechanics* ,Seventh edition, Taylor & Francis e-Library.
- Davis A. M. and Schultheiss P. J., 1980, *Seismic Signal Processing in Engineering Site - Investigation A Case History* ,Ground Engineering , May 1980.
- Department of Defense Handbook, 1997, *Soil Dynamics and Special Design Aspects*, MIL-HDBK-1007/3
- Doyle, H., 1995, *Seismology*, John Wiley & Sons, Chichester, New York.
- ECB report , 2013, *Installation of 10000 m<sup>3</sup> Oil Storage Tank in Shuaiba Warehouse in Basrah*, Engineering Consultancy Bureau, Aug.2013.
- Eurocode 8, 2004, *Design of Structures for Earthquake Resistance*, Part 1 , The European Union Per Regulation 305/2011, Directive 98/34/EC, Directive 2004/18/EC.
- FEMA, 2010, *Earthquake-Resistant Design Concepts, an Introduction to the NEHRP Recommended Seismic Provisions for New Buildings and Other Structures*, P-749 / Dec. 2010.
- Sitharam T. G. , GovindaRaju L. and Sridharan A., 2004, *Dynamic Properties and Liquefaction Potential of Soils*, Special Section: Geotechnics and Earthquake Hazards, Vol. 87, No. 10, 25 November.
- Terzaghi, K. and Peck, R.B., 1967, *Soil Mechanics in Engineering Practice*, John Wiley, New York. 729.
- *The Preliminary Draft of Iraqi Seismic Code* , 303, submitted to Central Organization for Standardization and Quality Control COSQC, 2013.

## NOMENCLATURE

$c$  = cohesion, kN/m<sup>2</sup>.

$E_d$  = dynamic modulus of elasticity, kN/m<sup>2</sup>.



$G_d$  = dynamic shear modulus,  $\text{kN/m}^2$ .

$N$  = no. of blows for standard penetration test (SPT), blow.

$q_u$  = unconfined compressive strength,  $\text{kN/m}^2$ .

$V_p$  = compression wave velocity, m/s.

$V_s$  = shear wave velocity, m/s.

$V_{s,30}$  = average shear wave velocity in the upper 30 m of soil, m/s.

$\gamma_{\text{dry}}$  = dry unit weight,  $\text{kN/m}^3$ .

$\gamma_{\text{wet}}$  = unit weight,  $\text{kN/m}^3$ .

$\nu$  = Poisson's ratio, dimensionless.

$\phi$  = friction angle, degree.

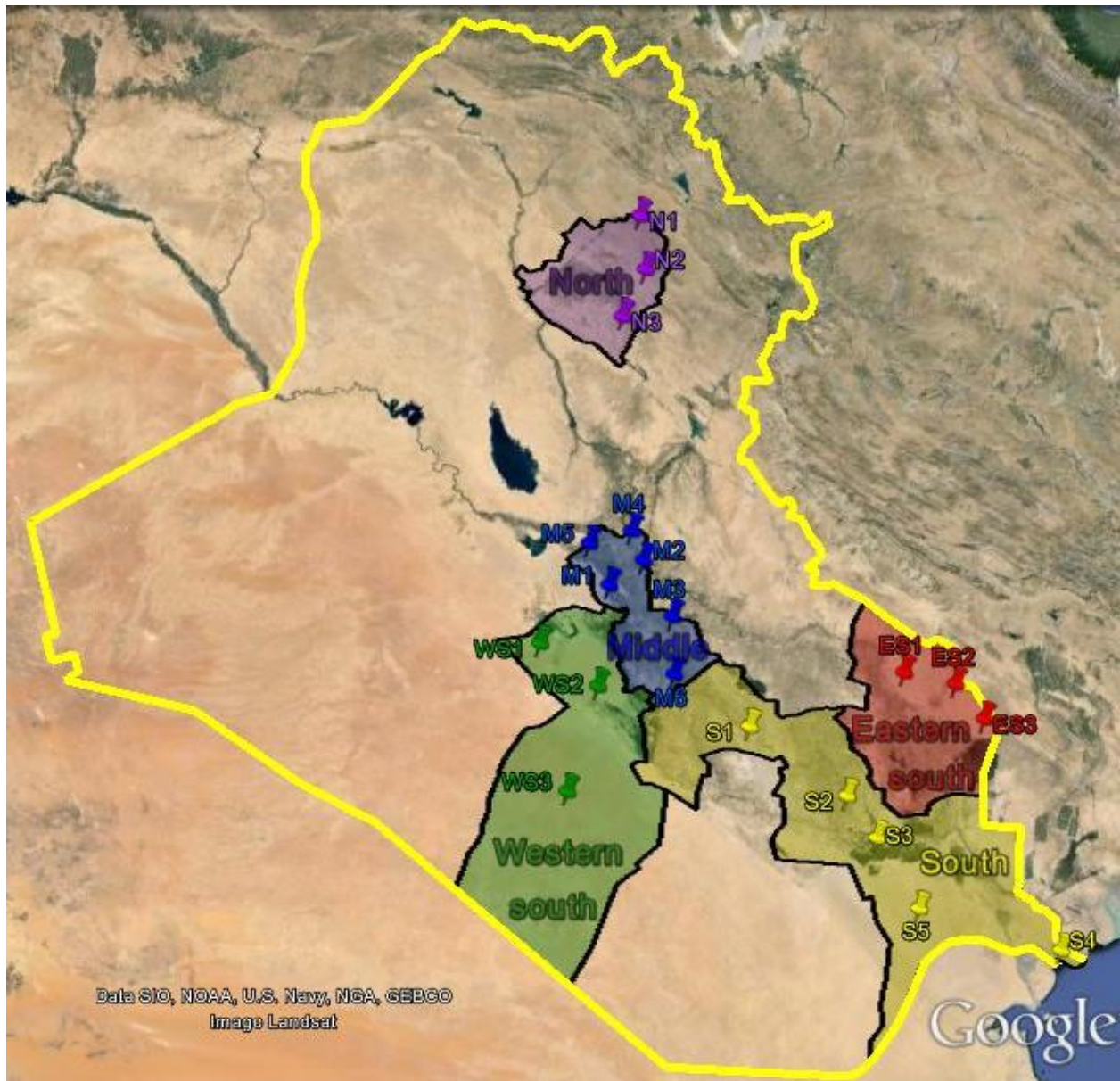


**Figure 1.** Projects locations in Iraq.

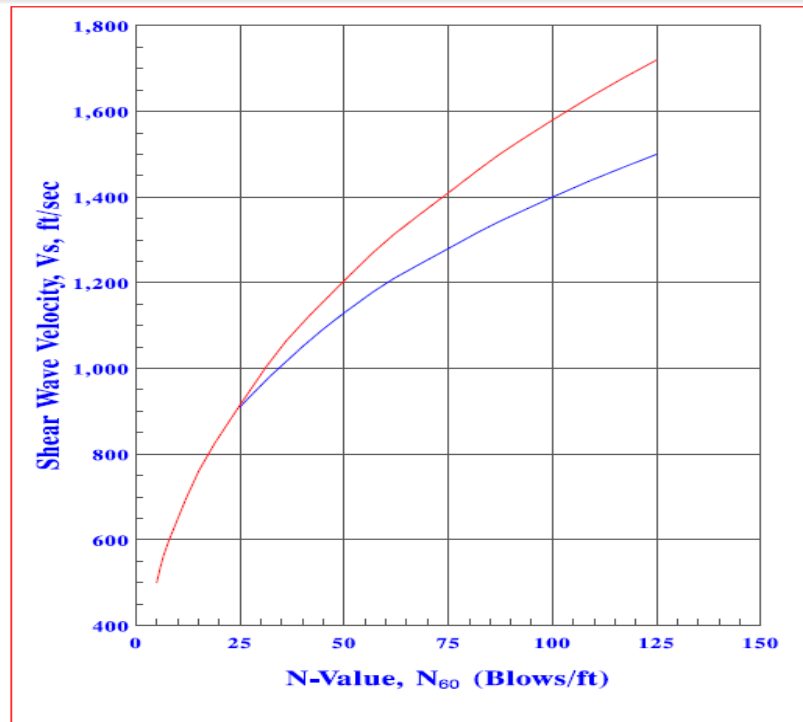


**Figure 2.** Relation between number of blowes per foot in standard penetration test and velocity of shear waves, after department of defense handbook, 1997.

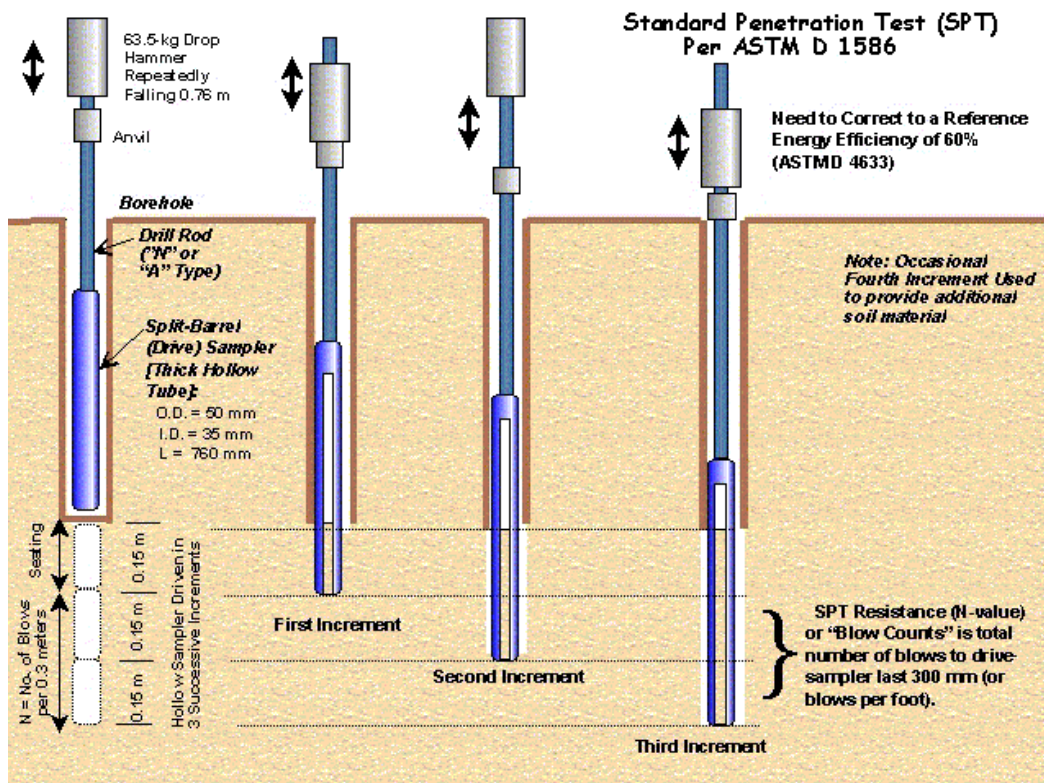


**Figure 3.** Standard penetration test ,after Clayton, 1995.



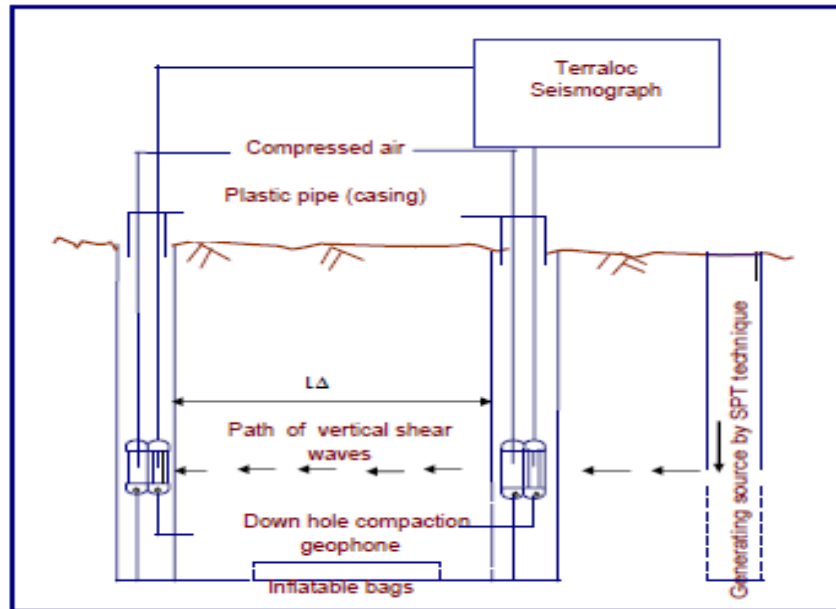


**Figure 4.** Cross hole test procedure, after Davis and Schultheiss 1980.

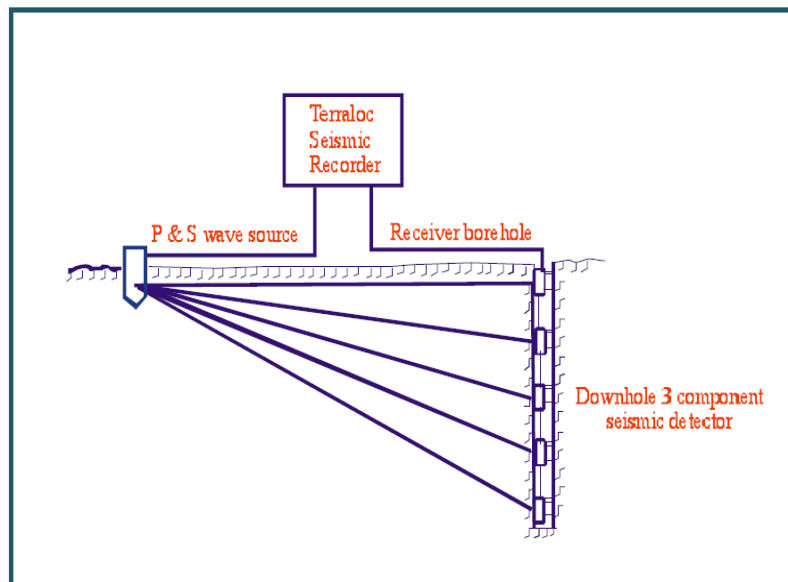


**Figure 5.** Down hole test procedure, after Davis and Schultheiss 1980.

**Table 1.** The available projects in Iraq with their site areas and symbols.

No.	Zone	Site	Project	Site Symbol
1	North	Kirkuk	Kirkuk North Gas Company 1 June Depot	N <sub>1</sub>
2		Kirkuk	Kirkuk Cement Factory	N <sub>2</sub>
3		Kirkuk	Kirkuk North Gas Company	N <sub>3</sub>
4	Middle	Baghdad	Al Karkh Pumping Station	M <sub>1</sub>
5		Baghdad	Al Zawra Stadium	M <sub>2</sub>
6		Baghdad	Eiwa'n Al Madain	M <sub>3</sub>
7		Baghdad	Al Taji Stadium	M <sub>4</sub>
8		Baghdad	Al Qudus Gas Turbine Power Plant	M <sub>5</sub>
9		Babylon	Hilla Power Plant	M <sub>6</sub>
10	Western South	Karbala	Karbala Cultural	WS <sub>1</sub>
11		Karbala	Karbala Al Abbasia Sacred Shrine	WS <sub>2</sub>
12		Al Najaf	Al Najaf Al Salam Housing Complex	WS <sub>3</sub>
13	Eastern South	Missan	Al Amarah Water Intake Depot	ES <sub>1</sub>
14		Missan	Halfaya Oil Field	ES <sub>2</sub>
15		Missan	Missan Oil Export Pipe Line	ES <sub>3</sub>
16	South	Al Dewaniya	Al Dewaniya Pumping Station	S <sub>1</sub>
17		Al Nasiriya	Al Nasiriya Oil Depot	S <sub>2</sub>
18		Al Nasiriya	Al Nasiriya Water Intake Refinery	S <sub>3</sub>
19		Al Basrah	Faw Depot Turbine	S <sub>4</sub>
20		Al Basrah	Al Sheiba Oil Refinery	S <sub>5</sub>

**Table 2.** Correlations with N values of cohesionless soils, after Bowles, 1997.

Description	Relative Density, $D_r$ (%)	Friction Angle, $\phi'$ (Deg.)	N Value
Very loose	Less than 15	25 - 28	< 4
Loose	15 - 60	29 - 32	4 - 10
Medium	60 - 75	33 - 35	10 - 30
Dense	75 - 90	36 - 40	30 - 50
Very dense	Over 90	41 - 45	Over 50

**Table 3.** Correlations of unconfined compressive strength  $q_u$ -N value ,after Terzaghi and Peck, 1967.

Consistency	N Value	$q_u$ (kN/m <sup>2</sup> )
Very soft	<2	>24
Soft	2-4	24-50
Medium	4-8	50-100
Stiff	8-15	100-200
Very stiff	15-30	200-400
Hard	>30	>400



Table 4. Soil properties in different locations of Iraq .

No.	Site	Depth (m)	Soil Type	WT (m)	$\gamma_{wet}$ (kN/m <sup>3</sup> )	$\gamma_{dry}$ (kN/m <sup>3</sup> )	$c$ (kN/m <sup>2</sup> )	$\phi$ (°)	$V_p$ (m/s)	$V_s$ (m/s)	$E_d \times 10^3$ (kN/m <sup>2</sup> )	$G_d \times 10^3$ (kN/m <sup>2</sup> )	$\nu$
1.	N <sub>1</sub>	0-10	Very stiff to hard brown lean CLAY (CL)	3.8	20.1	17	130	0	1250	312	585.43	199.53	0.467
2.	N <sub>2</sub>	0-2.5	Stiff brown sandy SILT (ML)	>25	19	16.8	0	32	1125	225	290.15	98.09	0.479
		2.5-15	Very stiff to hard brown lean to fat CLAY (CL,CH)		20.6	18.2	227	0	1250	321	634.86	216.38	0.467
		15-20	Very dense silty GRAVEL with SAND (GM)		20.6	18.2	0	42	2500	476	1409.8	475.98	0.481
3.	N <sub>3</sub>	0-10	Stiff to very stiff brown lean or fat CLAY (CL,CH)	2.58	21.0	18.1	120	0	1541	304	585.82	197.91	0.48
4.	M <sub>1</sub>	0-6	Medium stiff to stiff brown fat CLAY (CH)	0.63	19.8	15.8	50	0	641	189	209.16	72.13	0.45
		6-12	Very stiff brown lean CLAY (CL)		19.0	14.5	100	0	675	248	338.44	119.17	0.42
		12-15	Medium dense to dense silty clayey SAND to silty SAND with gravel		19.0	15.0	0	37	750	225	284.46	98.09	0.45
5.	M <sub>2</sub>	0-7	Medium to hard brown lean to fat CLAY (CL,CH)	2.3	19.6	15.8	60	3	914	276	441.56	152.26	0.45
		7-9	Very stiff grey sandy SILT (ML)		20.6	17.1	0	34	687	195	233.25	79.88	0.46
		9-14	Stiff to Hard brown lean CLAY (CL)		20.0	18.0	200	0	945	221	292.87	99.61	0.47
		14-15	Medium to dense grey silty SAND		20.0	18.1	0	41	1014	327	628.09	218.09	0.44
6.	M <sub>3</sub>	0-8.5	Medium to hard brown lean to fat CLAY (CL, CH)	3.86	20	16.3	35	0	454	161	151.00	52.8	0.428
		8.5-11	Very stiff brown SILT (ML)		19.6	17	200	0	625	232	305.41	107.54	0.42
		11-12	Very stiff brown fat CLAY(CH)		19.6	17.2	240	0	1000	227	303.29	102.95	0.473



No.	Site	Depth (m)	Soil Type	WT (m)	$\gamma_{wet}$ (kN/m <sup>3</sup> )	$\gamma_{dry}$ (kN/m <sup>3</sup> )	$c$ (kN/m <sup>2</sup> )	$\phi$ (°)	$V_p$ (m/s)	$V_s$ (m/s)	$E_d \times 10^3$ (kN/m <sup>2</sup> )	$G_d \times 10^3$ (kN/m <sup>2</sup> )	$\nu$
7.	<b>M<sub>4</sub></b>	0-7.5	Stiff to very stiff brown lean to fat CLAY (CL-CH)	2.2	19.8	17.1	65	10	841	165	162.7	54.97	0.48
		7.5-11	Medium to very dense grey silty SAND (SM)		19.0	16.5	0	38	1025	279	440.3	150.8	0.46
8.	<b>M<sub>5</sub></b>	0-1	Brown to grey clayey silt to sandy silt with filling materials, organic to salts (ML)	1.3	19.00	15.8	28.7	0	322	140	105	37.96	0.383
		1-15	Brown to Grey Silty CLAY to Clayey Silt (ML,CL,CH)		18.88	14.7	31.5	0	776	219	268.9	92.34	0.456
		15-20	Grey Sand to silty or clayey SAND to Gravilly SAND		22.31	17.04	0	38	1544	408	1107.4	378.73	0.462
9.	<b>M<sub>6</sub></b>	0-2.4	Grayish sandy silty CLAY soil, medium consistency	1.5	16.18	14.5	144	0	306	111	57.9	20.33	0.424
		2.4-16	Grayish silty sand soil, medium dense		18.44	16.5	0	38	450	183	176.33	62.98	0.4
10.	<b>WS<sub>1</sub></b>	0-4.5	Dense white to yellow slightly to moderately gypseous SAND with silt to silty SAND with gravel (SP,SM)	0.8	18.8	18	0	37	1433	284	457.0	154.6	0.478
		4.5-12	Dense to very dense white to yellow SAND with silt (SP,SM)		19.4	18	0	35	1733	550	1727.2	598.46	0.443
		12-22	Very dense white to yellow SAND with silt to silty SAND (SP,SM)		19.4	18	0	35	1650	563	1801	627.1	0.436
11.	<b>WS<sub>2</sub></b>	0-10.5	Stiff brown silty to moderately gypseous fat CLAY (CH)	1.5	18.5	14.7	100	0	1416	312	541.76	183.65	0.475
		10.5-14	Very loose to medium green to yellow marly SAND (SM)		19	17.1	0	50	1474	289	479	161.83	0.48
12.	<b>WS<sub>3</sub></b>	0-1.2	Medium- dense light brown slightly gypseous silty SAND (SM)	0.9	19.1	17	0	43	805	268	458.15	159.3	0.438
		1.2-7	Medium- dense to very dense light brown SAND (SP)		19.5	18	0	40	1450	557	1743.5	616.95	0.413
		7-10	Very dense light brown silty SAND (SM)		19.6	18	0	39	1812	659	2472.2	868.03	0.424



No.	Site	Depth (m)	Soil Type	WT (m)	$\gamma_{wet}$ (kN/m <sup>3</sup> )	$\gamma_{dry}$ (kN/m <sup>3</sup> )	$c$ (kN/m <sup>2</sup> )	$\phi$ (°)	$V_p$ (m/s)	$V_s$ (m/s)	$E_{ax}10^3$ (kN/m <sup>2</sup> )	$G_{ax}10^3$ (kN/m <sup>2</sup> )	$\nu$
13.	ES <sub>1</sub>	0-7.6	Medium stiff to stiff brown lean to fat CLAY (CL,CH)	0.6	19.5	15.1	80	0	500	176	175.96	61.57	0.429
		7.6-9	Loose grey silty SAND		19.5	15.7	0	29	600	200	228.51	79.51	0.437
		9-10	Stiff brown lean CLAY (CL)		19.5	15.7	60	8	600	250	346.6	124.23	0.395
14.	ES <sub>2</sub>	0-5	Medium stiff to stiff brown lean to fat CLAY (CL,CH)	0.6	18.0	14.6	65	0	377	131	90.15	31.5	0.431
		5-8	Stiff brown lean to fat CLAY (CL,CH)		19.5	15.8	60	0	604	250	347.98	124.28	0.4
		8-17	Stiff brown lean CLAY (CL)		20.8	15.9	60	8	1362	420	1082.8	374.17	0.447
15.	ES <sub>3</sub>	0-9	Medium stiff to stiff brown lean to fat CLAY (CL,CH)	0.6	19.7	15.7	80	0	696	179	188.5	64.37	0.464
		9-18	Stiff brown lean CLAY (CL)		20.9	16.1	60	0	1167	380	886.78	307.76	0.44
16.	S <sub>1</sub>	0-1.5	Brown lean CLAY(CL)	0.3	18.5	14.4	94	0	625	188	193.28	66.65	0.450
		1.5-2	loose grey silty SAND layer (SM)		20.0	15.0	0	30	909	185	213.45	72.21	0.478
		2-10	Medium stiff to very stiff brown to green marly lean to fat CLAY (CL,CH)		19.3	14.7	60	5	909	200	232.17	78.73	0.475
17.	S <sub>2</sub>	0-4	Very stiff brown lean CLAY (CL)	4	19.07	15.1	34	0	600	200	223.45	77.75	0.437
		4-10	Stiff to hard brown lean to fat CLAY (CL,CH)		19.93	15	112	0	750	240	337.6	117.1	0.442
18.	S <sub>3</sub>	0-12	Soft to medium black, brown, green light, green lean to fat CLAY (CL,CH)	1.7	19.5	15.2	90	3	434	110	70.54	24.06	0.466
		12-14	Loose grey silty SAND (SM)		20.8	18	0	41	500	145	129.7	44.6	0.454
		14-15	Very stiff brown, green lean CLAY(CL)		20.8	17	191	0	600	166	170.56	58.45	0.459
19.	S <sub>4</sub>	0-10	Very soft to very stiff brown lean or fat CLAY(CL,CH)	1.0	18.37	13.92	40	0	550	138	104.6	35.7	0.466
		10-13	Grey silty SAND (SM)		19.63	15.54	0	37	334	103	61.8	21.23	0.455
		13-15	Very soft to very stiff brown lean CLAY (CL)		20.02	16.03	48	0	450	102	62.57	21.24	0.473
20.	S <sub>5</sub>	0-3.7	Grey gypseous SAND (SM)	1.8	18.18	-	5.33	38.6	566	230	244.6	87.29	0.401
		3.7-15	Grey gypseous silty SAND (SM)		19.16	-	8.4	40.5	1404	365	682.52	233.14	0.463

**Table 5.** Site soil classification (after the Preliminary draft of Iraqi seismic code, submitted to Central Organization for Standardization and Quality Control COSQC, 2013 .

Site Class Definition	$V_s$	$N$ or $N_{ch}$	$S_u$
A Hard rock	>1500 m/s	-	-
B Rock	760 to 1500 m/s	-	-
C Very dense soil or soft rock	370 to 760 m/s	>50	>100kPa
D Hard soil	180 to 370 m/s	15 to 50	50 to 100 kPa
E Soft clayey soil	<180 m/s	<15	<50kPa
Each side section thickness greater than 3m for soil profile of the following characteristics: - Plasticity Index $PI > 20$ . - Water content $w \geq 40\%$ . - Undrained shear strength $S_u < 25\text{kPa}$ .			
F Soil types that require a special field assessment	1. Soil exposed to possibility of collapse. 2. Silt and/or clayey soil of high organic content. 3. Clayey soil of very high plasticity index. 4. Very thick clayey soil of weak /medium strength.		

**Table 6.** Site class and soil types ,after Fema, 2010.

Site Class	General Description	$V_s$	$N$ Blows/foot	$S_u$
A	Hard rock	>5000 ft/sec >1524 m/s	-	-
B	Rock	2500-5000 ft/sec 762-1524 m/s	-	-
C	Very dense soil and soft rock	1200-2500 ft/sec 365-762 m/s	>50	>2000 psf >95kPa
D	Stiff soil	600-1200 ft/sec 182-365 m/s	15 - 50	1000-2000 psf 47-95 kPa
E	Soft clay soil	<600 ft/sec <182 m/s	<15	<1000 psf <47kPa
F	Unstable soils	-	-	-



**Table 7. Ground Types according to the European Standard, after Eurocode 8, 2004.**

Ground type	Description of stratigraphic profile	Parameters		
		$V_{s,30}$ (m/ s)	$N$ SPT (blows/30cm)	$c_u$ (kPa)
A	Rock or other rock-like geological formation including at most 5m of weaker material at the surface.	> 800	-	-
B	Deposits of very dense sand, gravel, or very stiff clay, at least several tens of metres in thickness, characterized by a gradual increase of mechanical properties with depth.	360-800	> 50	> 250
C	Deep deposits of dense or medium- dense sand, gravel or stiff clay with thickness from several tens to many hundreds of metres.	180-360	15 - 50	70-250
D	Deposits of loose-to-medium cohesionless soil (with or without some soft cohesive layers), or of predominantly soft-to-firm cohesive soil.	< 180	< 15	< 70
E	A soil profile consisting of a surface alluvium layer with $V_s$ values of type C or D and thickness varying between about 5 m and 20 m, underlain by stiffer material with $V_s$ 800 m/s.			
$S_1$	Deposits consisting, or containing a layer at least 10m thick, of soft clays/silts with a high plasticity index ( $PI > 40$ ) and high water content	< 100 (indicative)		10-20
$S_2$	Deposits of liquefiable soils, of sensitive clays, or any other soil profile not included in types A E or $S_1$			

**Table 8.** Iraq site soil classification.

No.	Site	Max. depth of Geophysical Investigations (m)	$V_s$ (m/s)	Iraqi Seismic Code and FEMA 2010	Eurocode 8
1	N <sub>1</sub>	10	312	D	C
2	N <sub>2</sub>	20	330	D	C
3	N <sub>3</sub>	10	304	D	C
4	M <sub>1</sub>	15	217	D	C
5	M <sub>2</sub>	15	245	D	C
6	M <sub>3</sub>	12	177	E	D
7	M <sub>4</sub>	11	190	D	C
8	M <sub>5</sub>	20	240	D	C
9	M <sub>6</sub>	16	198	D	C
10	WS <sub>1</sub>	22	466	C	B
11	WS <sub>2</sub>	14	306	D	C
12	WS <sub>3</sub>	10	514	C	B
13	ES <sub>1</sub>	10	185	D	C
14	ES <sub>2</sub>	17	237	D	C
15	ES <sub>3</sub>	18	243	D	C
16	S <sub>1</sub>	10	198	D	C
17	S <sub>2</sub>	10	222	D	C
18	S <sub>3</sub>	15	116	E	D
19	S <sub>4</sub>	15	124	E	D
20	S <sub>5</sub>	15	319	D	C

## Identification Of Key Factors Affecting Waste Management In Life Cycle Of The Construction Project By Using Delphi Technique

Hatem Kh. B. Al-Agele

Assistant Professor

College of Engineering-University of Baghdad

E-mail: dr.hatem2999@yahoo.com

Sajjad A. M. Al-Kaabi

MSc. student

College of Engineering-University of Baghdad

E-mail: sajadnaji2014@gmail.com

### ABSTRACT

The problem of generated waste as a result of the implementation of construction projects, has been aggravated recently because of construction activity experienced by the world, especially Iraq, which is going through a period of reconstruction, where construction waste represents (20-40%) of the total generated waste and has a negative effect on the environment and economic side of the project. In addition, the rate of consumed amounts of natural resources are estimated to be about 40% in the construction industry, so it became necessary to reduce waste and to be manage well. This study aims to identify the key factors affecting waste management through the various phases of the project, and this is accomplished by using the Delphi technique. After conducting three questionnaire rounds of the Delphi to a group of experts, the results of this study identified forty four key factors affecting waste management distributed on the phases of the project, where found that the factor of frequent errors in the designs has the highest effect on the design phase, and the factor of the use of construction techniques that do not generate waste has highest effect on the construction phase. The purpose is to provide data base for decision-makers to control waste management well to avoid all affecting factors, with the possibility of building waste management system based on factors effective for each phase.

**Key words:** phases of construction project; key affective factors; waste management; Delphi technique.

### تحديد العوامل الرئيسية المؤثرة على ادارة المخلفات في دورة حياة المشروع الانشائي باستخدام تقنية دلفي

سجاد علي محمود الكعبي

طالب ماجستير

كلية الهندسة – جامعة بغداد

حاتم خليفة بريسم العجيلي

استاذ مساعد

كلية الهندسة – جامعة بغداد

### الخلاصة

مشكلة المخلفات المتولدة نتيجة تنفيذ المشاريع الانشائية تفاقمت في الاونة الاخيرة بسبب الحركة العمرانية التي يمر بها العالم وخصوصا العراق الذي يمر بمرحلة اعادة اعمار تشكل المخلفات الانشائية (20-40%) من المخلفات الكلية المتولدة، اضافة الى تأثيراتها السلبية على البيئة وعلى الجانب الاقتصادي للمشروع، علاوة على استهلاك كميات كبيرة من الموارد الطبيعية. تقدر بحوالي 40 % في الصناعة الانشائية، لذلك اصبح من الضروري تقليل كميات المخلفات المتولدة وادارتها بصورة جيدة. تهدف هذه الدراسة الى تحديد العوامل الرئيسية المؤثرة على ادارة المخلفات خلال مراحل المشروع المختلفة، ويتم تحقيق ذلك عن طريق استخدام تقنية دلفي. تم اجراء ثلاث جولات استبائية من دلفي لمجموعة من الخبراء كانت نتائج هذه الدراسة هي تحديد اربعة واربعون عاملاً رئيسياً مؤثراً على ادارة المخلفات موزعة على مراحل المشروع الانشائي، حيث وجد ان عامل الاخطاء المتكررة في التصميم هي الاكثر تأثيراً في مرحلة التصميم، وعامل استخدام التقنيات التنفيذية التي لاتولد مخلفات هو الاكثر تأثيراً في مرحلة التنفيذ. ان الفائدة من ذلك هي توفير قاعدة بيانات لاصحاب القرار لادارة المخلفات بصورة جيدة متلافياً بذلك جميع العوامل المؤثرة، مع امكانية بناء نظام لادارة المخلفات يستند على العوامل المؤثرة في كل مرحلة.

**كلمات البحث:** مراحل المشروع الانشائي؛ العوامل الرئيسية المؤثرة؛ ادارة المخلفات؛ تقنية دلفي.

## 1. INTRODUCTION

In the construction industry, especially during the construction, renovation and demolition projects achieving 'zero waste' will be a great strategy for a world in an environmental crisis, but, this is a highly challenging target in construction. However, by involving and committing all stakeholders to minimize waste from source and developing a good waste management strategies by both the reuse and recycle of materials, minimization of construction waste can be achieved at various phases of a construction project life cycle; and opportunities and responsibilities lie with all supply chain stakeholders, clients, designers, contractors and suppliers. The ratio of construction and demolition waste (C&DW) represents (20 – 40) % of the nation's total waste stream to landfills, **Altuncua & Kasapseçkina, 2011**, and the rate of consumed amounts of natural resources were estimated to be about 40% in the construction industry, **Winkler, 2010**. Despite some European countries have high rates for reuse and recycling up to 80%, this rate is still very low in many European countries, therefore, a plan should developed to make waste re-use, recycling and other material recovery rate increase to a minimum of 70% by weight in Europe by 2020, it is important publish initiatives that contribute to an effective waste management approach reaching high rates of construction and demolition waste recovery, **Gangoellis et al., 2014**. While in Iraq there is no system for managing waste in construction projects, in addition the relevant previous studies are focused on estimate the volume of C&DW that will be generated on a site and their impacts only. **Fig.1** shows a construction and demolition waste management framework. **Boyle, 2004**, reported that the principles of sustainability greatly contribute to preserving the natural resources and the environment by reduction of the C&DW quantities and increasing recycling/reusing of materials. In addition, decrease the environmental impact of construction materials, the term sustainability refers to development strategies that take into account the requirements of the present and future generations together and provide a balance of interests that serve all in the economic, social and environmental fields, so sustainable development is defined as meeting the needs of present generations without compromising the ability of future generations to meet their needs and requirements and that the idea of environmental sustainability is based on the principle of leaving the land in good condition for future generations, **A1, 2011**. The three dimensions of sustainability to achieve these requirements, **Blair, 2008**, are as follows:

- 1- Social equity: which includes safety at work, standards on consumer protection, and accessibility requirements for people with disabilities.
- 2- Integrity environmental: which includes standards on sustainability in relation to activities such as water and soil quality, the quality of water services and air, building construction, treatment of waste. Also standards on energy efficiency and renewable sources and support of the environmentally friendly practices are also included.
- 3- Economic growth: which provide tools for consolidating innovation, business transactions and eliminating barriers to trade, and contributing to interoperability and the dissemination of new technologies. In addition, to the "toolbox" of standards is used for conformity assessment, to increase confidence in products and services.

## 2. DELPHI TECHNIQUE

The Delphi name came from the island of Delphi, which was the hallowed site of the most respected oracle in ancient Greece, **Powell, 2002**. A Delphi procedure was selected as the most appropriate method for attaining consensus in a national panel of the subject matter experts (SMEs), **Farmer, 1998**. There are many definitions of the Delphi method. **Yousuf, 2007 and Mayburry, and Swanger, 2010**, defined Delphi technique as "a group process involving an

interaction between the researcher and a group of identifying experts on a specific topic or topics, usually through a series of questionnaires”. The development of the Delphi technique started in the 1940s with work of Olaf Helmer, and his associate, Norman Dalky, at the RAND Corporation, **Yousuf, 2007**. The development of Delphi was in five stages: secrecy and obscurity; novelty; popularity; scrutiny; and continuity, **Rowe, and Wright, 1999**. Finally, Delphi method has been applied in different fields such as higher education, marketing, information technology, library and information science, engineering and medicine, and it became a great assistance tool in reaching important results for a number of difficult issues, **Antoniades, 2014**.

## 2.1 Designing a Delphi Method

As in all applied research, attention must be paid to the detailed planning and then to effective execution of this study. This section focuses on four elements for planning of Delphi technique, they are as follows:

- 1- Problem Definition: A problem definition is an important initial step to ensure that both the nature and scope of the problem or issue to be investigated, to define expected outcomes of the study, as well as the appropriateness of the Delphi method to address the specific problem, **Welding, 2013**.
- 2- Selection of Experts: Careful selection of the panel of experts is the keystone to a successful Delphi study. The key aspects of panel selection include the experts' qualifications and the size of the participant's commitment, **Gohdes, and Crews, 2004**.
- 3- Panel Size: The careful selection of the panel is a key factor in the Delphi method because it enables a researcher confidently to use a small panel. There is no sample size advocated for Delphi studies. The literature on this subject suggests that the panel size be between (15-30) with heterogeneous population and (5-15) for a homogeneous population, **Adler, and Ziglio, 1996**. But, **Okoli, and Pawlowski, 2004**, gave the appropriate size of the group was between (10-18) experts.
- 4- Conducting the Delphi Rounds: Developing the questionnaire for rounds also called questions or iterations etc.) is based upon the clear identification of the study goals, and a critical literature review, among other preliminary research activities and enables the researcher to generate question items and response scales tapping the major questions and issue areas to be measured, and a Delphi study usually involves three or four rounds, **Welding, 2013**. The communication between panel members and researcher is usually conducted by mail, but the growing access to email and the web opens new channels for group communication that speeds up the timeline from many months to conduct all rounds in a few weeks, **Loo, 2002**.

## 3. IDENTIFICATION OF KEY FACTORS AFFECTING WASTE MANAGEMENT IN CONSTRUCTION PROJECTS

From the previous studies it was found there were many classifications of the construction project life cycles. Most, if not all, projects go through a life cycle that varied with the size and complexity of the project. A project consists of five phases as follows: (Brief Phase, Design Phase, Procuring Phase, Construction Phase, and Commissioning Phase), while the following studies: **Lu and Yuan, 2011; Llatas, 2013 and Lester et al., 2014**, reported the additional phase in the life cycle of the construction project, it is called Demolition or Decommissioning phase, this phase begins when ending the life of the project. So a construction project life cycle that adopted by the researcher consists of six phases as follows: (Brief Phase, Design Phase, Procuring Phase, Construction Phase, Commissioning Phase, and Demolition phase). The

researcher in this study had used the Delphi method for identifying the key factors affecting waste management in construction projects in Iraq, in each phase of project phases there are three processes:

- 1- Selection of the expert team.
- 2- Conducting Delphi rounds.
- 3- The conclusion.

### **3.1 Selection of the Expert Team**

A group of experts was selected to provide opinions on the key factors affecting on waste management based on the following criteria:

1. They have extensive working experience in the construction industry in Iraq.
2. They are involved in the management of construction projects in Iraq.

Twenty invitation were sent to individuals to participate. The invitation explained the purpose of the study; the experts were informed that there would be a number of rounds of questionnaire, and the method of the distribution of the questionnaire would be either by receiving it directly or by an E-mail. Sixteen participant responded and agreed to participate, four of them come from the private sector and twelve from the public sector, all the participating have experience of not less than twenty years in the construction industry, all experts' information has been listed in **Table 1**, the names of experts and their organizations are not revealed for anonymity. The academic degrees, field of specialization, and work sector for the experts, are given in **Figs. 2, 3, and 4** respectively.

### **3.2 Conducting Delphi Rounds**

#### **3.2.1 Delphi first round: identifies the effective factors**

In the first round of Delphi, the researcher prepared a list of effective factors depending on the relevant literatures and studies, this list is distributed on seven groups (according to the six phases of construction project, as well as other factors), then experts were asked to identify a specified number of the major factors from this list that they considered affecting waste management in the construction projects of Iraq. Also this list had additional request to the experts to advise if there are any other factors affecting waste management not listed. The researcher managed in this round to meet with ten of experts in one place at one time and began with them a round of brainstorming to identify the factors and for the remaining six experts the researcher conducted interviews with them for the purpose of answering the questionnaire of the first round of the Delphi technique.

##### **3.2.1.1 Result and analysis of the first round**

The factors identified and suggested by the experts in the first round were carefully analyzed and a list of factors was formed after excluding the factors which have similar meanings. This list include seventy four factors in all phases of a construction project, they were prepared to be used in the second round of Delphi method.

#### **3.2.2 Delphi second round: refining the selection factors**

In the second round questionnaire, the experts were asked to indicate the relevant importance of these seventy four factors that had been identified in the first round of the Delphi method, using a five-level Likert scale, as follows (very low important, low important, medium important, highly important, very highly important).



### 3.2.2.1 Results and analysis of the second round

**Table 2**, shows the indication of relative importance of all effective factor in the second round. This round used the (SPSS) program to conduct the statistical analysis, like Mean (M) and standard deviation (S.D) according to Eq. (1) & Eq. (2) respectively. The factors that got arithmetic mean less than number (3), were removed in third round of the Delphi method, like, **Mayburry and Swagner, 2010**, where (1= very low important, 2= low important, 3= medium important, 4= highly important, 5= very highly important). Forty four factors that resulted from the second round, were prepared for use it in the third round.

$$M=[(\sum_{i=1}^K x_i f_i)/n] \quad (1)$$

$$S.D=[(\sum_{i=1}^k (x_i - M)^2 f_i / (\sum_{i=1}^k f_i))]^{\frac{1}{2}} \quad (2)$$

Where:

M: mean.

S.D: standard deviation.

$x_i$  : weight value for particular.

$f_i$  : number of frequencies.

n : total number of answers.

### 3.2.3 Delphi third round: degree of consistency

In the third round of Delphi method, experts were asked to re-evaluate the relative importance of each factor that resulted from the second round by using the same five-level Likert scale. The aim of third round is to measure the consistency of experts' opinions between the second round and the third round. If the required consistency is not achieved the researcher will go to the fourth round for re-evaluation.

#### 3.2.3.1 Result and analysis of the third round

**Table 3** shows the indication of relative importance of each factor in third round. In this round also the (SPSS) program was used to conduct the statistical analysis. The results of the analysis show that all the factors got arithmetic mean of more than number (3). This means that all the effective factors that have been obtained from the third round are located between (medium to very high) importance and this result is similar to the result of the second round where there is no difference between the two rounds so there is no need to go to the fourth round. The researcher also conducted the validity and reliability test, for the experts' answers in this round, by extracting the alpha coefficient - Cronbach by using (SPSS) program, all the values of alpha were positive, because they reached the minimum value of (0.888), this indicates the answers of experts in this round, have a high stability and sincerity, while the value of Cronbach alpha should not be less than (0.70), **A2, 2013**.

## 4. CONCLUSIONS

The result of Delphi technique is forty four key factors affecting waste management in all phases of a construction project and were sorted by importance, starting from the highest for each phase, as shown in **Table 4**, found that the factor of weakness in knowledge about the project life cycle and quantity of the generated waste has highest effect in the brief phase, and the factor of frequent errors in the designs has the highest effect on the design phase, and the factor of imposing contractual clauses for the main contractor and sub-contractors in dealing with the

waste and the method used for their disposal in the procuring phase has highest effect, and the factor of the use of construction techniques that do not generate waste has highest effect on the construction phase, and the factor of instructions on how to use and maintain should be available for all occupants of the project has highest effect on commissioning phase, while the factor of use of the high-tech equipment in the demolition process has highest effect on the demolition phase. By all the key effective factors may manage waste by taking the necessary procedure to address these factors, so the researcher recommended the following some measures for that purpose: The need to form a special technical committee to manage the construction waste in large companies, the need for support from the state to process of construction waste management by allocating the needed funds to manage waste, work training courses to qualify engineers on waste management, in addition to held scientific conferences by the government on waste management, government encouragement of investors to invest in the field of waste recycling, and the need to use high-tech equipment in the implementation process. In addition, these factors may be relied on constructing the proposed system for managing waste in construction projects.

## REFERENCES

- Adler, M., Ziglio, E., 1996, *Gazing into the Oracle: The Delphi Method and its Application to Social Policy and Public Health*, London, England: Jessica Kingsley.
- Altuncua, D., Kasapşekina, M. A., 2011, *Management and Recycling of Constructional Solid waste in Turkey*, *Procedia Engineering*, vol. 21, PP. 1072 – 1077.
- Antoniadou, P., 2014, *SOA Maturity Model: A Delphi-Derived Proposal for Inter-Enterprise Setups*, Cham : Springer International Publishing.
- Blair, B., 2008, *The Role of Standards in Sustainability*, Standards Australia, October.
- Boyle, C., 2004, *The Sustainable Buildings in New Zealand*, IPENZ Presidential Task Committee, March.
- Farmer, E. A., 1998, *A Delphi Study of Research Priorities in Tech-Prep*, *Journal of Vocational and Technical Education*, vol. 15, NO. 1, PP. 42-49.
- Gangolells, M., Casals, M., Forcada, N., Macarulla, M., 2014, *Analysis of the Implementation of Effective Waste Management Practices in Construction Projects and Sites*, *Resources, Conservation and Recycling*, vol. 93, PP. 99–111.
- Gohdes, W. L., Crews, T. B., 2004, *The Delphi Technique: A Research Strategy For Career and Technical Education*, *Journal of Technology Education*, vol. 41, NO. 2, PP. 105 – 122.
- Lester, E. A., CEng, FICE, FIMech.E, FIStruct.E, FAPM, 2014, *Project Management, Planning and Control*, (Sixth Edition).
- LLATAS, C., 2013, *Methods for Estimating Construction and Demolition (C&D) Waste*, University of Seville, Spain.

- Loo, R., 2002, *the Delphi Method: A Powerful Tool for Strategic Management*, An international journal police, strategies & management, vol. 25, NO. 4, PP. 762 -769.
- Lu, W., Yuan, H., 2011, *A Framework for Understanding Waste Management Studies in Construction*, Waste Management, vol. 31, PP.1252–1260.
- Mayburry, T., Swanger, N. A., 2010, *Identification of Industry Needs for Baccalaureate Hospitality Graduates: A Delphi Study*, International CHRIE Conference-Refereed Track. Paper 4., July 31.
- Okoli, C., Pawlowski, S. D., 2004, *The Delphi Method as a Research Tool: An Example, Design Considerations and Applications*, Information & Management, vol. 42, Issue 1, PP. 15–29.
- Powell, T., 2002, *Quick Tips, Collecting Group Data: Delphi technique*, University of Wisconsin, Madison.
- Rowe, G., Wright, G., 1999, *The Delphi Technique as a Forecasting Tool: Issues and Analysis*, International Journal of Forecasting, vol. 15, PP. 353–375.
- Welding, A. K., 2013, *Project Evaluation: Lessons Learned Vs. Delphi Method*, Thesis of 6 ECTS credits submitted to the School of Science and Engineering at Reykjavík University in partial fulfillment of the requirements for the degree of Master of Project Management in MPM.
- Winkler, G., 2010, *Recycling Construction & Demolition Waste*, , A LEED-Based Toolkit.
- Yousef, M. I., 2007, *Using Experts' s Opinions Through Delphi Technique*, Practical Assessment, Research & Evaluation, vol. 12, NO. 4.

- (A1, 2011) الصفار، أ.، 2011، *الاستدامة والصناعة الإنشائية*، موقع الاستدامة الالكتروني.

- (A2, 2014) حسن، ع. ق.، 2014، *تخمين و إعادة تدوير النفايات الإنشائية في محافظة البصرة*، مجلة البصرة للعلوم الهندسية، المجلد 14، العدد الأول.

## ABBREVIATIONS

- AM: he Arithmetic Mean.
- C&D W: Construction and demolition waste.
- N: The sample size.
- S.D: The Standard Deviation.
- SMEs: Subject matter experts.
- SPSS: Statistical Package for Social Science.
- $\alpha$ : Cronbach's Alpha factor.

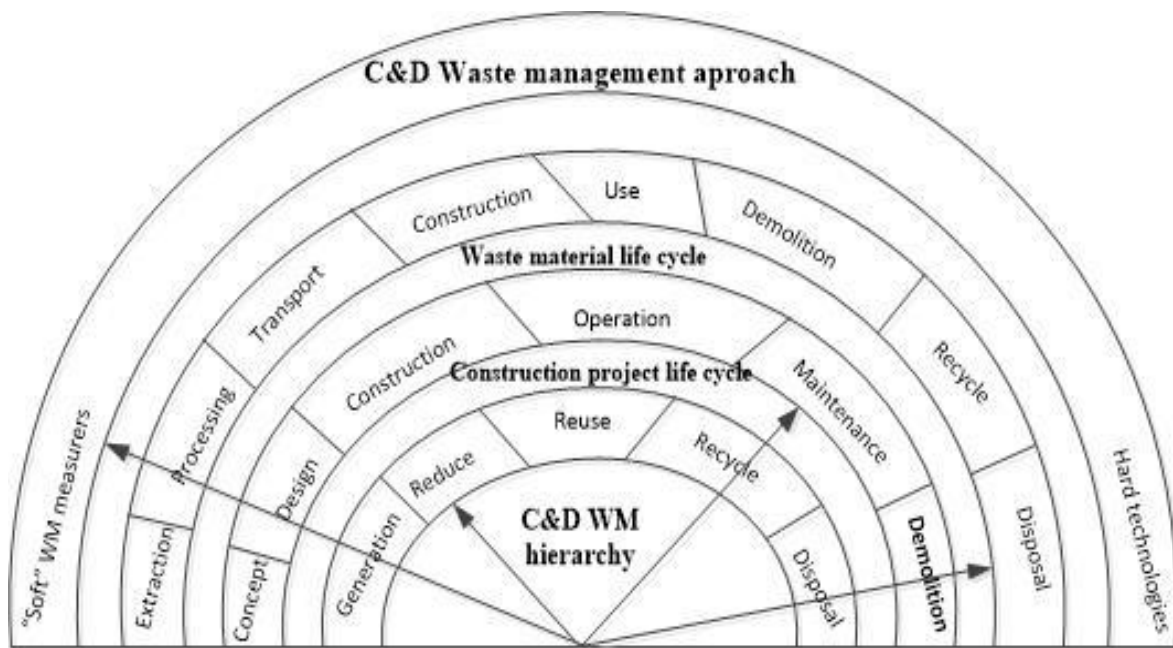


**Figure 1.** A Construction and demolition waste management framework, Lu & Yuan, 2011.

**Table 1.** List of qualifications for participants experts in delphi method.

NO.	Academic Degree	Eng. Field	Experience Year	Sector	Position	Organization
1	Ph.D.	Civil	29	Public	Construction Consultant	Ministry of Construction and Housing
2	Ph.D.	Civil	28	Public	Academic	University of X
3	Ph.D.	Environmental	25	Public	Academic	University of Y
4	Ph.D.	Architecture	21	Private	Construction Sup.	Company
5	Ph.D.	Architecture	21	Public	Department Manager	Ministry of Construction and Housing
6	M.Sc.	Civil	26	Public	Resident Engineer	Ministry of Construction and Housing
7	M.Sc.	Civil	21	Public	Construction Supervision	Ministry of Construction and Housing
8	M.Sc.	Architecture	20	Public	Site engineer	Ministry of Construction and Housing
9	B.Sc.	Mechanical	37	Public	Department Manager	Ministry of Construction and Housing
10	B.Sc.	Civil	35	Private	Construction Consultant	Company
11	B.Sc.	Civil	32	Private	Construction Cons.	Company
12	B.Sc.	Mechanical	30	Public	Project Manager	Ministry of Construction and Housing
13	B.Sc.	Civil	30	Public	Project Manager	Ministry of transportation
14	B.Sc.	Civil	25	Public	Construction Supervision	Ministry of Construction and Housing

15	B.Sc.	Architecture	21	Public	Department Manager	Ministry of Construction and Housing
16	B.Sc.	Electrical	20	Private	Site engineer	Company

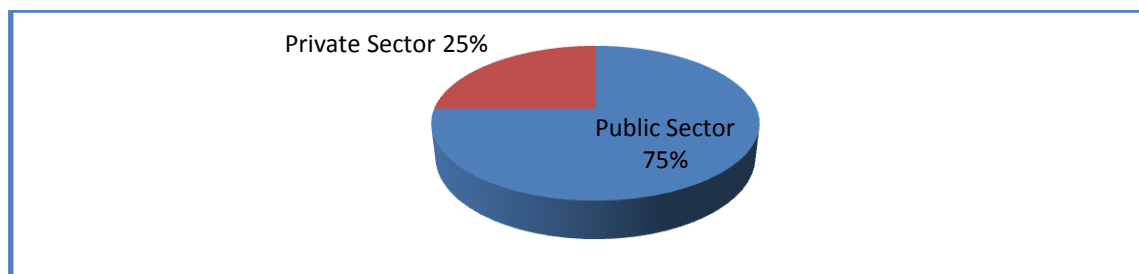


**Figure 2.** Experts from work sector.

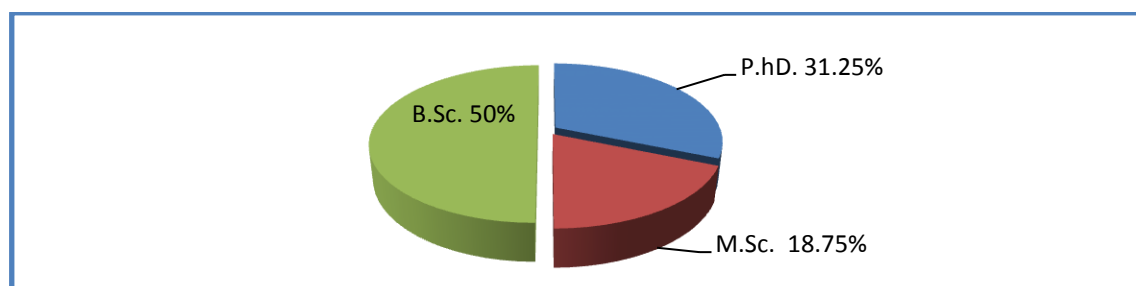


**Figure 3.** Experts academics degree.

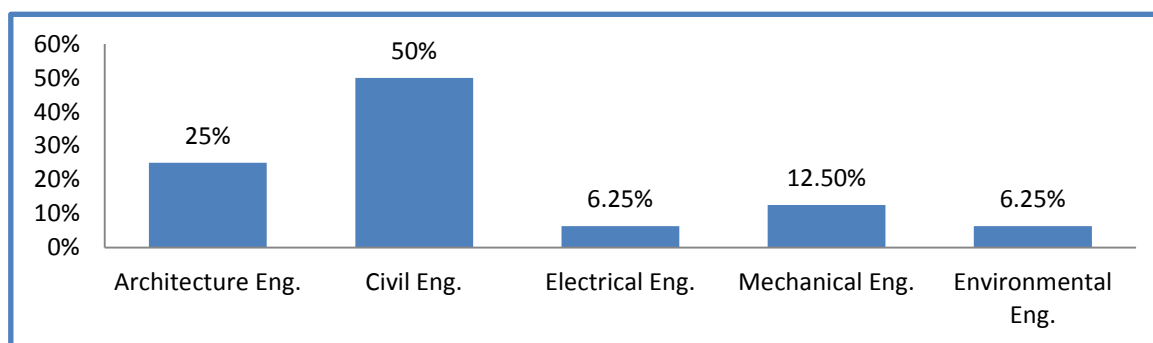


**Figure 4.** Field of specialization for experts.

**Table 2.** Delphi second round results: the mean and the standard deviation.

No.	The Factors	N	M	S.D
<b>The Briefing Phase:</b>				
1.	Awareness of the employer and the contractor of the project.	16	2.75	0.44721
2.	Keeping up the new ideas in the design in order to reduce the waste (the idea of sustainable design).	16	3.8125	0.75

3.	Lack of cooperation with the competent authorities.	16	3.0625	0.85391
4.	Lack of cooperation with the projects by the designers where the experience and information are limited to the consultant designer.	16	2.6250	0.88506
5.	Negligence in a way of the project management by using the technical means of modern science in the shipping and the contracting with suppliers.	16	3.5	0.89443
6.	The culture of preserving the environment.	16	4	0.89443
7.	The financial allocation for the project.	16	4.4375	0.62915
8.	Weakness in perception at the beginning of the project in the subject of waste.	16	3.4375	0.81394
9.	Weakness in the knowledge in the project life cycle and quantity of the generated waste.	16	3.9375	0.7719
<b>The Designing Phase:</b>				
1.	Accuracy in the preparation of BOQ.	16	3.8125	0.83417
2.	Changes in the design because of lack of clarity of the requirements of the employer.	16	4	0.5164
3.	Design using lengths and dimensions of the spaces that do not cause waste during execution of the project.	16	3.9375	0.68007
4.	Frequent errors in the designs.	16	3.8125	0.75
5.	The design and construction using standard materials.	16	3.5625	0.81394
6.	Use of prefabricated materials in implementation.	16	2.5	0.5164
7.	Use of sustainable materials that can be recycled or re-used after demolition.	16	2.375	0.7188
8.	Go to the idea of sustainable design in designs.	16	2.25	0.85635
9.	Application of environmental management systems in the designs.	16	2.1875	0.75
<b>The Rocuring Phase:</b>				
1.	Accuracy in the preparation of the contract documents.	16	3.5625	0.89209
2.	Application of waste management system.	16	4.25	0.68313
3.	Comprehensive and detailed schedule of all the activities, as well as a detailed schedule of construction materials to be purchased at the site before starting implementation.	16	3.625	0.88506
4.	Make sure of the executing company's ability to deal with waste.	16	4	0.6346
5.	Imposing contractual clauses for the main contractor and sub-contractors in dealing with the waste and the method used for their disposal.	16	4.4375	0.62915



6.	Waste management process coordination with municipal departments.	16	3.9375	0.57373
7.	Estimate the required costs to treat waste, in the contract document.	16	2.5	0.8165
8.	Incentives and priority in the bidding for the contractor who has a plan for reducing waste and increasing recycling	16	2.25	0.7746
9.	Simplify legal procedures for the provision of equipment for waste treatment.	16	2.1875	0.75
10.	Methods of recycling waste and how use it on the site.	16	2.0625	0.85391
<b>The Construction Phase:</b>				
1.	Activation of advanced technologies for the treatment and recycling of waste.	16	4.125	0.7188
2.	Allowing the use of recycled materials in the implementation.	16	2.875	0.80623
3.	Awareness and education in waste management system.	16	3.75	0.7746
4.	Bad the planning for the quantities required materials in the implementation, as well as sequence work activities.	16	4.1875	0.75
5.	Good storage and improving the traditional construction processes.	16	4.0625	0.57373
6.	Put separate containers according to the type of waste in the project.	16	2.75	0.68313
7.	The supervision system of the construction waste on-site	16	4.3125	0.60208
8.	The change in materials, specifications and type during execution the project.	16	3.75	0.60208
9.	The training to reduce the waste.	16	3.875	0.88506
10.	The use of construction techniques that do not generate waste.	16	4.25	0.85635
11.	Weak monitoring and control in the implementation of the project.	16	4	0.63246
12.	Workers' productivity and its technical skills.	16	4.125	0.80623
13.	Efficiency of the sub-contractors and cooperation among themselves in the management of waste.	16	2.75	0.57735
14.	Set a place for sorting waste and do it in the early stage of implementation.	16	2.875	0.61914
15.	Good storage and improving the traditional construction process.	16	2.875	0.34157
16.	Determine the controls on dealing with the originators of waste.	16	2.375	0.88506
17.	Communication and coordination system between the parties involved in the project.	16	2.9375	0.68007
18.	Technical training courses for project managers, technicians and workers.	16	2.9375	0.7719

19.	The needs of local markets for construction materials.	16	2.875	0.5
20.	Record retention for waste management (quantities, types, Etc).	16	2.625	0.61914
21.	Techniques on use of the handling materials.	16	2.9375	0.44253
<b>The Commissioning Phase:</b>				
1.	Develop a spare plan maintenance.	16	3.9375	0.68007
2.	Failure Repair the direct water and sewer pipes.	16	2.375	0.7188
3.	Lack of Periodical maintenance program.	16	4	0.7303
4.	Occupants culture of the building.	16	2.5	0.7303
5.	Penalize the projects that cause waste in the materials used And also punish for the person's negligence.	16	3.875	0.34157
6.	Proper storage of the remaining materials and the spare materials.	16	3.875	0.80623
7.	up the instructions on how to use and maintain should available for all occupants of the project.	16	4.1875	0.83417
8.	Referral the management of building during the Commissioning phase to professional people.	16	3.875	0.7188
9.	The accuracy and good work during maintenance operations.	16	4	0.8165
<b>The Demolition Phase:</b>				
1.	Allow the use of recycled materials.	16	2.375	0.80623
2.	Appointment of a place to sort the waste, and do this sorting in the early stage of implementation.	16	4	0.63246
3.	Awareness of the employer of issue to take advantage of the building after the end of the age.	16	3.8125	0.65511
4.	Determine the requirements of the local markets for construction materials.	16	2.625	0.88506
5.	Feasibility study on materials resulting from the demolition.	16	4.0625	0.68007
6.	Identify the recyclable materials.	16	4.125	0.80623
7.	Management of database for construction waste	16	2.8125	0.75
8.	The use of high-tech equipment in the demolition process.	15	4	0.63246
9.	Tight work site area.	16	2.5625	0.96393
<b>The other factors:</b>				
1.	Enact the laws for supporting waste management.	16	4.5625	0.51235
2.	Encourage citizens to use recycled materials.	16	2.5	0.5164

3.	Encouraged by the specialized agencies in this area.	16	2.5625	0.72744
4.	Increase the fees on mixed waste and reduce fees on classified waste.	16	2.6875	0.7932
5.	Number the landfill sites, and thier distance from the project site.	16	3.875	0.88506
6.	Put the severe sanctions by the government for violators of the laws relating to construction waste management.	16	4.3125	0.47871
7.	The tax exemption (Do not impose the tax) on the waste treatment equipment.	16	4.25	0.68313

**Table 3.** Delphi third round results; mean, standard deviation and cronbach's alpha factor ( $\alpha$ ).

No.	The Factors	N	M	S.D	$\alpha$
<b>The Briefing Phase:</b>					
1.	Keeping up the new ideas in the design in order to reduce the waste (the idea of sustainable design).	16	4.1875	0.54391	0.957
2.	Lack of cooperation with the competent authorities.	16	3.4375	0.62915	0.953
3.	Negligence in a way of the project management by using the technical means of modern science in the shipping and the contracting with suppliers.	16	3.75	0.68313	0.953
4.	The culture of preserving the environment.	16	4.3125	0.70415	0.951
5.	The financial allocation for the project.	16	4.1875	0.75	0.948
6.	Weakness in perception at the beginning of the project to the subject of waste.	16	3.8125	0.75	0.951
7.	Weakness in the knowledge in the project life cycle and quantity of the generated waste.	16	4.3125	0.60208	0.949
<b>The Designing Phase:</b>					
1.	Accuracy in the preparation of BOQ.	16	4.25	0.68313	0.925
2.	Changes in the design because of lack of clarity of the requirements of the employer.	16	4.1875	0.40311	0.949
3.	Design using lengths and dimensions of the spaces that do not cause waste during execution of the project.	16	4.1875	0.54391	0.908
4.	Frequent errors in the designs.	16	4.25	0.57735	0.908
5.	The design and construction using standard materials.	16	4.0625	0.68007	0.912
<b>The Procuring Phase:</b>					
1.	Accuracy in the preparation of the contract documents.	16	3.875	0.7188	0.935
2.	Application of waste management system.	16	4.3125	0.60208	0.918
3.	Comprehensive and detailed schedule of all the activities, as well as a detailed schedule of construction materials to be purchased at the site before starting implementation.	16	4.25	0.44721	0.930
4.	Make sure of the executing company's ability to	16	4.1875	0.54391	0.923

	deal with waste.				
5.	Imposing contractual clauses for the main contractor and sub-contractors in dealing with the waste and the method used for their disposal.	16	4.5	0.5164	0.933
6.	Waste management process coordination with municipal departments.	16	4.375	0.5	0.922
<b>The Construction Phase:</b>					
1.	Activation of advanced technologies for the treatment and recycling of waste.	16	4.1875	0.65511	0.969
2.	Awareness of and education in waste management system.	16	3.875	0.7188	0.971
3.	Bad the planning for the quantities required materials in the implementation, as well as sequence work activities.	16	4.3125	0.70415	0.970
4.	Good storage and improving the traditional construction process.	16	4.125	0.61914	0.970
5.	The supervision system of the construction waste on-site	16	4.375	0.5	0.973
6.	The change in materials, specifications and type during execution of the project.	16	3.875	0.80623	0.970
7.	The training to reduce the waste.	16	4.0625	0.85391	0.970
8.	The use of construction techniques that do not generate waste.	16	4.4375	0.62915	0.972
9.	Weak monitoring and control in the implementation of the project.	16	4.1875	0.54391	0.972
10.	Workers' productivity and their technical skills.	16	4.1875	0.75	0.969
<b>The Commissioning Phase:</b>					
1.	Develop a spare plan maintenance.	16	4.0625	0.57373	0.957
2.	Lack of Periodical maintenance program.	16	4.0625	0.68007	0.951
3.	Penalize the projects that cause waste in the materials used and also punish for the person's negligence.	16	4.0625	0.44253	0.971
4.	Proper storage of the remaining materials and the spare materials.	16	4.125	0.7188	0.952
5.	Up the instructions on how to use and maintain should available for all occupants of the project.	16	4.3125	0.70415	0.957
6.	Referral the management of building during the Commissioning phase to professional people.	16	4.1245	0.61914	0.953
7.	The accuracy and good work during maintenance operations.	16	4.1875	0.75	0.955
<b>The demolition Phase:</b>					
1.	Appointment of a place to sort the waste, and do this sorting in the early stage of implementation.	16	4.125	0.5	0.901
2.	Awareness of the employer of issue to take advantage of the building after the end of the age.	16	3.9375	0.57373	0.915
3.	Feasibility study on materials resulting from the demolition.	16	4.25	0.57735	0.888

4.	Identify the recyclable materials.	16	4.25	0.68313	0.905
5.	The use of high-tech equipment in the demolition process.	15	4.25	0.44721	0.915
<b>The other factors:</b>					
1.	Enact the laws for supporting waste management.	16	4.5	0.5164	0.930
2.	Number the landfill sites, and thier distance from the project site.	16	4.0625	0.85391	0.926
3.	impose the severe sanctions by the government for violators of the laws relating to construction waste management.	16	4.375	0.5	0.909
4.	The tax exemption (Do not impose the tax) on the waste treatment equipment.	16	4.3125	0.60208	0.903

**Table 4.** The key factors affecting on waste management during all construction project phases (starting from higher effect to the least for each phase).

No.	The Factors
<b>The Briefing Phase:</b>	
1.	Weakness in the knowledge in the project life cycle and quantity of the generated waste.
2.	The culture of preserving the environment.
3.	Keeping up the new ideas in the design in order to reduce the waste (the idea of sustainable design).
4.	The financial allocation for the project.
5.	Weakness in perception at the beginning on the project to the subject of waste.
6.	Negligence in a way of the project management by using the technical means of modern science in the shipping and the contracting with suppliers.
7.	Lack of cooperation with the competent authorities.
<b>The Designing Phase:</b>	
1.	Frequent errors in the designs.
2.	Accuracy in the preparation of BOQ.
3.	Changes in the design because of lack of clarity of the requirements of the employer.
4.	Design using lengths and dimensions of the spaces that do not cause waste during execution of the project.
5.	The design and construction using standard materials.
<b>The Procuring Phase:</b>	
1.	imposing contractual clauses for the main contractor and sub-contractors in dealing with the waste and the method used for their disposal.
2.	Waste management process coordination with municipal departments.
3.	Application of waste management system.
4.	Comprehensive and detailed schedule of all the activities, as well as a detailed schedule of construction materials to be purchased for the site before starting implementation.
5.	Make sure of the executing company's ability to deal with waste.
6.	Accuracy in the preparation of the contract documents.
<b>The Construction Phase:</b>	
1.	The use of construction techniques that do not generate waste.

2.	The supervision system on the construction waste on-site
3.	Bad the planning for the quantities of required materials in the implementation, as well as sequence of work activities.
4.	Weak monitoring and control in the implementation of the project.
5.	Activation of advanced technologies for the treatment and recycling of waste.
6.	Workers' productivity and their technical skills.
7.	Good storage and improving the traditional construction process.
8.	The training to reduce the waste.
9.	Awareness of and education on waste management system.
10.	The change in materials, specifications and type during execution of the project.
<b>The Commissioning Phase:</b>	
1.	Up instructions on how to use and maintain should available for all occupants of the project.
2.	The accuracy and good work during maintenance operations.
3.	Proper storage of the remaining materials and the spare materials.
4.	Referral the management of building during the Commissioning phase for professional people.
5.	Penalizing the projects that cause waste in the materials used And also punish for the person's negligence.
6.	Develop a spare maintenance plan.
7.	Lack of Periodical maintenance program.
<b>The Demolition Phase:</b>	
1.	The use of high-tech equipment in the demolition process.
2.	Feasibility study of materials resulting from the demolition.
3.	Identify the recyclable materials.
4.	Appointment of a place to sort the waste, and do this sorting in the early stage of implementation.
5.	Awareness of the employer of issue to take advantage of the building after the end of the age.
<b>The other factors:</b>	
1.	Enact the laws for supporting waste management.
2.	Impose the severe sanctions by the government on violators of the laws relating to construction waste management.
3.	The tax exemption (Do not impose the tax) on the waste treatment equipment.
4.	Number the landfill sites, and their distance from the project site.



## Nonlinear Behavior of Self -Compacting Reinforced Concrete Two-Way Slabs with Central Square Opening under Uniformly Distributed Loads

Dr. Ali Hussein Ali Al-Ahmed

Lecturer

College of Engineering - University of Baghdad-

ali\_hussein\_alahmed@yahoo.co.uk

### ABSTRACT

This research is carried out to investigate the behavior of self-compacting concrete (SCC) two-way slabs with central square opening under uniformly distributed loads. The experimental part of this research is based on casting and testing six SCC simply supported square slabs having the same dimensions and reinforcement. One of these slabs was cast without opening as a control slab. While, the other five slabs having opening ratios ( $O_R$ ) of 2.78%, 6.25%, 11.11%, 17.36% and 25.00%. From the experimental results it is found that the maximum percentage decrease in cracking and ultimate uniform loads were 31.82% and 12.17% compared to control slab for opening ratios ( $O_R$ ) of 11.11% and 6.25% respectively. Also the results showed that as  $O_R$  is increased from 0.00% to 11.11%, a significant increase in deflection was occurred. While the increase of  $O_R$  from 11.11% to 25.00%, a slightly decrease in deflection was occurred compared to control slab within the entire range of loading starting from first cracking load up to ultimate load. The theoretical part of this research is adopted for both simply supported and clamped ends square slabs according to yield line theory. For simply supported slabs, the results showed a decrease in ultimate uniform loads for  $O_R$  ranging between 0.00% and 25.00%. While beyond this value, an increase in the ultimate uniform load is occurred. In addition, it is found that as  $O_R$  was increased; the total ultimate load is decreased. Also from the theoretical analysis for clamped end slabs it is found that as  $O_R$  was increased, both the ultimate uniform load and the total ultimate load were increased.

**Key words:** self-compacting concrete, square opening, two-way slabs, yield lines, uniform load

التصرف اللاخطي للبلاطات الخرسانية المسلحة ذاتية الرص العاملة باتجاهين ذات فتحات مربعة في المركز تحت تأثير احمال منتشرة

د. علي حسين علي احمد

مدرس

جامعة بغداد-كلية الهندسة

### الخلاصة

في هذا البحث تم التحري عن تصرف البلاطات الخرسانية المسلحة ذاتية الرص العاملة باتجاهين ذات فتحات مربعة في المركز تحت تأثير احمال منتشرة منتظمة. تضمن الجانب العملي من هذا البحث صب وفحص ستة بلاطات خرسانية ذاتية الرص مربعة الشكل ذات اسناد بسيط لها نفس الابعاد وحديد التسليح. كانت احدى هذه البلاطات بدون فتحة حيث اتخذت كبلطة مرجعية للمقارنة. بينما احتوت البلاطات المتبقية على فتحات مربعة في المركز بنسب ( 2.78% ، 6.25% ، 11.11% ، 17.37% و 25.00%) من المساحة السطحية للبلاطة. وجد من النتائج العملية ان اكبر نسبة نقصان في حمل التشقق والحمل الاقصى المنتشر كان 31.82% و 12.17% لنسب فتحات 11.11% و 6.25% على التوالي مقارنة مع البلاطة المرجعية. كذلك اظهرت النتائج ان بزيادة نسبة الفتحة من 0.00% الى 11.11% حدثت زيادة في الهطول في حين ان زيادة نسبة الفتحة من 11.11% الى 25.00% ادت الى نقصان في الهطول مقارنة مع البلاطة المرجعية ضمن منطقة التصرف ابتداء من حمل التشقق الى الحمل الاقصى المنتشر. تبني الجانب النظري من هذا البحث نظرية خطوط الخضوع

لتحليل بلاطات ذات اسناد بسيط واخرى مقيدة الحافات. للبلاطات ذات الاسناد البسيط وجد بان هنالك نقصان في الحمل الاقصى المنتشر لنسبه فتحات تتراوح من 0.00 % الى 25.00%. بينما بعد هذه النسبة حدثت زيادة في قيمة الحمل الاقصى المنتشر. وجد كذلك ان بزيادة نسبة الفتحة ادى الى نقصان في قيمة الحمل الكلي. اما بالنسبة للبلاطات مقيدة الحافات فوجد بان زيادة نسبة الفتحات ادى الى زيادة في القيم القصوى للاحمال المنتشرة والاحمال الكلية سوية.

**الكلمات الرئيسية:** خرسانة ذاتية الرص، فتحات مربعة، بلاطات عاملة باتجاهين، خطوط الخضوع، احمال منتشرة منتظمة

## 1. INTRODUCTION

Reinforced concrete (RC) slabs are the most common elements in structural buildings and have been widely used for multi-storey buildings. Openings are often required in slabs for mechanical and electrical services such as heating, plumbing, electrical wiring, fire protection pipes, telephone, computer network, water supply, sewerage and ventilating reasons. Meanwhile, substantial size openings are required by lift, staircases and elevator shafts. The structural effect of small openings is usually not considered due to ability of the structure to redistribute the stresses. However, for large openings in slabs can severely reduce the strength and load carrying capacity of these slabs due to cut out of both concrete and steel reinforcement. This may lead to decrease the ability of structures to withstand the imposed loads and the structural needs, **Taljsten et. al, 2006; Mota, and Kamara, 2006.**

Two- way RC slab is a form of unique construction of reinforced concrete. It is an efficient, economic and widely used member. It is usually supported by all four sides and the ratio of long span to short span is less than two. So that, two- way RC slab will deflect in two directions and the loads are transferred to all supports. In general there are three types of RC two- way slabs: flat plates, flat slab and slab supported on beams, **Wang et. al, 2007.**

Self-Compacting Concrete (SCC) is an innovative concrete flows under its own weight and it does not require any external vibration for compaction. It was first developed in the late 1980's by Japanese researchers. SCC can flow through restricted sections without segregation and bleeding and completely filling formwork and achieving full compaction. Such concrete should have a relatively low yield value to ensure high flow ability, a moderate viscosity to resist segregation and bleeding, **Nagamoto, and Ozawa, 1997 and Khayat, and Ghezal, 1999.**

## 2. STRUCTURAL DESIGN OF REINFORCED CONCRETE SLABS WITH OPENINGS

The design of RC slab with openings is not clearly declared in the **BS 8110, 1997.** However, the **ACI 318, 2014** Code states that the openings are permitted in new slab system. The ACI Code provides guide lines for different location of openings in RC flat slabs. **Fig. 1** illustrates the openings size and their locations in flat slab. The flat slab is divided into column and middle strips in two orthogonal directions. The ACI Code suggests that any size of opening is permitted in the area of where middles strip intersects. For opening in the area intersecting column strip, the permissible opening size is only 1/8 the width of column strip in either span directions. Finally, for opening in the area that intersecting one column strip and one middle strip, the maximum permissible opening size is only 1/4 the width of column or middle strip in either span directions.

## 3. EXPERIMENTAL PROGRAM

### 3.1 Introduction

The main purpose of the experimental work is to investigate the behavior of SCC two-way slabs with central square opening under uniformly distributed load. The primary variable in this research is the opening ratio ( $O_R$ ) which is equal to the area of opening divided by the area of solid slab multiplied by 100.

The standard tests were carried out to determine the properties of hardened concrete and steel reinforcement. In addition, instrumentation, experimental setup and testing procedures adopted throughout this investigation are presented.

### 3.2 Specimens

The experimental work is based on casting and testing six SCC square slabs. All specimens have the same dimensions of (650×650×50 mm) were cast and tested up to failure under a uniform load. The slabs are designed as simply supported along four edges and supported on the (600×600 mm) perimeter at the bottom side of the slabs. One of these slabs was without opening (solid) which is taken as a control slab and denoted as S-0. While the other five slabs have different square openings located at the center of slab. Five openings with dimensions (100 x 100, 150 x 150, 200 x 200, 250 x 250 and 300 x 300 mm) were created at the center of the slabs, so that the opening ratios ( $O_R$ ) were (2.78%, 6.25%, 11.11%, 17.36% and 25.00%) respectively. These slabs are denoted as S-10, S-15, S-20, S-25 and S-30 for the above opening ratios ( $O_R$ ) as listed in **Table 1**.

All specimens were reinforced at bottom with  $\phi$  2.5 mm @ 50 mm steel bars in both directions with effective depth ( $d$ ) of 40 mm, so that the steel ratio ( $\rho$ ) is about 0.245% which lies within the ACI Code limits. Also, each corner of the openings was provided with 2 $\phi$ 2.5 mm additional diagonal steel bars to prevent stress concentration. Full details of the test slabs are shown in **Fig. 2**.

### 3.3 Material Used for Casting Specimens

#### 3.3.1 Cement

Ordinary Portland cement type (I) was used throughout this investigation. All quantity of cement was tested chemically and physically. The properties were conform to the **Iraqi Specifications No. 5, 1984** for Portland cement.

#### 3.3.2 Fine and coarse aggregate

Natural sand from Al-Akhaidher quarries was used for SCC mixes. The fine aggregate has (4.75mm) maximum size with rounded-shape particles and smooth texture. While, crushed gravel from Al-Sudor region with maximum size of 10 mm was used throughout this research. The sand and gravel have been washed and cleaned with water several times and they were conform to the **Iraqi specification No.45, 1984**.

#### 3.3.3 Limestone powder

To produce SCC, crushed limestone powder (LSP) was used in this investigation. This LSP is passed sieve No. 0.075 mm and tested physically and chemically.

#### 3.3.4 Superplasticizer

Glenium 51 was used in this research as a superplasticizer material to produce SCC. Glenium 51 is free of chlorides and it was conform to **ASTM C494** type A and F.

#### 3.3.5 Steel bars

$\phi$  2.5 mm plain steel bars were used for reinforcement. For these bars, yield stress ( $f_y$ ) and ultimate strength ( $f_u$ ) were 590 MPa and 690 MPa respectively. While, the modulus of elasticity ( $E_s$ ) was 205000 MPa.

### 3.4 Molds Fabrication

In the present research, six molds were used to cast the specimens. These molds were made from plywood plates (18 mm) thickness and had a base and four sides to form a square frame. In addition, five square wooden frames with different opening sizes are fabricated and located at the center of each slab to form the opening size required. Before casting the SCC, these molds were oiled and the reinforcement meshes were put into the required position as shown in **Fig. 3**.

### 3.5 Mix Design

In the present research, SCC was used for casting the specimens. After several trial mixes according to recommendations mentioned in **The European Guidelines for Self-Compacting Concrete, 2005**, concrete mixture was designed to achieve a cylindrical compressive strength ( $f_c$ ) of 30 MPa at 28 days. **Table 2** illustrates the mix design properties of SCC used in this investigation.

### 3.6 Test Rig Components and Loading Procedure

In the present research, the hydraulic testing machine at the Civil Engineering Department Lab. of the University of Baghdad was used. All specimens were white painted to facilitate the identification of cracks during the test. All test slabs were mounted on a supporting frame which have a 30 mm bar welded along each side at the upper of supporting frame to achieve simply supported condition. Several dial gauges were used in this investigation and attached the tension face of slabs. These dial gauges were located at distances of (150, 175, 200, 225, 250 and 300 mm) measured from supports for control slab (S-0). While for slabs with opening, one or more dial gauges were excluded according to opening size condition as illustrated in **Table 3**.

To apply a uniformly distributed load on slabs, an aluminum sand container was put on the top face of specimens and filled with sand. A steel plate with dimensions of (550 x 550 x 15 mm) was put on sand. Also a steel block of dimensions (550 x 450 x 50 mm) was put on steel plate to insure full distribution of load on specimens. Hydraulic jack and load cell were put respectively on steel block. The weight of sand, steel plate, steel block, hydraulic jack and load cell were taken into account and added to external applied load. **Fig. 4** shows full details of test rig components and setup of a typical tested slab.

The specimens were uniformly loaded with increasing load until failure. At each load step, deflections reading by dial gauges were recorded.

## 4. EXPERIMENTAL RESULTS

All beams were tested up to failure by applying uniformly distributed load with load division of (10 kN/m<sup>2</sup>) for steps before cracking. While for steps after cracking, the load division was reduced to (2.5 kN/m<sup>2</sup>).

### 4.1 Cracking and Ultimate Loads Results

All slabs are characterized by the formation of cracks at the tension face of slabs and yield lines propagated from corner of opening toward corner of supports till failure occur. **Fig. 5** shows tested slabs after forming yield lines and failure. From this figure it could be noticed that for slabs S-0, S-10 and S-15 only diagonal yield lines were occurred. While, for slabs S-20, S-25 and S-30 additional straight cracks were developed perpendicular to the sides of openings. This might be due large opening size effect. The experimental results for cracking and ultimate uniform loads of all specimens are given in **Table 4**. From this table it could be noticed that the control slab S-0 had maximum cracking and ultimate load capacities. The cracking and ultimate uniform loads were decreased as  $O_R$  was increased from 0.00% to 25.00%. The maximum

percentage decrease in cracking load was 31.82% for slab S-20 ( $O_R=11.11\%$ ) compared to control slab. Beyond this value of  $O_R$ , the percentage decrease in cracking load was decreased as  $O_R$  was increased from 11.11% to 25.00%.

The maximum percentage decrease in ultimate uniform load was 12.17% for slab S-15 ( $O_R=6.25\%$ ) compared to control slab. Beyond this value of  $O_R$ , the percentage decrease in ultimate uniform load was decreased when  $O_R$  was increased from 6.25% to 25.00%. For slab S-30 ( $O_R=25.00\%$ ), the ultimate load capacity is approximately similar to value obtained from control slab. This might be due concentration of the uniform load near supports and increasing slab stiffness. **Fig. 6** shows the percentage decrease in cracking and ultimate uniform loads with increasing opening ratio ( $O_R$ ).

Cracking to ultimate load ratios ( $w_{cr}/w_u$ ) were also calculated and listed in **Table 4**. The maximum and minimum ( $w_{cr}/w_u$ ) ratios are 0.507 and 0.386 for slab S-0 (control) and S-20 ( $O_R=11.11\%$ ) respectively.

#### 4.2 Load-Deflection Response

Deflections for each slab have been recorded during the test by using dial gauges located at the positions listed in **Table 3**. **Fig. 7** shows the load-deflection response for each tested slab at different dial gauge locations (i.e variable dial gauge locations with constant  $O_R$ ). From this figure it could be noticed that a linear behavior of the load-deflection response is evident. This stage covers the region up to the cracking load. Within this stage the materials are still elastic and no cracks occur in the specimens. When cracks have taken place, a sudden jump in deflection value was occurred. Those cracks are developed as the load increases and the response changes from linearity to nonlinearity because the rate of increase in deflection with respect to load continuously increases as the load is increased and the curve behaved nonlinearly as load increased. Finally as the applied load approaches its ultimate value, the rate of increase in deflection is substantially exceeding the rate of increase in the value of applied load till failure occurred. Also it is clear from this figure that for each tested slab, the deflection is increased as the location of dial gauge is far from supports.

**Fig. 8** shows the load-deflection response for each tested slab recorded by same dial gauge location (i.e constant dial gauge location with variable  $O_R$ ). It is clear from this figure that the increase in  $O_R$  has a significant effect on deflection through the entire range of loading starting from cracking load up to ultimate uniform load. For slabs S-10, S-15 and S-20 of  $O_R$  (2.78%, 6.25% and 11.11%) respectively, the load-deflection curve showed a significant increase in deflection values compared to control slab. While for slabs S-25 and S-30 with  $O_R$  of (17.36% and 25.00%) respectively, the load-deflection curve showed a slightly decrease in deflection values compared to control slab. This might be due to the effect of large opening size on shifting the concentration of the uniform load towards the supports and that will make the slab stiffer.

To obtain a reasonable comparison of deflections among tested slabs, **Table 5** summarizes the deflection recorded at different locations corresponding to a load level of 130 kN/m<sup>2</sup> which is about 85% of ultimate uniform load capacity of the control slab. Also **Fig. 9** shows the percentage increase and decrease in deflection with respect to distance of recorded deflection from supports for different values of  $O_R$ . While, **Fig. 10** shows the percentage increase and decrease in deflection with respect to  $O_R$  for different values of distances from supports. From these figures and **Table 5**, it may be noticed that the maximum percentage increase in deflection is 39.13% for slab S-10 ( $O_R=2.78\%$ ) at location of 250 mm from supports. While, the maximum percentage decrease in deflection is 11.47% for slab S-25 ( $O_R=17.36\%$ ) at location of 175 mm from supports corresponding to a load level of 130 kN/m<sup>2</sup>.



## 5. THEORETICAL ANALYSIS USING THE YIELD LINE THEORY

Simply supported and clamped ends square slabs with central square opening as shown in **Fig.11** were considered in this theoretical analysis. These slabs are considered to have isotropic reinforcement (i.e  $m_x = m_y$ ). Yield lines are assumed to propagate from the corner of opening toward the corner of slab. Also, these slabs are subjected to a uniformly distributed load ( $w$ ) and a unit displacement ( $\Delta=1$ ) is applied at the edge of opening.

### 5.1 Case-1 Simply Supported Slab

According to **Fig. 11-a**, the external work ( $WE$ ) done by the applied load is given by Eq. (1)

$$WE = w_u (\text{slab with opening}) \times 4 \left\{ \left( Z \times \frac{(L-Z)}{2} \times \frac{1}{2} \right) + \left( \left( \frac{1}{2} \times (L-Z) \times \frac{(L-Z)}{2} \times \frac{1}{3} \right) \right) \right\}$$
$$WE = w_u (\text{slab with opening}) \left\{ \frac{(L-Z)(L+2Z)}{3} \right\} \quad (1)$$

where:

$L$  = dimension of square slab.

$Z$  = dimension of central square opening.

If the positive resistance moment per unit length along the yield lines is defined as ( $m$ ), the internal work ( $WI$ ) done by this moment is given by Eq. (2)

$$WI = 4ml\theta$$

$$WI = 4m \times (L-Z) \times \frac{1}{\frac{(L-Z)}{2}}$$

$$WI = 8m \quad (2)$$

where:

$l$  = projected length of the yield line.

$\theta$  = rotation along the yield line.

Equating the external work with the internal work gives Eq. (3) which represents the relation between ( $w$ ) and ( $m$ ) for case of simply supported slab with opening. Multiplying Eq. (3) by the area of slab ( $L^2-Z^2$ ) gives Eq. (4) which represents the relation between total load ( $P$ ) and ( $m$ ) for the same case.

$$w_u (\text{slab with opening}) = \frac{24m}{(L-Z)(L+2Z)} \quad (3)$$

$$P_u (\text{slab with opening}) = \frac{24m(L+Z)}{(L+2Z)} \quad (4)$$

If  $Z=0$  (solid slab) then Eq. (3) gives Eq. (5) which represents the relation between ( $w$ ) and ( $m$ ) for case of simply supported solid slab. While, Eq. (4) gives Eq. (6) which represents the relation between ( $P$ ) and ( $m$ ) for the same case.

$$w_u (\text{solid slab}) = \frac{24m}{L^2} \quad (5)$$

$$P_u (\text{solid slab}) = 24m \quad (6)$$

Hence, the ratio of ultimate uniform load for a slab with opening to ultimate uniform load for a solid slab ( $UL_R$ ) is given by Eq. (7). This equation is obtained when Eq. (3) is divided by Eq. (5). While, the ratio of total ultimate load for a slab with opening to total ultimate load for a solid slab ( $TL_R$ ) is given by Eq. (8) when Eq. (4) is divided by Eq. (6).



$$UL_R = \frac{w_u (\text{slab with opening})}{w_u (\text{solid slab})} = \frac{L^2}{(L-Z)(L+2Z)} \quad (7)$$

$$TL_R = \frac{P_u (\text{slab with opening})}{P_u (\text{solid slab})} = \frac{(L+Z)}{(L+2Z)} \quad (8)$$

Since, area of solid slab= $L^2$ , area of opening= $Z^2$  and % Opening ratio ( $O_R$ ) =  $\frac{\text{Area of opening}}{\text{Area of solid slab}} \times 100$  so that Eqs. (7 & 8) can be expressed by Eqs. (9 & 10) respectively.

$$UL_R = \frac{w_u (\text{slab with opening})}{w_u (\text{solid slab})} = \frac{1}{(1 - \frac{\sqrt{\%O_R}}{10})(1 + \frac{\sqrt{\%O_R}}{5})} \quad (9)$$

$$TL_R = \frac{P_u (\text{slab with opening})}{P_u (\text{solid slab})} = \frac{(1 + \frac{\sqrt{\%O_R}}{10})}{(1 + \frac{\sqrt{\%O_R}}{5})} \quad (10)$$

By using Eqs. (9 & 10), **Figs. 12 and 13** are plotted to represent the effect of  $O_R$  on the  $UL_R$  and  $TL_R$  values respectively for simply supported square slabs. From **Fig. 12** it can be noticed that for  $O_R$  ranging between 0.00% to 25.00% the slabs with opening showed decreasing values of ultimate uniform load with respect to solid slab. The maximum decrease in  $UL_R$  is 0.889 occurred when  $O_R=6.25\%$ . This value is in agreement with the results obtained from the experimental test for slab S-15 ( $O_R=6.25\%$ ). Also **Fig. 12** shows that beyond  $O_R$  of 25.00%, a significant increase in the ultimate uniform load is occurred. This might be due to concentration of uniform load near supports for large opening ratios. So that larger load is needed for the external work to achieve equilibrium with the internal work. For  $O_R=60\%$ , the ultimate uniform load is about 1.75 times the uniform load of solid slab. From **Fig. 13** it can be noticed that as  $O_R$  is increased, the  $TL_R$  is decreased. For  $O_R=25\%$  and 60%, the total ultimate loads are 0.750 and 0.696 of total ultimate load of the solid slab respectively. It can be also noticed from **Fig. 13** that beyond  $O_R$  of 25.00%, a continuous decrease in  $TL_R$  is occurred which is unlike the behavior of  $UL_R$  noticed from **Fig. 12**.

**Table 6** summarizes the experimental and the theoretical values of  $UL_R$  and  $TL_R$ . This table show good agreement between the experimental and theoretical results.

## 5.2 Case-2 Clamped Ends Slab

According to **Fig. 11-b**, the external work done by the applied load is also given by Eq. (1) obtained for simply supported slab.

If ( $\beta$ ) is defined as the ratio of the negative resistance moment at clamped ends to the positive resistance moment along the positive yield lines, the internal work done by these moments is given by Eq. (11)

$$\begin{aligned} WI &= 4ml\theta + 4\beta mL\theta \\ WI &= 4m \times (L - Z) \times \frac{1}{\frac{(L-Z)}{2}} + 4\beta m \times L \times \frac{1}{\frac{(L-Z)}{2}} \\ WI &= 8m \left( \frac{L-Z+\beta L}{L-Z} \right) \end{aligned} \quad (11)$$

Equating the external work given by Eq. (1) with the internal work given by Eq. (11) gives Eq. (12) which represents the relation between ( $w$ ) and ( $m$ ) for clamped ends slab with central

opening. Total load ( $P$ ) is given by Eq. (13) which is also adopted by multiplying Eq. (12) by the area of slab ( $L^2 - Z^2$ ).

$$W_u (\text{slab with opening}) = \frac{24 m(L-Z+\beta L)}{(L-Z)^2(L+2Z)} \quad (12)$$

$$P_u (\text{slab with opening}) = \frac{24 m(L-Z+\beta L)(L+Z)}{(L-Z)(L+2Z)} \quad (13)$$

If  $Z=0$  (solid slab) then Eq. (12) gives Eq. (14) which represents the relation between ( $w$ ) and ( $m$ ) for solid clamped ends slab. While, Eq. (13) gives Eq. (15) which represents the relation between ( $P$ ) and ( $m$ ) for solid clamped ends slab.

$$W_u (\text{solid slab}) = \frac{24 m(1+\beta)}{L^2} \quad (14)$$

$$P_u (\text{solid slab}) = 24m(1+\beta) \quad (15)$$

Hence, the expression for  $UL_R$  and  $TL_R$  is given by Eqs. (16 & 17) respectively.

$$UL_R = \frac{W_u (\text{slab with opening})}{W_u (\text{solid slab})} = \frac{L^2(L-Z+\beta L)}{(L-Z)^2(L+2Z)(1+\beta)} \quad (16)$$

$$TL_R = \frac{P_u (\text{slab with opening})}{P_u (\text{solid slab})} = \frac{(L-Z+\beta L)(L+Z)}{(L-Z)(L+2Z)(1+\beta)} \quad (17)$$

Also similar to Eqs. (7 and 8), Eqs. (16 and 17) can be expressed by Eq. (18 & 19).

$$UL_R = \frac{W_u (\text{slab with opening})}{W_u (\text{solid slab})} = \frac{1 - \frac{\sqrt{\%O_R}}{10} + \beta}{(1+\beta)(1 - \frac{3(\%O_R)}{100} + \frac{\%O_R \sqrt{\%O_R}}{500})} \quad (18)$$

$$TL_R = \frac{P_u (\text{slab with opening})}{P_u (\text{solid slab})} = \frac{(1 - \frac{\sqrt{\%O_R}}{10} + \beta)(1 + \frac{\sqrt{\%O_R}}{10})}{(1+\beta)(1 - \frac{\sqrt{\%O_R}}{10})(1 + \frac{\sqrt{\%O_R}}{5})} \quad (19)$$

**Figs. 14 and 15** are plotted by using Eqs. (18 & 19). These figures show the effect of  $O_R$  on the  $UL_R$  and  $TL_R$  respectively for clamped end slabs for different values of  $\beta$ . From these figures it could be noticed that as  $O_R$  is increased, both  $UL_R$  and  $TL_R$  are increased for all values of  $\beta$  except ( $\beta=0.5$ ). When  $\beta=0.5$  and for  $O_R$  ranging between 0.00% to 25.00% the slabs with opening showed decreasing values of total ultimate load with respect to solid slab. While beyond  $O_R$  of 25.00%, a clear increase in the total ultimate load is noticed as shown in **Figs. 15**. Also these figures reveal that the increase in  $UL_R$  and  $TL_R$  values are increased with increasing the value of  $\beta$ . For values of  $\beta$  (0.5, 1.0, 1.5 and 2.0), the  $UL_R$  values are 3.73, 4.73, 5.33 and 5.73 respectively for opening ratio ( $O_R$ )=60%. While  $TL_R$  values are 1.49, 1.89, 2.13 and 2.29 respectively for the same above values.

## 6. CONCLUSIONS

1. From the experimental results for simply supported square slabs, the cracking and ultimate uniform loads were decreased as opening ratio ( $O_R$ ) is increased from 0.00% to 25.00%. The maximum percentage decrease in cracking and ultimate loads were 31.82% and 12.17% compared to the control solid slab for opening ratios ( $O_R$ ) of 11.11% and 6.25% respectively. Beyond the values of  $O_R=11.11\%$  and 6.25%, the percentages decrease in cracking load and ultimate uniform load were decreased respectively.

2. For opening ratio ( $O_R$ )=25.00%, the ultimate uniform load capacity is approximately similar to the value obtained for the control solid slab. This might be due concentration of the uniform load near supports which leads to increase the slab stiffness.
3. The maximum and minimum cracking to ultimate uniform load ratios ( $w_{cr}/w_u$ ) were 0.507 and 0.386 for the control solid slab and for the slab with opening ratio ( $O_R$ ) of 11.11% respectively.
4. From the experimental results, it can be noticed that the opening ratio ( $O_R$ ) has a significant effect on deflection values through the entire range of loading starting from crack and up to ultimate load. For slabs of  $O_R$  (2.78%, 6.25% and 11.11%), the load-deflection curve showed a significant increase in deflection compared to control solid slab. While for slabs with  $O_R$  of (17.36% and 25.00%), the load-deflection curve showed a slight decrease in deflection values compared to the control solid slab.
5. At a load level of 130 kN/m<sup>2</sup> which is about 85% of ultimate uniform load capacity of the control slab, it is found that the maximum percentage increase in deflection is 39.13% for slab of  $O_R$ =2.78% at location of 250 mm from supports. While, the maximum percentage decrease in deflection is 11.47% for slab of  $O_R$ =17.36% at location of 175 mm from supports.
6. Based on the theoretical analysis for simply supported slabs it is found that for opening ratio ( $O_R$ ) ranging between 0.00% and 25.00% a decrease in ultimate uniform load for a slab with central opening relative to the ultimate uniform load for a solid slab ratio ( $UL_R$ ) is occurred. The maximum decrease in  $UL_R$  was 0.889 for  $O_R$ =6.25%. While beyond  $O_R$  of 25.0%, a significant increase in ultimate uniform load is occurred. Also according to the theoretical analysis it is found that the total ultimate load for a slab with central opening relative to the total ultimate load for a solid slab ratio ( $TL_R$ ) is decreased as  $O_R$  is increased.
7. According to the theoretical analysis for clamped ends slab, it is found that as  $O_R$  is increased, both  $UL_R$  and  $TL_R$  are increased for all values of ( $\beta$ ) which represents the ratio of the negative resistance moment at clamped ends to the positive resistance moment along the positive yield lines. Except when the value of  $\beta$ =0.5 within  $O_R$  ranging between 0.00% to 25.00% the  $TL_R$  is decreased. While beyond  $O_R$  of 25.00%, a clear increase in the total ultimate load is noticed. Also, it is found that as the value of  $\beta$  is increased, both  $UL_R$  and  $TL_R$  values are increased.

## REFERENCES

- ACI Committee 318, 2014, *Building Code Requirements for Reinforced Concrete and Commentary (ACI 318-14 and ACI 318R-14)*, American Concrete Institute, Detroit.
- ASTM Designation C 494/C 494M-01b, 2001, *Standard Specifications for Chemical Admixture for Concrete*, Annual Book of ASTM Standards, American Society for Testing and Materials, Philadelphia, Pennsylvania.
- BS 8110-1, 1997, *Structural Use of Concrete, Code of Practice for Design and Construction*, British Standards Institution, London, PP 163.
- Iraqi Specification No. 5, 1984, *Portland Cement*, Baghdad.
- Iraqi Specification No. 45, 1984, *Natural Sources for Gravel That is Used in Concrete and Construction*, Baghdad.
- Khayat, K. H., and Ghezal, A., 1999, *Utility of Statistical Models in Proportioning Self-Compacting Concrete*, Proceedings, RILEM, International symposium on Self-Compacting Concrete, Stockholm, PP. 345-359.



- Mota, M. C., and Kamara, M., 2006, *Floor Openings in Two-Way Slabs*, Concrete International Journal, Vol.28, No.7, PP. 33-66.
- Nagamoto, N., and Ozawa, K., 1997, *Mixture Properties of Self-Compacting High-Performance Concrete*, Proceedings, Third CANMET, ACI International Conferences on Design and Materials and Recent Advances in Concrete Technology, SP-172, V. M. Malhotra, American Concrete Institute, Farmington Hills, Mich., PP. 623-637.
- Taljsten, B., Lundqvist, J., Enochsson, O., Rusinowski, P., and Olofsson, T., 2006, *CFRP Strengthened Openings in Two-way Concrete Slabs—An Experimental and Numerical Study*, Construction and Building Materials, PP. 810-826.
- The European Guidelines for Self-Compacting Concrete, 2005, *Specification, Production and Use*. PP. 28.
- Wang, C. K., Salmon, C. G., and Pincheira, J. A., 2007, *Reinforced Concrete Design*, Seventh Edition, John Wiley and Sons, New York, PP. 948.

## NOMENCLATURE

$d$  = depth of steel bars from top fiber of the section

$E_s$  =modulus of elasticity of steel bars

$f'_c$  = cylindrical compressive strength of self-compacting concrete

$f_y$  = yield stress of steel reinforcement

$f_u$  = ultimate strength of steel reinforcement

$L$  =dimension of square slab.

$l$  = projected length of yield line.

$LSP$ = limestone powder

$m$  = resistance moment per unit length

$O_R$  = opening ratio

$P_u$  =total ultimate load

$RC$  =reinforced concrete

$SCC$  = self- compacting concrete

$TL_R$  =ratio of total ultimate load for a slab with opening to total ultimate load for a solid slab

$UL_R$  =ratio of ultimate uniform load for a slab with opening to ultimate uniform load for a solid slab

$w_{cr}$  =cracking load

$WE$  =external work

$WI$  =internal work

$w_u$  =ultimate uniform load

$Z$  =dimension of central square opening.

$\beta$  =ratio of negative resistance moment at fixed end to positive resistance moment along positive yield lines

$\Delta$  =unit displacement

$\rho$  =steel ratio of section

$\theta$  =rotation along yield line

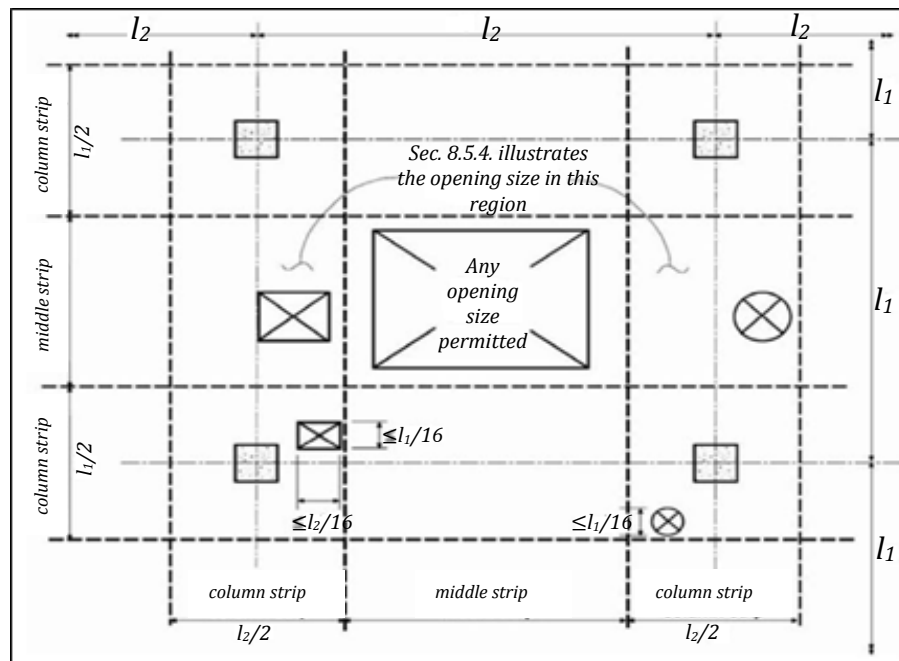


**Figure 1.** Suggested opening size and location in flat slab according to the *ACI-318, 2014 Code*.

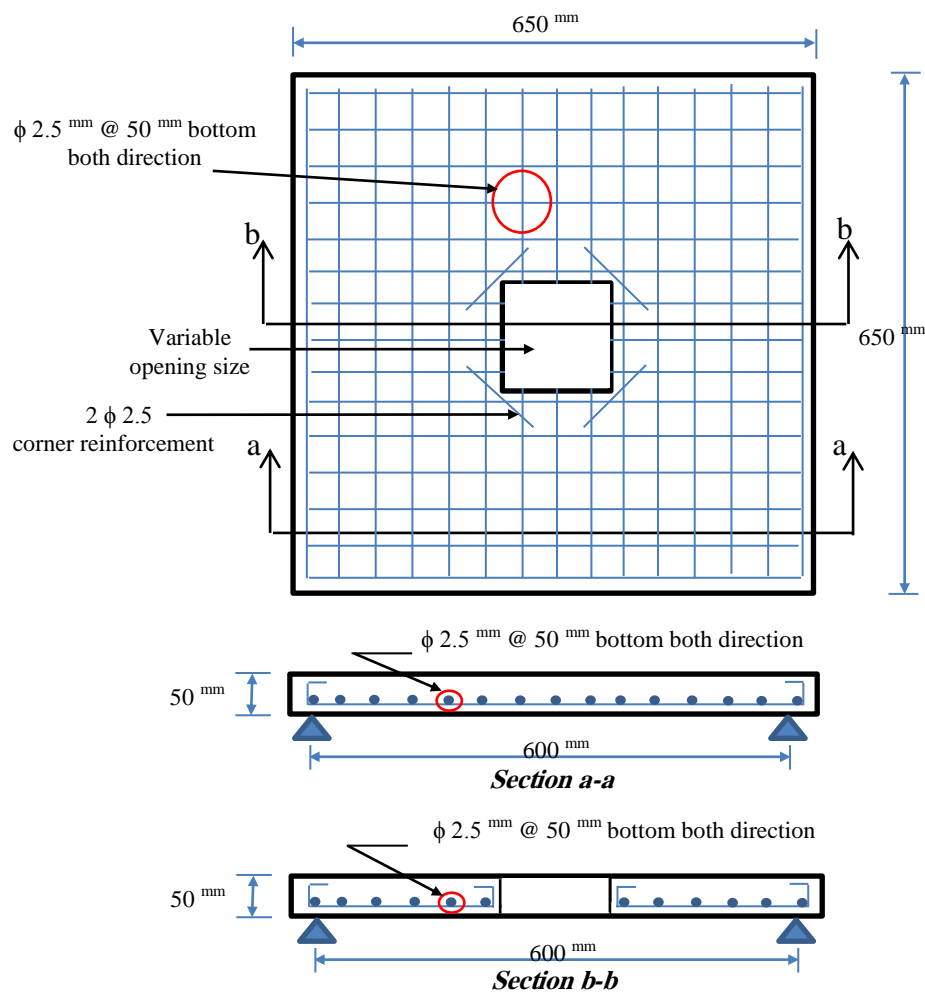


**Figure 2.** Layout of a typical tested slab.



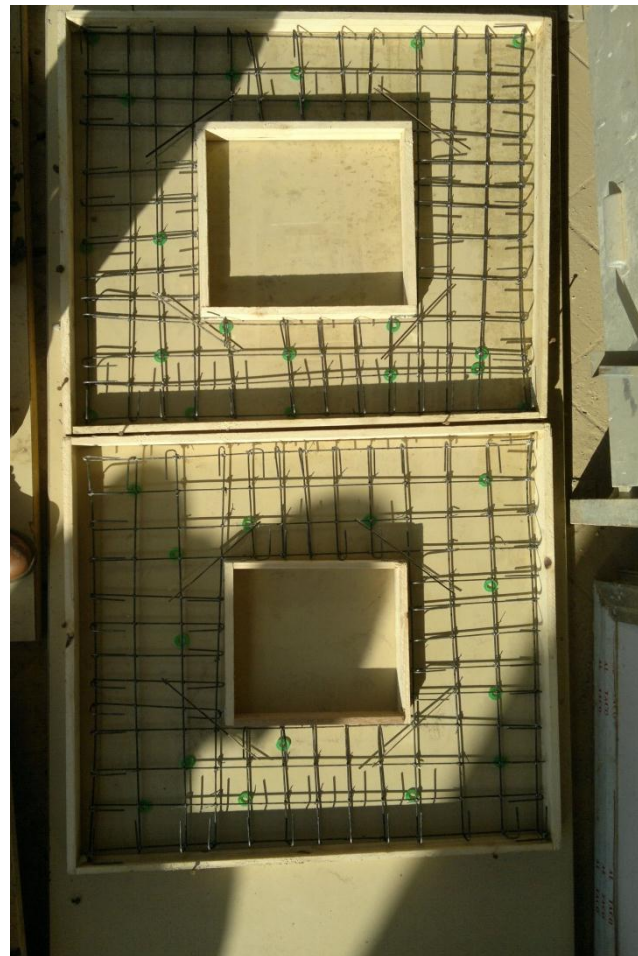


**Figure 3.** Molds fabrication and reinforcement meshes for some tested slabs.

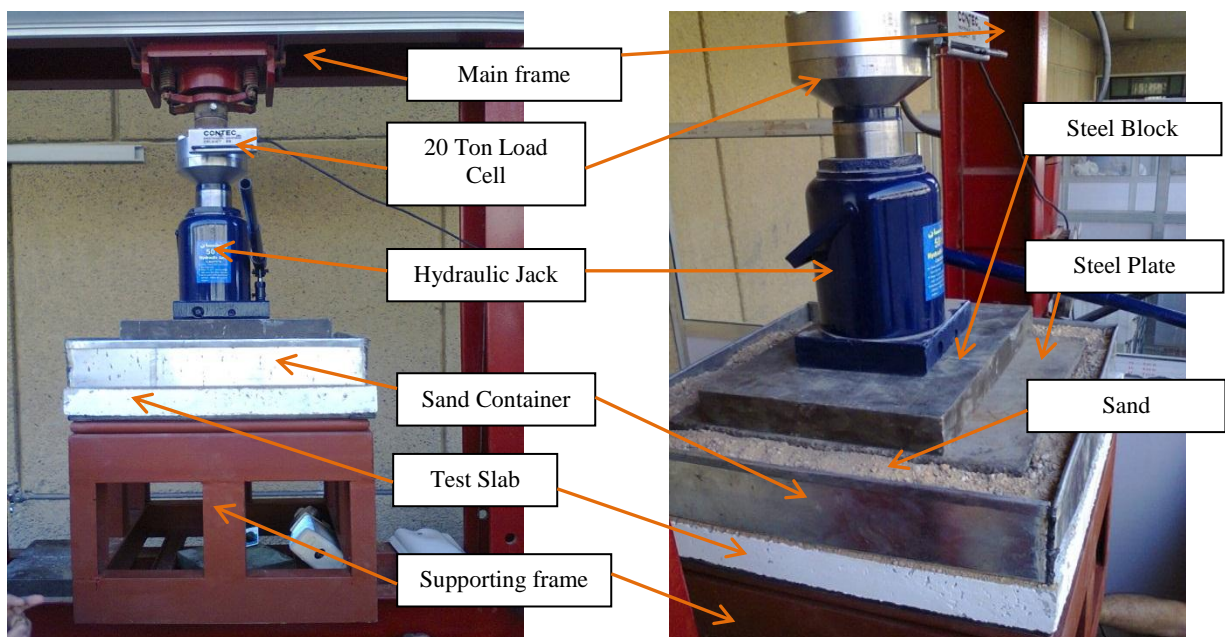


**Figure 4.** Setup of a typical tested slab.



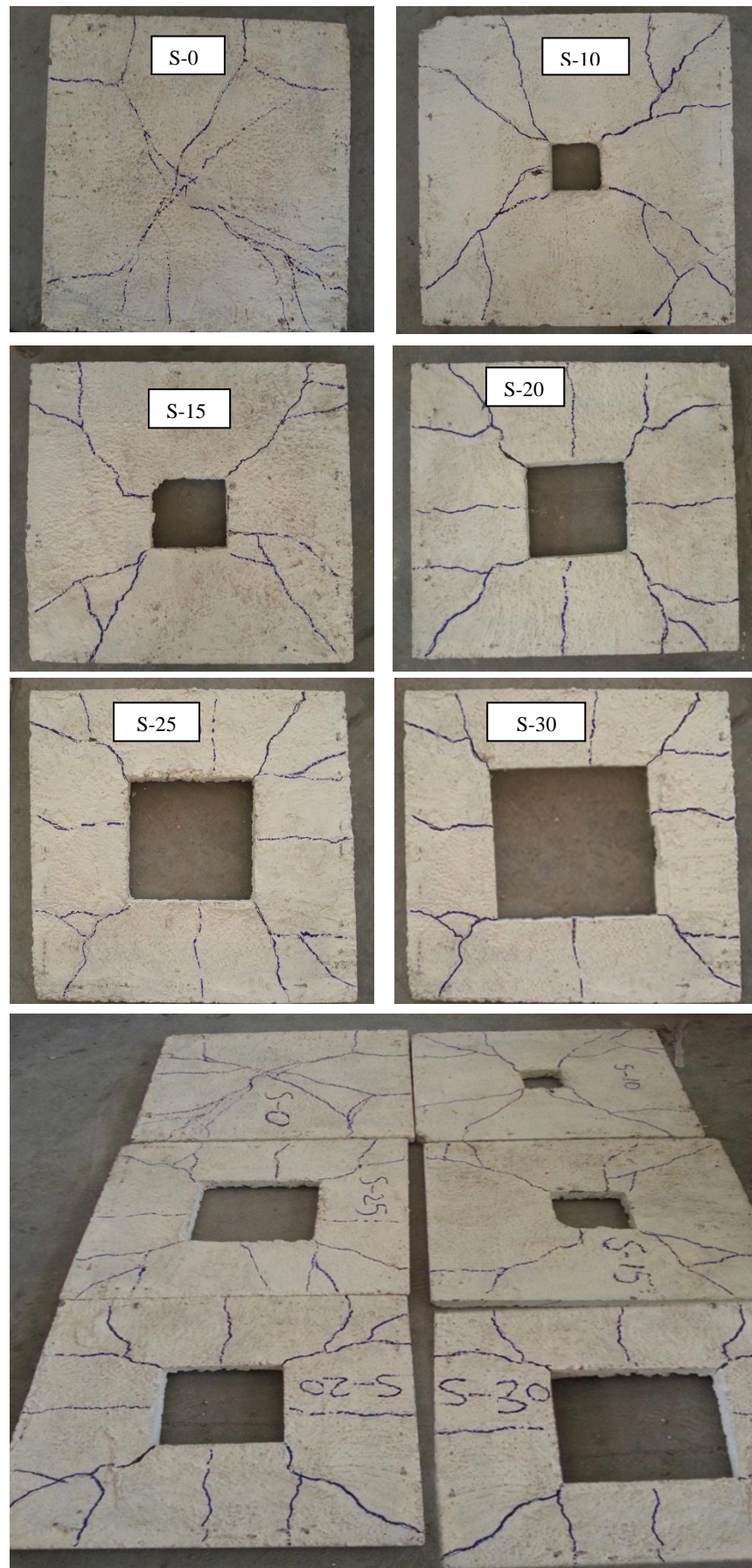


**Figure 5.** Bottom face of tested slabs after failure.

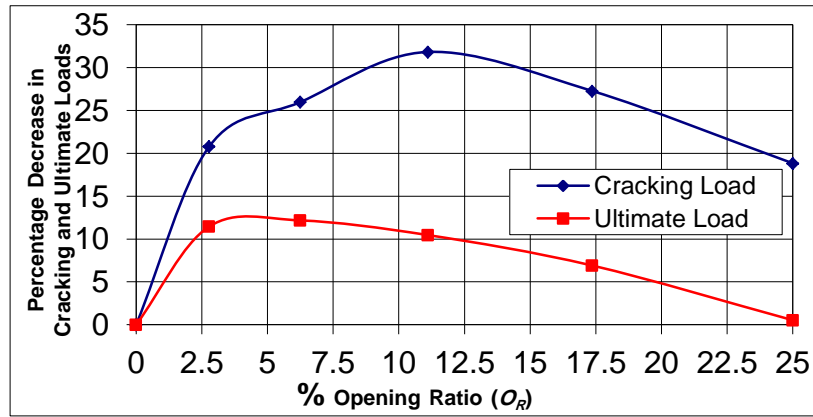


**Figure 6.** Percentage decrease in cracking and ultimate uniform loads with varying opening ratios.

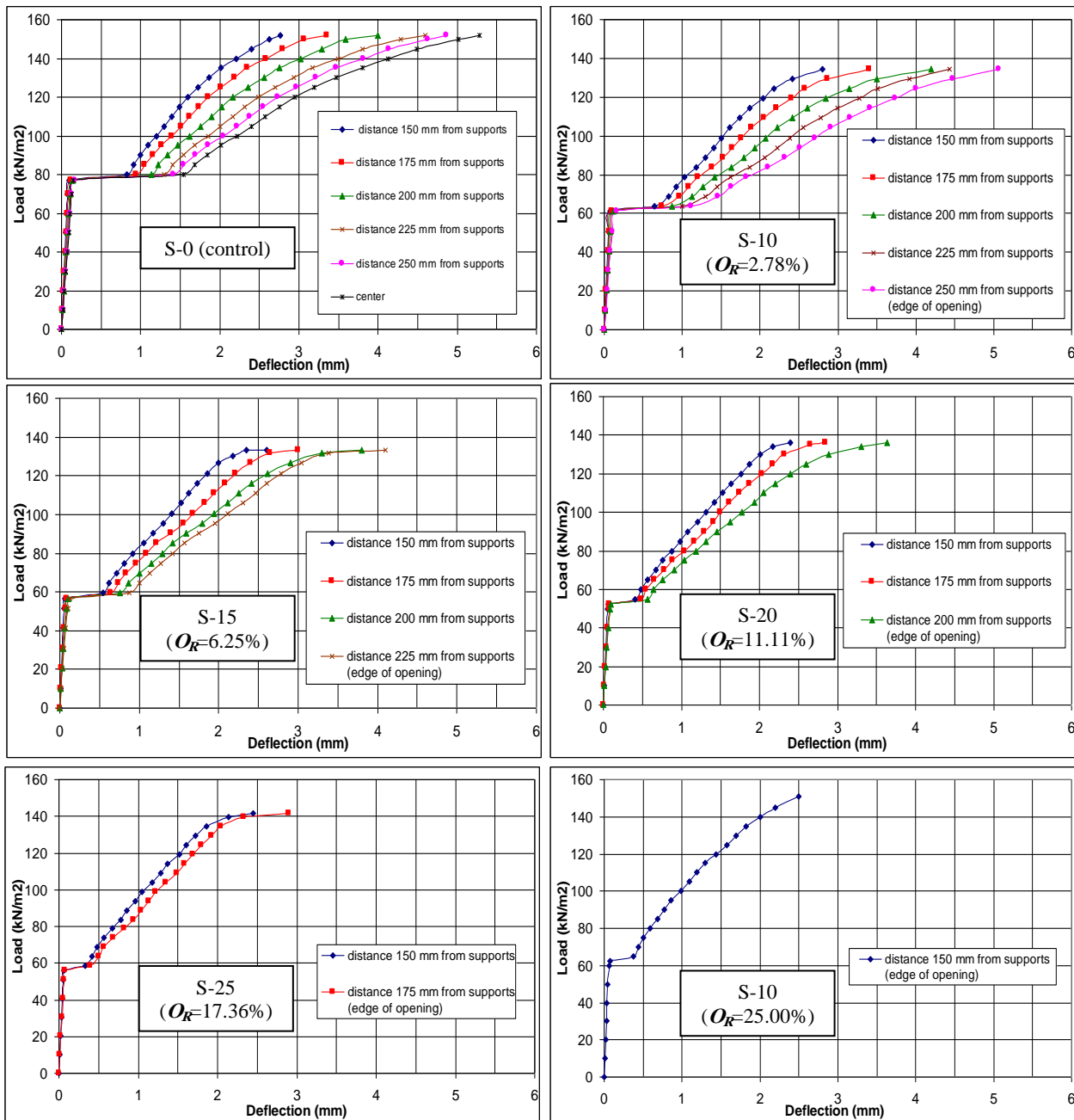


**Figure 7.** Load-deflection curves for tested slabs at different dial gauge locations.

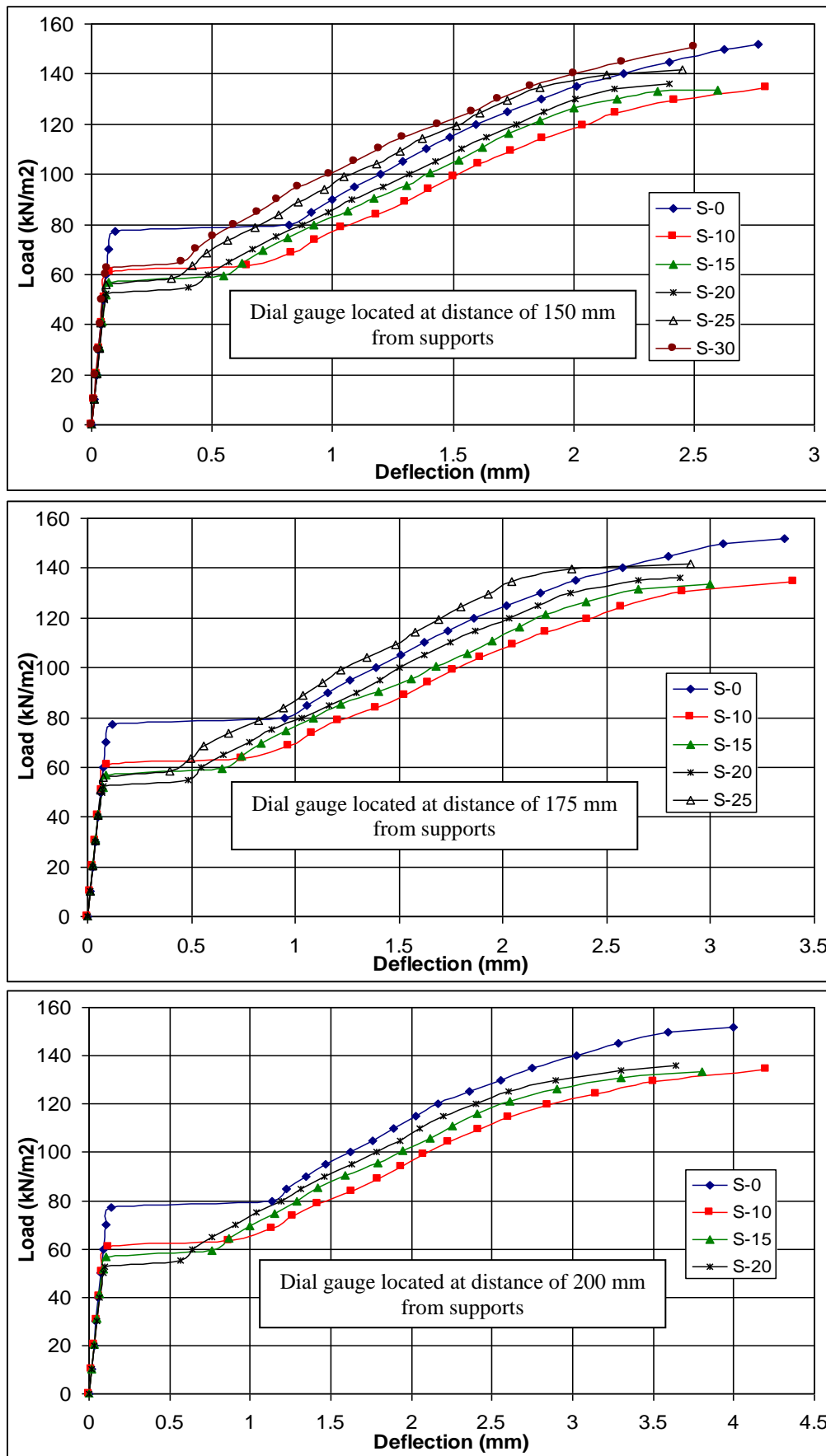


**Figure 8.** Load-deflection curves for tested slabs recorded by same dial gauge locations.

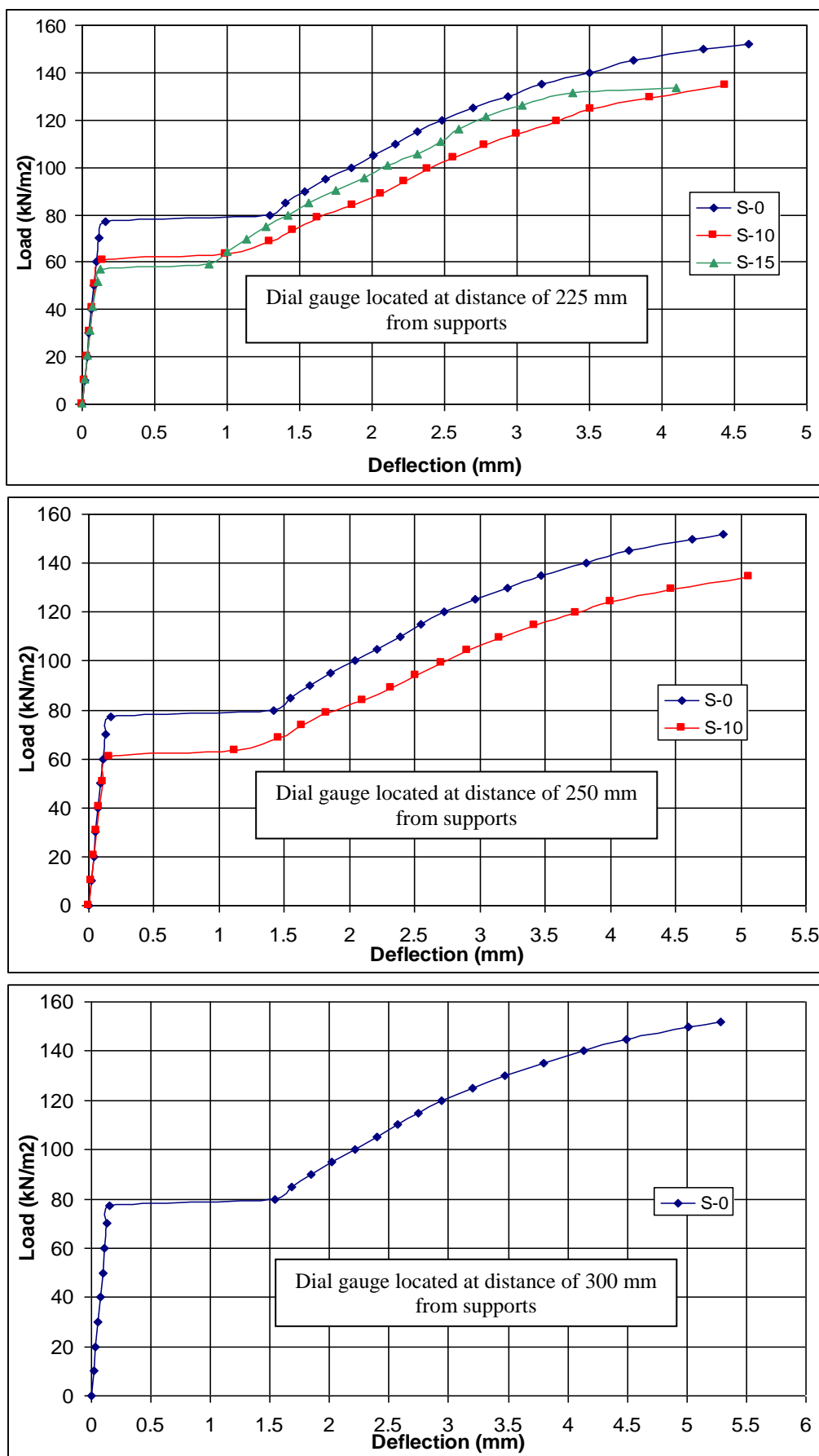
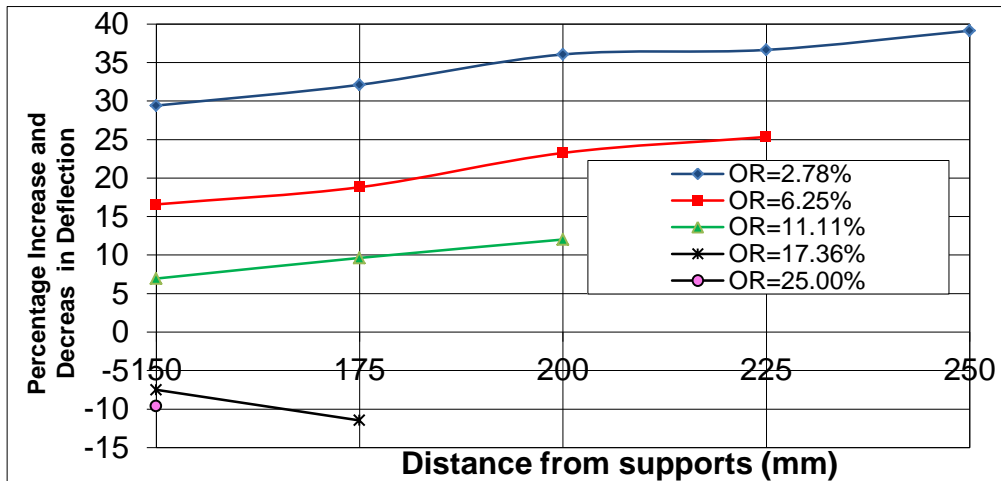
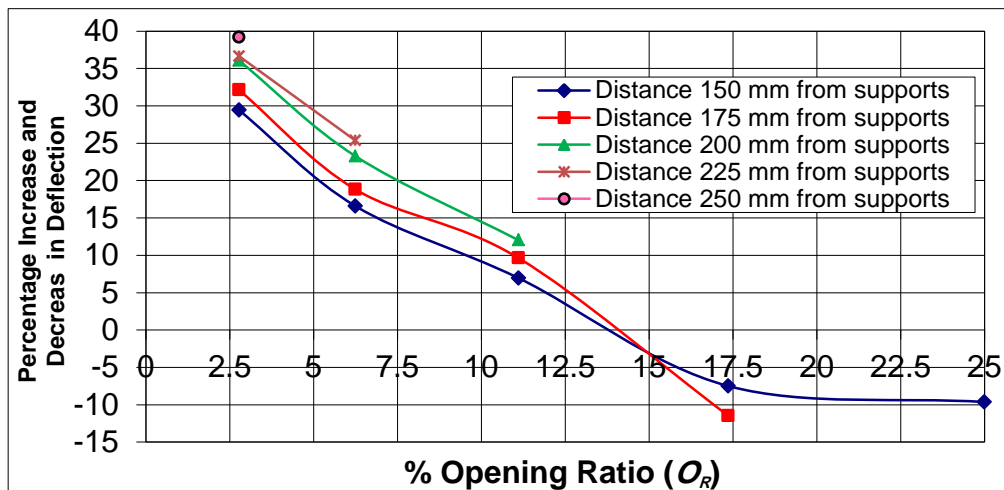


Figure 8. Continue.



**Figure 9.** Percentage increase and decrease in deflection with respect to distance of recorded deflection from supports corresponding to a load level of  $130 \text{ kN/m}^2$ .



**Figure 10.** Percentage increase and decrease in deflection with respect to opening ratios corresponding to a load level of  $130 \text{ kN/m}^2$ .

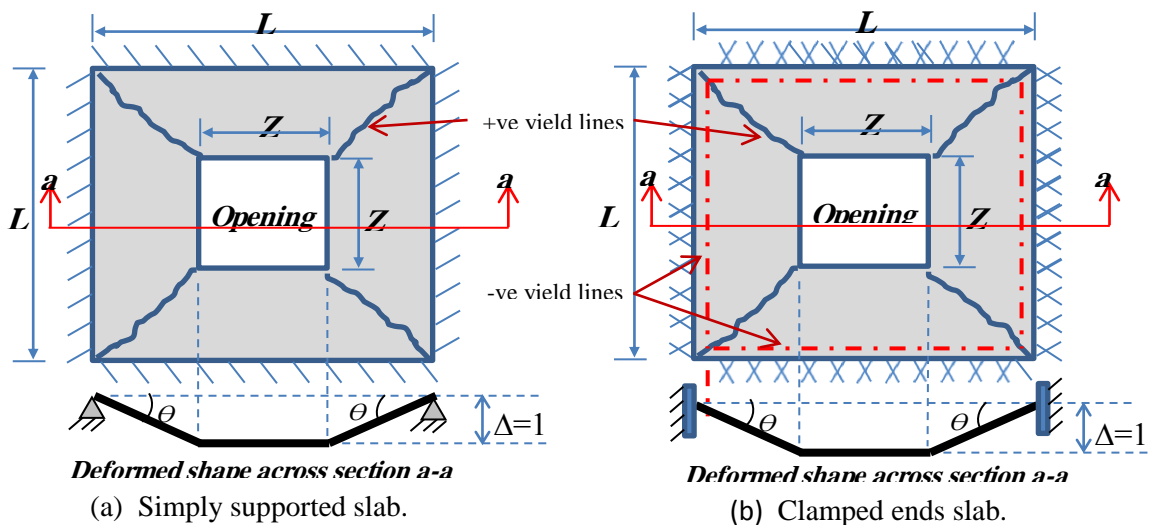


**Figure 11.** Yield lines and deformations of simply supported and clamped ends square slabs with central square opening.

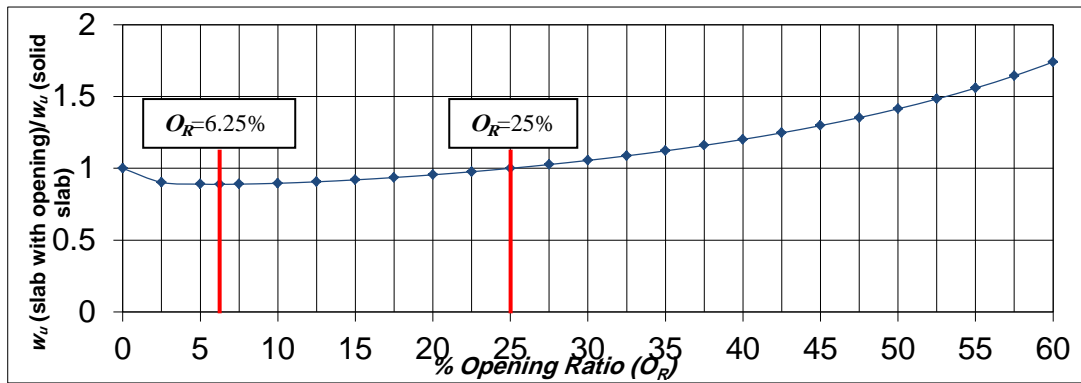


Figure 12. Effect of opening ratio on ultimate uniform load of simply supported slabs.

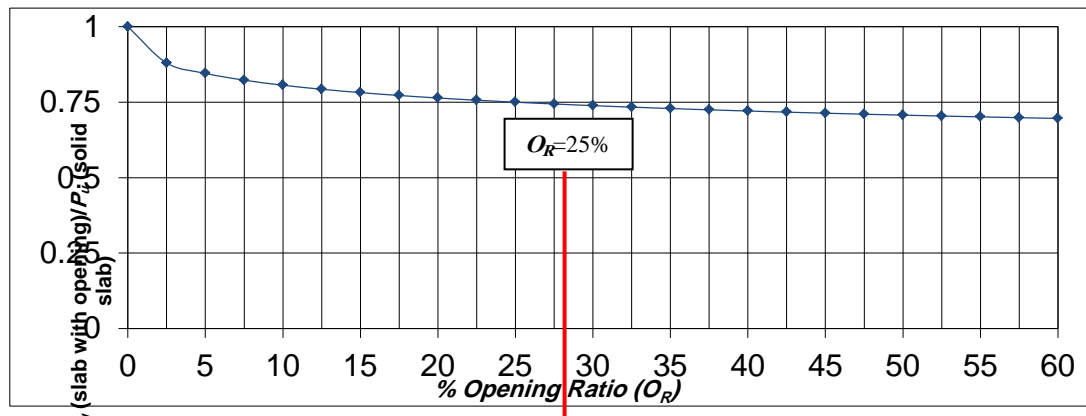


Figure 13. Effect of opening ratio on total ultimate load of simply supported slabs.

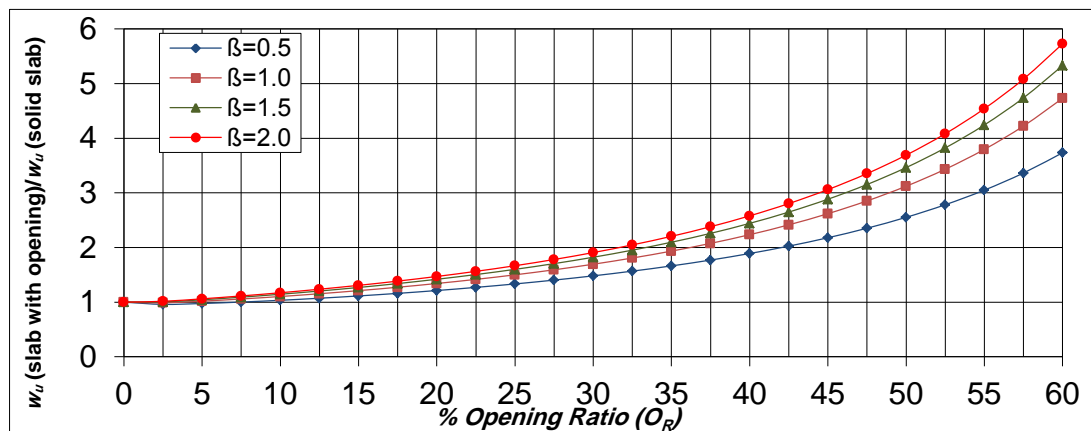


Figure 14. Effect of opening ratio on ultimate uniform load of clamped ends slabs.

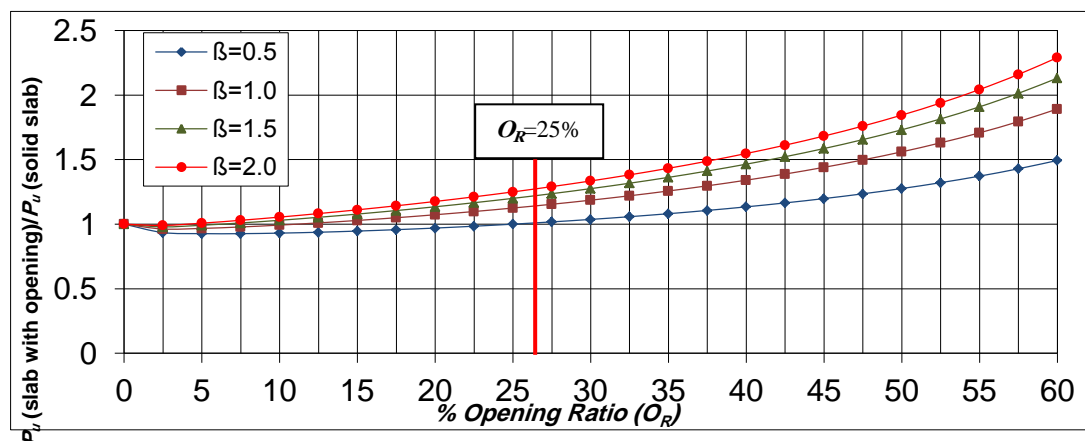


Figure 15. Effect of opening ratio on total ultimate load of clamped ends slabs.



**Table 1.** Properties of tested slabs.

<i>Slab designation</i>		<i>Slab dimensions center to center of supports (mm)</i>	<i>Opening dimensions (mm)</i>	<i>% Opening ratio(<math>O_R</math>)</i>
S-0	control	600 x 600	-	0.00
S-10		600 x 600	100 x 100	2.78
S-15		600 x 600	150 x 150	6.25
S-20		600 x 600	200 x 200	11.11
S-25		600 x 600	250 x 250	17.36
S-30		600 x 600	300 x 300	25.00

$$\% \text{ Opening ratio } (O_R) = \frac{\text{Area of opening}}{\text{Area of solid slab}} \times 100$$

**Table 2.** Mix properties for SCC used in this research

<i>Cement (<math>\text{Kg/m}^3</math>)</i>	<i>Sand (<math>\text{Kg/m}^3</math>)</i>	<i>Gravel (<math>\text{Kg/m}^3</math>)</i>	<i>LSP (<math>\text{Kg/m}^3</math>)</i>	<i>Water (litter/<math>\text{m}^3</math>)</i>	<i>Superplasticizer (litter/<math>\text{m}^3</math>)</i>
371	845	792	199	185	4

**Table 3.** Dial gauges location .

<i>Slab designation</i>		<i>Opening dimensions (mm)</i>	<i>No. of dial gauges used</i>	<i>Location of dial gauge No.1 from supports (mm)</i>	<i>Location of dial gauge No.2 from supports (mm)</i>	<i>Location of dial gauge No.3 from supports (mm)</i>	<i>Location of dial gauge No.4 from supports (mm)</i>	<i>Location of dial gauge No.5 from supports (mm)</i>	<i>Location of dial gauge No.6 from supports (mm)</i>
S-0	control	-	6	150	175	200	225	250	300 (center)
S-10		100 x 100	5	150	175	200	225	250 (edge of opening)	N.A
S-15		150 x 150	4	150	175	200	225 (edge of opening)	N.A	N.A
S-20		200 x 200	3	150	175	200 (edge of opening)	N.A	N.A	N.A
S-25		250 x 250	2	150	175 (edge of opening)	N.A	N.A	N.A	N.A
S-30		300 x 300	1	150 (edge of opening)	N.A	N.A	N.A	N.A	N.A

N.A Not applicable

**Table 4.** Experimental cracking and ultimate loads results .

Slab designation		% Opening ratio( $O_R$ )	Cracking Load $w_{cr}$ ( $kN/m^2$ )	% Decrease in cracking load	Ultimate load $w_u$ ( $kN/m^2$ )	% Decrease in ultimate load	$w_{cr}/w_u$
S-0	control	0.00	77.0	control	152.0	control	0.507
S-10		2.78	61.0	20.78	134.6	11.45	0.453
S-15		6.25	57.0	25.97	133.5	12.17	0.427
S-20		11.11	52.5	31.82	136.1	10.46	0.386
S-25		17.36	56.0	27.27	141.5	6.91	0.396
S-30		25.00	62.5	18.83	151.2	0.53	0.413

$$\% \text{ Decrease} = \frac{W_{\text{control slab}} - W_{\text{slab with opening}}}{W_{\text{control slab}}} \times 100$$

**Table 5.** Deflections coressponding to a load level of 130  $kN/m^2$ .

Slab designation	A	AA	B	BB	C	CC	D	DD	E	EE	F	FF
S-0 control	1.87	control	2.18	control	2.58	control	2.92	control	3.22	control	3.47	control
S-10 ( $O_R=2.78\%$ )	2.42	+29.41	2.88	+32.11	3.51	+36.05	3.99	+36.64	4.48	+39.13	N.A	N.A
S-15 ( $O_R=6.25\%$ )	2.18	+16.58	2.59	+18.81	3.18	+23.26	3.66	+25.34	N.A	N.A	N.A	N.A
S-20 ( $O_R=11.11\%$ )	2.00	+6.95	2.39	+9.63	2.89	+12.02	N.A	N.A	N.A	N.A	N.A	N.A
S-25 ( $O_R=17.36\%$ )	1.73	-7.49	1.93	-11.47	N.A	N.A	N.A	N.A	N.A	N.A	N.A	N.A
S-30 ( $O_R=25.00\%$ )	1.69	-9.63	N.A	N.A	N.A	N.A	N.A	N.A	N.A	N.A	N.A	N.A

A Deflection (mm) recorded at location of 150 mm from supports

B Deflection (mm) recorded at location of 175 mm from supports

C Deflection (mm) recorded at location of 200 mm from supports

D Deflection (mm) recorded at location of 225 mm from supports

E Deflection (mm) recorded at location of 250 mm from supports

F Deflection (mm) recorded at location of 300 mm from supports

$$XX \text{ Percentage increase or decrease in deflection with respect to control slab} = \frac{\text{def. control slab} - \text{def. slab with opening}}{\text{def. control slab}} \times 100$$

(+) Sign for increasing in deflection and (-) sign for decreasing in deflection

N.A Not applicable

**Table 6.** Effect of opening ratio on ultimate loads results for simply supported slabs.

Slab designation	% Opening ratio( $O_R$ )	Experimentally		Experimentally		Theoretically		$\frac{UL_R (Exp.)}{UL_R (Theo.)}$	$\frac{TL_R (Exp.)}{TL_R (Theo.)}$
		$w_u$ ( $kN/m^2$ )	$P_u$ (kN)	$UL_R$	$TL_R$	$UL_R$ Applying Eq. (9)	$TL_R$ Applying Eq. (10)		
S-0 control	0.00	152.0	54.72	1.0000	1.0000	1.0000	1.0000	1.0000	1.0000
S-10	2.78	134.6	47.11	0.8855	0.8609	0.8999	0.8750	0.9840	0.9839
S-15	6.25	133.5	45.06	0.8783	0.8235	0.8889	0.8333	0.9881	0.9882
S-20	11.11	136.1	43.55	0.8954	0.7959	0.8999	0.8000	0.9950	0.9949
S-25	17.36	141.5	42.10	0.9309	0.7694	0.9350	0.7727	0.9956	0.9957
S-30	25.00	151.2	40.82	0.9947	0.7460	1.0000	0.7500	0.9947	0.9947

$$UL_R = \frac{w_u (\text{slab with opening})}{w_u (\text{solid slab})}, TL_R = \frac{P_u (\text{slab with opening})}{P_u (\text{solid slab})}, P_u = w_u \times \text{area of slab}$$

## Aluminum Rubbish as a Coagulant for Oily Wastewater Treatment

Hasan Ferhood Makki

College of Engineering-University of Baghdad

Email: [hs\\_fmfm@yahoo.com](mailto:hs_fmfm@yahoo.com)

Imama Raed Abdulameer

College of Engineering-University of Baghdad

Email: [emamaraed1991@gmail.com](mailto:emamaraed1991@gmail.com)

### ABSTRACT

In this study an experimental work was done to study the possibility of using aluminum rubbish material as a coagulant to remove the colloidal particles from oily wastewater by dissolving this rubbish in sodium hydroxide solution. The experiments were carried out on simulated oily wastewater that was prepared at different oil concentrations and hardness levels (50, 250, 500, and 1000) ppm oil for (2000, 2500, 3000, and 3500) ppm  $\text{CaCO}_3$  respectively. The initial turbidity values were (203, 290, 770, and 1306) NTU, while the minimum values of turbidity that have been gained from the experiments in NTU units were (1.67, 1.95, 2.10, and 4.01) at best sodium aluminate dosages in milliliters (12, 20, 24, and 28) for oily wastewater of concentrations (50, 250, 500, and 1000) ppm of oil. Zeta potential and particle size measurements have been carried out to the samples of oily wastewater before treatment and during the coagulation- flocculation process at 2, and 22 minutes after the addition of the optimum coagulant doses in order to determine and investigate the operation conditions. The results were presented graphically in two dimensional co-ordinates showing particle size distribution and growth that have (greater intensity, largest volume, and greater surface area) as a function with time.

**Key words:** wastewater, emulsion, coagulation, zeta potential, particle size.

### استخدام نفايات الألمنيوم كمادة مخثرة لمعالجة المياه الملوثة بالزيوت

إمامة راند عبد الأمير

كلية الهندسة – جامعة بغداد

د. حسن فرهود مكي

كلية الهندسة-جامعة بغداد

### الخلاصة

في هذه الدراسة تم إجراء عمل تجريبي لدراسة إمكانية استخدام مخلفات مادة الألومنيوم لإزالة الجسيمات الغروية من مياه الصرف الملوثة بالزيوت عن طريق إذابة هذه المخلفات في محلول هيدروكسيد الصوديوم. تم إجراء التجارب على مياه الصرف الملوثة بالزيوت الذي أعد في تراكيز مختلفة من الزيت ومستويات مختلفة من العسرة و هي (50، 250، 500، و 1000) جزء في المليون من الزيت ل (2000، 2500، 3000، و 3500) جزء في المليون من كربونات الكالسيوم  $\text{CaCO}_3$  على التوالي. كانت قيم التعكر الأولية (203، 290، 770، و 1306) وحدة عكورة، بينما كانت أدنى قيم للعكورة التي تم الحصول عليها من التجارب في وحدات (1.67، 1.95، 2.10، و 4.01) و لجرعات ألومينات الصوديوم المثلى (12، 20، 24، و 28) مليلتر لمياه الصرف الملوثة بالزيوت بتراكيز (50، 250، 500، و 1000) جزء من المليون من الزيت على التوالي. تم قياس جهود زيتا المحتملة وحجم الجسيمات لعينات من مياه الصرف الملوثة بالزيوت قبل المعالجة وأثناء عملية التلبد- التخثر في زمن 2 و 22 دقيقة بعد إضافة جرعة المخثر المثلى من أجل تحديد ودراسة ظروف العملية. عرضت النتائج الثنائية الأبعاد بيانياً والتي تبين توزيع حجم الجسيمات والنمو للجزيئات التي تمتلك (أعلى شدة، أعلى حجم، وأعلى مساحة سطحية) بوصفها متغيرة مع مرور الوقت.

**الكلمات الرئيسية:** مياه صناعية، مستحلب، تخثر، جهد زيتا، حجم الجسيمات.

## 1. INTRODUCTION

With industrial development, there is an increase in the amount of oil used, Oil polluted wastewater arises from diversity of sources like crude oil production, oil refinery, petrochemical industry, lubricant, metal processing, cooling agents, car washing, compressor condensates, and restaurants. Oily wastewater comprises toxic substances such as phenols, poly-aromatic hydrocarbons, petroleum hydrocarbons, which are inhibitory to plant and animal growth, equally, carcinogenic and mutagenic to human being. Likewise, oily wastewater comprises high oil content, chemical oxygen demand (COD) and color. Oil and grease is well-defined as a group of allied materials rather than a particular chemical composite extractable by certain solvents, like hexane. They are nonpolar and, as a result, are hydrophobic in nature, **Alade et al., 2011**. Oily wastewater pollution is mainly manifested in the following aspects:

(1) affecting drinking water and groundwater resources, endangering aquatic resources; (2) endangering human health; (3) atmospheric pollution; (4) affecting crop production; (5) destructing the natural landscape, **Yu et al., 2013**. Oil and grease in wastewater can exist in several forms: free, dispersed or emulsified. The differences are based primarily on size. In oil in water mixture, free oil is characterized with droplet sizes greater than 150  $\mu\text{m}$  in size, dispersed oil has a size range of 20 to 150  $\mu\text{m}$  and emulsified oil has droplets typically less than 20  $\mu\text{m}$ , **Cheryan and Rajagopalan, 1998**. Environmental limitations require that highest total oil and grease concentration in dispose waters to be 10–15 ppm for mineral and synthetic oils and 100–150 ppm for those of animal and vegetable origin, **The World Bank Group, 1999**.

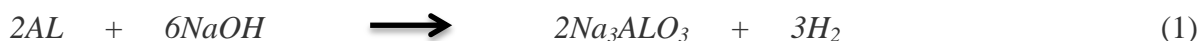
Oily waters are commonly in the formula of oil-in-water (O/W) emulsions. Emulsions are heterogeneous systems in which the external phase (dispersion medium) is water, and the internal phase (dispersed phase) is oil. Therefore emulsion can be conveniently classified according to the distribution of oil and aqueous phases. Hence, a system which consists of oil droplets in an aqueous phase is called as oil-in-water or O/W emulsion and a system with water droplets dispersed in oil phase is termed as water-in-oil or W/O emulsion. The usage of emulsifiers, extreme heat, agitation and pumping in the milling process further assist the formation of these undesirable oil droplets, **Sethupathi, 2004**. Emulsifiers can be present as singular molecules in small amounts, or form poly-molecular aggregates which are called "micelles" **Fig.1**. The number of molecules per micelle can increase and concentrate at the interface. They may then become more water soluble or oil soluble and become soluble in one or the other phase. The function of the emulsifier is to migrate to the interface of the internal and external phase. It consists of a molecule with a hydrophilic portion and a hydrophobic portion. At the interface it forms a protective sheath (barrier) around the droplets of the dispersed phase (oil droplets). It does this in a manner that the hydrophobic end of the molecule migrates or partitions into the oil droplets and the hydrophilic end stays in the water. The stability that results from the addition of the emulsifier depends on its physical nature. When well dispersed it forms an interfacial film around the oil droplets, preventing oil droplets from approaching each other and coalescing. It accomplishes this by changing the interfacial tension of the internal and external phase. Emulsions form when the interfacial tensions between oil and water are reduced. When the interfacial tension value is reduced to zero, an emulsion spontaneously forms. This means that the surface area of the internal phase, (i.e. the oil droplets) has increased to its maximum. This means that very fine droplets have formed giving the emulsion a milky appearance and the oil particles are probably less than 1 micron in size, **Alther, 1997**. An important parameter of a surfactant is the hydrophilic-lipophilic balance (HLB), which correlates surfactant structures with their effectiveness as emulsifiers. The HLB value is given on an arbitrary scale of 0 to 18. An HLB = 0 corresponds to a completely hydrophobic molecule and

HLB = 18 would correspond to a molecule made up completely of hydrophilic components: the higher the HLB number the more hydrophilic is the surfactant. The type of emulsion formed depends on the type of emulsifier, o/w emulsions are produced with a hydrophilic surfactant (high HLB), and w/o emulsions are generated by a hydrophobic surfactant (low HLB). This rule states that, contrary to common sense, what makes an emulsion either o/w or w/o is not the relative percentages of oil or water, but the phase where the emulsifier is more soluble, **Coca et al., 2011**.

Currently the treatment of oily wastewater applies a primary treatment to separate the floatable oils from the water and emulsified oils. A secondary treatment phase is then required to break the oil–water emulsion and separate the remaining oil from the water. Several mechanical processes have been used to try to remove the oil, among which include filtration, and Flotation. The chemical processes have devised the addition of coagulating or flocculating agent that favors the formation of aggregates with drops of oil dispersed so that they can be removed mechanically **Rubi et al., 2009**. For the present work chemical destabilization (coagulation- flocculation processes) has been used, coagulation is an essential process in water and industrial wastewater treatment. It is one of the most important physicochemical processes. Coagulation has been defined as the addition of a positively charged ion of metal salt or catalytic polyelectrolyte that results in particle destabilization and charge neutralization. Coagulation targets the colloid particles of size  $10^{-7}$  to  $10^{-14}$  cm in diameter. Flocculation refers to the successful collision that occurs when destabilized particles are driven toward each other by the hydraulic shear force in the rapid mix and flocculation basin. It agglomerates of a few colloids then quickly bridge together to form micro flocs which is turned into visible floc masses. The process of coagulation separation comprises of four steps. The initial step is simple: the chemical is added to wastewater. This is followed by the second step, where the solution is mixed rapidly in order to make certain that the chemicals are evenly and homogeneously distributed throughout the wastewater. In the third step, the solution is mixed again, but this time in a slow fashion, to encourage the formation of insoluble solid precipitates. The final step is the removal of the coagulated particles by way of filtration or decantation. Coagulant chemicals come in two essential types' primary coagulants and coagulant aids. Primary coagulants neutralize the electrical charges of particles into the water which causes the particles to cluster together. Chemically, coagulants are either metallic salts (such as alum) or polymers. Polymers are human-made organic composites made up of a long chain of smaller molecules. Polymers can be either cationic (positively charged), anionic (negatively charged), or nonionic (neutrally charged). On the other hand, coagulant aid is an inorganic material, when used along with chief coagulant, increases or quickens the process of coagulation and flocculation by generating quick forming, thick and rapid-settling flocs, **Sahu and Chaudhari, 2013**.

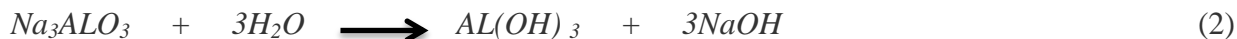
### 1.1 Aluminum Rubbish as a Coagulant

The aluminum rubbish used in this study was dissolved in sodium hydroxide solution to produce 0.5 M from sodium aluminate according to the following equation:



Sodium aluminate is a significant marketable inorganic chemical. It has been used as an active source of aluminum hydroxide for many applications. The commercial importance of sodium aluminate is due to the versatility of its technological applications. In water treatment methods it is used as an assistant to water softening systems, as a coagulant to eliminate

suspended solids and several metals (Cr, Ba, Cu), and for removing dissolved silica. In building technology, sodium aluminate is working to increase speed of the solidification of concrete, generally when working during cold episodes. It is also used in the paper industry, refractory brick production and alumina production, etc. Furthermore, it is used as a transitional in the production of zeolites for detergents, adsorbents molecular sieves, and catalysts. Sodium aluminate aids in the removal process, reacting with the precipitated hardness to form particles that can be removed more effectively, **Makki et al., 2010**. Sodium aluminate, which is alkaline, releases caustic soda and aluminum hydroxide as it dissolves in water.



Aluminum hydroxide will produce a gelatinous precipitate of oil and impurities that presented in water. Also the Hydroxide ion will react with the Calcium bicarbonate and precipitate it as Carbonate ion which will react with the Calcium ion and precipitate it as salt in water. Likewise the Hydroxide ion will react with the Magnesium ion and precipitate it as Magnesium hydroxide, **Makki and Omran, 1995**.



## 1.2 Zeta Potential

Nearly all particulate or macroscopic materials in an interaction with a liquid obtain an electronic charge on their surfaces. Zeta potential is a significant and convenient pointer of this charge which can be used to expect and regulate the stability of colloidal suspensions or emulsions, **Ferhan, 2014**. Negatively charged particulates accumulate positive counter ions on and near the particle's surface to satisfy electro neutrality. A layer of cations will bind tightly to the surface of a negatively charged particle to form a fixed adsorption layer. This adsorbed layer of cations, bound to the particle surface by electrostatic and adsorption forces, is about 5 °Å thick and is known as the Helmholtz layer (also known as the Stern layer after Stern, Beyond the Helmholtz layer, a net negative charge and electric field is present that attracts an excess of cations (over the bulk solution concentration) and repels anions, neither of which are in a fixed position. These cations and anions move about under the influence of diffusion (caused by collisions with solvent molecules), and the excess concentration of cations extends out into solution until all the surface charge and electric potential is eliminated and electro neutrality is satisfied, **Crittenden et al., 2012**, this potential is greatest at the surface and decreases to zero at the bulk of the solution. The potential at a distance from the surface at the location of the shear plane is called the zeta potential. Zeta potential meters are calibrated to read the value of this potential. The greater this potential, the greater is the force of repulsion and the more stable the colloid, **Sincero and Sincero, 2003**. Electrical double layer around a negatively charged oil droplet and the distribution of electrical potential around it has been presented in **Fig.2**.

In aqueous media, the pH of the sample is one of the most important factors that affect its zeta potential. A zeta potential value on its own without defining the solution conditions is a virtually meaningless number. Imagine a particle in suspension with a negative zeta potential. If



more alkali is added to this suspension then the particles tend to acquire more negative charge. If acid is added to this suspension then a point will be reached where the charge will be neutralized. Further addition of acid will cause a buildup of positive charge. Therefore a zeta potential versus pH curve will be positive at low pH and lower or negative at high pH, **Malvern Instruments Ltd, 2011**. Theories describing how the charge density around a particle varies with distance always use the concept of the diffuse double layer. In the simplest theory, the electrostatic potential decays exponentially with distance away from the shear plane. The inverse of the decay constant is a distance called the Debye double layer thickness. It is a function of free salt ion concentration (as embodied in the value of the ionic strength): the higher the concentration, the faster the decay, the smaller the double layer thickness. At high enough salt, the double layer collapses to the extent that the ever present attractive van der Waals forces overcome the charge repulsion. This is one example of the so-called “salting out” effect. Electrostatically stabilized colloidal suspensions will become unstable with the addition of enough salt, **Brookhaven Instruments, 2015**. The effect of the concentration of a formulation component on the zeta potential can give information to assist in formulating a product to give maximum stability. The influence of known contaminants on the zeta potential of a sample can be a powerful tool in formulating the product to resist flocculation for example, **Malvern Instruments Ltd, 2011**.

### 1.3 Particle Size and Distribution Application in Water Treatment

Physical properties of particles, such as size, shape, density, porosity, surface charge, and settling velocity, may influence their behavior in water and have some relationship to water treatment efficiency. As previously mentioned, particle size is the most significant property responsible for the stability of colloidal dispersion in water. Analysis of sizes of flocs formed in the coagulation and flocculation processes are not routinely conducted. Particle size distribution (PSD) analysis can produce direct information about particulate material in water. Through measuring and analyzing the amount of different-sized particles in the raw water as well as in the effluent of each unit, we can evaluate water treatment process efficiency, assess operational problems, and design treatment processes in water and wastewater engineering **Geng, 2005**.

Dynamic light scattering (DLS) is an important experimental technique in science and industry. The principle behind dynamic light scattering is particles, emulsions and molecules in suspension undergo Brownian motion. This is the motion induced by the bombardment by solvent molecules that themselves are moving due to their thermal energy. If the particles or molecules are illuminated with a laser, the intensity of the scattered light fluctuates at a rate that is dependent upon the size of the particles as smaller particles are “kicked” further by the solvent molecules and move more rapidly. Analysis of these intensity fluctuations yields the velocity of the Brownian motion and hence the particle size using the Stokes-Einstein relationship. Note that the radius that is measured in DLS is a value that refers to how a particle diffuses within a fluid so it is referred to as a hydrodynamic diameter **Fig.2**. The radius that is obtained by this technique is the radius of a sphere that has the same translational diffusion coefficient as the particle, **Murarishetty, 2012**.

The Intensity Distribution defines how much light is scattered by the particles in different size bins. This distribution is the most truthful and dependable distribution, and is closely related to the raw measurements that the instrument takes. When understanding these data, it is imperative to save in mind that there is a very strong dependency of the intensity of light scattered, with respect to particle diameter. These two values have a sixth-power relationship, which incomes, for example, that a 100 nm particle will scatter one million times as much light as a 10nm particle. The Volume Distribution measurement displays the entire volume



of particles in the different size bins. This distribution is calculated from the intensity distribution, the visual possessions of the material (specifically, Refractive Index and Absorption at 632 nm), and the formulation for the volume of a sphere:  $V = (4/3) \pi r^3$ . Note in the formulation, that particle diameter (or more definitely, radius) has a third power relationship with volume. This means that, alike to the intensity distribution, the volume distribution will be extra heavily weighted towards the larger, more voluminous particles in a distribution, **Nanocomposix Laboratory, 2015**. In any DLS measurement, the Surface Area standpoint is resulting from the Intensity (Volume) data; since it involve expectations about particle shape, this viewpoint is somewhat detached from the original data and may be less accurate for your measurement, **MNC, 2014**.

## 2. EXPERIMENTAL WORK

### 2.1 Materials

#### 2.1.1 Hard water preparation

The hard water, its solutions, and reagents have been prepared according to the (US EPA, 2013).

##### 2.1.1.1 Hard water solutions and reagents

###### A. Hard Water Solution 1

7.94 g  $\text{MgCl}_2$  (anhydrous) or 16.94 g ( $\text{MgCl}_2 \cdot 6\text{H}_2\text{O}$ ), and 18.50 g  $\text{CaCl}_2$ , have been dissolved in boiled de-ionized  $\text{H}_2\text{O}$ , and then brought to a volume of 250 mL volumetrically .

###### B. Hard Water Solution 2

14.01 g  $\text{NaHCO}_3$ , (Table 3.4) has been dissolved in boiled de-ionized  $\text{H}_2\text{O}$ ; and then brought to a volume of 250 mL volumetrically.

The two solutions have been filtered and sterilized by using a 0.2  $\mu\text{m}$  filter unit. These two solutions have been used for the preparation of hard water at various concentrations.

##### 2.1.1.2 Hard water (as $\text{CaCO}_3$ ) preparation

1 mL of hard water solution 1 has been added for each 100 ppm of hardness desired. For example, for the preparation of 1 L of 400 ppm hard water, 4 mL hard water solution 1 and 4 mL hard water solution 2 have been added to a 1 L flask and bring to volume with sterile de-ionized water. The pH of the hard water sample has been determined. The pH should be between 7.6 and 8.0.

#### 2.1.2 Mixed emulsifier preparation

A mixture of two emulsifiers has been used for the O/W emulsion preparation, where a mixture of 38% Span 85 and 62% Tween 80 has been used for the mixed emulsifier preparation .The calculation of how much of Span 85to blend with Tween 80 to attain a given HLB (hydrophilic- lipophilic balance) of X (oil HLB), the following equations have been used, **Croda Europe Ltd, 2010**:

$$A\% = \frac{X - \text{HLB of } B}{(\text{HLB of } A - \text{HLB of } B)} \quad (6)$$

$$B\% = 1 - A\% \quad (7)$$

##### 2.1.3 Oily wastewater (emulsion) preparation



Oil in water emulsion was prepared by mixing of oil, mixed emulsifier, and the prepared hard water. The emulsion was prepared by using homogenizer of 10000 rpm for 30 seconds. Gasoline and diesel fuel engine oil (Helix 15W-40) has been used in this preparation. The percent of the emulsifier has been taken as 10% of the oil (i.e. for 1000 ppm of oily water 0.9 g of oil and 0.1 g of the mixed emulsifier has been used per 1 liter volume). The emulsion has been prepared at different oil concentration and hardness levels. The oily wastewater has been prepared at four different hardness levels (2000, 2500, 3000, and 3500) ppm for (50, 250, 500, and 1000) ppm oil concentrations respectively.

#### 2.1.4 Coagulant preparation

Aluminum rubbish has been brought from aluminum factories waste. Sodium Hydroxide (NaOH) solution was prepared at a concentration of 1.5 M by dissolving 30g of NaOH in 500ml of deionized water. Sodium Aluminate was prepared at a concentration of 0.5 M by dissolving 6.75g of aluminum rubbish in NaOH solution. The reaction has been completed when all the aluminum dissolved in NaOH and Sodium Aluminate has been produced. The reaction container must not be covered during the reaction because of the hydrogen gas releasing.

#### 2.2 Methods

1. For jar testing, a conventional unit capable of variable speeds from (50 – 250) rpm was used with six beakers, each 1000 ml in capacity.
2. System type Lovibond instrument has been used for turbidity measurement with a turbidity range from (0 to 800) NTU.
3. The pH values of the samples were measured by one device which is (Model 2906, Jenway Ltd, UK) with a pH range (0-14) pH.
4. The hardness of water was measured in parts per million (ppm), expressed in terms of Calcium as  $\text{CaCO}_3$ . Actually the hardness is due both to Calcium and Magnesium salts, but the two are determined together in the titration.
5. The measurements of the oil content in water samples have been done by a simple device TD500-D<sup>TM</sup> Handheld Oil in water meter.
6. The zeta potential has been measured by Zeta-Meter System 4.0, Zeta-meter, Inc.
7. The particle size measurement have been done by Nano Brook zeta plus device (zeta potential and particle size analyzer), Brookhaven Instrument.

#### 2.3 Procedure

Six dosages (4 ml, 12 ml, 20 ml, 24 ml, 28 ml, and 32 ml) of the chemical coagulant (Sodium Aluminate) have been added to the O/W emulsion. The jar tester has been worked at a high speed of 250 rpm for two minutes (Coagulation process), and then slow mixing at a speed of 50 rpm for 20 minutes (Flocculation process). After the slow mixing the tester has been stopped to allow the settling operation for 15 min, and after settling, samples of the clear part of water have been taken for farther analysis (i.e. turbidity, pH, hardness, and oil content measurements). From the turbidity measurements the optimum dose has been found for each concentration. The zeta potential measurements have been done to the optimum dose of chemical coagulant for each selected concentration of oil and hardness and to the oily wastewater before treatment. The measurement samples have been taken after the addition of the optimum dose and during jar testing at time of 2 min (after coagulation), at 22 min (after flocculation), and after the sedimentation. Likewise the particle size measurements have been done to the optimum dose of chemical coagulant for each selected concentration of oil and hardness. The particle size

measurements were done to the oily wastewater before the treatment and after the addition of the optimum dose, during jar testing samples of water have been taken at time of 2 min (after coagulation) and at 22 min (after flocculation). All the water samples have been filtrated with a whatman 44,  $3\mu\text{m}$  pore size filter paper before measurement.

### 3. RESULTS AND DISCUSSION

#### 3.1 Optimum Coagulant Dosages

**Figs.3 to 6** illustrate the results of the effect of different dosages of sodium aluminate as a coagulant on the residual turbidity through coagulation-flocculation and settling time. The residual turbidity has been decreased as the sodium aluminate dose increased until reaching the minimum value of turbidity at the optimum coagulant dose, then the turbidity has been increased with increasing sodium aluminate dosages. This may be explained as the particulates can be destabilized by adsorption of oppositely charged ions or polymer. Most particulates in natural waters are negatively charged (oils, clays, humic acids, and bacteria) in the neutral pH range (pH 6 to 8); consequently, hydrolyzed metal salts can be used to destabilize particles through charge neutralization. When the proper amount of coagulant has adsorbed, the charge is neutralized and the particle will flocculate. When too much coagulant has been added, the particles will attain a positive charge and become stable once again. For coagulant dosages up to optimum value, the electrophoretic mobility becomes more positive and the amount adsorbed increases. Higher dosage causes charge reversal, particle stability, and a higher residual turbidity. At the optimum dosage of coagulant, the particle charge is just neutralized and the collision efficiency reaches a maximum value and this agreed with **Makki et al., 2010**. The minimum values of turbidity that have been gained from the experiments in NTU units were (1.67, 1.95, 2.10, and 4.01) at optimum sodium aluminate dosages in milliliters (12, 20, 24, and 28) for oily wastewater of concentrations (50, 250, 500, and 1000) ppm of oil respectively.

#### 3.2 Effect of Coagulant Dosages on pH Value

Sodium aluminate is a very strong alkaline. The reasons for the addition of some form of alkali were to establish the optimum pH value at which coagulation can take place and to rise the final pH value after treatment to reduce corrosiveness. In coagulation, the pH value is important. Floc formed in any given water tends to be heaviest at specific pH value **Putros, 2001**. The effect of adding sodium aluminate on the pH value has been illustrated in **Fig.7**, where the increase of sodium aluminate dosages from 4 ml to 32 ml has been increased the pH value of the water of four different concentrations (50, 250, 500, and 1000) ppm with increasing rate of (46, 49, 52, and 52) % respectively.

#### 3.3 Effect of Coagulant Dose on Hardness ( $\text{CaCO}_3$ ) Removal

The oily wastewater has been prepared at four different hardness levels (2000, 2500, 3000, and 3500) ppm for (50, 250, 500, and 1000) ppm oil concentrations respectively. **Fig.8** illustrates the effect of sodium aluminate coagulant on the oily wastewater hardness, where the hardness has been decreased with the increase of the sodium aluminate dose, this can be explained as the Hydroxide ion will react with the Calcium bicarbonate and precipitate it as Carbonate ion which will react with the Calcium ion and precipitate it as salt in water. Likewise the Hydroxide ion will react with the Magnesium ion and precipitate it as Magnesium. The removal rates were (77, 90, 84, and 93) % for (2000, 2500, 3000, and 3500) ppm hardness levels of (50, 250, 500, and 1000) ppm respectively oily wastewater at the optimum coagulant dose.

### 3.4 Effect of Coagulant Dose on Oil Removal

Jar tests were performed using the prepared oily wastewater and the experimental results have been shown in **Fig.9**. The results suggest that the oil in water can be effectively removed by a suite coagulation, flocculation, and sedimentation processes, where the residual oil concentration has been decreased with the increase of the coagulant dose and this can be regarded that Oil droplets in an O/W emulsion exhibit a net charge the droplet surface. It is usually negative charge, if aluminum ions of positive electric charge are added, it neutralizes the electric negative charge, precipitate the oil particles and other presented pollutants in the wastewater, as hydroxides and facilitate their removal by physical separations through the sedimentation process. The oil removal rates were (100, 93, 96, and 97) % for oily wastewater of oil concentrations (50, 250, 500, and 1000) ppm respectively. The behavior observed in the oil removal denotes that the amount of sodium aluminate coagulant necessary to produce the destabilization of the emulsion is proportional to the oil concentration.

### 3.5 Zeta Potential Measurement

**Fig.10** illustrates the effect of time of coagulation, flocculation and sedimentation on the value of zeta potential. Initially the zeta potential has been measured for the prepared oily wastewater (O/W emulsion) and the values were (-36, -35, -31, and -26) mv for oil concentrations of (50, 250, 500, and 1000) ppm respectively, so the prepared emulsions of concentrations of 50, 250, and 500 ppm oil are considered to be moderately stable because their zeta potential values were in the range of (-31 to -40), but for the emulsion of 1000 ppm oil concentration it considered to be plateau of slight stability because its zeta potential value was in the range of (-21 to -30). The time variation in the zeta potential that has presented in Figure 8 suggests that the addition of  $AL^{+3}$  ions neutralize the negative charges on the particle surfaces. The zeta potential that has been measured at pH=7 becomes positive when the emulsion is demulsified, and this can be explained as that initially, the negative colloid attraction effects some of the positive ions to form a definitely attached layer round the colloid surface, this layer of counter ions is identified as the stern layer, because of that the zeta potential will be a positive value. During flocculation the additional positive ions are still attracted by the negative colloid so the value of the zeta potential raises more until the colloids are repelled by the positive stern layer as well as by the other near-by positive ions that are trying to reach to the colloid. After sedimentation all the agglomerates have been settled out of the water, so the values of the zeta potential will be negative again due to the remained (OH-) ions in the water, except for 28 ml coagulant sample where the zeta potential value has been remained positive after sedimentation and this may be due to the remained positive charge flocs that didn't settle out and may need more sedimentation time.

### 3.6 Particle Size Measurements

Several experimental runs have been carried out to examine the particle size of oily wastewater before the clarification process (i.e. before treatment), after coagulation-filtration, and after coagulation-flocculation-filtration without the sedimentation step in order to study the effect of the coagulation and flocculation time on the effective diameter, volume, surface area, intensity (i.e. the fate of Nano particles and flocs), where the fate of the larger particles and flocs is well known during coagulation and flocculation process.



### 3.6.1 Effective diameter of the particles of highest intensity

DLS experiment first order result is the intensity distribution of particle sizes. According to the scattering intensity of each particle fraction or family the intensity distribution is logically weighted. **Fig. 11** illustrates the relation of the effective diameter of the particles that have the highest intensity and time. The effective diameter has been measured for oily wastewater and the results before treatment were (310.95, 543.13, and 575.88) nm for concentrations of (250, 500, and 1000) ppm oily wastewater respectively. The particle size is an indicator of the emulsion stability and the type of the oil in water, where smaller particle sizes and higher surface charge (zeta potential) will typically improve suspension and emulsion stability, and therefore the 250 ppm oily wastewater emulsion is more stable than the others, and since all the particle sizes are below 5 microns so the oil can be considered dissolved in water. After coagulation –filtration process, the effective diameter of the particles has been increased to (323.38, 587.26, and 577.63) nm for concentrations of (250, 500, and 1000) ppm oily wastewater respectively, and after coagulation – flocculation –filtration, the effective diameter has been more increased to (329.89, 668.87, and 762.05) nm for concentrations of (250, 500, and 1000) ppm oily wastewater respectively. This can be explained as that the effective diameter is the hard sphere diameter where this hard sphere diffuses at the identical speed as the molecule or particle being measured. The translational diffusion coefficient will not only depend on the particle size “core”, but also on any surface structure, the concentration, and type of ions in the medium. The medium ions and the total ionic concentration may affect the diffusion speed of the particle by varying the electric double layer thickness during coagulation and flocculation. Any variation in the particle surface that affects the diffusion speed will correspondingly change the particle apparent size, where smaller particles are further “reflexed” by the molecules of the solvent and move more rapidly and vice versa.

### 3.6.2 Diameter of the particles of highest surface area

Before treatment the diameters of the particles and flocs that have the highest surface area were (455, 320.25, and 669) nm for oily wastewater of concentrations (250, 500, and 1000) ppm respectively. After coagulation –filtration step the results were (332, 332, and 790) nm for oily wastewater of (250, 500, and 1000) ppm oil respectively, so the diameters have been increased after this step except for 250 ppm oil concentration and this can be due to the high speed of mixing (250)rpm during this step. After the coagulation- flocculation- filtration step the results were (487.5, 660, and 410) nm for (250, 500, and 1000) oily wastewater respectively and there is an increase in the diameters except for the 1000 ppm oily wastewater, so for this concentration this step is not sufficient. **Fig.12** illustrates the relation between the time and the surface area that has been calculated depending on the assumption that the particles and flocs have the form of a spherical ball.

### 3.6.3 Diameter of particles of highest volume

Before treatment the results were (462, 850, and 1342.85) nm for oily wastewater of concentrations (250, 500, and 1000) ppm oil respectively. After coagulation-filtration step the results were (1002, 1690, and 860) nm for wastewater of (250, 500, and 1000)ppm respectively, so there is an increase in the diameters except for the 1000 ppm concentration sample and this may be explained as it need more time to achieve a larger diameter. After coagulation-flocculation –filtration step the diameters have been decreased to the values (782.5, and 1062) nm for the wastewater of concentrations of (250, and 500) ppm oil respectively, and increased for the 1000 ppm oil wastewater to (1524) nm, in spite of that there is an increment in the





diameter values after this step than the values before treatment. **Fig.13** illustrates the relation between the time and the volume that has been calculated depending on the assumption that the particles and flocs have the form of a spherical ball.

## CONCLUSIONS

1. Successful in using aluminum rubbish as a coagulant for oily wastewater treatment with removing the bicarbonates, calcium, and magnesium ions that causing hardness and this coagulant can be used for treating the oily wastewater from different industries.
2. Within the range of the oil concentrations that have been studied, the optimum coagulant doses were (12, 20, 24, and 28) ml for oily wastewater of (50, 250, 500, and 1000)ppm oil and (2000, 2500, 3000, and 3500) ppm  $\text{CaCO}_3$  respectively.
3. The pH values increases with increasing the coagulant dose, while the hardness level ( $\text{CaCO}_3$  concentration), and the oil content decreases with increasing the coagulant dose.
4. Zeta potential values have been reversed from negative to positive charge values after the coagulation-flocculation process, where the initial values were (-36, -35, -31, and -26) mv, while the final values after coagulation-flocculation process were (20.2, 29.1, 24.56, and 27) mv for oily wastewater of initial concentrations (50, 250, 500, and 1000) ppm of oil respectively.
5. The results were presented graphically in two dimensional co-ordinates showing particle size distribution and growth that have (greater Intensity, largest volume, and greater surface area) as a function with time. For the particles and flocs that have the highest intensity the initial effective diameter values were (310.95, 543.13, and 575.88) nm, while the final values after coagulation-flocculation process were (329.89, 668.87, and 762.05) nm, but for the particles and flocs that have the highest surface area the initial diameter values were (455, 320.25, and 669) nm, while the final values after coagulation-flocculation process were (487.5, 660, and 410) nm, while for the particles and flocs that have the largest volume the initial diameter values were (462, 850, and 1342.85) nm, while the final values after coagulation-flocculation process were (782.5, 1062, and 1524) nm for oily wastewater of initial concentrations (250, 500, and 1000) ppm of oil respectively.

## REFERENCES

- Alade A. O., Jameel A. T., Muyubi S. A., Abdulkarim M. I., and Alam M., 2011, *Removal of Oil and Grease as Emerging Pollutants of Concern (EPC) in Wastewater Stream*, IIUM Engineering Journal, Vol. 12(Special Issue on Biotechnology), Pages (161-169).
- Alther G. R., 1997, *Oils Found in Wastewater: What are they?, How to Separate and Eliminate them from Wastewater?*, Biomin Incorporated
- Brookhaven Instrument Corporation, 2015, *Colloidal Stability in Aqueous Suspensions*, Holtville, New York, USA
- Cheryan, M. and Rajagopalan N., 1998, *Membrane processing of Oily Streams*, Journal of Membrane Science, Vol. 151, Pages (13-28).
- Coca J., Gutierrez G., and Benito J. M., 2011, *Tratment of Oily Wastewater, In Water Purification and Management*, Pages (1-55), Spain, Springer Science+Business Media B.V
- Crittenden J. C., Trussell R. R., Hand D. W., Hawe K. J., and Obanoglous G. T., 2012, *MWHS Water Treatment: Principles and Design*, Third Eddition.
- Croda Ltd., Croda Europe Limited, 2010, *Span-Tweem*, from Croda Europe Web site: [www.croda.com/europe](http://www.croda.com/europe).



- Ferhan M. I., 2014, *Effect of Particle and Floc Size on Water Treatment by Physico-Chemical Process for River Water*, M.Sc. Thesis, University of Technology, Baghdad.
- Geng Y., 2005, *Application of Flocs Analysis for Coagulation Optimization at the Split Lake Water Treatment Plant*, M.Sc. Thesis, University of Manitoba, Manitoba.
- Makki H. F., Al-Alawy A. F., Abdul-Razaq N. N., and Mohammed M. A., 2010, *Using Aluminum Refuse as a Coagulant in the Coagulation and Flocculation Processes*, Iraqi Journal of Chemical and Petroleum Engineering, Pages (15– 22)
- Makki H. F., and Omran I. I., 1995, *The Possibility of Using Aluminum Waste as a Precipitated in Drinking Water Purification Projects*. Journal of Technical Research, Pages (10-17).
- Malvern Instruments Limited, 2011, *Dynamic Light Scattering: Common Terms Defined*, Worcestershire, UK. : [www.malvern.com/contact](http://www.malvern.com/contact)
- MNC, University of Minnesota Nano Center, 2014, *Calibration and Size Correction of the DLS*.
- Murarishetty S. K., 2012, *Characterization of Polymeric Phthalocyanine Nano Particles Using Dynamic Light Scattering Laser*, M.Sc. Thesis, Governors State University.
- Nanocomposix Laboratory, 2015, *Nanocomposixs Guide to Dynamic Light Scattering Measurements and Analysis*, from Nanocomposix Web site: [https://cdn.shopify.com/s/files/1/0257/8237/files/nanoComposix\\_Guidelines\\_for\\_DLS\\_Measurements\\_and\\_Analysis.pdf](https://cdn.shopify.com/s/files/1/0257/8237/files/nanoComposix_Guidelines_for_DLS_Measurements_and_Analysis.pdf)
- Putros L. E., 2001, *Quality Improvement of the Locally Produced Alum and its Use in Water Treatment Plants*. M.Sc. Thesis. Baghdad , Iraq: Baghdad University.
- Rubi H., Fall C., and Ortega R. E., 2009, *Pollutant Removal from Oily Wastewater Discharged from Car Washes Through Sedimentation–Coagulation*, Water Science & Technology, Pages (2359-2369).
- Sahu O. P. and Chaudhari P. K., 2013, *Review on Chemical Treatment Of Industrial Waste Water*, J. Appl. Sci. Environ, Pages (241-257).
- Sethupathi S., 2004, *Removal of Residue Oil From Palm Oil Mill Effluent (Pome) Using Chitson* . University Sains Malaysia.
- Sincero A. P., and Sincero G. A., 2003, *Physical-Chemical Treatment of Water and Wastewater*, Maryland
- The World Bank Group, 1999, *Pollution Prevention and Abatement Hand Book*, The World Bank, Washington D.C.
- US EPA, Environmental Protection Agency, 2013, *Standard Operating Procedure for Preparation of Hard Water and Other Diluents for Antimicrobial Products*, USA
- Yu L., Han M., and He F., 2013, *A Review of Treating Oily Wastewater*, Arabian Journal of Chemistry.
- Zouboulis A. I. and Avranas, 2000, *Treatment of Oil-In-Water Emulsions by Coagulation and Dissolved-Air Flotation*. Colloids and Surfaces A: Physicochemical and Engineering Aspects, Pages (153–161).

## NOMENCLATURE

A%= volume percent of Tween 80 emulsifier.

B%= volume percent of Span 85 emulsifier.

X= HLB number of oil has been used for emulsion preparation (HLB=10 for Helix oil).

HLB of A = hydrophilic- lipophilic balance of Tween 80 =15.

HLB of B = hydrophilic- lipophilic balance of Span 85 = 1.8.

**Abbreviations**

API	American Petroleum Institute
COD	Chemical Oxygen Demand
DAF	Dissolved Air Flotation
DLS	Dynamic Light Scattering
Dp	Particle Diameter
HLB	Hydrophilic Lipophilic Number
MF	Microfiltration
NF	Nanofiltration
NTU	Nephelometric Turbidity Unit
O/W	Oil in Water Emulsion
RO	Reverse Osmosis
UF	Ultrafiltration
W/O	Water in Oil Emulsion

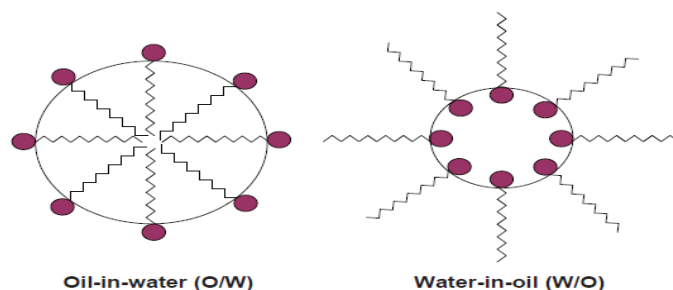


**Figure 1.** Surfactant stabilized micelles, **Sethupathi, 2004.**

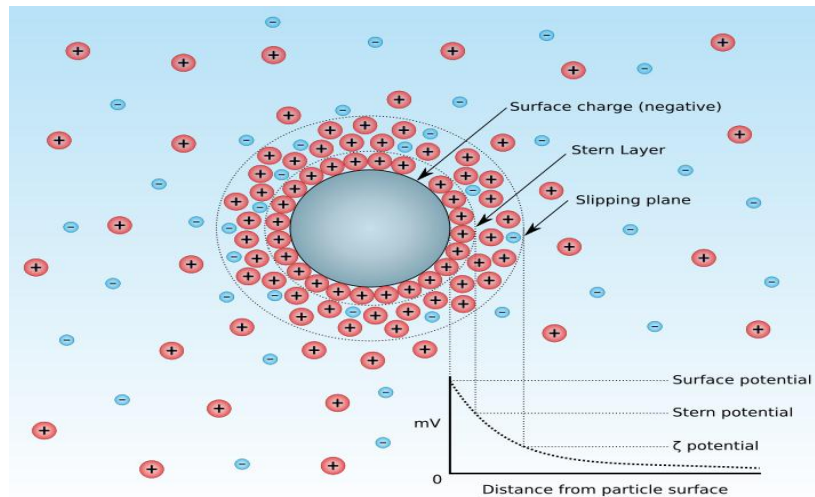


**Figure 2.** Electrical double layer surround a negatively charged oil droplet and the distribution of electrical potential around it, **Zghair, 2014**.

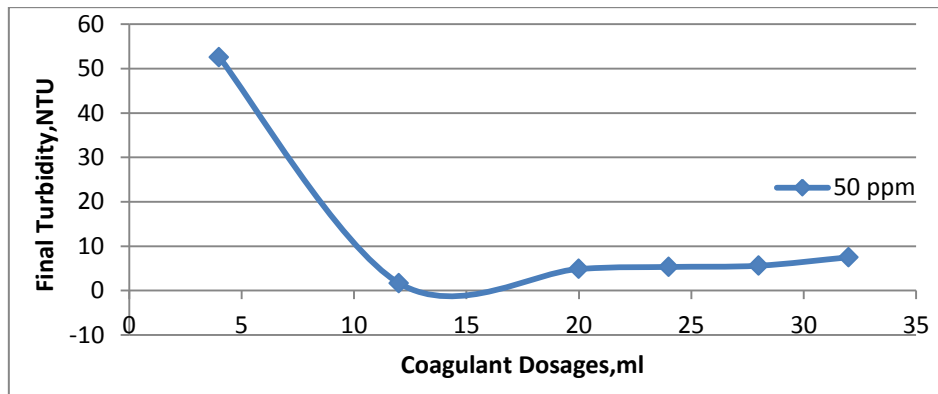


**Figure 3.** Final turbidity vs. coagulant dose for 50 ppm oily wastewater, initial turbidity=203 NTU.

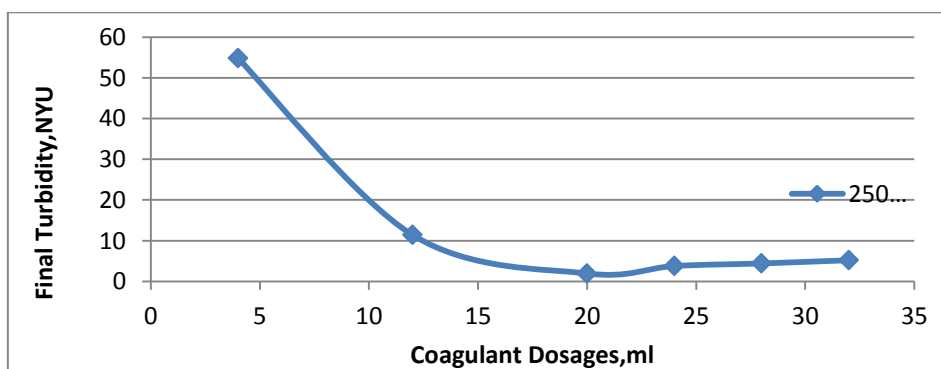


**Figure 4.** Final turbidity vs. coagulant dose for 250 ppm oily wastewater, initial turbidity=290 NTU.

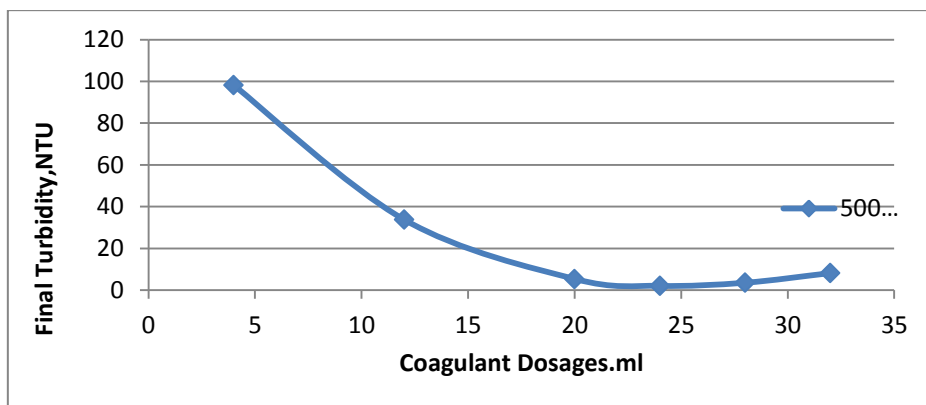


**Figure 5.** Final turbidity vs. coagulant dose for 500 ppm oily wastewater, initial turbidity=770 NTU.

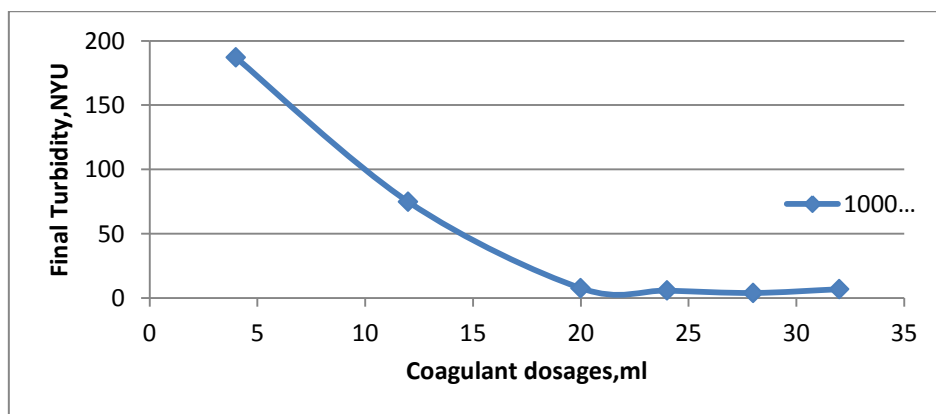


**Figure 6.** Final turbidity vs. coagulant dose for 1000 ppm oily wastewater, initial turbidity=1306 NTU.

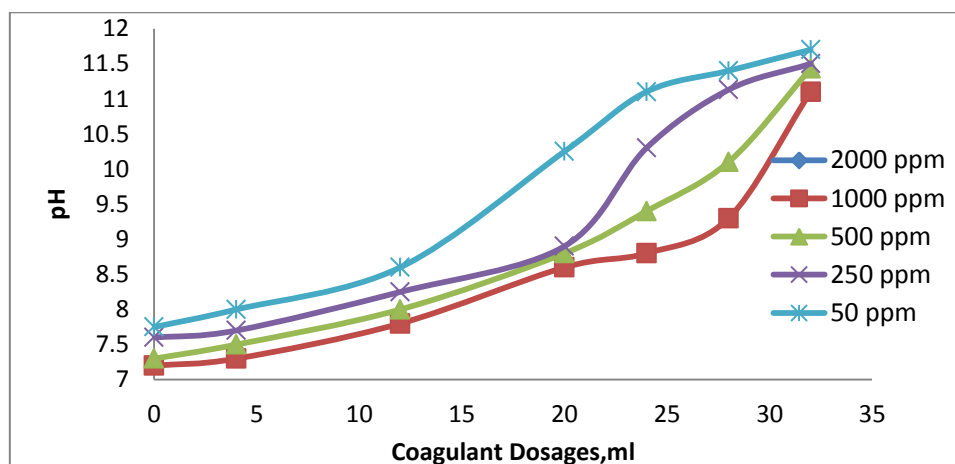


**Figure 7.** pH vs. coagulant dose.

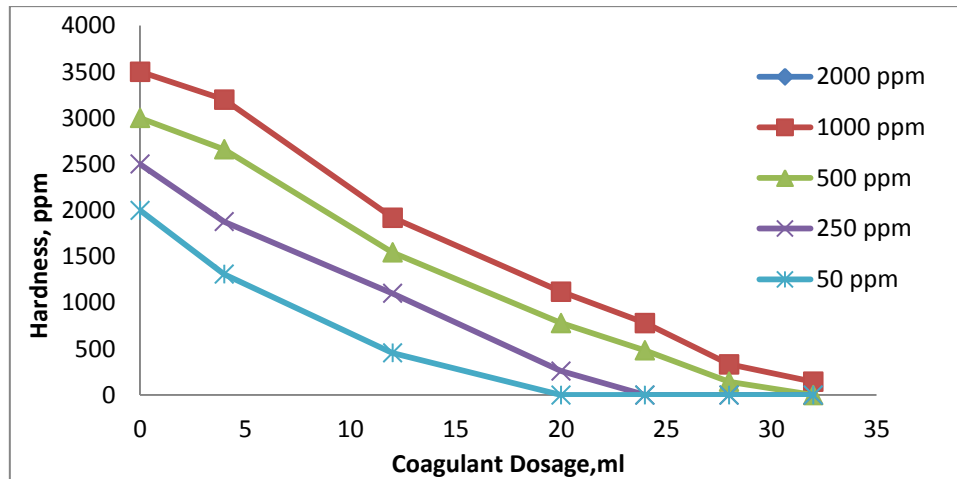


**Figure 8.** Oily wastewater hardness vs. coagulant dose.

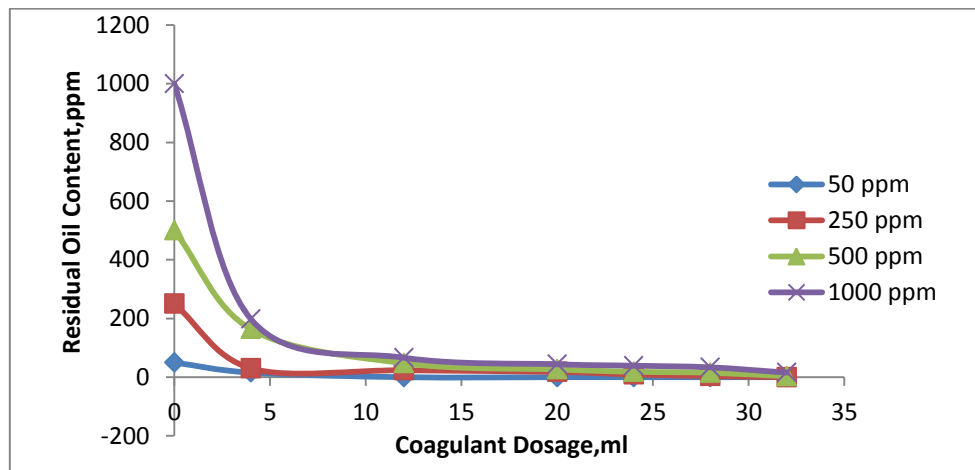


**Figure 9.** Residual oil content vs. coagulant dose.

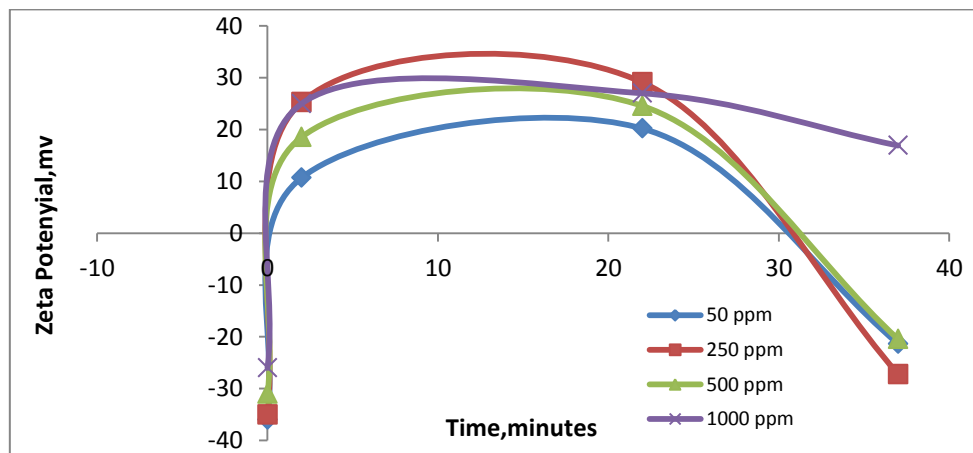


**Figure 10.** Zeta potential vs. time.



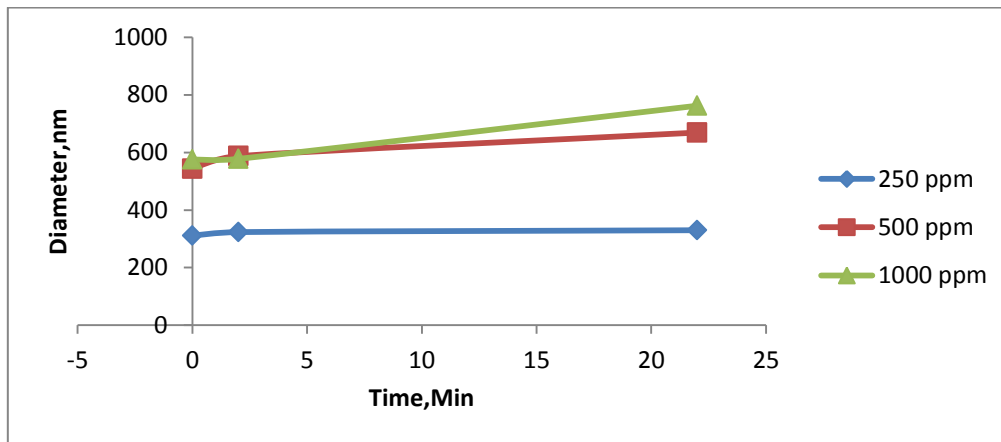


**Figure 11.** Effective diameter of particles and flocs that have highest intensity vs. time.

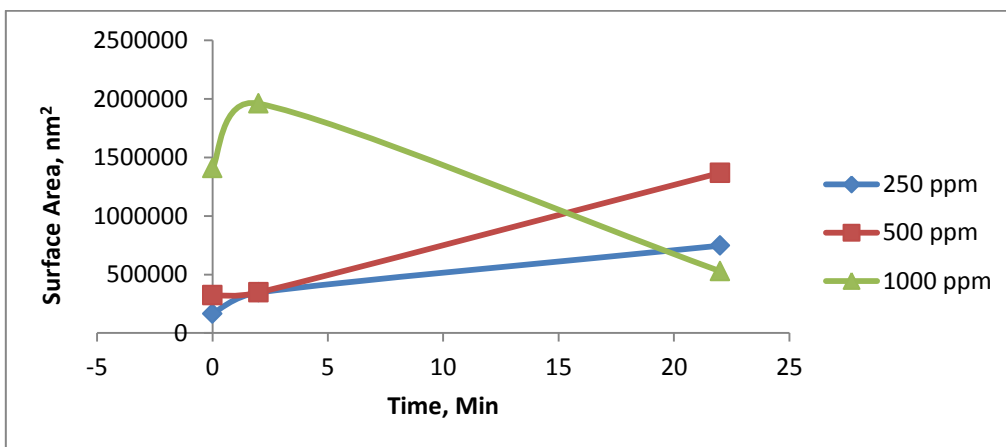


**Figure 12.** Surface area vs. time.

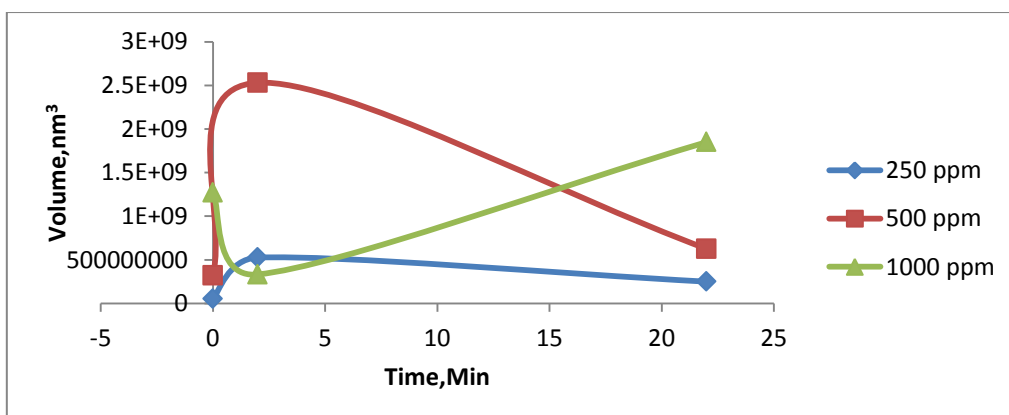


**Figure 13.** Volume of particles and flocs vs. time.

## Hydrogen Production by Water Electrolysis Via Photovoltaic Panel

**Prof. Dr. Karima Esmail Amori**  
Department of .Energy Engineering  
College of Engineering-University of Baghdad  
E-mail: [drkarimaa@yahoo.com](mailto:drkarimaa@yahoo.com)

**Ass. Prof. Dr. Sameer Mohammed Salman**  
Department of .Energy Engineering  
College of Engineering-University of Baghdad  
E-mail: [Dr.Samir88@yahoo.com](mailto:Dr.Samir88@yahoo.com)

**Zahraa Hashim Kareem**  
Energy Engr. Dept. , (MSc. Student)  
College of Engineering-University of Baghdad  
E-mail: [Zahraa\\_hashim89@yahoo.com](mailto:Zahraa_hashim89@yahoo.com)

### ABSTRACT

Hydrogen fuel is a good alternative to fossil fuels. It can be produced using a clean energy without contaminated emissions. This work is concerned with experimental study on hydrogen production via solar energy. Photovoltaic module is used to convert solar radiation to electrical energy. The electrical energy is used for electrolysis of water into hydrogen and oxygen by using alkaline water electrolyzer with stainless steel electrodes. A MATLAB computer program is developed to solve a four-parameter-model and predict the characteristics of PV module under Baghdad climate conditions. The hydrogen production system is tested at different NaOH mass concentration of (50,100, 200, 300) gram. The maximum hydrogen production rate is 153.3 ml/min, the efficiency of the system is 20.88% and the total amount of hydrogen produced in one day is 220.752 liter.

**Key words :** photovoltaic module, four parameter model, electrolyzer, hydrogen.

### إنتاج الهيدروجين بواسطة التحليل الكهربائي للماء عن طريق اللوح الكهروضوئي

سمير محمد سلمان  
أستاذ مساعد  
قسم هندسة الطاقة- كلية الهندسة - جامعة بغداد

كريمة أسما عيل عموري  
أستاذ  
قسم الهندسة الميكانيكية - كلية الهندسة - جامعة بغداد

زهراء هاشم كريم  
طالبة ماجستير  
قسم هندسة الطاقة- كلية الهندسة - جامعة بغداد

### خلاصه

وقود الهيدروجين هو بديل جيد للوقود الأحفوري. يمكن إنتاجه باستخدام الطاقة النظيفة دون انبعاثات ملوثة. هذا العمل يهتم بدراسة عملية إنتاج الهيدروجين عن طريق الطاقة الشمسية. يستخدم اللوح الكهروضوئي لتحويل الإشعاع الشمسي إلى طاقة كهربائية. يتم استخدام الطاقة الكهربائية لتحليل الماء إلى هيدروجين وأوكسجين باستخدام المحلل القلوي مع أقطاب فولاذية مقاوم للصدأ. تم تطوير برنامج ماتلاب لحل نموذج الاربعة متغيرات والتنبؤ بخصائص اللوح الكهروضوئي في ظل الظروف المناخية للعراق. يتم اختبار نظام إنتاج الهيدروجين في تراكيز مختلفة لهيدروكسيد الصوديوم (50، 100، 200، 300) غرام. أقصى إنتاج للهيدروجين هو (153.3) مل/دقيقة. كفاءة المنظومة هي (20.88)% وإجمالي كمية الهيدروجين المنتجة في يوم واحد هي (220.752 لتر).

الكلمات الرئيسية : اللوح الكهروضوئي، نموذج الاربعة متغيرات ، المحلل الكهربائي ، هيدروجين.

## 1. INTRODUCTION

Solar energy presents the prime source of energy for life on earth, **Sharma, et al., 2009**. Photovoltaic (PV) is the most direct way to convert solar radiation into electricity, **Pamplona, 2008**. Hydrogen gas is a good alternative to fossil flues, when considering environmentally friendly hydrogen production, the obvious choice for the input energy is renewable energy, mainly solar energy, **Dincer, and Joshi, 2013**. Increasing the temperature of water and electrolyte concentration led to net increase of volume flow of hydrogen gas and efficiency of the electrolyzer, **Chennouf, et al., 2012**. Different electrodes (aluminum, stainless steel, graphite) used in hydrogen production using photovoltaic cell, the highest accumulative hydrogen gas was obtained with aluminum electrodes and the lowest was with graphite electrodes, **kargi, 2011**. Increase the electrical efficiency of the PV-electrolysis system by matching the maximum power output and voltage of the photovoltaic to the operating voltage of a proton exchange membrane (PEM) electrolyzer by using DC-DC convertor connected to the PV power circuit (battery system) studied by, **Gibson, and Kelly, 2010**. The objectives of this work are to evaluate theoretically and experimentally the photo-hydro characteristics of solar hydrogen generator under outdoor test for Iraq climate conditions. Mono-crystalline PV panel of 50 W is used to generate hydrogen with stainless steel electrodes used to electrolysis of water.

## 2. THEORETICAL MODEL

There are many mathematical models in the literature to describe photovoltaic cells, from simple to more complex models. Some of them is used two-diode model and other used one-diode model, **Eicker, 2003**. In present work one-diode model is used. The current-voltage (I-V) characteristic of a photovoltaic module can be described with a single diode such as **Fanny, et al., 2002**.

$$I = I_L - I_o \left[ \exp \left( \frac{V + IR_s}{N_s n_I V_t} \right) - 1 \right] - \frac{V + IR_s}{R_{sh}} \quad (1)$$

where  $I$  is current of the module (A),  $I_L$  is the light-generated current (A),  $I_o$  is the reverse saturation current of the p-n diodes (A),  $V$  is the voltage of the module (v),  $R_s$  is the series resistance of the cells ( $\Omega$ ),  $R_{sh}$  is the shunt resistance of the cells ( $\Omega$ ),  $N_s$  is the number of cells in series,  $n_I$  is the diode ideality factor,  $V_t$  is the thermal voltage (V) depending on the cell temperature, which is defined as

$$V_t = \frac{kT_c}{q} \quad (2)$$

where  $k$  is Boltzman's constant  $= 1.381 \times 10^{-23}$  J/K,  $T_c$  is the cell temperature (K),  $q$  is electron charge  $= 1.602 \times 10^{-19}$  Coulomb.

### 2.1 Four - Parameter Model

The four parameters model adopted in this work is based on  $I_L$ ,  $I_o$ ,  $R_s$ ,  $a$ , as given in the work of **Kou, et al., 1998**. Where  $a$  is curve fitting parameter for the four-parameter model. Assume  $R_{sh}$  as infinite so the third term in Eq.(1) yields:

$$I = I_L - I_o \left[ \exp \left( \frac{V + IR_s}{mV_t} \right) - 1 \right] \quad (3)$$

where  $m$  is the product of  $N_s n_i$ . To evaluate the power generated by PV module, the simple relationship is used;

$$P = IV \quad (4)$$

where  $P$  is power of the module (W),  $V$  is voltage of the module (V). Introducing Eq.(3) into Eq. (4), the power would be

$$P = IV = \left\{ I_L - I_o \left[ \exp \left( \frac{V + IR_s}{mV_t} \right) - 1 \right] \right\} V \quad (5)$$

where  $R_s$  is series resistance, the series resistance is assumed to be independent of both temperature and solar radiation so that  $R_s = R_{s,ref}$  and  $R_{s,ref}$  is series resistance at reference condition ( $\Omega$ ), and it is calculated as :

$$R_{s,ref} = \frac{a_{ref} \ln \left( 1 - \frac{I_{mp,ref}}{I_{L,ref}} \right) - V_{mp,ref} + V_{OC,ref}}{I_{mp,ref}} \quad (6)$$

where

$a_{ref}$  is curve-fitting parameter for the four-parameter model at reference condition. It is calculated by:

$$a_{ref} = \frac{\mu_{V,oc} T_{c,ref} - V_{oc,ref} + E_g N_s}{\frac{T_{c,ref} \mu_{I,sc}}{I_{L,ref}} - 3} \quad (7)$$

$I_{mp,ref}$  is current at maximum-power point at reference condition (A),  $I_{L,ref}$  is light-generated current at reference condition =  $I_{sc,ref}$  (A),  $V_{mp,ref}$  is voltage at maximum-power point at reference condition (V),  $V_{OC,ref}$  is open-circuit voltage at reference condition (V),  $\mu_{V,oc}$  is temperature coefficient of open-circuit voltage (V/K),  $T_{c,ref}$  is cell temperature at reference condition = 298 (K),  $E_g$  is energy-band gap = 1.124(eV) for mono crystalline silicon photovoltaic module,  $\mu_{I,sc}$  is temperature coefficient of short-circuit current (A/K). The electrical efficiency of the module at maximum-power point can be calculated as

$$\eta = \frac{P}{G \times A} \times 100 \quad (8)$$

where  $G$  is incident solar radiation at reference condition ( $W/m^2$ ),  $A$  is module area ( $m^2$ ). The current produced by incident light is computed by :

$$I_L = \left( \frac{G}{G_{ref}} \right) [I_{L,ref} + \mu_{I,sc} (T_c - T_{c,ref})] \quad (9)$$

where  $G_{ref}$  is solar irradiance at reference condition = 1000 ( $\text{W/m}^2$ ). The reverse saturation current of p-n diodes is computed by :

$$I_o = I_{o,ref} \left( \frac{T_c}{T_{c,ref}} \right)^3 \exp \left[ \left( \frac{E_g N_s}{a} \right) \left( 1 - \frac{T_{c,ref}}{T_c} \right) \right] \quad (10)$$

where  $I_{o,ref}$  is diode reverse saturation-current at reference condition (A), calculate by

$$I_{o,ref} = \frac{I_{L,ref}}{\exp \left( \frac{V_{oc,ref}}{a_{ref}} \right) - 1} \quad (11)$$

$a$  is calculated as

$$a = a_{ref} \frac{T_c}{T_{c,ref}} \quad (12)$$

## 2.2 Mathematical Analysis of Hydrogen Generation Cell

The core of an electrolysis unit is an electrochemical cell, which is filled with pure water and has two electrodes connected with an external power supply. The following equations represents the cathode , anode and the total reaction existed for electrolysis of water, **Neagu, et al., 2000**.



The hydrogen flow rate, can be evaluated as, **El-shenawy, et al., 2012**:

$$Q = \eta_F \frac{I_{ely}}{nF} \times 3600 \times 0.224136 \times 1000 \quad (16)$$

where  $I_{ely}$  is the measured current of electrolyzer (A),  $\eta_F$  is Faraday efficiency, it expresses how much current is converted in the desired reaction and it is the ratio of the experimental volume of hydrogen and the theoretical volume of hydrogen, **Papagiannakis, 2005**.

$$\eta_F = \frac{V_{H_2 \text{ experimental}}}{V_{H_2 \text{ theoretical}}} \times 100 \quad (17)$$

where  $V_{H_2 \text{ experimental}}$  is the experimental volume of hydrogen can be obtained from the experimental data,  $V_{H_2 \text{ theoretical}}$  is the theoretical volume of hydrogen can be calculate as:

$$V_{H_2 \text{ theoretical}} = \frac{I \times t \times v_m}{n F} \quad (18)$$

where  $I$  is the current (A),  $t$  is the time measured during the experiment (second),  $v_m$  is the molar volume of hydrogen = 24 at 20°C (l/mol), The total efficiency of the electrolyzer is found from Eq.(19), **Papagiannakis, 2005**.

$$\eta = \frac{H_{H_2} \times V_{H_2 \text{ experimental}}}{U \times I \times t} \times 100 \quad (19)$$

where  $H_{H_2}$  is the calorific value of hydrogen = 11920 kJ/m<sup>3</sup> at 20°C,  $U$  is voltage (Volt).

### 2.3 Computer Algorithm for Determine PV Model Parameters

Matlab 2014 is used to compute the four-parameter model and establishing (I-V) and (P-V) characteristic curves. The steps of computer algorithm are shown in **Fig.1**.

### 3. EXPERIMENTAL SETUP

The experimental setup shown in **Fig. 2** consists of mono-crystalline photovoltaic module was south oriented at 45 ° with the horizontal. Each experiment was carried out from 09:00 AM to 16:00 PM for clear days and for Baghdad climate conditions. Electrical characteristics data of the solar module at reference

condition are as follows: short circuit current = 3.1A, open circuit voltage = 22V, current at maximum power point = 2.9A, voltage at maximum power point = 17.5V, power at maximum power point = 50W, with 36 cells. The hydrogen production system consist of two stainless steel plate electrodes (140×80×1) mm connect to 9Ah/12V sealed type lead-acid battery to provide the electricity needed to start water electrolysis and the battery connected to PV panel through solar charge controller type (HBSC201) 12/24V 20A. The two electrodes inserted inside two plastic graduated cylinders of 260 mm length and 90 mm diameter to collect hydrogen gas, the cylinders upside down immersed in a basin filled with water, one of electrodes is connected to the positive pole of battery to work as an anode and the other is connected to the negative pole of battery to make it as a cathode. The Schematic diagram of the experimental set-up is shown in **Fig.3**. PROVA 200 solar module analyzer shown in **Fig.4** is used to present (I-V) and (P-V) curves for solar module, calculate the maximum solar power ( $P_{\max}$ ), identify the maximum voltage ( $V_{\max}$ ), maximum current ( $I_{\max}$ ), voltage at open circuit ( $V_{\text{open}}$ ), current at short circuit ( $I_{\text{short}}$ ) and predict the electrical efficiency. Solar power meter type TES (1333R) shown in **Fig. 5** is used to measure the solar irradiation in W/m<sup>2</sup>, it has four digit display with 0.1W/m<sup>2</sup> resolution. A digital thermometer type (TPM-10) probe, LCD display, temperature range -50°C to +70°C, accuracy of ±1°C and of resolution of 0.1 located on the back side of the module to measure its temperature ( $T_c$ ) and the temperature of the basin water used in electrolysis ( $T_w$ ) as well as the ambient temperature ( $T_a$ ). An electronic balance unit type (TE214S) of 400 g capacity, 0.1mg readability, seven digit, 3second response time (average), allowable ambient operating temperature 5 °C to 40 °C, is used to measure the mass of NaOH.



### 3.1 Water Displacement Method

This method is used to measure the volume of hydrogen generated. The gas collecting cylinders are filled with water and located upside down in the basin. When the electrolysis of water begins and hydrogen with oxygen released, the gas displaces the water inside the cylinder down and takes his place and the displacement of water continues until the cylinder is filled with gas.

### 3.2 Data Analysis Processing

The electrical efficiency of the solar module is calculated using Eq.(8). The efficiency of hydrogen production system is calculated using Eq.(19). The gas pressure is evaluated as

$$P = P_{atm} - \rho gh \quad (20)$$

where  $P_{atm}$  is the atmospheric pressure,  $\rho$  is density of the liquid  $\text{kg/m}^3$ ,  $g$  is acceleration due to gravity  $= 9.8 \text{ m/s}^2$ ,  $h$  is the difference between the water level inside cylinder and the water level outside cylinder.

### 3.3 Experimental Procedure

Connect the solar module analyzer to solar module and use solar power meter to measure the solar radiation and input the value in analyzer and connect the solar module analyzer to the laptop and click auto scan button to measure open circuit voltage, short circuit current, maximum power, maximum voltage, maximum current and efficiency for each hour. Use the digital thermometer to measure the hourly temperatures for module and ambient ( $T_c$ ,  $T_a$ ) respectively. Fill the basin with 10 liters of water and dissolve 50 gram of NaOH into the basin water. Fill the cylinders with water and upside down in the basin. Insert the electrodes into the cylinders. Connect the two electrode to the power supply (battery or solar module) the electrolysis of water will begin. Insert thermometer in water basin to measure the  $T_w$ . Measure the total gas produced by using water displacement method. Record the time required to collect 100 ml of hydrogen and repeat this for (200, 300, 400, 500, 600, 700, 800, 900, 1000) ml. Change the NaOH concentration (100, 200, 300) gram and repeat the previous steps for each concentration. The results of theoretical and experimental studies were presented in Tables 1- 6.

## 4. RESULTS AND DISCUSSION

The discussions of photovoltaic module used for hydrogen generation are presented. The hydrogen production system and the effects of NaOH concentration on hydrogen production are discussed also. **Fig. 6** shows the characteristics curve for PV panel on 11<sup>th</sup> of October 2015. The current and power increase gradually from sunrise to reach their maximum value (2.73 A, 38.49 W) at 11:00 a.m because the solar radiation reach the largest value of  $1160 \text{ W/m}^2$  and decreases after that, they reach lowest value at 16:00 p.m (close to sunset) at which solar radiation was  $150 \text{ W/m}^2$ . The short circuit current ( $I_{sc}$ ) increases with solar radiation from (2.46 A) at 09:00 a.m to its maximum value (3.36 A) at 10:00 a.m and decreases gradually with solar radiation to its lowest value (0.33 A) (close to sunset). The open circuit voltage ( $V_{oc}$ ) also increases with solar radiation but it is affected by temperature of cell. ( $V_{oc}$ ) decreases when the temperature of cell increases and reach its maximum value at 15:00 p.m when solar radiation reaches

500 W/m<sup>2</sup> and solar cell reaches 39.8°C. **Fig. 7** shows theoretical calculated characteristics curve of PV panel on 11<sup>th</sup> October 2015, the power and current increase gradually from sunrise to reach their maximum value (52.33 W, 3.6 A) at 11:00 a.m and decreases after that to reach lowest value (7.06 W, 0.46 A) at 16:00 p.m. **Fig. 8** shows a comparison between experimental and theoretical work in electrical efficiency with time, the theoretical efficiency is better than experimental by (26.43%). **Fig. 9** shows the maximum power with time, the power in theoretical is better than experimental by (26.44%). This difference between theoretical work and experimental work is due to weather conditions that effect on PV panel and due to the accuracy of devices used in the measurement. Four concentration of NaOH have been tested to exhibit its effect on hydrogen production. The concentrations adopted are (50,100,200,300) gram in 10 kg of water or mass concentration of (0.5,1,2,3 %) respectively. **Fig. 10** shows accumulative volume and pressure with accumulative time for 50 gram of NaOH (0.5%) percentage mass concentration and inlet water temperature of 40°C. This figure reports a linear increase of accumulative volume accompanied by a slight increase of gas pressure (which agrees with gas law  $PV=mRT$ ) since the accumulated mass is increased by (0.2%). **Fig. 11** shows the same trend in accumulation behavior for NaOH concentration mass of (100 gram, 1% by mass). The time required to accumulate (1000 ml) was (1200 s) while that for concentration mass of (50 gram) was (2160 s) i.e. there is a saving in accumulation time equals to (960 s). **Fig. 12** represents the accumulative hydrogen volume generated for NaOH concentration mass of (200 gram, 2% by mass). It illustrates a time saving of (420 s) compared with concentration mass of 100 gram. **Fig. 13** shows accumulative volume and pressure with accumulative time at (300 gram, 3% by mass) the time saving was by (390 s) compared with 200 gram. **Fig. 14** shows the accumulative time with accumulative volume at different concentration of NaOH. An obvious improvement is reported, the time required to collect 1000 ml of hydrogen was 2160 seconds at 100 gram but at 300 gram the time decrease to 390 seconds. The inlet water temperature is higher than the ambient temperature this due to the interaction between water and sodium hydroxide, the reaction is exothermic.

#### 4.1 Comparison with Previous Results

To verify the results obtained from the present work, a comparison was made with the results achieved by previous studies. **Fig.15** shows the comparison in characteristics curve for PV panel between present study and ,**Chennouf, et al., 2012** for the same PV panel specifications, the present work shows improvement in current by (21.8 %) and in power by (20.9%). **Fig. 16** shows a comparison in time required to collect 1000 ml of hydrogen between present work and ,**Kargi, 2011** under the same type and different (shape,size) of electrodes and different type of electrolyte. The improvement in accumulative time in present work is (99.77) %.

#### 5. CONCLUSION

The present work investigates the hydrogen production using solar photovoltaic panel. The conclusion is that the power of PV panel increases by the increase of solar radiation. The short circuit current ( $I_{sc}$ ) and open circuit voltage ( $V_{oc}$ ) increases gradually with increases solar radiation. Increase the mass concentration of NaOH

decreases the time required to collect 1000 ml and therefore increases the hydrogen production rate.

## REFERENCES

- Chennouf, N., Settout, N., Negrou, B., Bouziane, K., and Dokkar, B., 2012, *Experimental Study of Solar Hydrogen Production Performance by Water Electrolysis in the South of Algeri*, Energy Procedia, Vol. 8, PP. 1280-1288.
- Dincer, I., Joshi, A. S., 2013, *Solar Based Hydrogen Production Systems*, Springer New York Heidelberg Dordrecht London.
- Eicker, U., 2003, *Solar Technologies for Buildings*, New York:Wiley.
- El-shenawy, E. T., El-seesy, I. E., and Ahmed, M. H., 2012, *Efficient Design of Hybrid PV/hydrogen System*, World Applied Sciences Journal, Vol. 9, No. 9, PP.1315-132.
- Fanne, A. H., Dougherty, B. P., and Davis, M. W., 2002, *Evaluation Building-Integrated Photovoltaic Performance Models*, In: proceedings of 29<sup>th</sup> IEEE photovoltaic specialists conference (PVSC), PP. 9-194.
- Gibson, T. L., Kelly, N. A., 2010, *Predicting Efficiency of Solar Powered Hydrogen Generation using Photovoltaic-Electrolysis Devices*, International Journal of Hydrogen Energy, Vol. 35, PP. 900-911.
- Kargi, F., 2011, *Comparison of Different Electrodes in Hydrogen Gas Production from Electrolysis of Wastewater Organics using Photovoltaic Cells (PVC)*, International Journal of Hydrogen Energy, Vol. 36, PP. 3450-3456.
- Kou, Q., Klein, A., and Beckman, W. A., 1998, *A Method for Estimating the Long-Term Performance of Direct Coupled PV Pumping System*, Solar Energy, Vol. 64, PP. 33-40.
- Neagu, C., Jansen, H., Gardeniers, H., and Elwenspoek, M., 2000, *The Electrolysis of Water : An Actuation Principle for MEMS with a Big Opportunity*, Mechatronics, PP. 571-581.
- Pamplona, D. S., 2008, *Dynamic Modeling of Hybrid PV/ Thermal Solar System for Hydrogen Production*, M.Sc. Thesis, University of Gävle, Sweden.
- Papagiannakis, I., 2005, *Studying and Improving the Efficiency of Water Electrolysis using a Proton Exchange Membrane Electrolyser*, M.Sc. Thesis, Strathclyde University, Scotland.
- Sharma, A., Tyagi, V. V., Chen C. R., and Buddhi D., 2009, *Review on Thermal Energy Storage with Phase Change Materials and Applications*, Renew sustain Energy Rev, Vol. 13, PP. 45-318.

## NOMENCLATURE

$a$  = curve-fitting parameter for the four-parameter model, dimensionless.

$a_{ref}$  = curve-fitting parameter for the four-parameter model at reference condition, dimensionless.

$A$  = module area, m<sup>2</sup>.

$E_g$  = energy-band gap, eV.

$F$  = Faraday's constant, C/mol.



$G$  = solar irradiance,  $\text{W/m}^2$ .

$G_{ref}$  = solar irradiance at reference condition,  $\text{W/m}^2$ .

$H_{H2}$  = calorific value of hydrogen,  $\text{kJ/m}^3$ .

$I$  = current of the module, A.

$I_{L,ref}$  = light-generated current at reference condition, A.

$I_{mp}$  = current at maximum-power point, A.

$I_{mp,ref}$  = current at maximum-power point at reference condition, A.

$I_o$  = diode reverse saturation-current, A.

$I_{o,ref}$  = diode reverse saturation-current at reference condition, A.

$I_{sc,ref}$  = short-circuit current at reference condition, A.

$K$  = Boltzmann's constant, J/K.

$n$  = number of electrons that are exchanged in order to release one particle at the electrode, dimensionless.

$n_I$  = diode ideality factor, dimensionless.

$N_s$  = number of cells in series in one module, dimensionless.

$P$  = power of the module, W.

$Q$  = hydrogen flow rate, 1/h.

$q$  = electron charge, Coulomb.

$R_s$  = series resistance,  $\Omega$ .

$R_{s,ref}$  = series resistance at reference condition,  $\Omega$ .

$R_{sh}$  = shunt resistance,  $\Omega$ .

$t$  = Time, s.

$T_c$  = cell temperature, K.

$T_{c,ref}$  = cell temperature at reference condition, K.

$V$  = voltage of the module, V.

$V_{H2}$  = volume of hydrogen, L.



$V_m$  = molar volume of hydrogen, l/mol.

$V_{mp,ref}$  = voltage at maximum-power point at reference condition, V.

$V_{OC,ref}$  = open-circuit voltage at reference condition, V.

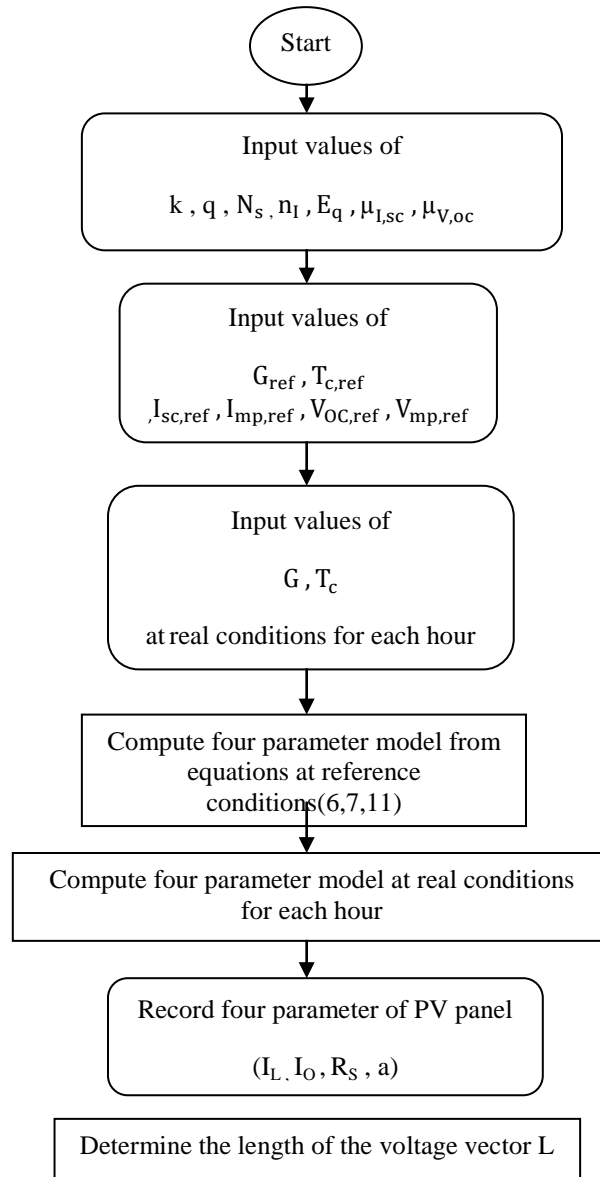
$V_t$  = thermal voltage, V.

$\eta$  = efficiency of the module at maximum-power point, dimensionless.

$\eta_F$  = Faraday efficiency, dimensionless.

$\mu_{I,sc}$  = temperature coefficient of short-circuit current, A/K.

$\mu_{V,oc}$  = temperature coefficient of open-circuit voltage, V/K.



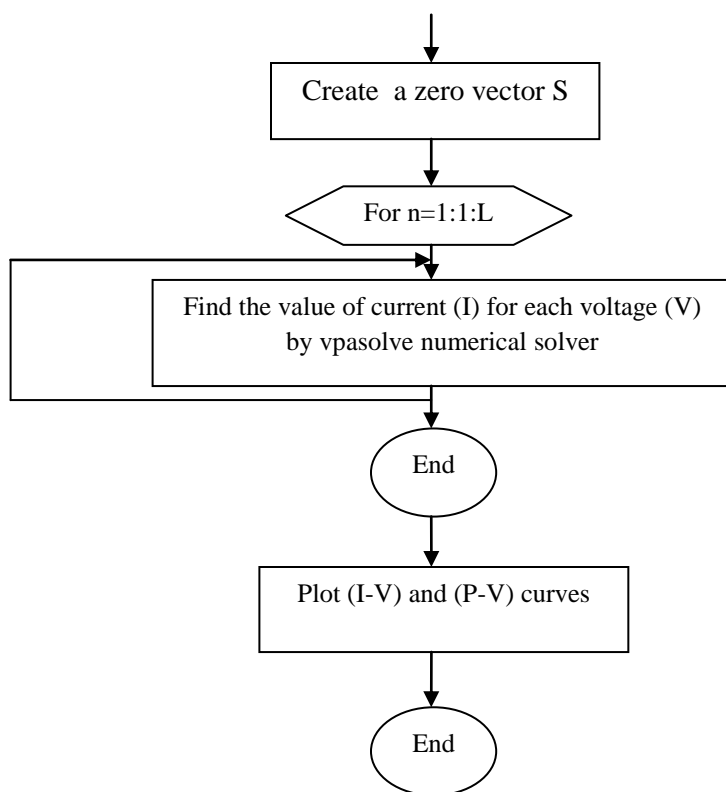


**Figure 1.** Flowchart of computer algorithm for PV panel.

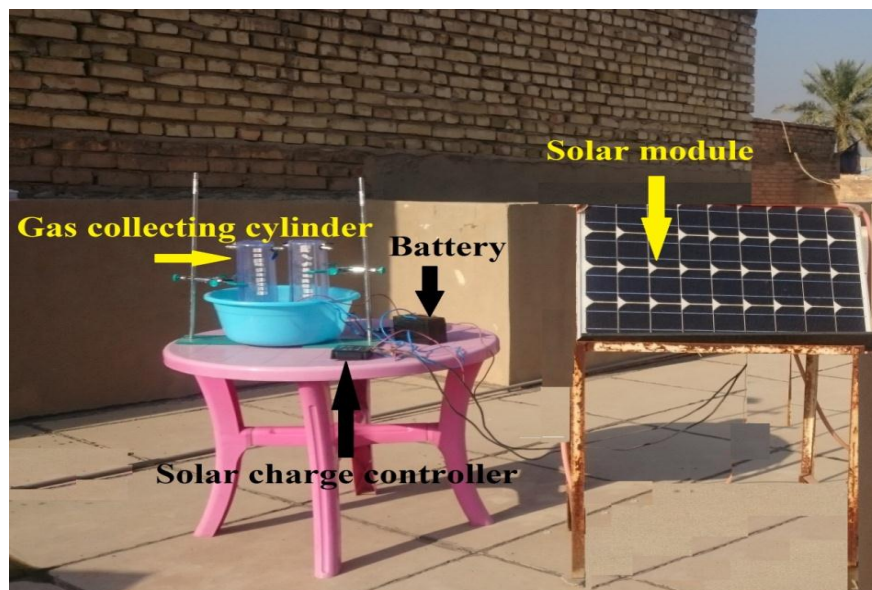


**Figure 2.** Experimental setup.



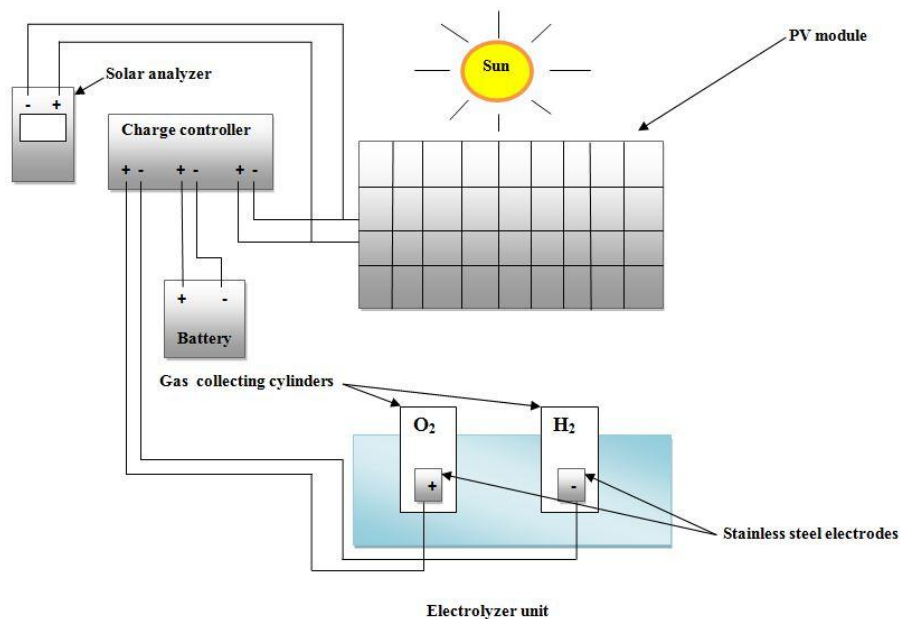


**Figure 3.** Schematic diagram of the experimental setup.

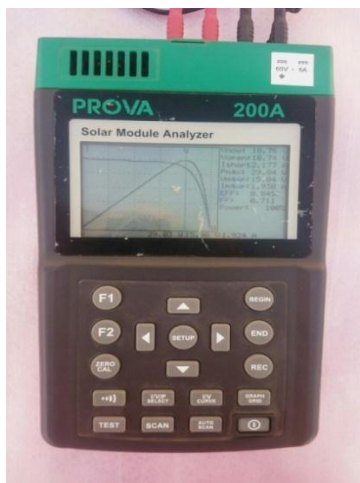
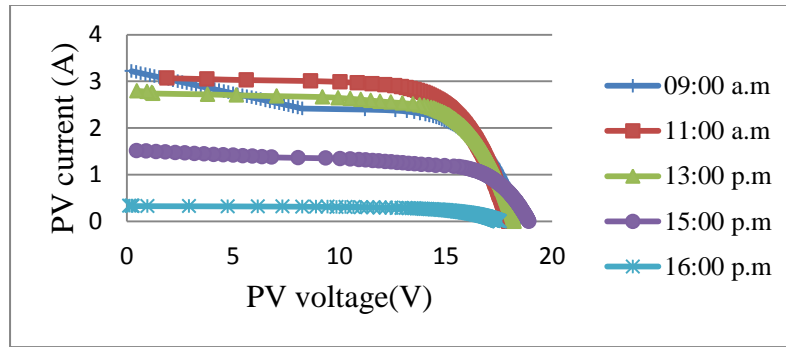


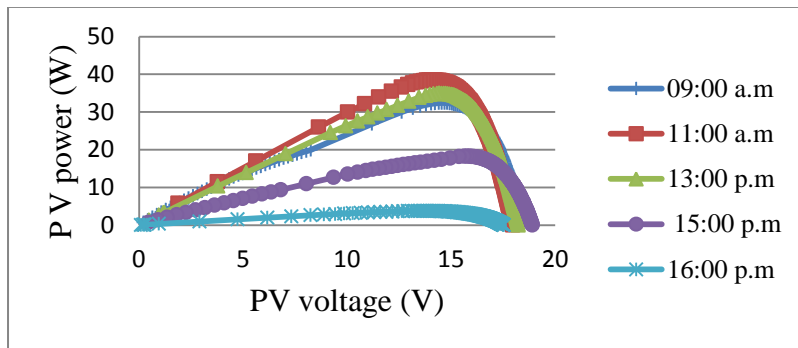
**Figure 4.** The PROVA 200 solar panel analyzer.



**Figure 5.** Solar power meter

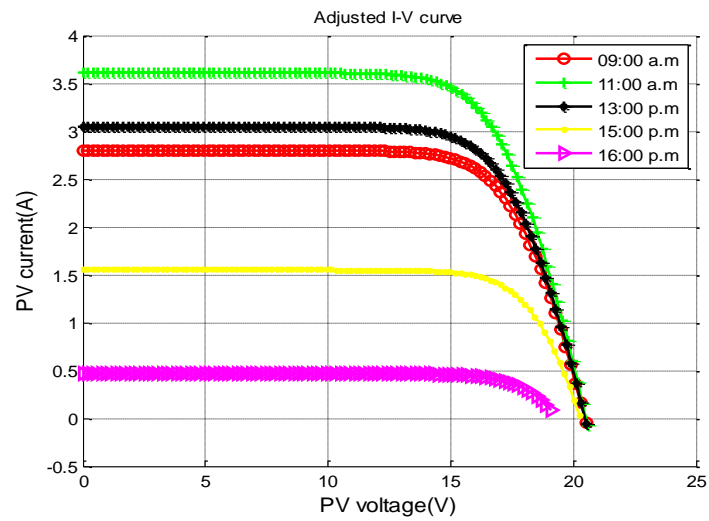


(a)

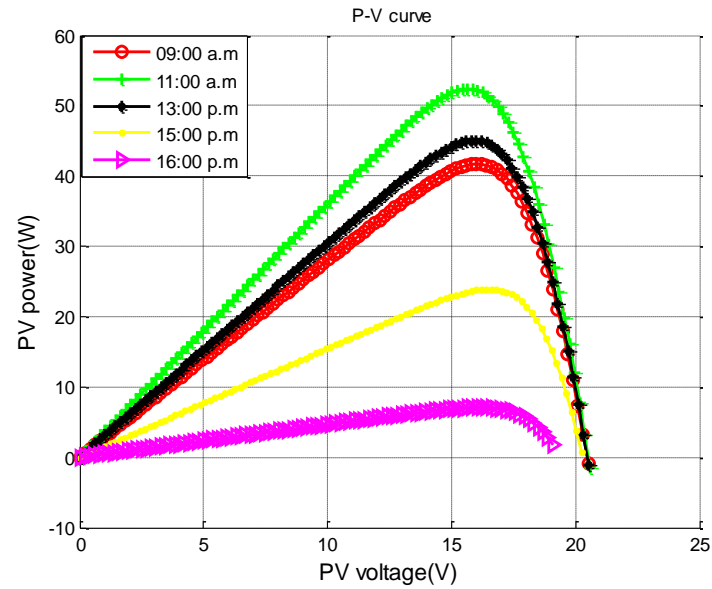


(b)

**Figure 6.** Characteristics curve of PV panel on 11<sup>th</sup> of October 2015 case I (a) I-V curve (b) P-V curve.



(a)



(b)

**Figure 7.** Theoretical characteristics of PV panel on 11<sup>th</sup> of October 2015 (a) I-V curve (b) P-V curve.

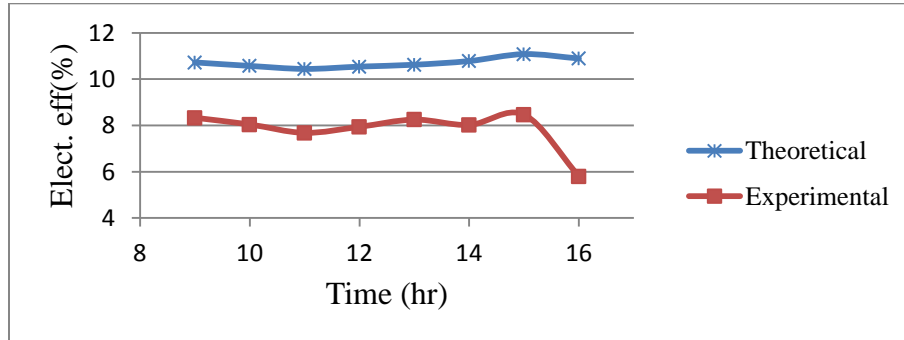


**Figure 8.** Electrical efficiency with time on 11<sup>th</sup> of October 2015.

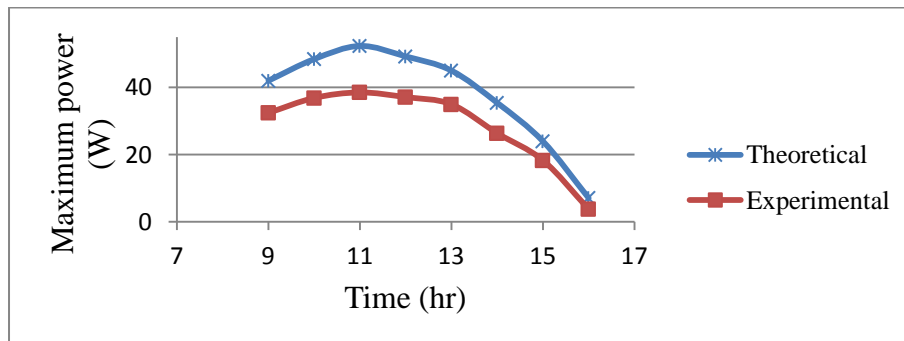


**Figure 9.** Maximum power with time on 11<sup>th</sup> of October 2015.

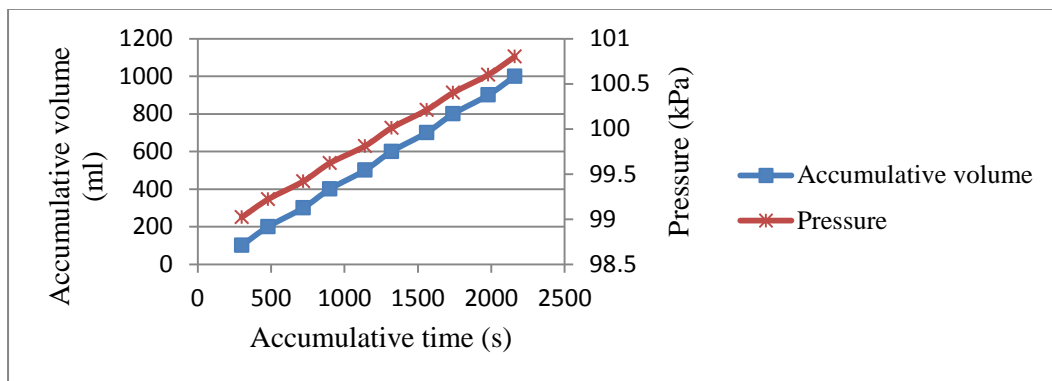


**Figure 10.** Accumulative volume and pressure with accumulative time for 50 gram NaOH concentration , 40 °C inlet water temperature and 38°C ambient temperature.

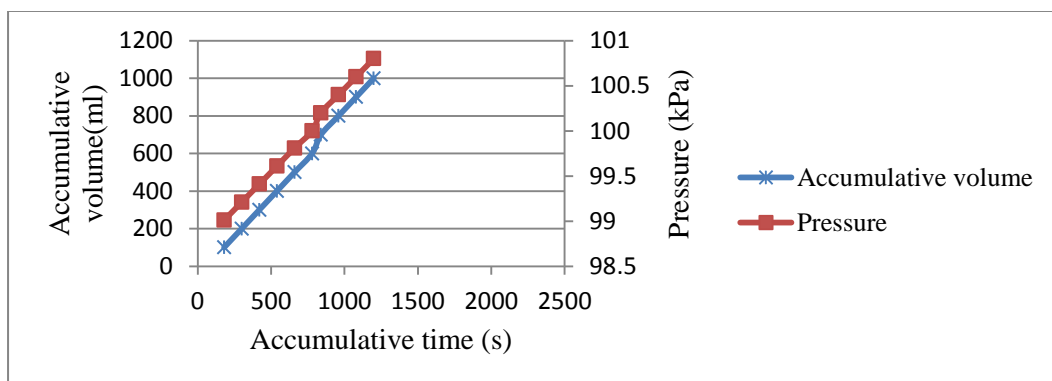


**Figure 11.** Accumulative volume and pressure with accumulative time for 100 gram NaOH concentration , 40 °C inlet water temperature and 38°C ambient temperature.

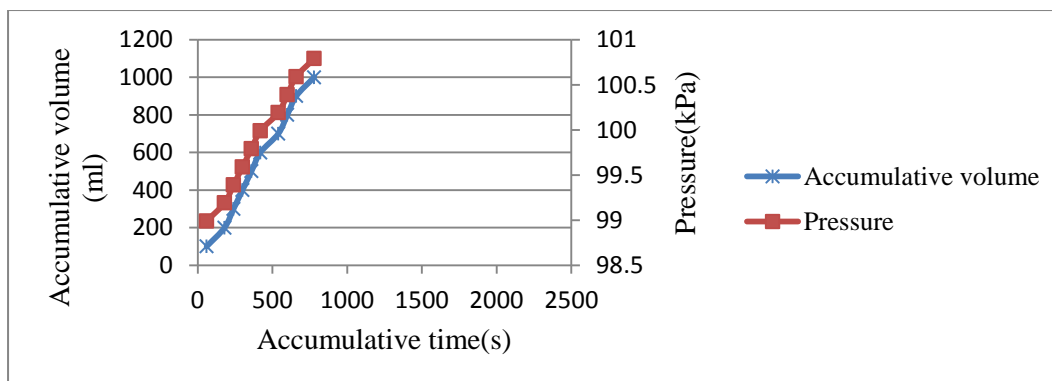


**Figure 12.** Accumulative volume and pressure with accumulative time for 200 gram NaOH concentration , 40°C inlet water temperature and 38°C ambient temperature.

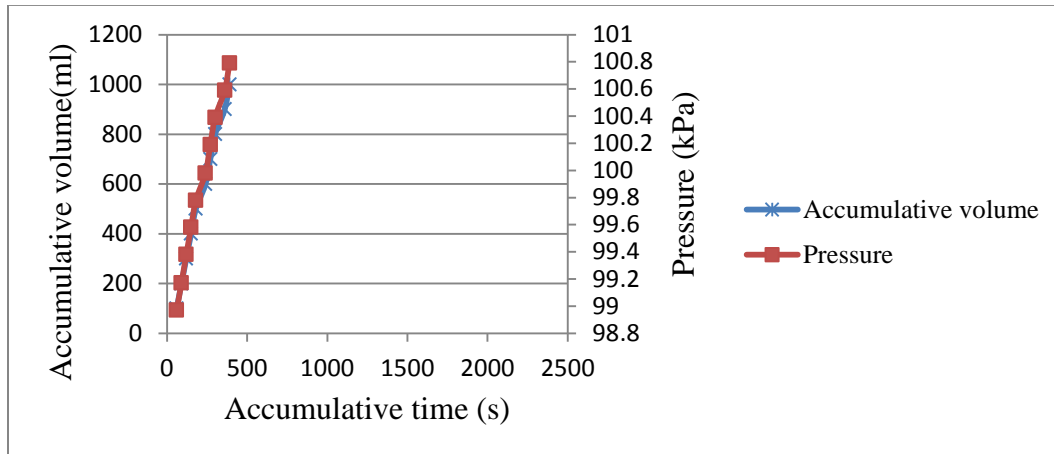


**Figure 13.** Accumulative volume and pressure with accumulative time for 300 gram NaOH concentration, 40 °C inlet water temperature and 38°C ambient temperature.

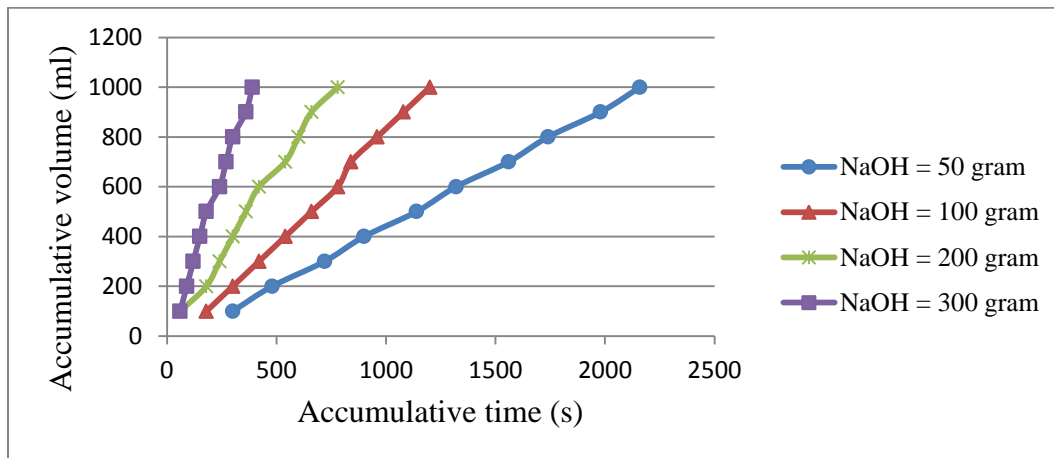


**Figure 14.** Accumulative volume with accumulative time at different concentration of NaOH.

**Table 1.** Theoretical data of photovoltaic panel at reference and real working conditions on 11<sup>th</sup> of October 2015.

Hours	a (--)	$I_L$ (A)	$R_s$ ( $\Omega$ )	$I_o$ (A)	$V_{OC}$ (A)	$P_{max}$ (W)	$\eta$ (%)
Ref.	1.01	3.10	0.58	$1.29 \cdot 10^{-9}$	22.00	50.00	11.57
09:00	1.09	2.79	0.58	$2.16 \cdot 10^{-8}$	20.51	41.69	10.72
10:00	1.10	3.29	0.58	$2.73 \cdot 10^{-8}$	20.59	48.41	10.57
11:00	1.11	3.60	0.58	$3.40 \cdot 10^{-8}$	20.58	52.33	10.44
12:00	1.10	3.35	0.58	$2.85 \cdot 10^{-8}$	20.59	49.21	10.54
13:00	1.10	3.04	0.58	$2.56 \cdot 10^{-8}$	20.52	44.99	10.62
14:00	1.09	2.36	0.58	$2.02 \cdot 10^{-8}$	20.33	35.40	10.78
15:00	1.06	1.55	0.58	$9.00 \cdot 10^{-9}$	20.23	23.95	11.08
16:00	1.05	0.46	0.58	$4.69 \cdot 10^{-9}$	19.07	7.06	10.89

**Table 2.** Experimental data of photovoltaic panel on 11<sup>th</sup> of October 2015.

Hours	P <sub>max</sub> (W)	I <sub>max</sub> (A)	V <sub>max</sub> (V)	V <sub>open</sub> (V)	I <sub>short</sub> (A)	T <sub>a</sub> (C)	T <sub>c</sub> (C)	G (W/m <sup>2</sup> )	η (%)
09:00	32.40	2.21	14.61	18.46	2.46	31.4	47.5	900	8.33
10:00	35.85	2.59	14.18	18.14	3.36	33.0	49.7	1060	8.04
11:00	38.49	2.73	14.05	17.99	3.08	34.2	51.8	1160	7.68
12:00	37.09	2.61	14.21	18.02	2.96	34.9	50.1	1080	7.94
13:00	34.95	2.42	14.43	18.25	2.81	35.1	49.1	980	8.25
14:00	26.35	1.79	14.64	18.29	2.09	34.9	46.9	760	8.02
15:00	18.28	1.15	15.77	18.93	1.52	34.2	39.8	500	8.46
16:00	3.76	0.27	13.64	17.56	0.33	33.6	34.5	150	5.80

**Table 3.** Data of hydrogen production system for NaOH=50 gram ,T<sub>w</sub> =40 °C and 38°C

No.	Accumulative time (s)	Height difference (mm)	Accumulative volume (ml)	Pressure (kPa)
1	300	200	100	99.02
2	480	180	200	99.22
3	720	160	300	99.42
4	900	140	400	99.62
5	1140	120	500	99.81
6	1320	100	600	100.01
7	1560	80	700	100.21
8	1740	60	800	100.40
9	1980	40	900	100.60
10	2160	20	1000	100.80

ambient temperature.





**Table 4.** Data of hydrogen production system for NaOH=100 gram,  $T_w = 40^\circ\text{C}$  and  $38^\circ\text{C}$  ambient temperature.

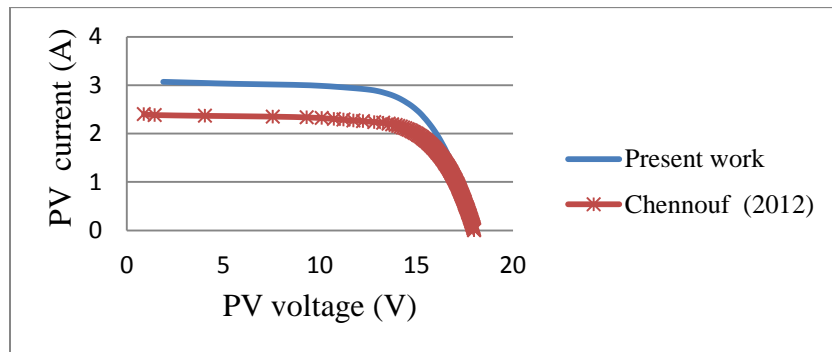
No.	Accumulative time(s)	Height difference (mm)	Accumulative volume(ml)	Pressure (kPa)
1	180	200	100	99.01
2	300	180	200	99.21
3	420	160	300	99.41
4	540	140	400	99.61
5	660	120	500	99.81
6	780	100	600	100
7	840	80	700	100.20
8	960	60	800	100.40
9	1080	40	900	100.60
10	1200	20	1000	100.80

**Table 5.** Data of hydrogen production system for NaOH=200 gram,  $T_w = 40^\circ\text{C}$  and  $38^\circ\text{C}$  ambient temperature.

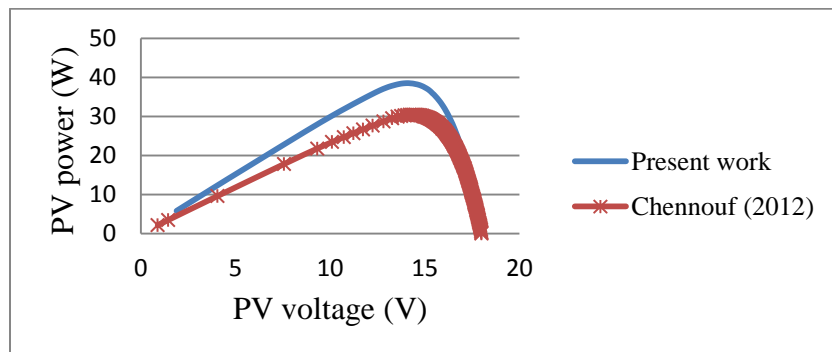
No.	Accumulative time(s)	Height difference (mm)	Accumulative volume(ml)	Pressure (kPa)
1	60	200	100	98.99
2	180	180	200	99.19
3	240	160	300	99.39
4	300	140	400	99.59
5	360	120	500	99.79
6	420	100	600	99.99
7	540	80	700	100.19
8	600	60	800	100.39
9	660	40	900	100.59
10	780	20	1000	100.79

**Table 6.** Data of hydrogen production system for NaOH=300 gram , $T_w = 40^\circ\text{C}$  and  $38^\circ\text{C}$  ambient temperature.

No.	Accumulative time(s)	Height difference (mm)	Accumulative volume(ml)	Pressure (kPa)
1	60	200	100	98.97
2	90	180	200	99.17
3	120	160	300	99.38
4	150	140	400	99.58
5	180	120	500	99.78
6	240	100	600	99.98
7	270	80	700	100.19
8	300	60	800	100.39
9	360	40	900	100.59
10	390	20	1000	100.79

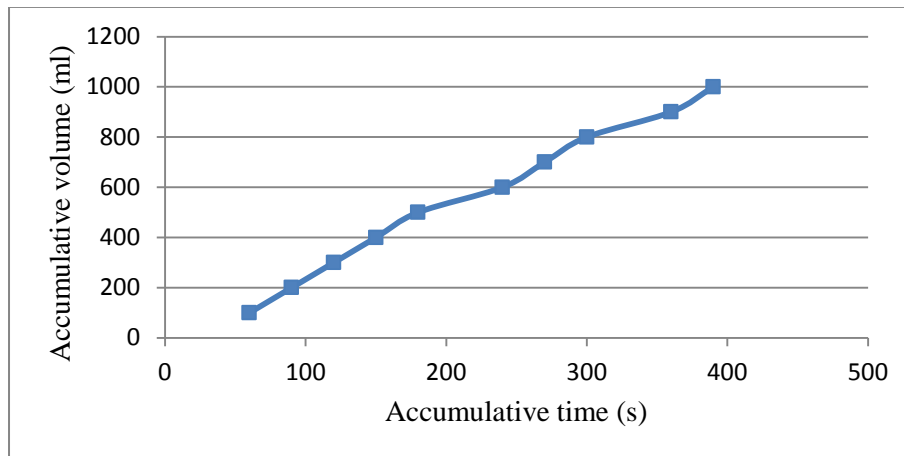


(a)

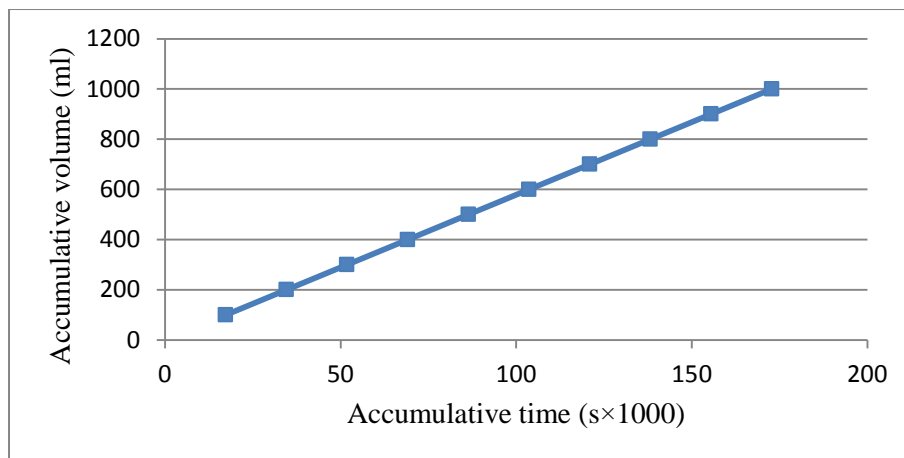


(b)

**Figure 15.** Comparison with previous results (a) (I-V) curve (b) (P-V) curve.



(a)



(b)

**Figure 16.** Accumulative time with accumulative volume (a) present work (b) **Kargi, 2011.**

## Determination of Mono-crystalline Silicon Photovoltaic Module Parameters Using Three Different Methods

Emad Talib Hahsim

Assistant Professor

Department of Energy Engineering/ College of Engineering / University of Baghdad

emadchem70@yahoo.com

### ABSTRACT

For modeling a photovoltaic module, it is necessary to calculate the basic parameters which control the current-voltage characteristic curves, that is not provided by the manufacturer. Generally, for mono crystalline silicon module, the shunt resistance is generally high, and it is neglected in this model. In this study, three methods are presented for four parameters model. Explicit simplified method based on an analytical solution, slope method based on manufacturer data, and iterative method based on a numerical resolution. The results obtained for these methods were compared with experimental measured data. The iterative method was more accurate than the other two methods but more complexity. The average deviation of the iterative method not more than 5% of current- voltage values with the corresponding experimental data. The average deviation for the other two method 9.3% for slope method and 7.9% for simplifies method.

**Key words:** photovoltaic; module parameters; modeling; temperature effect;

### حساب عوامل لوح السلكون الفوتوفولتائي احادي التبلور باستخدام ثلاث طرق مختلفة

د. عماد طالب هاشم

أستاذ مساعد

قسم هندسة الطاقة/كلية الهندسة/جامعة بغداد

### الخلاصة

من الضروري لنمذجة اللوح الفوتوفولتائي حساب العوامل الاساسية التي تحكم بمنحنيات التيار- الفولتية والتي لا تعطى من قبل الجهة المصنعة. تم انجاز عمل جاد لحساب تلك العوامل. بشكل عام ، مقاومة التوالي تكون عالية بالنسبة للوح الشمسي نوع السيليكون احادي التبلور وفي هذا النموذج يمكن اهمالها. وبهذه الدراسة تم استخدام ثلاث طرق . الطريقة الضمنية المبسطة وتعتمد على الحل التحليلي، طريقة الميل وتعتمد على بيانات المصنع وطريقة التكرار وتعتمد على حل عددي. تمت مقارنة النتائج المستخلصة من الطرق المذكورة مع نتائج القياسات المختبرية وكانت طريقة التكرار الاكثر دقة ولكن الاكثر تعقيدا من بين الطرق الثلاث. معدل الانحراف لطريقة التكرار لم تكن اكثر من 5% لقيم التيار – الفولتية مقارنة مع القيم العملية. معدل الانحراف للطريقتين الاخرى كانت 9.3% لطريقة الميل و 7.9% لطريقة للطريقة الضمنية المبسطة.

## 1. INTRODUCTION

The world faces a big problem of depletion of conventional sources of energy which have to be replaced by new ones. The solar energy is one of the fast developing renewable energy sources. Solar energy may be used to produce thermal energy for residential requirements and can be used to produce electricity indirectly by converting the heat generated to electrical energy through heat engine or directly using photovoltaic (PV) solar system.

Solar is envisaged to be an important source of energy in the future. In particular, the photovoltaic (PV) power system, which converts solar energy to electrical power, is becoming a popular renewable energy source due to its long term economic prospect and ease of maintenance. However, due to high initial cost of such a system, optimal capturing of the available solar energy has to be ensured. Enormous amount of work has been carried out to physically improve the performance of solar cells/modules **Wang Y. et al, 2009**. However, it appears that a proper system design also plays a vital role in increasing the overall efficiency. One area that could complement this effort is the development of a reliable and efficient PV simulator which can be used to optimize the system design prior to installation **Ishaque K et al, 2011**. The accuracy of commercially available software for PV module or system simulation mainly depends on the accuracy of the solar cell/module models and the extraction method being used to determine the model's parameters. The choice of a model that closely emulates the characteristics of solar modules is very crucial; a model is known to be accurate if it fits the measured I–V data at all operating conditions. Over the years, several models are introduced – among the more popular ones are the circuit based single diode and the two diode model. The latter, despite it is more computationally extensive, is preferable because its I–V characteristics closely resemble the behavior of a physical module **Walker, 2001**.

Generally, there are two possible approaches to extract the solar module parameters: (1) the analytical **Chan DSH, 1987**, and (2) numerical extraction techniques **Liu C-C, 2008**. The former requires information on several key points of the I–V characteristic curve, i.e. the current and voltage at the maximum power point ( $M_{PP}$ ), short-circuit current ( $I_{SC}$ ), open-circuit voltage ( $V_{OC}$ ), and slopes of the I–V characteristic at the axis intersections. Accuracy depends on the correctness of the selected points (short current, open current voltage, and maximum power point) on the I–V curve. It has to be noted that the I–V curve is highly non-linear and any wrongly selected points may result in significant errors in the computed parameters. Furthermore, a typical module datasheet provides only information at Standard Test Condition (STC).

However, it is known that the parameters vary with environmental conditions such as irradiance and temperature. On the other hand, the numerical extraction technique is based on certain mathematical algorithm to fit all the points on the I–V curve. More accurate results can be obtained because all the points on the I–V curve are utilized. Deviation of several data points may not severely affect the accuracy of the parameters as in the case of the analytical approach. However, the curve-fitting algorithm requires extensive computation. Its accuracy depends on the type of fitting algorithm, the cost function and the initial values of the parameters to be extracted **Gottschalg R., 1999**. As the number of

parameters in the model increases, the conventional extraction methods lose their ability to provide accurate values.

The growing of PV technologies led many researchers to focus on the various sides of PV system components from the basic fundamental cell manufacturing to the large PV power station modeling, sizing and performance of PV modules with the environmental conditions changes **Hernanz et al., 2010, Andrews et al., 2012, Chouder et al., 2012, and Chakrasali et al., 2013**. Modeling of PV module provides ways to understand the voltage, current, and power relationships. The estimation of mathematical models is affected by various factors, which ultimately alter the behavior of voltage and current.

Solar cells are the basic components of the PV systems to convert solar radiation into electrical power. They are connected in series or in parallel to form a PV module. The electric behavior of a photovoltaic device under given operating conditions is characterized by its electrical parameters and the current-voltage (I-V) curves describing its operation. Equivalent electrical circuit of PV cell, module and array is configured with either single or double diode with taking in consideration the connection of the cells or the modules in either series or parallel. The single diode models usually have seven, five, four, or even three unknown parameters. The four unknown parameters of a single diode model the photocurrent ( $I_{ph}$ ), the saturation current ( $I_o$ ), diode ideality factor ( $A$ ) and the series resistance ( $R_s$ ). These parameters are determined from measurements of the I-V characteristic at reference values of irradiance and temperature ( $G_{ref} = 1000 \text{ W/m}^2$ ,  $T_{ref} = 25 \text{ }^\circ\text{C}$ , spectrum AM1.5), many researchers have presented methods to extract these parameters from data mainly provided by manufacturers **De Soto et al., 2006, Carrero et al., 2011 and Sera et al., 2007**. The four parameter model assumes that the shunt resistance is infinite and it is ignored **Kuo et al., 2001**. In three parameters model the series resistance assumed to be zero in addition to the infinite shunt resistance.

In this work, three different methods are used to determine the unknown parameters: the photocurrent ( $I_{ph}$ ), the saturation current ( $I_o$ ), diode ideality factor ( $A$ ) and the series resistance ( $R_s$ ) of a mono-crystalline silicon solar module. The models provide the calculation of the equation of the I-V characteristic curves and compare the results with the I-V curves extracted from experimental measurements.

## 2. FOUR PARAMETERS MODEL

For simplicity, the single-diode model shown in **Fig. 1** offers a good compromise between simplicity and accuracy and has been used by numerous authors **Arab et al., 2004, Carrero et al. 2007 and Celik and Acikgoz, 2007**. The four-parameter model assuming the shunt resistance as infinite, the four-parameter model is obtained from the basic equation of output current  $I$  of the PV module **Townsend, 1989**:

$$I = I_{ph} - I_o \left[ \exp \left( \frac{q (V + I R_s)}{N_s A k_B T} \right) - 1 \right] \quad (1)$$



where,  $I$ : output current of photovoltaic module,  $A$ ,  $I_{ph}$ : photo-generated current,  $A$ ,  $I_o$ : reverse saturation current,  $A$ ,  $q$ : the charge of electron  $=1.6 \times 10^{-19}$  C,  $V$ : output voltage of photovoltaic module,  $V$ ,  $R_s$ : series resistance,  $\Omega$ ,  $N_s$ : the number of solar cells connected in series,  $A$ : diode ideality factor,  $k_B$ : Boltzmann's constant  $=1.38 \times 10^{-23}$ ,  $T$ : solar module temperature,  $^{\circ}C$ .

Three important points on the I-V curve are given by manufacturer at STC (short circuit current, open circuit voltage and maximum power point) so, Eq. (1) can be written as **Townsend, 1989**:

Short circuit current point  $(0, I_{sc})$ :

$$I_{sc} = I_{ph} - I_o \left[ \exp \left( \frac{q I_{sc} R_s}{N_s A k_B T} \right) - 1 \right] \quad (2)$$

Open circuit voltage point  $(V_{oc}, 0)$ :

$$0 = I_{ph} - I_o \left[ \exp \left( \frac{q V_{oc}}{N_s A k_B T} \right) - 1 \right] \quad (3)$$

Maximum power point  $(V_m, I_m)$ :

$$I_m = I_{ph} - I_o \left[ \exp \left( \frac{q (V_m + I_m R_s)}{N_s A k_B T} \right) - 1 \right] \quad (4)$$

### 3. PARAMETERS IDENTIFICATION METHODS

Three different methods will be used to evaluate the four parameters. The first one is the explicit simplified method which is based on a purely mathematical solution with some simplifications. The second one is the method of slope which is based in part of its algorithm on a geometry calculation, and the third one is the iterative method which is based in part of its algorithm on a numerical resolution.

#### 3.1 Simplified explicit method

This method considers the following assumptions **Eckstein, 1990**:

$$I_{ph} = I_{sc} \quad (5)$$



From Eq. (3) the value of exponential is much greater than one, so:

$$0 = I_{ph} - I_o \left[ \exp \left( \frac{q V_{oc}}{N_s A k_B T} \right) \right] \quad (6)$$

From Eq. (5) and Eq. (6) one can deduce the saturation current:

$$I_o = I_{sc} \exp \left( - \frac{q V_{oc}}{N_s A k_B T} \right) \quad (7)$$

From that Eq. (1) becomes:

$$I = I_{sc} \left[ 1 - \exp \left( \frac{q (V - V_{oc} + I R_s)}{N_s A k_B T} \right) \right] \quad (8)$$

From Eq. (4) the value of exponential is much greater than one, so:

$$I_m = I_{sc} - I_o \left[ \exp \left( \frac{q (V_m + I_m R_s)}{N_s A k_B T} \right) \right] \quad (9)$$

Substituting Eq. (7) in Eq. (9):

$$I_m = I_{sc} \left[ 1 - \exp \left( \frac{q (V_m + I_m R_s)}{N_s A k_B T} \right) \right] \quad (10)$$

Then the series resistance can easily found from:

$$R_s = \frac{\frac{N_s A k_B T}{q} \ln \left( 1 - \frac{I_m}{I_{sc}} \right) + V_{oc} - V_m}{I_m} \quad (11)$$

The ideality factor A, is determined from the fact that the derivative of the maximum power equals zero:

$$\frac{\partial P}{\partial V} = \frac{\partial (IV)}{\partial V} = V \frac{\partial I}{\partial V} + I = 0 \quad (12)$$

Substituting the derivative of Eq. (1), Substituting  $I_o$  from Eq. (7) and  $R_s$  from Eq. (11). Then A can be found:

$$A = \frac{q}{N_s k_B T_c} \cdot \frac{2V_m - V_{oc}}{\left[ \frac{I_m}{I_{sc} - I_m} + \ln \left( 1 - \frac{I_m}{I_{sc}} \right) \right]} \quad (13)$$

### 3.2 Slope Method

The difference given by this method in comparison of the previous method is in the manner of calculating the series resistance **Walker, 2001, Gow and Manning, 1999**. It is based on the fact that the series resistance influences remarkably the slope of the characteristic curve I-V in the vicinity of the point  $(V_{oc}, 0)$ . So, in order to calculate  $R_s$  one uses the derivative of current described in Eq. (1) as:

$$\frac{dI}{dV} = -I_o \left[ \exp \left( \frac{q(V + I R_s)}{N_s A k_B T} \right) - 1 \right] \frac{q}{N_s k_B T_c} \left( 1 + R_s \frac{dI}{dV} \right) \quad (14)$$

$$R_s = - \frac{dV}{dI} \text{ at } V_{oc} - \frac{1}{\frac{I_o q}{N_s k_B T_c} \exp \left( \frac{q V_{oc}}{N_s A k_B T} \right)} \quad (15)$$

The slope  $\frac{dV}{dI}$  at the point  $(V_{co}, 0)$  is deduced geometrically from manufacturer data (**Fig. 2**).

### 3.3 Iterative Method

This method differs from the two previous methods in the way of calculating of the series resistance, where the temperature coefficient of the open circuit voltage given by experimental data may be used to provide an additional equation for calculating the series resistance. The temperature coefficient of the open circuit voltage can be evaluated theoretically from the derivative of the open circuit voltage with respect to temperature as follows:

$$\mu_{V_{oc}} = \frac{\partial V_{oc}}{\partial T} = \frac{A N_s k_B}{q} \left[ \ln\left(\frac{I_{sc}}{I_o}\right) + \frac{T \mu_{I_{sc}}}{I_{sc}} - 3 - \frac{q E_g}{A k_B T} \right] \quad (16)$$

In this method, the value of  $R_s$  is calculated, Using an iterative method in the interval  $[0, R_{s,max}]$ , where  $R_{s,max}$  is the maximum possible value of series resistance **Celik and Acikgoz, 2007, Townsend, 1989**. The value of A is close to 1 for  $R_{s,max}$ , so set  $A = 1$  in Eq. (11), that yields to:

$$R_{s,max} = \frac{\frac{N_s k_B T}{q} \ln\left(1 - \frac{I_m}{I_{sc}}\right) + V_{oc} - V_m}{I_m} \quad (17)$$

The other three parameters are calculated using the same equations Eq. (5), Eq. (7) and Eq. (11) as the first method.

The behavior of the PV module output with change in solar radiation and temperature is presented by many authors. The short circuit current has a linear relationship with the solar irradiance while the open circuit voltage has a logarithmic with solar irradiance. The temperature coefficients provided by the manufacturer or evaluated experimentally used to predict the variations of different PV output parameters with temperature. That can be presented in the following formulas:

$$I_{sc} = I_{sc,ref} \frac{G}{G_{ref}} + \mu_{sc}(T - T_{ref}) \quad (18)$$

$$V_{oc} = V_{oc,ref} + V_T \ln\left(\frac{G}{G_{ref}}\right) + \mu_{oc}(T - T_{ref}) \quad (19)$$

where,  $V_T$  is the thermal voltage which is given by:

$$V_T = \frac{N_s A k_B T}{q} \quad (20)$$

The ideality factor varies with temperature as given by **Villalva, 2009**:

$$\frac{A}{A_{ref}} = \frac{T}{T_{ref}} \quad (21)$$

The change of the reverse saturation current with temperature as given by Villalva, 2009:

$$I_o = I_{o,ref} \left( \frac{T}{T_{ref}} \right)^3 \exp \left[ \frac{q E_g}{A k_B} \left( \frac{1}{T|_{ref}} - \frac{1}{T|_T} \right) \right] \quad (22)$$

#### 4. EXPERIMENTAL WORK

A mono-crystalline silicon solar PV module is used with electrical specification listed in **Table 1**. The performance of the module is tested at different conditions in the Energy Engineering Department/College of Engineering / University of Baghdad. The exponential work have made during the five months from April to June 2015. This work is done at an average ambient temperature of 38 °C and average wind speed 2.3 km/hr.

The output parameters of the module are measured by Prova200 solar panel analyzer which is a device used for testing of PV modules. When it is used in the installation of solar panels, the Prova 200 solar panel analyzer assists in determining the proper inverter size as well as optimum power output position of panels and helps identify defective cells or panels that have worn out over time.

The solar panel analyzer also provides the user with current and voltage (IV) test curves, maximum solar power as well as current and voltage. Solar cell properties are easily determined using the following units: I-V Curve Test for Solar Cell, Single Point I-V Test, Maximum Solar Power ( $P_m$ ) search by auto-scan, Maximum Voltage ( $V_m$ ) at  $P_m$ , Maximum Current ( $I_m$ ) at  $P_m$ , Voltage at open circuit ( $V_{oc}$ ), Current at short circuit ( $I_{sc}$ ), I-V curve with cursor, Efficiency (%) calculation of solar panel, Scan delay setting (0 ~ 9999ms) (*i. e. solar module analyzer will be operate with load resistance (0-  $\infty$   $\Omega$ ) connected with the solar module range with a time not more than 9999 ms (approximately 10 sec)*), Solar panel area setting range (0.001 m<sup>2</sup> ~ 9999 m<sup>2</sup>), Standard light source setting. (10 W/m<sup>2</sup> ~ 1000 W/m<sup>2</sup>), Min. power setting for alarm function, Built-in Calendar Clock, Rechargeable batteries with built-in charging circuit, Optical USB cable for PC and The terminals of solar cell.

TES-1333R solar power meter has been used to measure the incident solar radiation on the PV module. The measuring range of the solar power meter is 0-2000 W/m<sup>2</sup> with resolution of 0.1 W/m<sup>2</sup> and induced error of  $\pm 0.38$  W/m<sup>2</sup>/°C. The temperature of the back side of the module is measured by a simple thermometer TPM-10 thermocouple.

#### 5. RESULTS AND DISCUSSION

Firstly, the unknown parameters are evaluated by the different methods using Matlab based on the data provided by the manufacturer in STC. Secondly, from the results it is possible to estimate the performance of solar module for different radiations and temperatures. To validate the four parameter model, an experimental data extracted from outdoor measured data. The outdoor exposure tests were done on May 21, 2015 in the Energy Engineering Department/College of Engineering / University of Baghdad.

Matlab code used for the calculation process of the four parameter at STC and the results of the program are tabulated in **Table 2**. Two cases of different solar radiation and temperature were considered and introduced in **Table 3** and **Table 4**. Based on these values of the four parameters, it is possible to plot the I-V and P-V curves at specific conditions.

**Fig. 4** and **Fig. 5** give the results of I-V and P-V curves of the three methods and from the experimental results at different operating module temperature 25°C and 50°C. When the operating module temperature increases, the output current increases marginally while the output voltage decreases dramatically, which results in a net reduction in the output power. There was a deviation at the open circuit region because of the difference in the approaches to determine the series resistance. The slope method showed the largest deviation from the experimental curves followed by the simplified explicit method. The iterative method has been shown a good agreement with the experimental results.

To show the effect of irradiance on the performance of a module, the temperature was kept fixed at 25°C and measurements was taken for two incident solar radiations 750 and 1000W/m<sup>2</sup>. From **Fig. 6** and **Fig. 7** the short circuit current increased from 1.27A to 1.7A while the open circuit voltage showed a small raise.

The average deviation of the iterative method not more than 5% of current- voltage values with the corresponding experimental data. The average deviation for the other two method 9.3% for slope method and 7.9 for simplifies method.

## 6. CONCLUSION

In order to evaluate the PV module parameters defining and measuring its characteristic curves (I-V and P-V curves) are achieved. Three different methods of PV module parameters extracting have been examined. The values of the parameters were used to simulate the current-voltage and power-voltage characteristics of the module. The three methods were, explicit simplified method based on an analytical solution, slope method based in part of on an experimental data, and iterative method based on a numerical resolution. The iterative method was more accurate than the other two methods but more complexity. The average percentage error of the iterative method not more than 5% of current- voltage values with the corresponding measured data. The average percentage error for the slope method is 9.3% while for simplified method is 7.9%.

## REFERENCES

- Andrews R. B., Pollard A., and Pearce J. M., 2012, *Improved parametric empirical determination of module short circuit current for modeling and optimization of solar photovoltaic systems*, Solar Energy, vol. 86, pp. 2240–2254.
- Arab, A. H., Chenlo, F., Benghanem, M., 2004. *Loss of load probability of photovoltaic water pumping systems*, Solar Energy 76: 713–723.





- Carrero, C., Amador, J. and Analtes, S., 2007. *A single procedure for helping PV designers to select silicon PV modules and evaluate the loss resistances*, Renewable Energy 32 : 2579–2589.
- Carrero, C., Ramirez, D., Rodriguez, J., Platero, C.A., 2011. *Accurate and fast convergence method for parameter estimation of PV generators based on three main points of I–V curve*. Renew. Energy 36, 2972–2977.
- Celik A. N., Acikgoz N., 2007. *Modelling and experimental verification of the operating current of mono-crystalline photovoltaic modules using four- and five-parameter models*, Applied Energy 84, 1–15.
- Chakrasali R. L., Sheelavant V. R., and Nagaraja H. N., 2013. *Network approach to modeling and simulation of solar photovoltaic cell*, Renewable and Sustainable Energy Reviews, vol. 21, pp. 84–88.
- Chan DSH, Phang JCH, 1987. Analytical methods for the extraction of solar-cell single- and double-diode model parameters from I–V characteristics. Electron Dev IEEE Trans;34:286–93.
- Chouder A., S. Silvestre, N. Sadaoui, and L. Rahmani, 2012. *Modeling and simulation of a grid connected PV system based on the evaluation of main PV module parameters*, Simulation Modeling Practice and Theory, vol. 20, no. 1, pp. 46–58.
- De Soto, W., Klein, S.A., Beckman, W.A., 2006. *Improvement and validation of a model for photovoltaic array performance*. Sol. Energy 80, 78–88.
- Eckstein J. H., “*Detailed modeling of photovoltaic components*”. MS thesis, Solar Energy Laboratory, University of Wisconsin, Madison, 1990.
- Gottschalg R., 1999. The influence of the measurement environment on the accuracy of the extraction of the physical parameters of solar cells. Meas Sci Technol ;10:796.
- Gow, J.A., Manning, C. D., 1999. “*Development of a photovoltaic array model for use in power electronics simulation studies*,” IEE Proceedings on Electric Power Applications, vol. 146, no. 2, pp. 193–200.
- Hernanz J. A. R., Ampayo Martin J. J. C., Belver I. Z., Lesaka J. L., Guerrero E. Z., and Perez E. P., March 2010. *Modeling of photovoltaic module*, in Proceedings of the International Conference on Renewable Energies and Power Quality (ICREPQ '10), Granada, Spain.



- Ishaque K, Salam Z, Taheri H, Syafaruddin, 2011. Modeling and simulation of photovoltaic (PV) system during partial shading based on a two-diode model. *Simul. Model Pract. Theory* 19:1613–26.
- Kuo, Y.C., Liang, T.J. and Chen, J.F., 2001. *Novel maximum-power point-tracking controller for photovoltaic energy conversion system*,” *IEEE Transactions on Industrial Electronics*, vol. 48, no. 3, pp. 594–601.
- Liu C-C, Chen C-Y, Weng C-Y, Wang C-C, Jenq F-L, Cheng P-J, et al., 2008. Physical parameters extraction from current–voltage characteristic for diodes using multiple nonlinear regression analysis. *Solid-State Electron* ;52:839–43.
- Sera, D., Teodorescu, R., Rodriguez, P., 2007. *PV panel model based on datasheet values*. In: *IEEE International Symposium on Industrial Electronics*, 2007. *ISIE 2007*. IEEE, pp. 2392–2396.
- Townsend, T. U., 1989. *A method for estimating the long term performance of direct-coupled photovoltaic systems*. MS Thesis, Solar Energy Laboratory, University of Wisconsin, Madison.
- Villalva M. G., J. R. Gazoli, and E. R. Filho, “*Comprehensive Approach to Modeling and Simulation of Photovoltaic Arrays*”, *IEEE Transactions On Power Electronics*, 2009, vol. 24, no. 5, pp 1198-1208
- Walker G., 2001. *Evaluating MPPT converter topologies using a MATLAB PV model*, *Journal of Electrical & Electronics Engineering*, Australia, *IE Aust*, vol.21, No. 1, pp.49-56.
- Wang Y, Fang Z, Zhu L, Huang Q, Zhang Y, Zhang Z, 2009. liquids The performance of silicon solar cells operated in. *Applied Energy* ;86:1037–42.

## NOMENCLATURE

A =diode ideality factor

$I_{sc}$  =short circuit Current, A

$I_{ph}$  =photo-generated current, A

G =solar radiation,  $W/m^2$

$I_m$  =current at maximum power point, A

$I_o$  =reverse Saturation current, A

$N_s$  =number of cells



$q$  =charge of electron, C

$k_B$  =Boltzmann constant.

$V_{oc}$  =open circuit Voltage, V

$R_s$  =series resistance,  $\Omega$

$V_m$  =voltage at maximum power point, V

$P_m$  =maximum Power output, W

**Table 1.** Solar module specifications.

Area	0.26 m <sup>2</sup>
Short circuit current $I_{sc \text{ ref}}$	1.9
Open circuit voltage $V_{oc \text{ ref}}$	22
$P_{maxref}$	30
Current at maximal power point	1.76
Voltage at maximal power point $V_{m \text{ ref}}$	17
Temperature coefficient of open circuit voltage $\mu V$	-0.073
Temperature coefficient of short circuit current $\mu_{Isc}$	0.00086
Number of cell in series	36
Slope at open circuit region	-1.142

**Table 2.** Four parameters values at reference STC.

	Simplified method	Slope method	Iterative method
$I_{ph}$	1.9000	1.9000	1.9000
$I_o$	2.2171e-08	2.2171e-08	1.26619e-10
$A$	1.3021	1.3021	1.015099
$R_s$	1.0562	0.506	1.458200

**Table 3.** Four parameters values at 750W/m<sup>2</sup> and 25°C.

	Simplified method	Slope method	Iterative method
$I_{ph}$	1.425	1.425	1.425
$I_o$	2.16E-08	2.22E-08	1.18E-10
$A$	1.612892	0.861567	1.33696
$R_s$	0.540277	0.506	-1.02309

**Table 4.** Four parameters values at  $1000\text{W/m}^2$  and  $50^\circ\text{C}$ .

	Simplified method	Slope method	Iterative method
$I_{ph}$	1.911801	1.911801	1.911801
$I_o$	2.32E-08	2.16E-08	1.21E-10
$A$	0.322334	1.196524	1.218119
$R_s$	1.997061	0.849815	2.323333

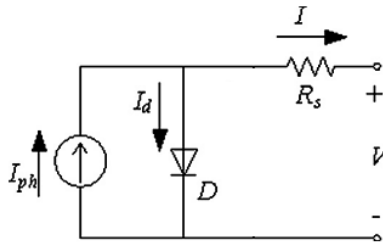


**Figure 1.** Equivalent circuit for four parameters model of a solar cell

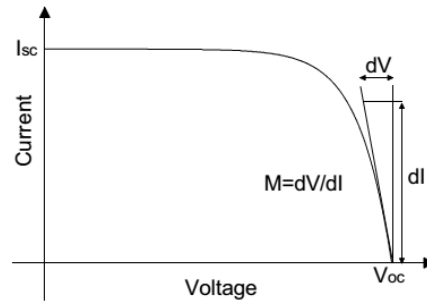


**Figure 2.** The slope at the open circuit voltage region at the I-V curve

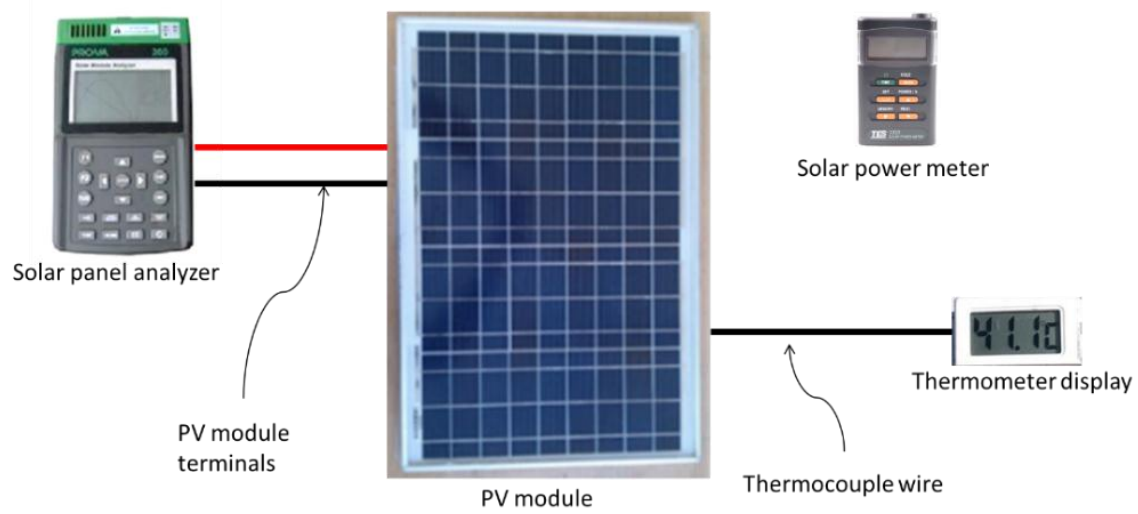


**Figure 3.** Measurement apparatus (left) PROVA200A solar module analyzer, (right) TES133R solar power meter

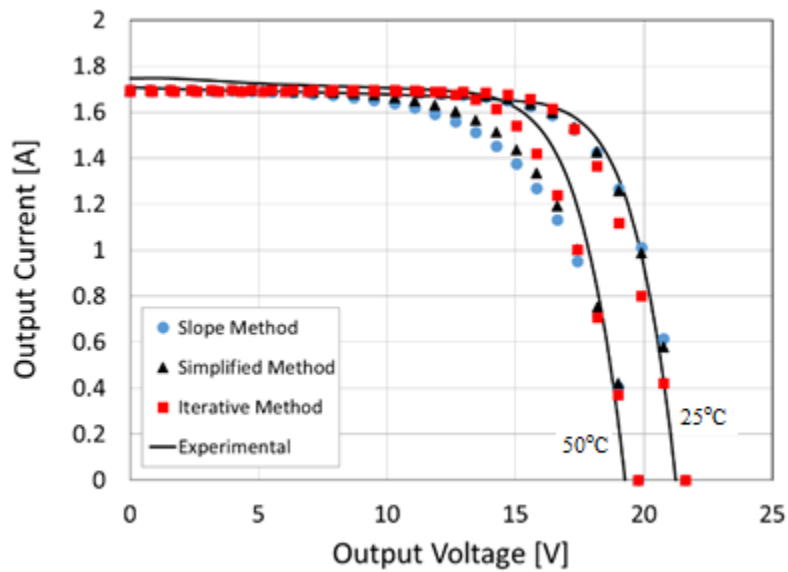


**Figure 4.** Current-voltage curve at 1000W/m<sup>2</sup> solar radiation and two different temperatures 25°C and 50°C.

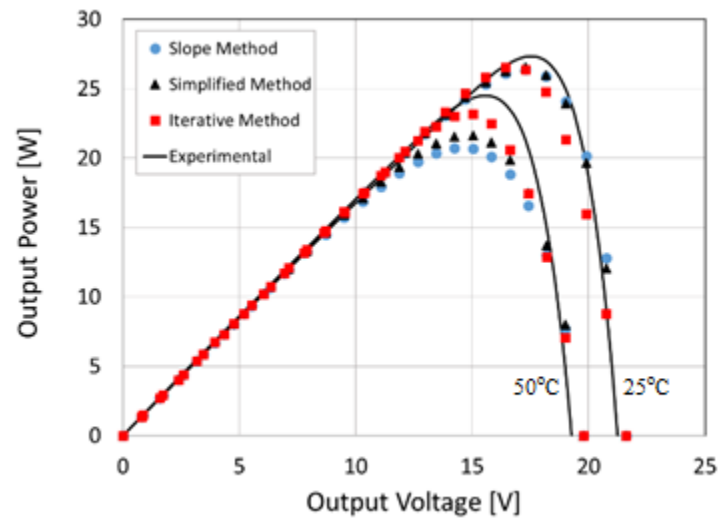


**Figure 5.** Power-voltage curve at  $1000 \text{ W/m}^2$  solar radiation and two different temperatures  $25^\circ\text{C}$  and  $50^\circ\text{C}$ .

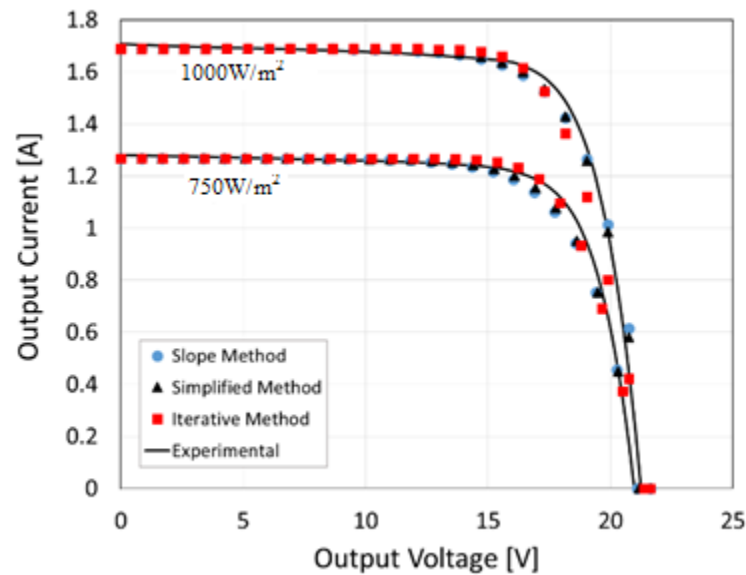


**Figure 6.** current-voltage curve at  $25^\circ\text{C}$  and two different solar radiation:  $750 \text{ W/m}^2$  and  $1000 \text{ W/m}^2$

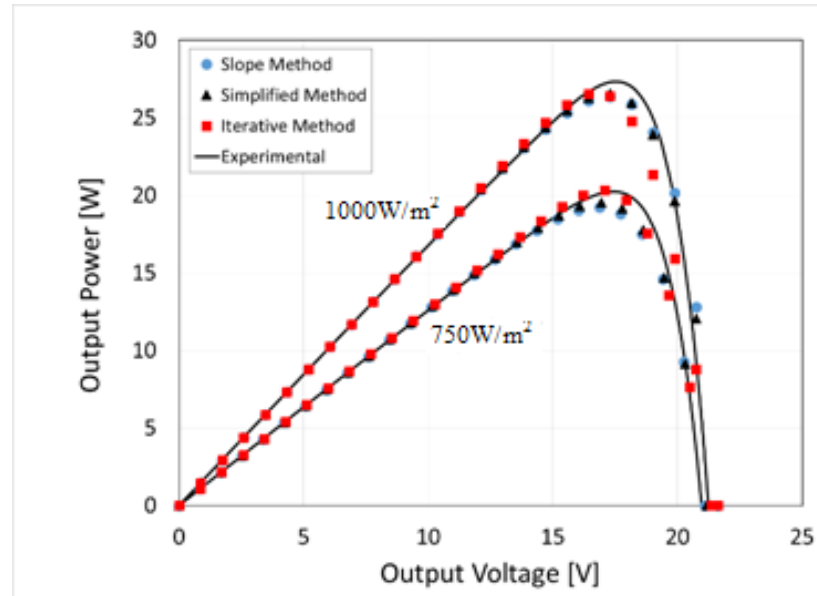


**Figure 7.** Power-voltage curve at 25°C and two different solar radiation: 750W/m<sup>2</sup> and 1000W/m<sup>2</sup>



## Optimization of Hole Cleaning In Iraqi Directional Oil Wells

Ayad A. Al-Haleem, Abd Al-Razzaq

Assistant Professor

Email: ayadah62@yahoo.com

College of Engineering –University of Baghdad

Abdul-Aali Dabbaj

Instructor

Ministry Of Oil

Email: resaldabaj@yahoo.com

Firas Mohammed Hadi

Master Student

College of engineering-University of Baghdad

Email: firasmoh\_70@yahoo.com

### ABSTRACT

Efficient cuttings transport and hole cleaning are very important factors for obtaining an effective drilling operation. In an inclined and horizontal drilling, hole cleaning issue is a common and complex problem.

The scope of this research is to study the drilling parameters which affect hole cleaning in Iraqi directional wells through studying and analyzing some drilled wells ( vertical , directional (30 degree) , directional (60 degree) and horizontal ).An excel sheet is prepared to calculate carrying capacity index which represents an indicator for good hole cleaning in different sections. The study indicated through the field investigations, practical experiences and theoretical calculations that the most effective drilling parameters for optimum hole cleaning were flow rate, yield point, mud weight, plastic viscosity, rotation of the drill string, and pH.

**Key words:** hole cleaning, rate of penetration, equivalent circulating density, directional well, cuttings bed

### التنظيف الامثل للتجاويف المحفورة في الابار الاتجاهية النفطية العراقية

أياد عبد الحليم عبد الرزاق

استاذ مساعد

كلية الهندسة – جامعة بغداد

فراس محمد هادي  
الباحث

عبد العالي الدباج  
خبير  
وزارة النفط

### الخلاصة

ان كفاءة نقل القطع الصخرية وتنظيف تجويف البئر تعتبر من العوامل المهمة في زيادة فعالية عمليات حفر الابار النفطية . يعتبر تنظيف تجويف البئر من المشاكل المألوفة والمعقدة وخاصة في الابار المحفورة اتجاهيا " او افقيا" . هذا البحث يركز على دراسة القيم التي تؤثر على عملية التنظيف ورفع القطع الصخرية للآبار النفطية العراقية المحفورة بصورة مائلة او افقية من خلال دراسة وتحليل بعض الابار المحفورة (عموديا" ، مائلة بزاوية 30 درجة ، مائلة بزاوية 60 درجة والافقية ) .

اعدت حسابات مؤشر رفع القطع الصخرية باستخدام ملف Excel بعد ادخال القيم والحصول على النتائج التي تبين كفاءة التنظيف ورفع القطع الصخرية في مختلف المقاطع المحفورة .

أظهرت الدراسة من خلال المشاهدات الحقلية والخبرة العملية والحسابات النظرية ان اهم العوامل التي تؤثر على التنظيف الامثل هي : معدل التدفق (Q)، نقطة الخضوع (Yp)، كثافة سائل الحفر ، اللزوجة البلاستيكية ، دوران خيط الحفر وقاعدية او حامضية سائل الحفر .

الكلمات الرئيسية: تنظيف البئر، معدل التثقيب، كثافة التدوير المكافئه، البئر الاتجاهي.

## 1. INTRODUCTION

Poor hole cleaning can cause severe drilling problems including : excessive over pull on trips, high rotary torque , stuck pipe , hole pack – off , excessive equivalent circulating density(ECD), formation break down , slow rates of penetration and difficulty running casing and logs. The sticking of the drill string is very expensive to remedy, **Fig. 1, Adari, et al., 2000.**

Insufficient hole cleaning is responsible for a large portion of all stuck pipe. Some would argue that it is the number one cause of stuck pipe around the world, especially in high - angle holes. Previous study in the North Sea attributed 33% of the stuck pipe incidents to poor hole cleaning alone, **Sifferman, et al.,1990.**

A study showed that drill string rotation has a moderate to significant effect on hole cleaning, and that this effect also depends on the hole angle and other cuttings properties. Also the drill string rotation enhances hole cleaning more when the used mud has a higher viscosity with smaller cuttings sizes. It was found that for hole angle at 65 degrees, and at horizontal, the effect drill string rotation caused an improvement in cuttings transport, **Bassal, 1995.** A new mathematical method for estimating the minimum fluid transport velocity for system with the inclination between 55° to 90° was developed. It was found that the model worked fairly well within inclination angle 55° to 90° and there were no correction factors yet for inclination less than 55°. From Larsen method it was known that there are three parameters which affect determination of minimum fluid annular velocity for inclined hole: inclination, ROP, and mud density, **Larsen et al., 1997.**

A new simulations show drill pipe rotation can improve the cuttings transport but the effect is more renounced for smaller particle size. Cutting transport efficiency has a decreasing trend with increase in annular velocity. In addition, inclination and ROP also have major impacts on cuttings concentration, **Bilgesu,et al., 2002.**

Another study was investigated the effect of fluid rheology and cuttings sizes on the circulation rate required to ensure that the drilling cuttings in horizontal wells are efficiently transported to the surface. The results of this study observed that much higher annular velocities are required for effective hole cleaning in horizontal wells. It was also observed that higher viscosity drilling fluid yield better transport than lower viscosity drilling fluid within the same flow regime, **Al-Zubaidi, 2007.**

### 1.1 Area of Study

Iraqi West Qurna oil field has been selected to simulate a study for the possibility of using hole cleaning in directional and horizontal well to minimize the problems which happen because that. Also, a horizontal well in Halfaya oil field have been selected.

West Qurna oil field is one of the largest oil fields in Iraq with a reserve of about 43 billion barrel of crude oil. This field located on the south-eastern part of Iraq, about 45 km north-westwards from Basra and 30 km from Zubair oil field, **BP Company, 2010.**

## RESULTS AND DISCUSSION:

### 1- Field Investigations

Below a list of results based upon field observations and practical experiences:

A) During connection process of additional drill pipe to the string, an increasing in pressure can be noticed because of shut off the mud pump until the pipe connection is finished .An obstruction may be happened due to settling of cuttings on the bit .

B) When there is remarkable changes on the hole inclination and azimuth during drilling, drilling parameters such as (weight on bit, rate of penetration, flow rate) and BHA should be adjusted immediately to correct the hole trajectory.

- C) Wiper trip should be make to break building up of any cutting bed at high angle hole regularly with high viscosity pill pump down for better hole cleaning.
- D) When the flapper valve is used, fill in mud every 10 – 15 stands to avoid the flapper valve from damage.
- E) At the end of drilling the 8.5" hole, circulate to clean the hole and make wiper trip with reamers to control the hole condition before logging and casing.
- F) In case of lost circulation, stop drilling and pull out of hole as fast as possible meanwhile fill in mud. Pull the string inside the 9<sup>5/8</sup>" casing and check the flow and loss rate, If necessary.
- G) Monitoring the shale shakers before trip out or pull out of the hole (POOH) in order to ensure that cuttings return rate has reduced.
- H) During drilling operation, it is common to circulate wellbore several times (the process is called circulate bottom-up) before starting tripping out of hole. The purpose is to avoid stuck of drill pipe during pull out and be able to reach the bottom hole with drill bit or casing, when running into the hole again(RIH). The common practice is to have at least three bottoms-up with slow pipe rotation before tripping out of the hole. If ECD measurement tool is available on the BHA, it has to be controlled that the ECD has dropped to normal level.

## 2- Concentration of the Cuttings

An increase in rate of penetration will increase the concentration of cuttings in the hole and a longer time will be needed for cleaning the hole, **Fig. 2**.

The figure indicates that an increasing in the ROP lead to an increase in the cuttings concentration, therefore, more than one cycle to clean the hole is needed besides additional time. If a comparison has been made between the wells to show the total time of drilling, for the state of wells, we can notice:

In WQ-404, the total time to complete the drilling operation is (30) days, **Fig. 3**.

While the total time for drilling operation of directional well less than 30 degree well (WQ-416) is about thirty-two (32) days, **Fig. 4**.

The similarity in needed time can be attributed to use the same drilling factors which affect on hole cleaning in vertical wells and directional wells less than 30 degree.

Accordingly, for the directional well with high deviated angle (WQ-271) (62degree) the total time of drilling operation is about fifty- five(55) days, **Fig. 5**, whereas for horizontal well (HF-69) the total time is ninety (90)days, **Fig. 6**. From the previous cases, it is evident that time values increases rapidly as hole inclination increases.

## 3- Sample of Calculations

Following a sample of Carrying Capacity Index (CCI), and flow rate for selected sections of some wells, which prepared to show the optimality of the field data in achieving the best hole cleaning. **Tables 1, 2, and 3** show the CCI and calculations using field data for the 1<sup>st</sup> hole, 2<sup>nd</sup> hole, and 3<sup>rd</sup> hole respectively. Such as CCI for the second hole for the well WQ-416:

$$\begin{aligned} n &= 3.32 \log [(2 \mu p + Y_p) / (\mu p + Y_p)] \\ n &= 3.32 \log [(2 * 60 + 15) / (60 + 15)] \\ &= 0.848 \end{aligned} \quad (1)$$

$$\begin{aligned} \mu_e &= 511^{(1-n)} (\mu p + Y_p) \\ \mu_e &= 194 \text{ cp} \end{aligned} \quad (2)$$

$$V = \frac{24.5 Q}{Dh^2 - Dp^2} \quad (3)$$

$$=155.4 \text{ ft/min.}$$

$$\begin{aligned} CCI &= (\rho \mu_e V)/400000 \\ &= 0.703 \end{aligned} \quad (4)$$

Where:

n = Power Law Index

$\mu_p$ : Plastic Viscosity cp

$Y_p$ : Yield Point lb/100ft

$\mu_e$ : Effective Viscosity cp

Q: Flow Rate gpm

Dh: Hole Diameter in , Dp: pipe diameter in

V : Annular Velocity ft/min

CCI: Carrying Capacity Index

It can be noticed in the second hole (WQ-416) that the CCI value which equal to 0.7 represent poor hole cleaning and this case may be cause many problems especially the stuck pipe so increasing yield point value is necessary to obtain proper hole cleaning. Absolutely, the CCI results for the selected section show that the drilling parameters used in different well types are the same. Simply, the need to change the parameters begins with high deviated wells.

Finally, a horizontal drilling program for West Qurna oil field was prepared and a plan to drill a horizontal well in this oil field due to absence of such well type. The present proposal consist of four holes shown in **Fig. 7**

## CONCLUSIONS:

Based on the theoretical and experimental observations and analysis, the following conclusions can be drawn regarding optimization of hole cleaning in horizontal oil well:

1- The rheological properties play a crucial role to ensure adequate hole cleaning, i.e. proper rheology is the key for efficient solids removal. So the yield point was maintained to 15-20 lb/100 ft<sup>2</sup>, which were enough to clean the hole while drilling vertical & directional wells.

2- In case of highly inclined or tight well, it is important to ream the wellbore with help of a back reamer. It helps creating a bigger hole that can eliminate risk of stuck drill-pipe.

3-The flow rate should be high enough (during drilling operation) or increased to its upper level, especially in the range of higher angles between 55° to 90° degrees to obtain optimum hole cleaning.

4-The hole cleaning in deviated holes can be assisted by the following topics:

- Turbulent flow

- Low viscosity and high flow rates

- Maximize flow rates at all times unless ECD problems require lower rates

- Low Viscosity Sweeps (10-20 bbl)

- Followed by High Viscosity Weighted sweep to remove cuttings

- Pipe rotation at high rpm

- Reaming and wiper trips can stir up cuttings beds

## RECOMMENDATIONS:

Some of the issues which should be investigated in future studies are listed below:

1- OBM or Polymer drilling fluid system has the outstanding abilities on cuttings lifting, lubrication, hole cleaning etc., so it is very important to be used for the successful drilling in the build- up and horizontal sections.



2- In cases, where drill pipe does not rotate, it is difficult to remove cuttings bed. In these situations, wiper trips are necessary to improve hole cleaning. Usually, a normal range of drill pipe rotation is around 90 to 180 rpm. The pipe can rotate up to 120-rpm when drill bit is on-bottom, and 180-rpm drill bit is off-bottom.

3- One has to be aware that inclinations between 40° to 45° degrees are critical since cuttings can slide down during connections when pumps are off.

#### REFERENCES:

- Adari, R.B., Miska, S., Kuru, E., Bern, P. and Saasen, A.,2000, *Selecting Drilling Fluid Properties and Flow Rates for Effective Hole Cleaning in High Angle and Horizontal Wells* SPE Paper 63050 presented at the Dallas Texas.
- Al-Zubaidi , N. S. ,2007, *Experimental Study of Cuttings Transport in Horizontal Wells*, Ph.D. Dissertation , Univ. of Baghdad , Iraq
- Bassal, A.A. 1995, *the Effect of Drill Pipe Rotation on Cuttings Transport in Inclined Wellbores*. Thesis. 1995
- Bilgesu H.I., M.W. Ali, K. Aminian, and S. Ameri, 2002, *Computational Fluid Dynamics (CFD) as a Tool to Study Cutting Transport*. At the SPE Eastern Regional Meeting, pp. 1-4.
- Larsen et. al.,1997, *Development of a New Cutting Transport Model for High – Angle Wellbores Including Horizontal Wells* , paper SPE 25872.
- Ministry of Oil (British Petroleum Company Data),2010.
- Sifferman, T.R.,& Becker T.E,1990, *Hole Cleaning in Full-Scale Inclined Well Bores*. SPE 20422,65<sup>th</sup> Ann.Tech.Conference of SPE in New Orlands

#### NOMENCLATURES AND ABBREVIATIONS:

BHA = bottom hole assembly.

CCI = carrying capacity index.

Dp = pipe diameter in

Dh = hole diameter in

ECD = equivalent circulating density, ppg .

FWB = fresh water bentonite .

HF = halfaya oil field .

OBM = oil base mud

POOH = pull out of the hole .

Q = flow rate gpm

RIH = running in the hole .

ROP = rate of penetration ft/hr .

Rpm = rotation per minute .

V = annular velocity ft/min .

WQ = west qurna oil field .

Yp = yield point lb/100 ft<sup>2</sup>

pf = fluid density ppg

$\mu_p$  = plastic viscosity cp  
 $\mu_e$  = effective viscosity cp

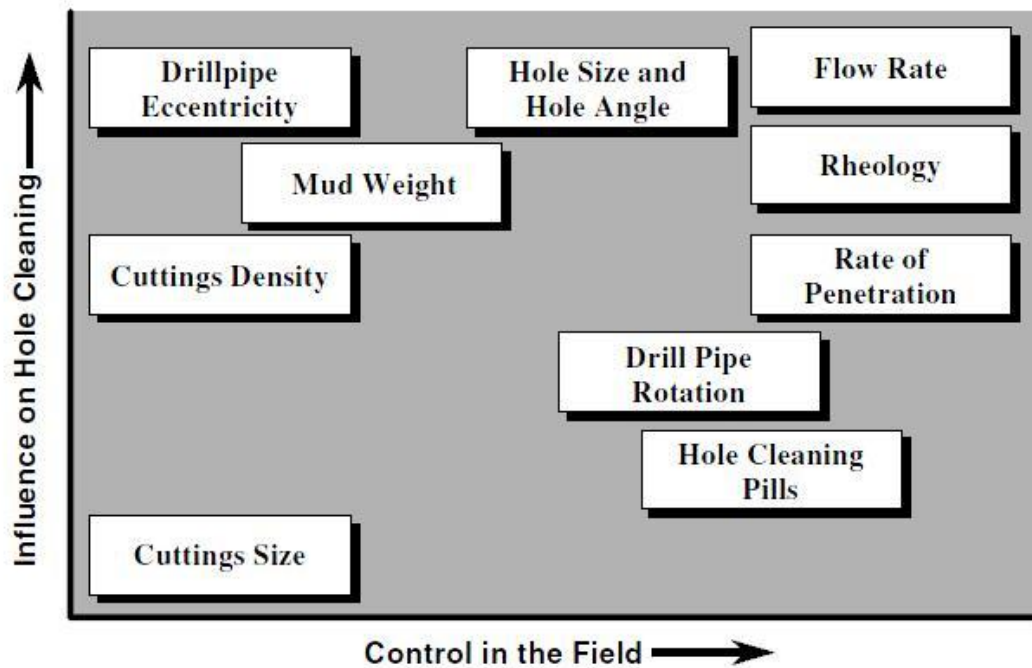


**Figure 1.** Key variables controlling cuttings transport, Adari, et al., 2000.

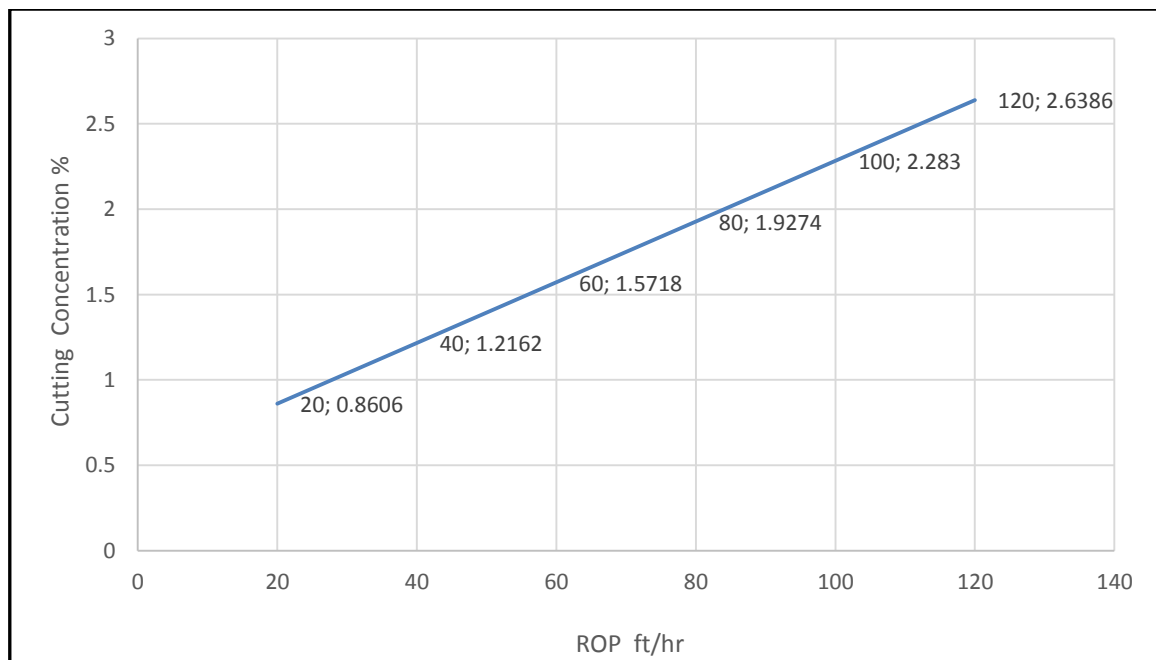


**Figure 2.** Relationship between ROP and cuttings concentration.

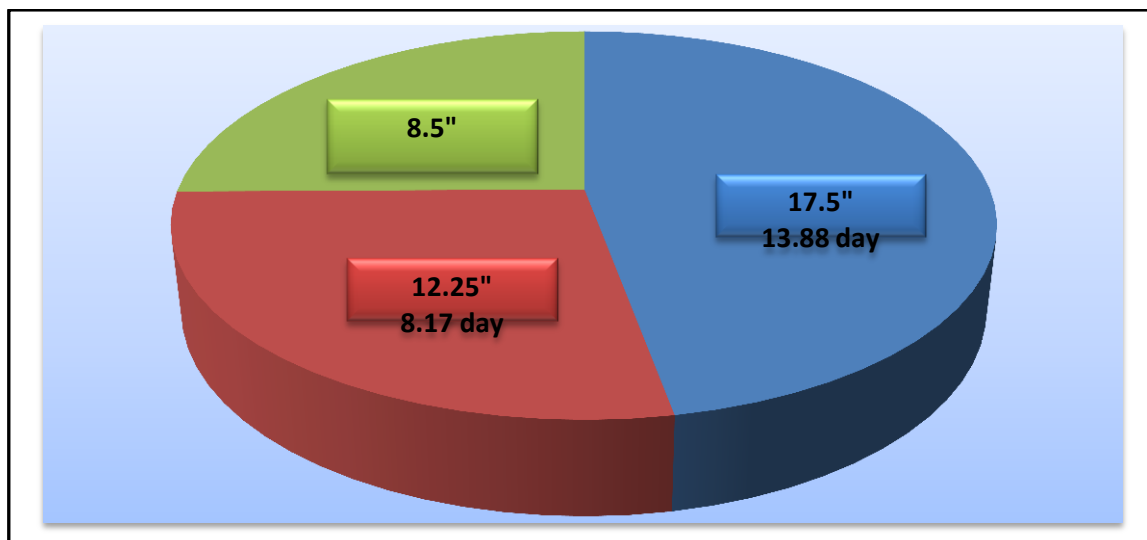


**Figure 3.** Pie chart show time vs hole size for vertical well (WQ-404).

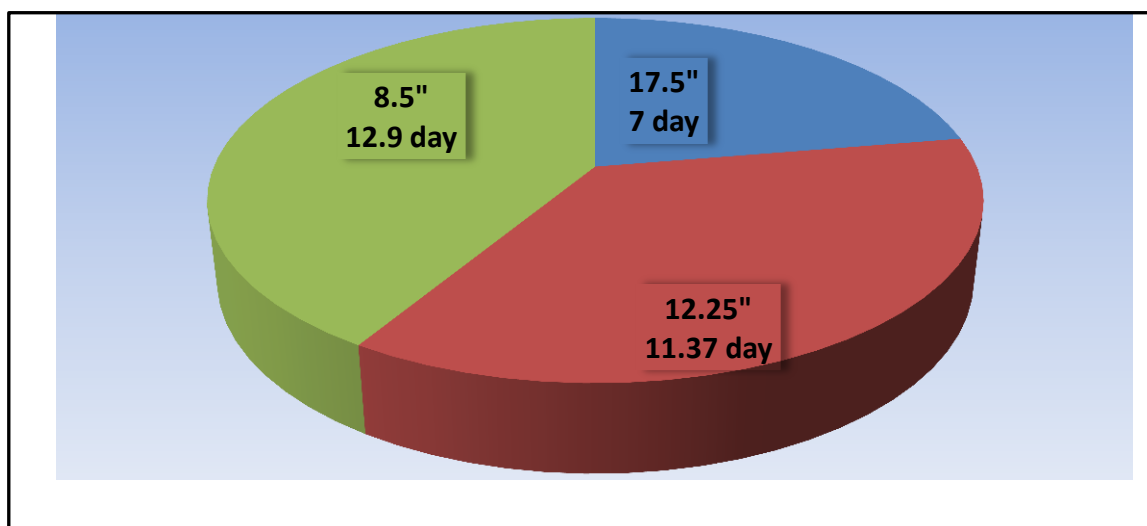


**Figure 4.** Pie chart show time vs hole size for directional well (WQ-416).

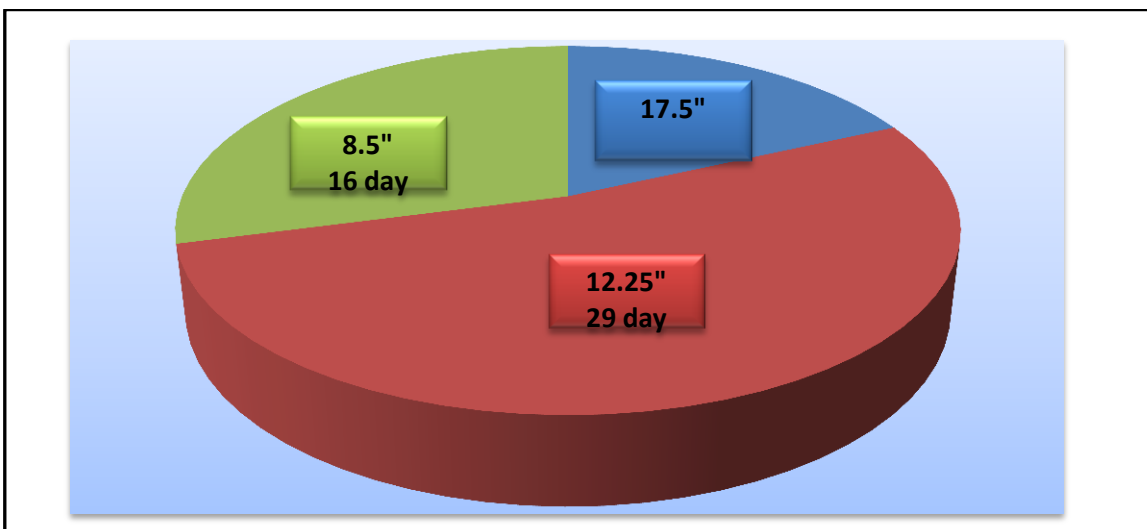


**Figure 5.** Pie chart show time vs hole size for directional well.



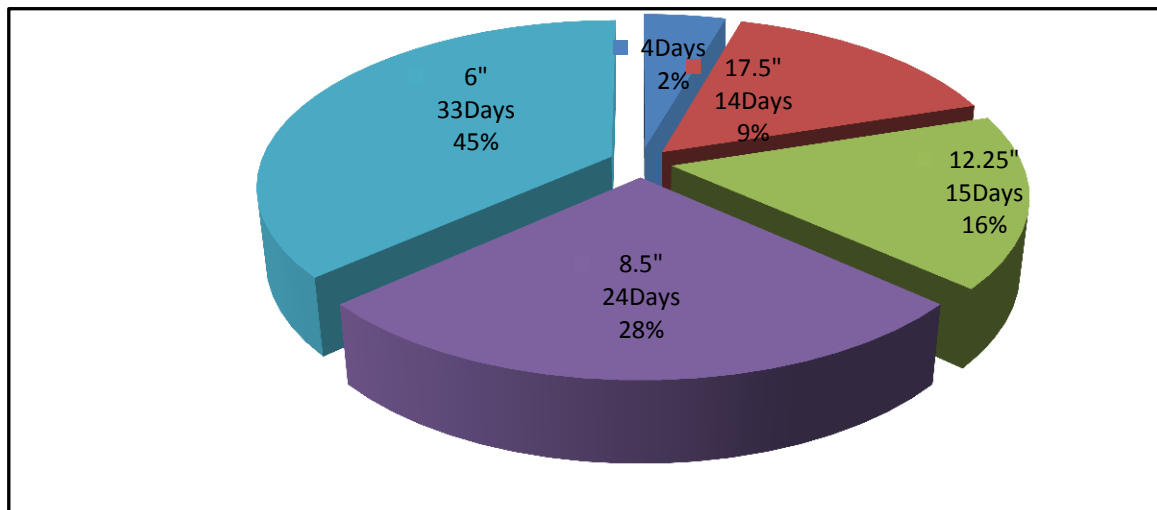


**Figure 6.** Pie chart show time vs hole size for well (HF-69).

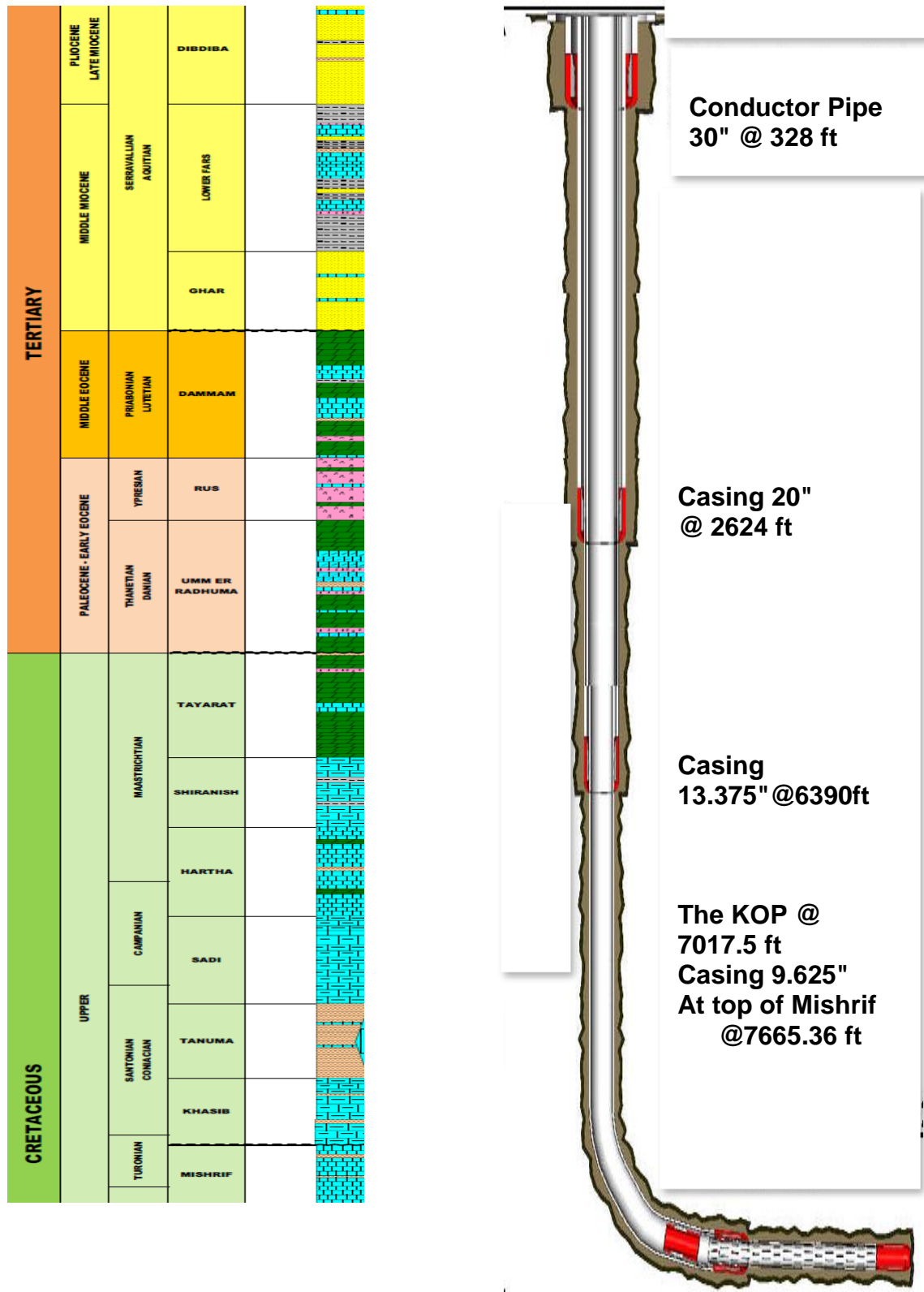


**Figure 7.** Casing program for the proposal horizontal well in west Quran oil field

**Table 1.** Excel sheet of CCI calculation for 17.5" hole.

Variable	Calculated value	Units
$\rho_f$	8.75	ppg
$Y_p$	20	lb/100ft <sup>2</sup>
$\mu_p$	14	cp
N	0.497	
$\mu_e$	782.1	cp
Dp	5	in
Dh	17.5	in
Q	700	gpm
V	60.98	ft/min
CCI	1.043	

**Table 2.** Excel sheet calculation CCI for 12.25" hole

Variable	Calculated value	Units
$\rho_f$	10.4	Ppg
$Y_p$	17	lb/100ft <sup>2</sup>
$\mu_p$	12	Cp
N	0.499	
$\mu_e$	659	Cp
Dp	5	In
Dh	8.5	In
Q	425	Gpm
V	220.3	ft/min
CCI	3.7	

**Table 3.** Excel sheet calculation CCI for 8.5" hole

Variable	Calculated value	Units
$\rho_f$	10.4	Ppg
$Y_p$	17	lb/100ft <sup>2</sup>
$\mu_p$	12	Cp
N	0.499	
$\mu_e$	659	Cp
Dp	5	In
Dh	8.5	In
Q	425	Gpm
V	220.3	ft/min
CCI	3.7	

## FRACTURE PROPERTIES OF LOCAL ASPALT CONCRETE

**HAMED M. H. AL-HAMDOU**

Professor Emeritus

Civil Eng. Dept./Eng. College/Baghdad University

e mail: profhamedalani@yahoo.com

**Dr. ABDUL-HAQ HADI ABED-ALI**

Assistant Professor

Highways & Transportation Dept./Eng. College

Al-Mustansiriyah University

e mail: abdulhaq-alhaddad@yahoo.com

**Dr. MOHAMMED Z. MOHAMEDMEKI**

Lecturer

Highways & Transportation Dept./Eng. College

Al-Mustansiriyah University

e mail: moh7312@gmail.com

### ABSTRACT

The local asphalt concrete fracture properties represented by the fracture energy, J-integral, and stress intensity factor are calculated from the results of the three point bending beam test made for pre notches beams specimens with deformation rate of  $1.27 \text{ mm/min}$ . The results revealed that the stress intensity factor has increased by more than 40% when decreasing the testing temperature  $10^\circ\text{C}$  and increasing the notch depth from 5 to  $30 \text{ mm}$ . The change of asphalt type and content have a limited effect of less than 6%.

**Key words:** Stress intensity factor, Fracture Energy, J-integral

### خواص الكسر للخرسانة الاسفلتية المحلية

حامد محمود حمدو

استاذ مشارك

قسم الهندسة المدنية / كلية الهندسة / جامعة بغداد

د. محمد زهير محمد مكي

مدرس

قسم هندسة الطرق / كلية الهندسة / الجامعة المستنصرية

د. عبد الحق هادي عبد علي

استاذ مساعد

قسم هندسة الطرق / كلية الهندسة / الجامعة المستنصرية

### الخلاصة

خلال هذه البحث تم دراسة خصائص التصدع للخرسانة الاسفلتية المحلية المتمثلة بطاقة التصدع؛ J-Integral و معامل شدة الاجهاد والتي تم احتسابها لنماذج العتبات المسبقة الشق من خلال فحصها باستخدام فحص الانثناء وبسرعة تشوه مقدارها  $1.27 \text{ mm/min}$ . اوضحت الدراسة بان معامل شدة الاجهاد قد ارتفع اكثر من 40% بخفض درجة حرارة الفحص 10 درجات مئوية وبزيادة عمق الشق المسبق (pre notch) من  $5 \text{ mm}$  الى  $30 \text{ mm}$  بينما كان لتغييرنسبة ونوع الاسفلت تأثير محدود لم يتجاوز 6%.

## 1. INTRODUCTION

Cracking is one of the major distresses in flexible pavement, results from exposure of pavement structure to environmental conditions and traffic loading. Accurate prediction of crack initiation and propagation aids in the design and maintenance of asphalt pavement structures. Crack initiation and its relation with material mechanical behavior can be used to describe the remaining service life of the existing pavements. Several test methods were developed to study the cracking behavior in Hot Mix Asphalt (HMA) under different sample geometries, loading configurations, and material properties **Denneman, et. al., 2009, Im, 2012**. In most tests, a notch was introduced into the sample so that the crack would initiate at the notch **Kim, and El Hussein, 1995**. In many of these studies, linear elastic fracture mechanics and elastic plastic fracture mechanics principles were applied to characterize material response.

## 2. FRACTURE MECHANICS

Fracture mechanics is the material mechanical behavior when subjected to load in the presence of cracks; in other words, it is the stress/strain characteristics of the pre-cracked material subjected to load or deformation **Saadeh, and Hakimelahi, 2012**.

### 2.1 Crack modes

Generally, there are three crack modes; these modes depend on the crack nature of cracked bodies. **Fig.1** shows these modes and a short description for each one is given below **Saxena, 1998**:

*Mode I: Opening mode, the crack surfaces separate symmetrically with respect to X-Y and X-Z planes.*

*Mode II: Sliding mode, the crack surfaces relatively slide to each other symmetrically with respect to X-Y plane and symmetrically skew with respect to X-Z plane.*

*Mode III: Tearing mode, the crack surfaces relatively slide to each other symmetrically with respect to X-Y and X-Z planes.*

For the purpose of this research, *mode I (Opening mode)* is adopted because it mostly represents the nature of pavement structure crack as shown in the **Fig.2**. Furthermore, widely accepted theories for fracture under mode II, III, and mixed mode conditions are currently not available **Saxena, 1998**.

### 2.2 Stress Intensity Factor

The stress intensity factor (K) represents the amplitude of the crack tip stress singularity and is dependent on body geometry, crack size, load level, and loading configuration. The **Eq.(1)** of estimating the (K) is:

$$K = \frac{P}{BW^{1/2}} F(a/W) \quad (1)$$

Where: *P*: Reaction point load,  
*B*: Specimen thickness,  
*W*: Specimen depth,  
*a*: Crack length, and

$F(a/W)$ : Dimensionless calibration functions for various geometries, as shown in **Table 1** as reported by **Saxena ,1998**.

### 2.3 The J-Integral Approach

In 1968, Rice, published papers in which he discussed the potential of a path-independent integral (J) for characterizing fracture in nonlinear-elastic materials **ASM, 1997**. This integral is identical in form to the static component of the energy moment tensor for characterizing generalized forces on dislocations and point defects introduced by Eshelby G.P. Cherapov, working independently in the former Soviet Union during the same time of Rice. Cherapov, 1967 also presented a formulation of an integral similar to Rice's (J). Rice defined the J-Integral for a cracked body, shown in **Fig.3**, as follows in **Eq. (2 and 3)**:

$$J = \int_S (Ws.n - T \partial u_i / \partial x) ds \quad (2)$$

$$J = \int_S Ws.dy - T \partial u_i / \partial x . ds \quad (3)$$

Where:  $Ws$  : elastic strain energy,

$T$  : Traction vector defined according to the out word normal  $n$  the contour  $S$ , and

$u$  : Displacement vector( $u_1i + u_2j$ ).

J can be shown to relate to the rate of changes of potential energy with respect to change in crack size. This interpretation of J is useful in showing that under linear elastic condition,  $J=Y$  **Eq.(4)**:

$$U = \int_A W(X,Y) dA - \int_S T_i u_i ds \quad (4)$$

Where:  $A$  : Body area,  
 $T_i$  : Traction, and  
 $u_i$  : Displacement. } applied along the boundary

by differentiating the previous equation get **Eq.(5)**:

$$\frac{dU}{da} = \int_A \frac{dW}{da} dA - \int_S T_i \frac{du_i}{da} ds \quad (5)$$

The contour of the line integral can be extended along the boundary  $S$  of the body in the counterclockwise direction from the lower crack face to the upper one, since  $\frac{dU}{da} = 0$ , on the boundary  $S_u$ , the displacements are prescribed independently of  $a$ , as shown in **Fig.4**.

By substituting the coordinate system attached to the crack tip, and using the symmetry of the stress tensor with the application of the divergence theorem, the equation becomes as shown in **Eq. (6 and 7)**:

$$\frac{dU}{da} = - \int_S W dy - \int_S T_i \frac{\partial u_i}{\partial x} ds \quad (6)$$

$$\left. \begin{array}{l} \text{For unit thickness body} \\ \text{For a body with thickness (B)} \end{array} \right\} J = \left. \begin{array}{l} - \frac{dU}{da} \\ - \frac{1}{B} \frac{dU}{da} \end{array} \right\} \quad (7)$$

Under certain restriction,  $J$  can be used as an elastic-plastic energy release rate. The path independence of  $J$ -integral expression allows calculation along a contour remote from the crack tip; such a contour can be chosen to contain only elastic loads and displacements. Thus, an elastic-plastic energy release rate can be obtained from an elastic calculation along a contour for which loads and displacements are known. In 1972, Begley, J. A. and Landes, J. D. **ASM, 1997** developed an experimental method for determining  $J$  from generating load-displacement curves for samples of unit thickness with different initial crack lengths.

### 3. ASPHALT CONCRETE FRACTURE

**Uzan, and Levenberg, 2001** studied the phenomenology of asphalt concrete (AC) fracture in the laboratory under uniaxial-tension with strain control of  $0.6^{\text{mm/min}}$  at the room temperature of  $24^{\circ}\text{C}$  for beam samples of about  $(60 \times 90 \times 225^{\text{mm}})$ . The study showed that the pre-peak stress conditions induced damage is a result of formation, growth and coalescence of micro cracks; the study also found in post-peak stress condition that the process of damage localization occurs within the Representation Volume Element (RVE) (the zone across the sample of 2-4 times their nominal maximum size of mix aggregate Witczak, 2000 at which the crack will propagate) leading to the creation of a dominant failure surface and eventually fracture. The study added that the cracking behavior of an AC MIX of RVE size, three scales of load induced cracks should be considered as shown in **Fig.5**:

1. Micro-cracks: small flows up to few millimeters (the air voids entrapped during compaction process may represent these flows).
2. Meso-cracks: resulting from micro cracks coalescence; their length may reach the maximum aggregate size in the mix.
3. Macro-cracks: at which the strength of AC is reduced to zero and of a minimal RVE in size.

**Kim, et. al. 2008** used a bilinear cohesive softening model to simulate the crack initiation and propagation in asphalt concrete. The meso-crack representation of material morphology was incorporated into the model using high-resolution imaging.

Kim and co-researchers explained the bilinear cohesive softening model concept as follows and as shown in **Fig.6**. In general the cracking of asphalt concrete can occur in any weak point within the fracture process zone **Fig.6-a** and cohesive fracture concept at the crack tip can be simplified as shown in **Fig.6-b**. In **Fig.6**,  $\sigma_{\text{max}}$  represents the location of cohesive crack tip and  $\delta_{\text{sep}}$  is the complete material separation or the material crack tip, and  $\sigma_{\text{max}}$  is the normal cohesive strength. Point B represents the starting point of unrecoverable material degradation (or micro-crack initiation) and point c represents the condition where a crack face was fully separated and released the energy potential associated with losing of cohesive strength.

In **2008** at Cambridge University UK, **Portillo and Cebon** investigated the fracture mechanics of idealized asphalt mix (bitumen of penetration grade of 40-50 and fraction of sub spherical sand between  $150\text{-}300^{\mu\text{m}}$ ) using a systematic 3-point bending test for beam samples of  $(50 \times 50 \times 225^{\text{mm}})$  with middle notch of length equal to half of depth, in order to develop fracture mechanism maps classifying the brittle, ductile, and transition response of the materials as a function of temperature and load rate. The experimental data of this study was analyzed in terms of stress intensity factor, fracture energy, and  $J$ -integral at the temperature range of  $-30^{\circ}\text{C}$  to  $30^{\circ}\text{C}$  with two deformation rate of  $0.01$  and  $0.05^{\text{mm/sec}}$ .

The study showed that, for typical force vs. deflection curves, the peak force increases with temperature; at  $0^{\circ}\text{C}$ , the crack arrests in the vicinity of peak load and the crack grows in a smooth fashion a more brittle behavior and less energy is required to propagate the crack. **Fig.7** shows the



typical load line displacement curve for tested sample at  $-20^{\circ}\text{C}$  with displacement rate of  $0.05\text{mm/sec}$  made by this study.

### 3.1 Materials

For the purpose of this study, two types of local asphalt cement, obtained from AL-Daurah refinery, including 40-50 and 60-70 penetration graded and quartzite crushed aggregates were selected to be used in this study. The crushed aggregates were obtained from AL-Nebai quarry, due to the extensive usage of this type of aggregates for asphaltic mixtures in the middle of Iraq especially in Baghdad city. The limestone dust, from Karbala governorate, was used as a filler material.

The main properties of selected materials for the purpose of this research, which include two types of asphalt cement, quartzite crushed aggregates and limestone dust as mineral filler, are presented in the following **Tables 2 to 6**.

### 3.2 Mix design and optimum binder content determination

For the purpose of this study the Hot Mix Asphalt concrete (HMA) was designed volumetrically according to the SUPERPAVE requirements, the aggregates gradation was selected to meet the Iraqi specification beside the SUPERPAVE to be as shown in the gradation curve presented in **Fig.8** with  $0.5^{\text{in}}$  as a maximum nominal aggregate size representing wearing layer.

Based on the results of rotational viscometer (ASTM D4402, AASHTO T316) the HMA was mixed and compacted at the required equiviscous temperatures shown in **Table 7**.

The HMA was compacted by using the gyratory compactor (ASTM D6925-09, AASHTO T312) after aging period of 4 hours @  $135^{\circ}\text{C}$  with 8,100, and 160 as a number of gyration initial, designed, and maximum respectively as presented in **Table 8** to meet the mix design subjected to number of equivalent axels to be passed on pavement during its design life which used here between 3.0 to 30.0 million ESALs.

The results of volumetric properties represented by Air Voids, Voids in Mineral Aggregates (VMA), and Voids Filled with Asphalt (VFA) for the gyratory compacted specimens shown on the **plate 1** are fitted with asphalt content and the Optimum Binder Content (OBC) of 4.7% is found to get the required properties as needed by SUPERPAVE criteria as shown in **Table 9**, it is worth to mentioned here that there is no significant difference is found on OBC between asphalt penetration graded 40-50 and 60-70.

### 3.3 Study parameters

The following parameters are considered at this study

- Two testing temperature  $20^{\circ}\text{C}$  and  $30^{\circ}\text{C}$ ,
- Three pre crack depth (notch) 5, 15, and  $30^{\text{mm}}$ ,
- Two asphalt type 40-50 and 60-70 penetration graded, and
- Three asphalt content, optimum and  $\pm 0.5\%$ .

So, and according to these parameters the required specimens number are 36 beams which prepared as describe in the following section.

### 3.4 Specimens preparation

In order to study the fracture properties of HMA subjected to bending stress beams specimens of  $3 \times 3 \text{in}$  ( $7.62 \times 7.62^{\text{cm}}$ ) cross section and  $15^{\text{in}}$  ( $38.1^{\text{cm}}$ ) length with gross mass of about 5150gm were made with different notch depth. A steel rectangular mold of ( $15^{\text{in}}$  length X  $4^{\text{in}}$  depth X  $3^{\text{in}}$  width ) ( $38.1 \times 10 \times 7.62^{\text{cm}}$ ) inside dimensions with two spacers made by **Fadthl, 2007**, is used for producing beams specimens as shown in **Plate 2**.

The specimens were compacted by using the uniaxial digital compression machine having a capacity of 2000<sup>kN</sup> as shown in **Plate 2**, to get the required air voids ( $4\% \pm 1\%$  for wearing layer) for specimens with different asphalt content; the relations between applied stress and %G<sub>mm</sub> were made as shown in **Fig.10**, so from these relations, the required applied stress was found for mixes of different asphalt content as presented in the same figure.

A steel plate of (3<sup>mm</sup> thickness) which welded perpendicularly on base plate of (6<sup>mm</sup> thickness) were used to make a notch on the specimens by placing it in the mold before applying the mix in the mold and then by removing it after the completion of the compaction process. To make a different notch depth, three plates arrangements were used with different perpendicular plate height of (5, 15, and 30<sup>mm</sup>) as shown in **Plate 3**.

### 3.5 Testing

A load frame device, manufactured by Humboldt company in the USA model HM-2800, with digital control unit for multi deformations rates (ranging from 0.001(0.0254) to 2<sup>in/min</sup> (50.8<sup>mm/min</sup>)) was used to test the specimens monotonically in order to generate the Load- Displacement (L-D) curves for tested specimens. Some modifications were made on device as shown in **Plate 4**, by adding load cell and fully isolated chamber made with aluminum frame and sandwich panel of 5<sup>cm</sup> thickness and double glasses door in addition to that heating and cooling sources were provided with thermometer sensor and digital thermostat to maintain the specified temperature during the test.

### 3.6 Bending Beam Test (BBT) fracture energy and J-Integral

In order to specify the fracture properties of local asphalt concrete, the value of J-integral was estimated using the experimental method. As pointed in Chapter Two, J-integral was defined and shown to characterize the process of ductile tearing under elastic-plastic and fully plastic conditions. Further, its magnitude should be easily measurable in test specimens used for characterizing crack growth resistance.

Experimental method which was developed by J.A. Begley and J.D. Lands in 1972 needs to generate Load-Displacement (L-D) for specimens of unit thickness with different initial crack lengths. Each specimen is loaded to displacement levels that can be sustained without crack extension. The areas under load displacement curves to specified values of displacement D1, D2, D3, ... Di are obtained graphically to determine the corresponding values of the potential energy U1, U2, U3, ... Ui. For each fixed value of displacement, Ui can be plotted as a function of crack length ai. The slope of U-a curve, dU/da, is then measured at various points to yield the values of J. If the specimen thickness is other than unity, dU/da must be divided by the thickness, B, in order to obtain the value of J. The resulting J values can be plotted as a function of the applied displacement for various crack size **Saxena, 1998**.

The fracture properties were estimated by generating the Load-Displacement (L-D) curves for beams specimens made as explained in the previous chapter with initial cracks (notches) of 5, 15, and 30<sup>mm</sup> lengths. A three point BBT test was made by using digital load frame device, as shown in **Plate 4**, with deformation rate of 0.05<sup>in/min</sup> (1.27<sup>mm/min</sup>). The specimens reaction load was indicated by employing a load cell of 5.0<sup>kN</sup> capacity; the load reaction history was recorded by using a digital camera which faced to the load cell reader.

**Figers 11-a to c** show the application of experimental method explained earlier to estimate the fracture properties which include fracture energy and J-integral; the load displacement curves were divided into two parts: pre peak and post peak.

The pre peak part represents the tested specimen before cracks initiate. This part is divided to segments as shown in **Fig. 11-a** of 0.75<sup>mm</sup> at horizontal axis which represent the displacement;

then the areas under the curves were calculated through integrating the polynomial equations of each curves at incremental value of  $0.75^{\text{mm}}$  until  $3\text{mm}$  and then the relation was made between the fracture energy and crack length as shown in **Fig. 11-b**. The slopes were found for previous relations and the values of J-integrals were calculated and the relations between J-integrals and displacement were made for different notch depths as shown in **Fig. 11-c**. **Figures 11-a, b, and c** illustrate the results of tests which were made for beams specimens made with asphalt cement of 40-50 penetration graded at optimum binder content tested at  $20\pm 1^{\circ}\text{C}$ ; while **Figures 12-a, b, and c** show the results of the same tests but at  $30\pm 1^{\circ}\text{C}$ .

### 3.7 Stress intensity factor

The stress intensity factor (K) represents the amplitude of the crack tip stress singularity and is dependent on body geometry, crack size, load level, and loading configuration. The **Eq.1** presented in section of stress intensity factor is used here to calculate the magnitude of (K) for beams specimens as shown below:

$F(a/W)$  = dimensionless calibration functions for various geometries and different notch depth as given in **Eq.8**:

$$F(a/W) = \frac{3\left(\frac{S}{W}\right)\left(\frac{a}{W}\right)^{\frac{1}{2}}\left[1.99 - \frac{a}{W}\left(1 - \frac{a}{W}\right)\left(2.15 - 3.93\left(\frac{a}{W}\right) + 2.7\left(\frac{a}{W}\right)^2\right)\right]}{2\left(1 + \frac{2a}{W}\right)\left(1 - \frac{a}{W}\right)^{3/2}} \quad (8)$$

where:

S : clear span =  $4W$  (12"), see **Table 1**.

So, the calibration function for studied notch depths are calculated and illustrated in **Table10**. Accordingly and by using **Eq.1**, the magnitudes of stress intensity factor was calculated for beams specimens and it was found that the (K) value increased with increasing notch depth, due to increasing crack length which means reducing the depth to the crack tip and increasing the stress concentration for the same applied load. In other words, the load required to bend and crack the specimen is decreased with increasing the crack length. **Fig.13** shows the effect of notch depth on stress intensity factor for beams specimens tested at  $20\pm 1^{\circ}\text{C}$  and  $30\pm 1^{\circ}\text{C}$ ; based on this figure, the effect of notch depth is decreased when raising the test temperature.

## 4. SENSITIVITY ANALYSIS

The effect of study parameters on stress intensity factor are shown and discussed at following sections

### 4.1. Notch depth

Three notch depths (5, 15, and  $30^{\text{mm}}$ ) were made for beam specimens tested monotonically with constant deformation rate of  $0.05^{\text{in/min}}$ , at two testing temperatures  $20\pm 1^{\circ}\text{C}$  and  $30\pm 1^{\circ}\text{C}$ ; the effect of notch depths on the stress intensity factor was illustrated in **Fig.14**.

The figure gives an idea about the effect of notch depths on the stress concentration at the crack tip, as the notch depth increase the stress concentration increased; that explained the rapid deterioration of asphalt concrete section having cracks if compared with non cracked section.

### 4.2. Testing Temperatures

When raising the testing temperature from  $20\pm 1^{\circ}\text{C}$  to  $30\pm 1^{\circ}\text{C}$ , the behavior of asphalt concrete changed from brittle material to plastic material and that led to reducing the stress intensity factor and increasing deformation before cracking initiation. The reduction increases with increasing

notch depth due to decreasing the load required to bend and break the specimens with increasing testing temperature. **Fig.15** shows the effect of testing temperature on the stress intensity factor for the tested beam specimens of different notch depths.

#### 4.3. Asphalt Type

It was found that the asphalt type has no significant effect on the stress intensity factor for the tested specimens especially at low testing temperature at which the effect did not exceed 1% for 5<sup>mm</sup> notch depth; when rising the testing temperature, the effect increased to be about 3% for the same notch depth. The stress intensity factor reduced slightly when changing the asphalt type from 40-50 to 60-70 penetration graded because the asphalt 40-50 is harder than 60-70 and that led to decreasing the load required to bend and break the beam specimens made with asphalt type of 60-70 penetration graded. **Fig.16** shows the effect of asphalt type on stress intensity factor of tested beam specimens of different notch depths.

#### 4.4. Asphalt Content

The effect of asphalt content on stress intensity factor increased with decreasing the notch depth which was ranging from  $\pm 0.5\%$  to  $\pm 2\%$  at  $20 \pm 1^\circ\text{C}$  testing temperature and from  $\pm 1.5\%$  to  $\pm 6\%$  at  $30 \pm 1^\circ\text{C}$  testing temperature as presented in **Figures 17** and **18**. The stresses concentration decreased when decreasing the asphalt content due to decreasing the cementing material and increasing the air voids which form a discontinuity points in the mix that led to decreasing the load needed to bending and breaking the beam specimens.

### 5. CONCLUSION

From the results of this study it can be concluded that the fracture properties of asphalt concrete are mainly affected by decrease the temperature and presence of cracks that increase the stress concentration at the crack tip. The decrease in temperature causes the asphaltic material to become harder with low ductility and brittle behavior under the effect of traffic wheel loads. The presence of crack decreases the effective pavement depth that can resist the crack propagation. More deterioration is expected in pavement section with high flaws, which necessitate an early preventive maintenance. The sensitivity of stress intensity factor for the various study parameters, is shown in **Table 11**.

### REFERENCES

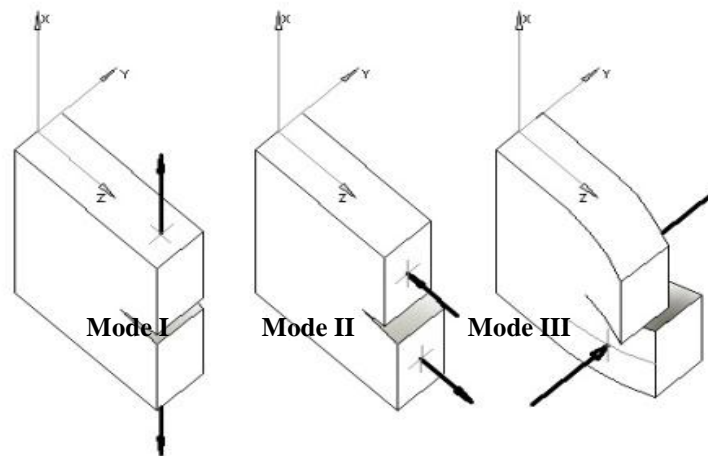
- American Association of State Highway and Transportation Officials AASHTO ,1993,"*Guide for Design of Pavement Structures*" Washington, D. C., USA.
- American Association of State Highway and Transportation Officials AASHTO ,2010,"*Standard Specifications for Transportation Materials and Methods of Sampling and Testing*" , Washington, D. C., USA.
- American Society of Metals ASM ,1997, "*Fatigue and Fracture*" Handbook, Volume 19, 2<sup>nd</sup> Printing, USA.



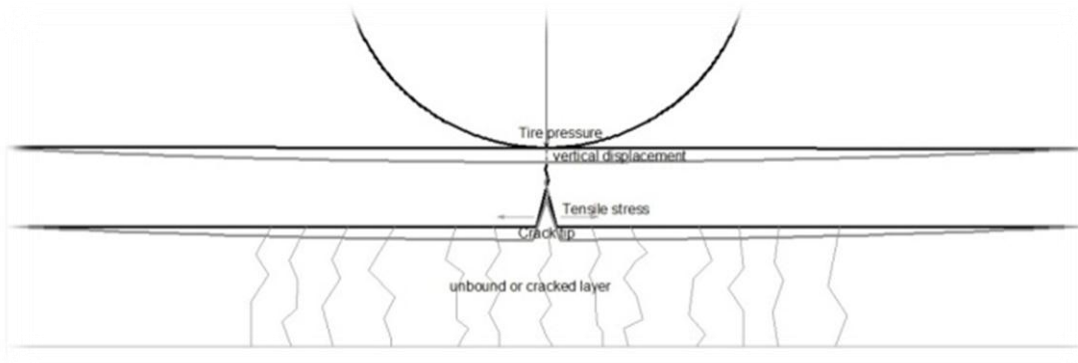
- American Society for Testing and Materials ASTM ,2009, "*Road and Paving Materials*" Annual Book of ASTM Standards, Volume 04.03, West Conshohocken, USA.
- Asphalt Institute ,2003, "*Performance Grade Asphalt Binder Specification and Testing*" Manual Series No.2, SP-2, Lexington, Kentucky.
- Denneman, E., R. Wu, E.P. Kearsley, and A.T. Visser, 2009, "*Fracture Mechanics in Pavement Design*" Proceedings of the 28<sup>th</sup> Southern African Transport Conference, PP. 255-262, 6-9July.
- Fadhel, T. H., 2007, "*Some Requirements to Control Reflective Cracking of Overlay Asphalt Pavement*" Ph.D. Thesis, Civil Engineering Department, College of Engineering, University of Baghdad.
- Im S. , 2012, "*Characterization of viscoelastic and fracture properties of asphaltic materials in multiple length scales*", Ph. D thesis, University of Nebraska, May.
- Kim, H., W.G. Buttler, M.N. Partl, 2008, "*Investigation of Fracture Toughening Mechanisms of Asphalt Concrete Using the Clustered Discrete Element Method*" Proceeding of the 8<sup>th</sup> Swiss Transport Research Conference, Monte Verita / Ascona, October 15-17.
- Kim, K.W., and H.M. El Hussein, 1995, "*Effect of Differential Thermal Contraction on Fracture Toughness of Asphalt Materials at Low Temperatures*" Proceeding of the Association of Asphalt Paving Technologists, volume 64, Portland, Oregon, March 27-29.
- Perng, J. , 1989, "*Analysis of Crack Propagation in Asphalt Concrete Using a Cohesive Crack Model*" MS c. thesis, Ohio State University.
- Portillo, O. and D. Cebon, 2008, "*An Experimental Investigation of the Fracture Mechanics of Bitumen and Asphalt*" Proceeding of the 6<sup>th</sup> Rilem International Conference on Cracking in Pavements, Chicago, USA, 16-18 June, PP. 627-636.
- Saadeh, S. and Hakimelahi, H. , 1998, "Investigation of Fracture Properties of California Asphalt Concrete Mixtures" Project No. 11-21, California state university long beach, department of civil engineering and construction engineering management, September, 2012.
- Saxena, A. "*Nonlinear Fracture Mechanics for Engineers*" CRC Press LLC, USA.
- State Corporation of Roads and Bridges SCRB, 2003, "*General Specification for Roads and Bridges/ Section R9, Hot Mix Asphalt Concrete Pavements*" Revised Edition, Ministry of Housing and Construction, Republic of Iraq.
- Uzan, J. and E. Levenberg , 2001, "*Strain Measurements in Asphalt Concrete Specimens towards the Development of a Fracture Model*" International Journal Pavement Engineering, Volume 2(4), PP. 243-258, Overseas Publishers Association OPA.

**NOMENCLATURE**

- P*: Reaction point load  
*B*: Specimen thickness  
*W*: Specimen depth  
*a*: Crack length  
*F(a/W)*: Dimensionless calibration functions for various geometries  
*Ws*: elastic strain energy  
*T*: Traction vector defined according to the outward normal *n* the contour *S*  
*u*: Displacement vector ( $u_1i + u_2j$ )  
*A*: Body area,  
*T<sub>i</sub>*: Tractions, and  
*u<sub>i</sub>*: Displacement.  
*S*: Clear span = 4W (12")

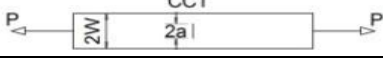
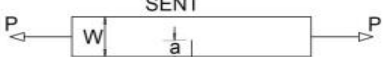


**Figure 1.** Crack modes, **Saxena, 1998.**



**Figure 2.** Crack in pavement.

**Table 1.** Dimensionless calibration functions for various geometries **Saxena, 1998.**

Geometry	$F(a/W)$
<p>Center Crack Tension CCT</p> 	$\frac{1}{2} \sqrt{\pi \frac{a}{W} \sec \frac{\pi}{2} \left( \frac{a}{W} \right)} \left[ 1 - .25 \left( \frac{a}{W} \right)^2 + 0.06 \left( \frac{a}{W} \right)^4 \right]$
<p>Single Edge Notch Tension SENT</p> 	$\frac{\left( 2 \tan \frac{\pi a}{2W} \right)^{1/2}}{\cos \frac{\pi a}{2W}} \left[ 0.752 + 2.02 \left( \frac{a}{W} \right) + 0.37 \left( 1 - \sin \frac{\pi a}{2W} \right)^3 \right]$



<p>Double Edge Notch Tension DENT</p>	$\frac{\frac{1}{2} \left( \frac{\pi a}{W} \right)^{1/2}}{\left( 1 - \frac{a}{W} \right)^{1/2}} \left[ 1.122 - 0.561 \left( \frac{a}{W} \right) - 0.205 \left( \frac{a}{W} \right)^2 + 0.471 \left( \frac{a}{W} \right)^3 - 0.19 \left( \frac{a}{W} \right)^4 \right]$
<p>Single Edge Notch Bending SENB</p>	$\frac{3 \left( \frac{S}{W} \right) \left( \frac{a}{W} \right)^{1/2} \left[ 1.99 - \frac{a}{W} \left( 1 - \frac{a}{W} \right) \left( 2.15 - 3.93 \left( \frac{a}{W} \right) \right) + 2.7 \left( \frac{a}{W} \right)^2 \right]}{2 \left( 1 + \frac{2a}{W} \right) \left( 1 - \frac{a}{W} \right)^{3/2}}$

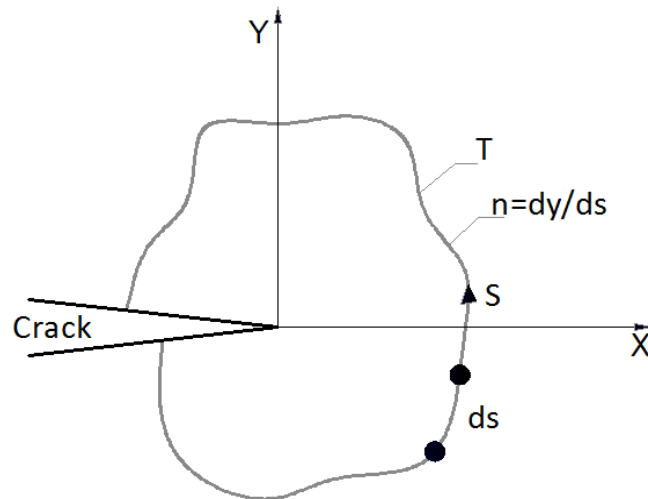


**Figure 3.** A 2-dimensional cracked body with a contour  $S$  originating from the lower cracked surface and going counterclockwise terminating at the upper crack surface, **Saxena, 1998.**

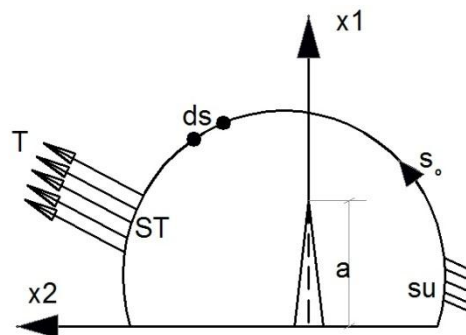


**Figure 4.** A planar cracked non linear elastic body with a boundary defined by  $S$ .  $ST$  and  $Su$  represent regions where the traction and displacement along the boundary are defined, **Saxena, 1998.**

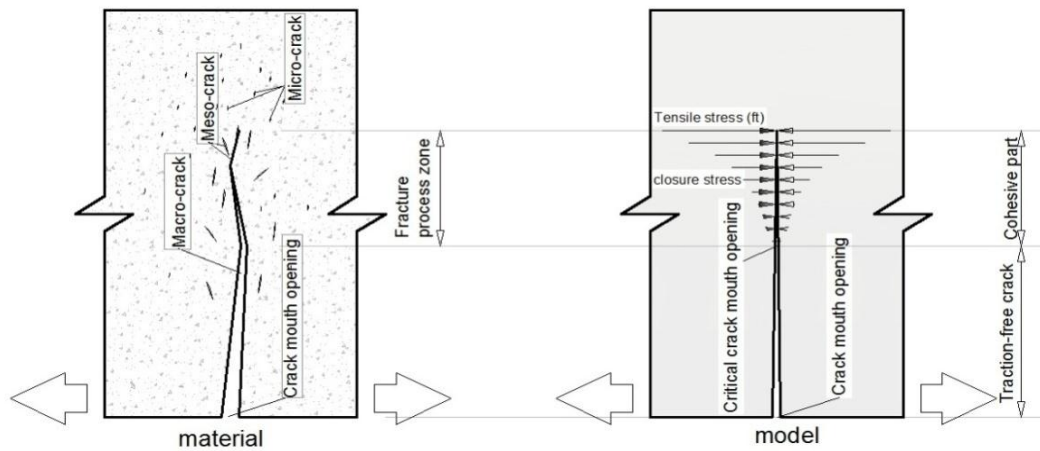


**Figure 5.** Crack scale in asphalt concrete material, **Uzan and Levenberg, 2001.**

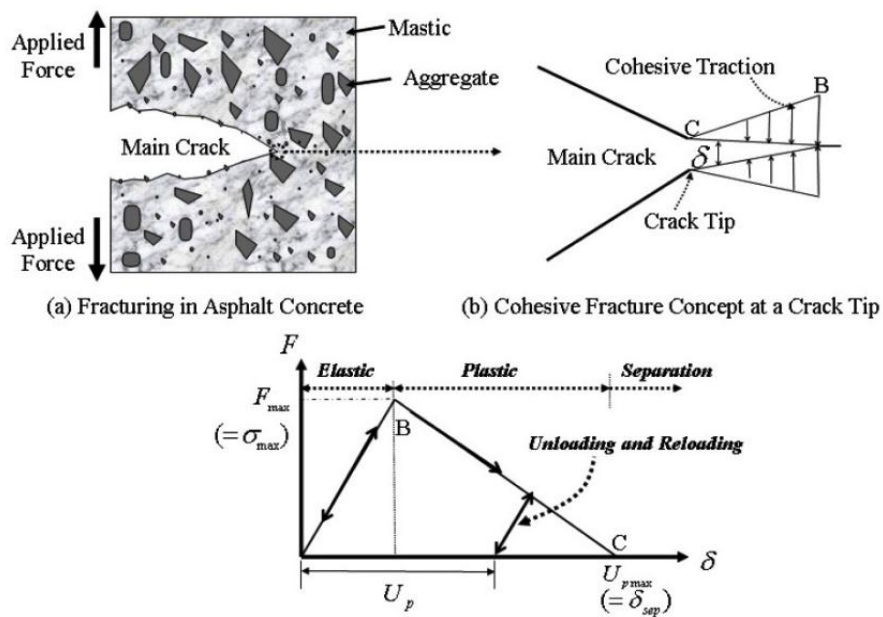


**Figure 6.** The schematic concept of bilinear cohesive softening model, **Kim, H., et. al., 2008.**

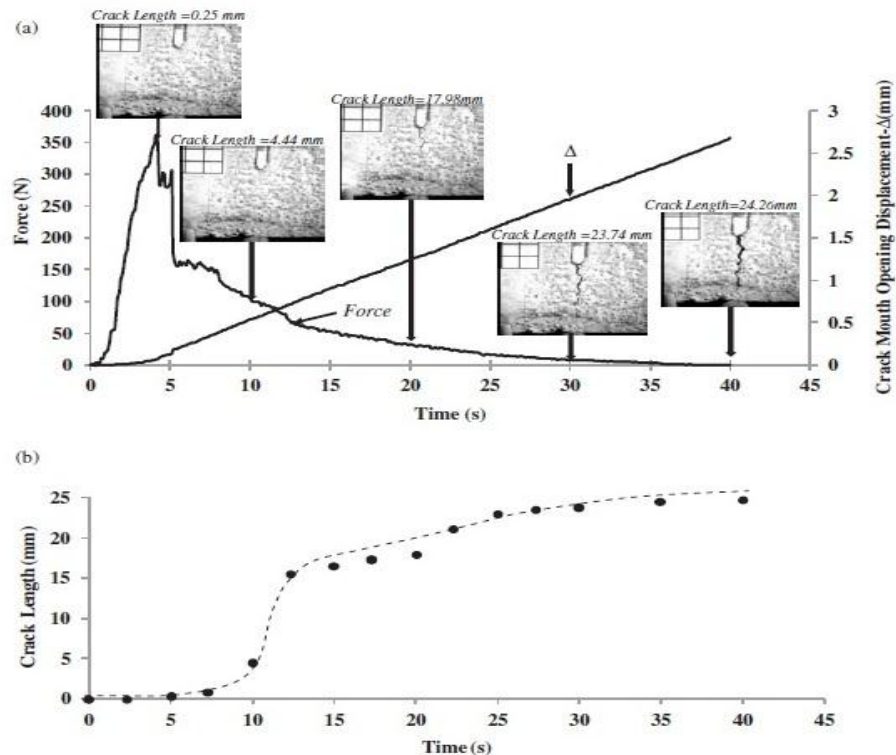


**Figure 7.** Typical load line displacement curve for tested beam sample at -20°C with displacement rate of 0.05mm/sec, Portillo and Cebon, 2008.

**Table 2.** Asphalt cements physical properties

Test	Test Conditions	ASTM, Designation (2010)	Units	Asphalt Cement		*SCRB criteria (2003)	
				40-50	60-70		
Penetration	100 gm, 25 °C, 5sec., 0.1 mm	ASTM D5	1/10 mm	47	64	40-50	60-70
Rotational Viscosity	135°C	ASTM D4402	Pas.sec	0.4625	0.353	---	---
	165 °C			0.125	0.113	---	---
Specific Gravity	25 °C	ASTM D70	----	1.04	1.03	---	---
Ductility	25 °C, 5 <sup>cm</sup> /min	ASTM D113	cm	>100	>100	>100	>100
Flash Point	-----	ASTM D92	°C	287	270	>232	>232
Solubility in trichloroethylene	-----	ASTM D2042	% wt	99.5	99.6	> 99	> 99
% Loss After Thin Film Oven Test	5hr @ 163°C, 50 gm	ASTM D1754	% wt	0.30	0.33	<0.75	<0.75
% from origin Penetration after Thin Film Oven Test	100 gm, 25°C, 5sec., 0.1 mm	ASTM D5	%	60	64	>55%	>52%
Ductility after Thin Film Oven Test	25 °C, 5 <sup>cm</sup> /min	ASTM D113	cm	75	>100	>25	>50

\*SCRB: State Corporation for Roads and Bridges

**Table 3.** Physical properties of coarse and fine aggregates of AL Nebai quarry.

Property	ASTM Test Designation (2010)	Coarse Aggregate	Fine Aggregate	SCRB Specification (2003)
<i>Bulk Specific Gravity</i>	<i>C-127 and C-128</i>	<i>2.610</i>	<i>2.630</i>	
<i>Apparent Specific Gravity</i>	<i>C-127 and C-128</i>	<i>2.690</i>	<i>2.708</i>	
<i>Percent Water Absorption</i>	<i>C-127 and C-128</i>	<i>0.464</i>	<i>0.715</i>	
<i>Percent Wear (Los Angeles Abrasion)</i>	<i>C-131</i>	<i>22.00</i>	<i>-----</i>	<i>30 max</i>
<i>Soundness loss by sodium sulfate solution, %</i>	<i>C-88</i>	<i>3.55</i>	<i>-----</i>	<i>10 max</i>
<i>Fractured pieces, %</i>	<i>-----</i>	<i>96</i>	<i>-----</i>	<i>95 min</i>
<i>Sand Equivalent, %</i>	<i>D-2419</i>	<i>-----</i>	<i>53</i>	<i>45 min.</i>

**Table 4.** Chemical composition of AL-Nebai quarry aggregates.

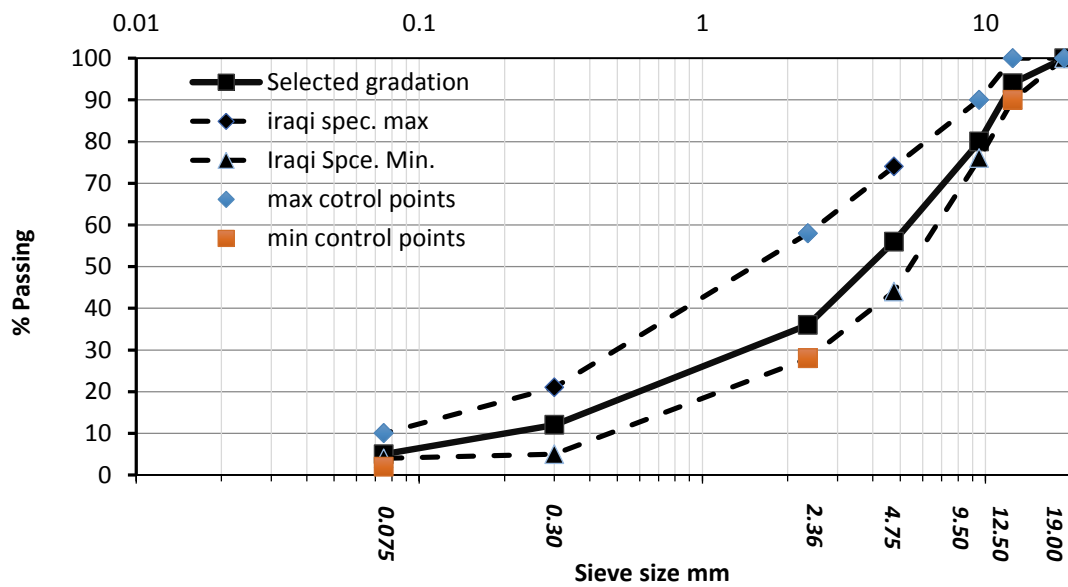
Mineral Composition	% content
<i>Quartz</i>	<i>80</i>
<i>Calcite</i>	<i>11</i>
<i>Total Soluble Salts TSS</i>	<i>2.0</i>
<i>Gypsum</i>	<i>0.45</i>
<i>Organic Matter</i>	<i>0.50</i>

**Table 5.** Mineral composition of AL-Nebai quarry aggregates.

Chemical compound	% content
<i>Silica SiO<sub>2</sub></i>	<i>82.52</i>
<i>Lime CaO</i>	<i>5.37</i>
<i>Magnesia MgO</i>	<i>0.78</i>
<i>Alumina Al<sub>2</sub>O<sub>3</sub></i>	<i>0.48</i>
<i>Ferric Oxide Fe<sub>2</sub>O<sub>3</sub></i>	<i>0.70</i>
<i>Sulfuric Anhydride SO<sub>3</sub></i>	<i>2.7</i>
<i>Loss on Ignition</i>	<i>6.55</i>
<i>Total</i>	<i>99.10</i>

**Table 6.** Physical properties of mineral filler.

<i>Property</i>	<i>Test Result</i>
<i>Specific Gravity</i>	<i>2.720</i>
<i>Passing Sieve No.200 (0.075 mm)</i>	<i>95%</i>


**Figure 8.** Selected aggregates gradation.

**Table 7.** Mixing and compaction temperatures for asphalt binder penetration graded.

Asphalt Binder Penetration Graded	Temperature °C	
	Mixing temperature	Compaction temperature
(40-50)	158	148
(60-70)	153	142

**Table 8.** *SUPERPAVE* gyration levels design ,SP-2, 2003.

ESALs (millions)	Number of Gyration		
	N initial	N design	N max
<0.3	6	50	75
0.3 to 3.0	7	75	115
3.0 to 30.0	8	100	160
≥ 30.0	9	125	205

**Table 9.** HMA volumetric properties of wearing mix at OBC ,SP-2, 2003.

<i>Mix Property</i>	<i>Optimum Binder Content 4.70%</i>	<i>SUPERPAVE Criteria</i>
<i>Air voids</i>	<b>4.00%</b>	<b>4.00%</b>
<i>VMA</i>	<b>15.10%</b>	<b>Min. 14%</b>
<i>VFA</i>	<b>73.25%</b>	<b>65%-75%</b>
<i><math>G_{mb}/G_{mm}</math> @ <math>N_{initial}</math> 8</i>	<b>85.10%</b>	<b>Max. 89%</b>
<i><math>G_{mb}/G_{mm}</math> @ <math>N_{design}</math> 100</i>	<b>96.00%</b>	<b>96.00%</b>
<i><math>G_{mb}/G_{mm}</math> @ <math>N_{maximum}</math> 160</i>	<b>96.742%</b>	<b>Max. 98%</b>



**Plate 1.** Optimum binder content determination using SUPERPAVE requirements.

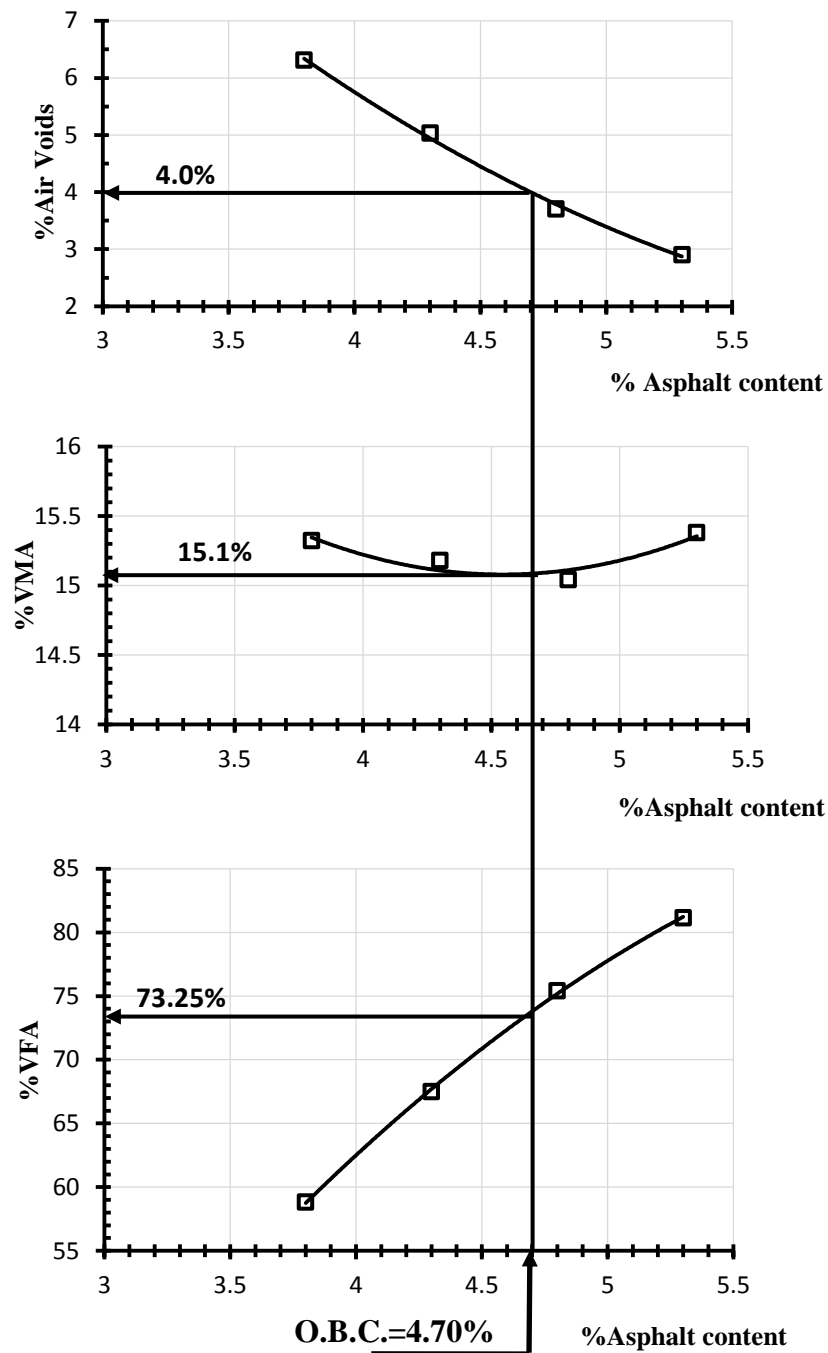
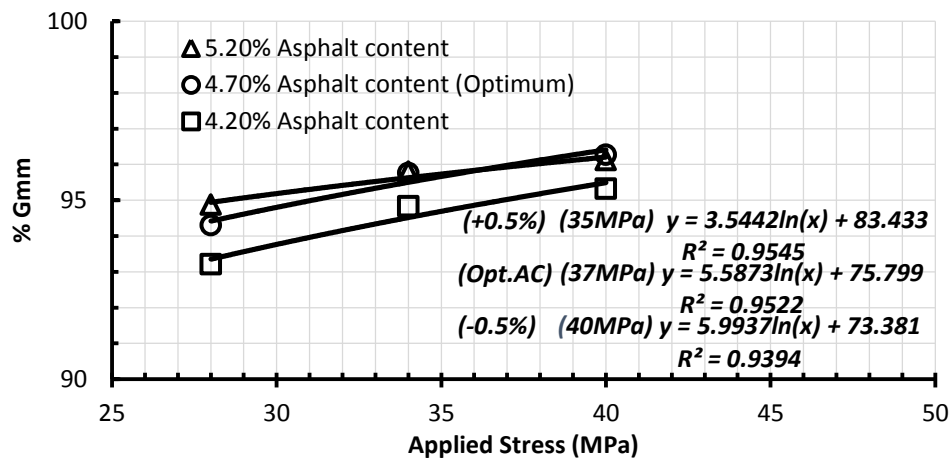


**Figure 9.** OBC determination for wearing layer according to *SUPERPAVE* criteria.

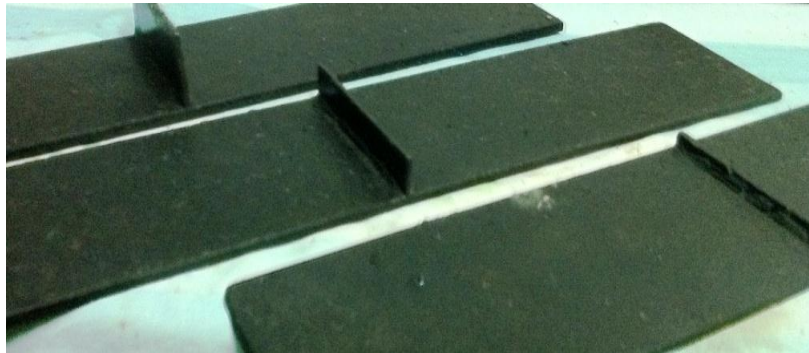




**Plate 2.** Beams specimens preparation.



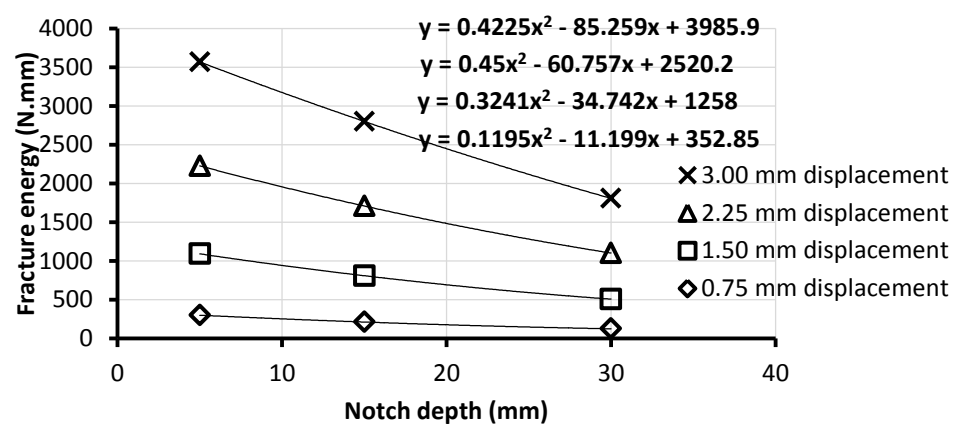
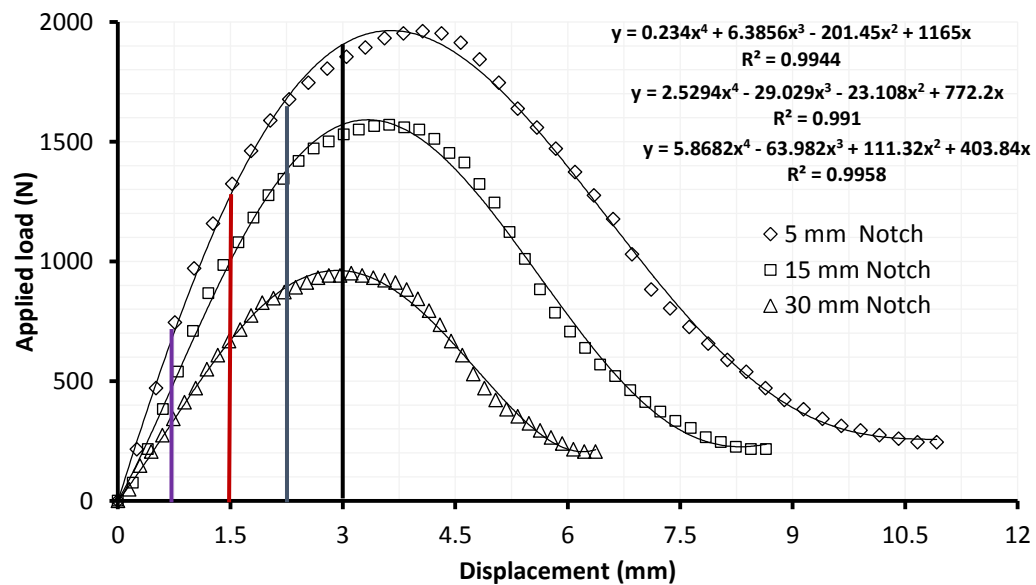
**Figure 10.** Applied stress and %  $G_{mm}$  relations for beams specimens with different asphalt content.

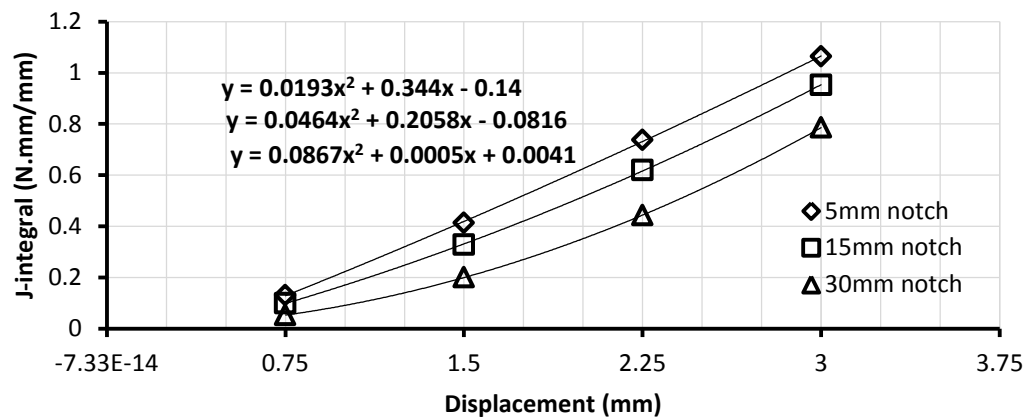


**Plate 3.** Steel plates arrangements which used for making notches.

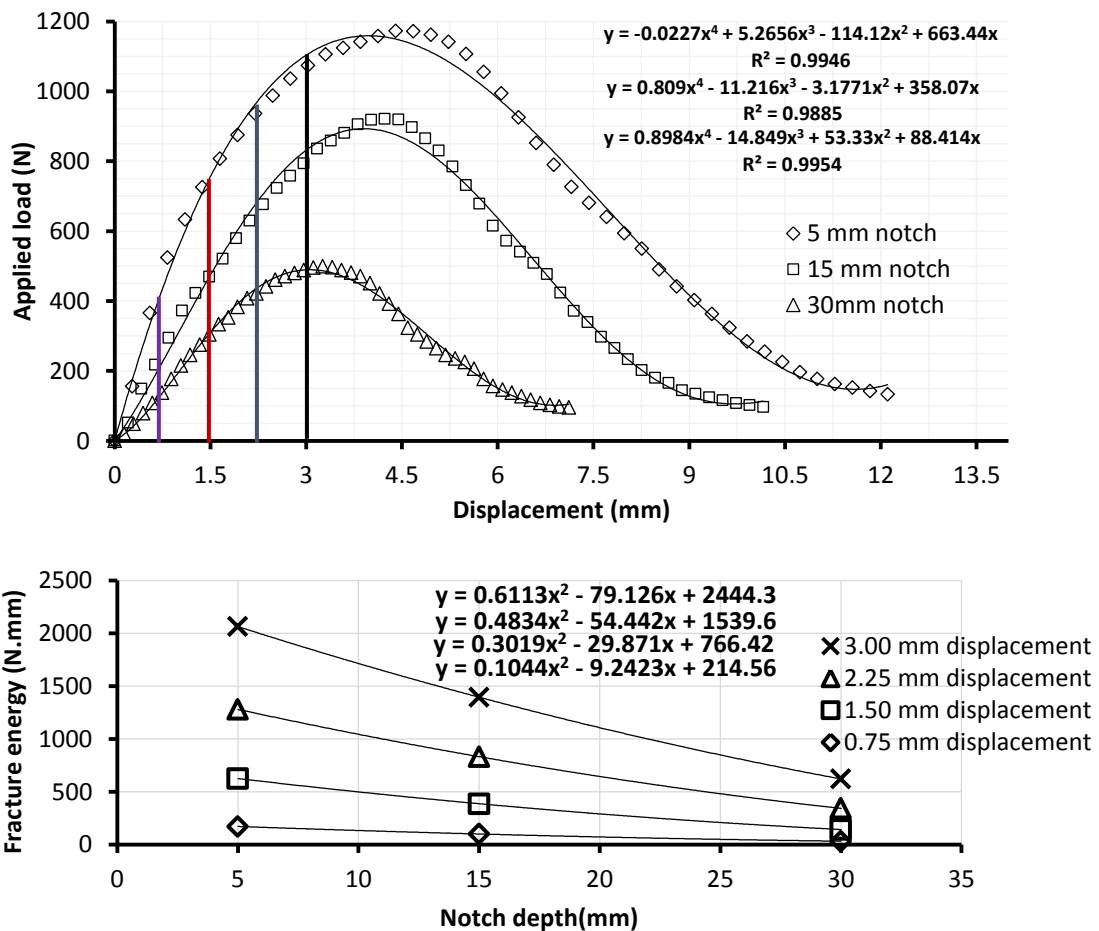


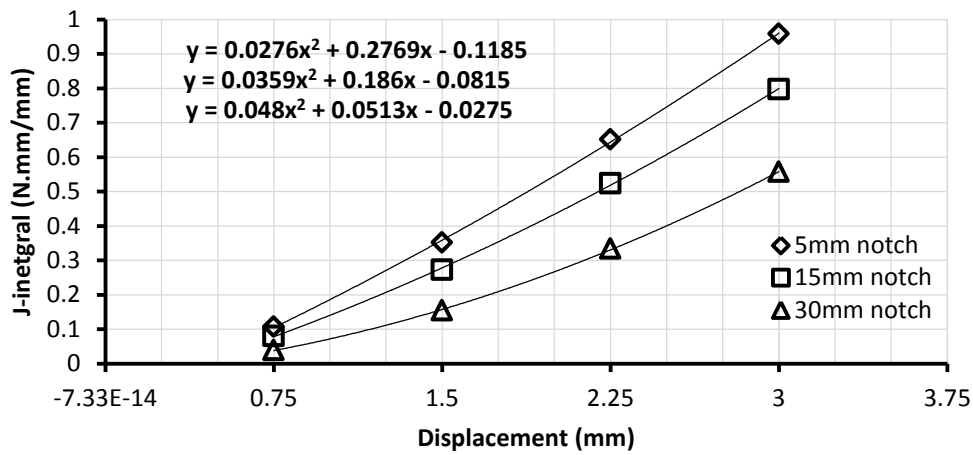
**Plate 4.** Load frame device of multi deformations rates and tested specimens.





Figures 11-a, b, and c. Estimating fracture properties, in-terms of (U) fracture energy and J-integral for beams specimens with different notch depths tested with 3-point BBT at  $20 \pm 1^\circ\text{C}$ .





**Figures 12-a, b, and c.** Estimating fracture properties, in-terms of (U) fracture energy and J-integral for beams specimens with different notches depths tested with 3-point BBT at  $30 \pm 1^\circ\text{C}$ .

**Table 10.** Calibration function  $F(a/W)$  magnitude for studied notch depth.

Notch depths	5 <sup>mm</sup>	15 <sup>mm</sup>	30 <sup>mm</sup>
$F(a/W)$	2.836	4.981	10.107

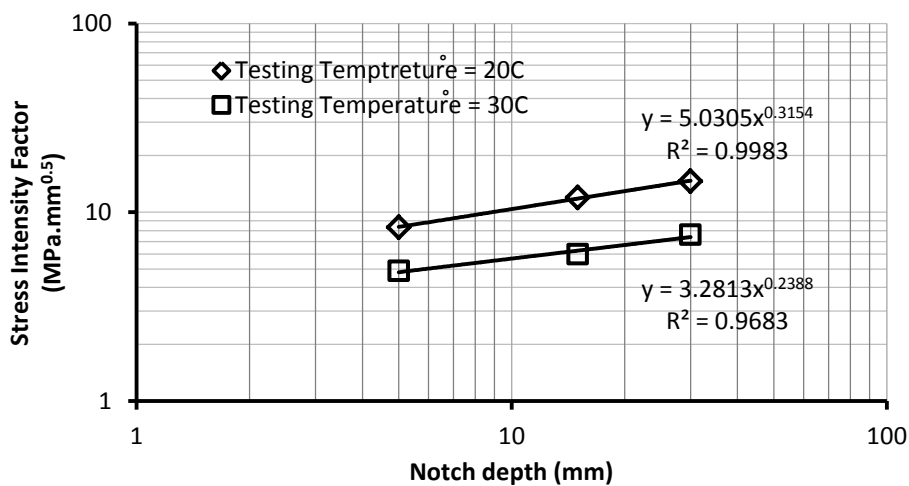


**Figure 13.** Stress Intensity Factor (K) for beams specimens of different notch depth tested monotonically at  $20 \pm 1^\circ\text{C}$  and  $30 \pm 1^\circ\text{C}$ .

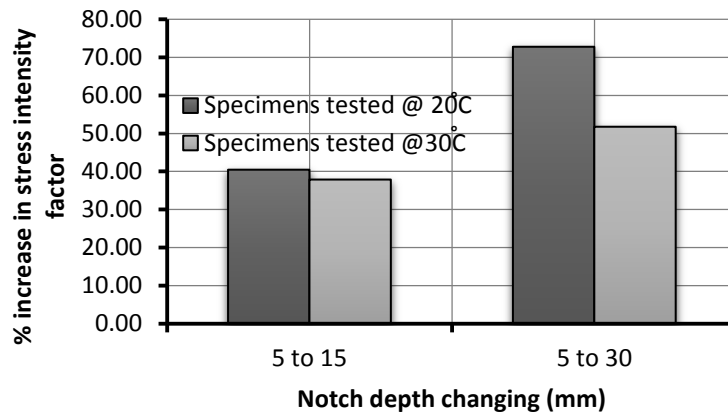


**Figure 14.** Percentage increase in stress intensity factor with increasing notch depth for beam specimens tested at  $20\pm 1^\circ\text{C}$  and  $30\pm 1^\circ\text{C}$  with different notch depths.

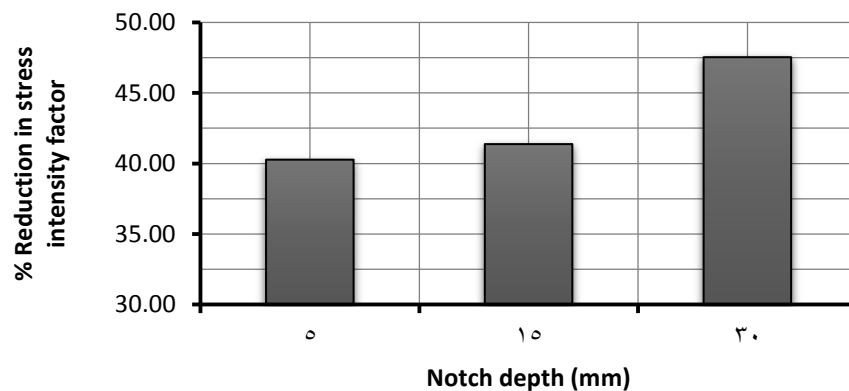


**Figure 15.** Percentage drop in stress intensity factor with increasing testing temperature for beam specimens tested at  $20\pm 1^\circ\text{C}$  and  $30\pm 1^\circ\text{C}$  with different notch depths.

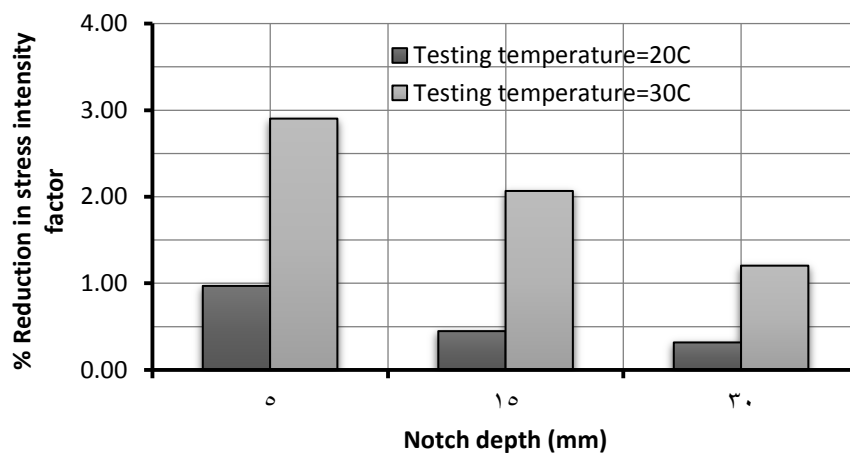


**Figure 16.** Percentage reduction in stress intensity factor for beam specimens tested at  $20\pm 1^\circ\text{C}$  and  $30\pm 1^\circ\text{C}$  with different notch depths due to change the asphalt type.

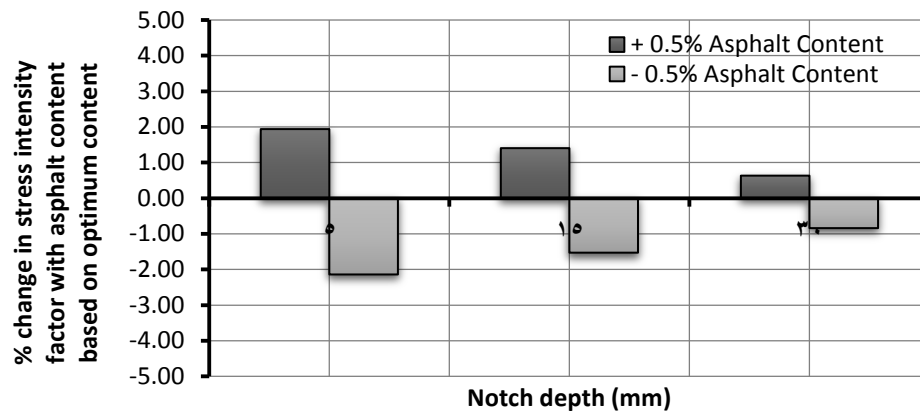


**Figure 17.** Percentage of change in stress intensity factor for beams specimens tested at  $20\pm 1^{\circ}\text{C}$  with notch depths.

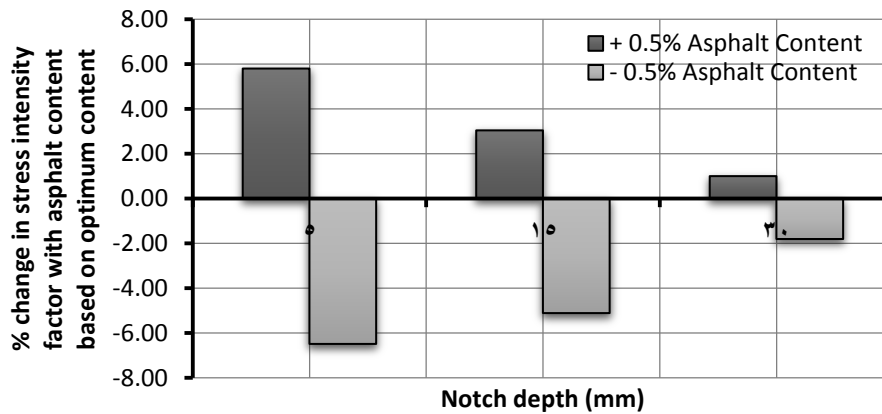


**Figure 18.** Percentage of change in stress intensity factor for beams specimens tested at  $30\pm 1^{\circ}\text{C}$  with notch depths.

**Table 11.** Stress intensity factor sensitivity according to study parameters.

Parameters	Percentage Effect	Sensitivity
Testing Temperature	>40%	Relatively High
Notch depth	>40%	Relatively High
Asphalt Content	<6%	Relatively low
Asphalt Type	<3%	Relatively low



## Estimation and Improvement of Routing Protocol Mobile Ad-Hoc Network Using Fuzzy Neural Network

**Dr. Tarik Zeyad Ismaeel**

professor

College of engineering-University of Baghdad

Email: tarikismaeel@yahoo.com

**Dhurgham Razaq Mohsen**

Instructor

College of engineering-University of Baghdad

Email: dego\_977@yahoo.com

### ABSTRACT

**A**d-Hoc Networks are a generation of networks that are truly wireless, and can be easily constructed without any operator. There are protocols for management of these networks, in which the effectiveness and the important elements in these networks are the Quality of Service (QoS). In this work the evaluation of QoS performance of MANETs is done by comparing the results of using AODV, DSR, OLSR and TORA routing protocols using the Op-Net Modeler, then conduct an extensive set of performance experiments for these protocols with a wide variety of settings. The results show that the best protocol depends on QoS using two types of applications (+ve and -ve QoS in the FIS evaluation). QoS of the protocol varies from one protocol to another depending on the applications used in the network. The network design is done using the program (Op-Net V14.5 modular) with core i7 computer for multiple nodes deployed randomly in several area (100 \* 100, 200 \* 200, 400 \* 400, 800 \* 800, 1000 \* 1000)m<sup>2</sup> accomplished by changing the number of nodes in the network (10, 20, 40 and 80). There are three programs designed using (MATLAB 2012A programming language). The first one evaluates the (QoS) using the organizational structure of the mysterious system (HFS), which relied on the standard applications that should be provided by the protocols to make the applications accepted by the nodes requirements. After the evaluation the QoS for all cases, we design Neural Network to assist in estimation of the best protocol for any network through QoS for all protocols (AODV, DSR, OLSR and TORA). Neural network has four entrances (area, number of nodes, real time application ratio and non-real time application ratio). The results show that the QoS estimated is (0.5401) of (OLSR) which has been improved to (0.6421) by reducing to mobility speed and making some nodes fixed and using more than one protocol in the network to provide the best QoS .

**Keywords:** Estimation, protocol, QoS, Simulator



## اقتراح وتحسين بروتوكولات توجيه الشبكة المخصصة باستخدام جودة الخدمة بواسطة الشبكات العصبية الغامضة

ضرغام رزاق محسن

الباحث الثاني

جامعة بغداد – كلية الهندسة

أ.د. طارق زياد إسماعيل

الباحث الأول

جامعة بغداد – كلية الهندسة

### الخلاصة

شبكات (Ad-Hoc) جيل من الشبكات التي لا تحتوي على أي اتصال سلكي بالإضافة إلى أنه يمكن بناؤها بسهولة ولا تحتاج إلى أي مشغل. وهناك بروتوكولات لإدارة هذه الشبكات ومن أهم العناصر التي تحدد فعالية هذه البروتوكولات هي جودة الخدمة للبروتوكول (QoS) (تم استخدام الـ QoS الموجبة والسالبة في تقييم الـ FIS). تختلف (QoS) من بروتوكول لآخر اعتماداً على تطبيقات المستخدمة في تلك الشبكة. تم تصميم شبكة بأستخدام برنامج (Op-Net 14.5 modular) لعدة مستخدمين تم نشرهم بشكل عشوائي في عدة مساحات متغيرة (100\*100, 200\*200, 400\*400, 800\*800, 1000\*1000) وتم تغيير عدد المستخدمين للشبكة من (10, 20, 40, 80). وقد تم تصميم ثلاثة برامج باستخدام (MATLAB 2012A programming language) الأول وقد تم احتساب جودة الخدمة باستخدام نظام الهيكل التنظيمي الغامض (HFS) والذي اعتمد على متطلبات التطبيقات القياسية التي ينبغي أن يقدمها البروتوكول لجعل التطبيق مقبول من قبل المستخدمين النهائيين. والثاني لتوقع البروتوكول الأفضل وذلك من خلال إعطاء جودة الخدمة لكل بروتوكول (AODV, DSR, OLSR, TORA) للشبكة المطلوبة وقد اعتمد البرنامج الثالث على تصميم شبكة عصبية لها أربعة مداخل وهي (المساحة و عدد المستخدمين و نسبة استخدامات تطبيقات الاتصالات المباشرة ونسبة تطبيقات الغير مباشرة). من أهم النتائج التي ظهرت لنا هي الاختبار الثالث حيث ان جودة الخدمة ظهرت لأفضل بروتوكول هي (0.5401) للـ (OLSR) وقد تم تحسينها إلى (0.6421) من خلال تقليل السرعة او جعل بعض المستخدمين ثابت او وضع مستخدمين فقط لتوفير الخدمة لباقي المشتركين واستخدام أكثر من بروتوكول بالشبكة لتوفير أفضل جودة خدمة للشبكة.

مفاتيح الكلمات : اقتراح ، بروتوكولات ، جودة الخدمة ، محاكاة



## 1. INTRODUCTION

A mobile ad-hoc network (MANET) is a set of wireless mobile nodes that can communicate with each other without using any fixed infrastructure. It is also necessary for MANET devices to communicate in a seamless manner. There are multiple protocols that have been developed for MANETs. There is a need to support real time and non real time applications in MANETs as they gain popularity. MANETs require an efficient routing protocol and quality of service (QoS) mechanism in order to support multimedia applications such as voice and Email. Such applications have strict QoS requirements such as bandwidth, latency, PDR and jitter. Design and development of routing algorithms with QoS support is experiencing increased research interest. This paper evaluates the QoS performance of MANETs using fuzzy interface system for AODV, DSR,OLSR and TORA routing protocols. Through the OPNET Modeler program, we have conducted an extensive set of performance experiments for these protocols with a wide variety of settings. On-demand routing protocols are widely used because they use much lower routing overhead than proactive protocols, **Jasani, 2011**.

Characteristics of WAN's such as lack of central coordination, mobility of hosts, dynamically varying network topology and limited availability of resources make QoS provisioning very challenging for all difficulties, **Reddy, 2006**. Some nodes may behave maliciously, resulting in degradation of the performance of the network or even disruption of its operation altogether. The results obtained show that the overall performance of the Ad-Hoc network is significantly improved, **Hallani, 2008**.

## 2. WIRELESS AD-HOC NETWORKS

A mobile Ad-Hoc network (MANET) is Unlike cellular wireless networks, no static or fixed infrastructure exists and no centralized control can be available. The network can be formed anywhere, **Lewis, 2007**. The mobile nodes can perform the roles of both hosts and routers. The presence of mobility makes a MANET challenging for designing and implementation in real life. It is a huge challenge to design topology



control, routing, (QoS) and resources management, services discovery, network operations and management, security services, **Misra, et al. 2009.**

**2.1 Mobility** The mobility of nodes is the key function of mobile Ad-Hoc networks, and the performance of MANET needs to be studied in presence of mobility. It is known that the Real-life mobility patterns can be very complex depending on the mission objectives of mobile nodes that are part of the autonomous system, **Misra, et al. 2009.**

**2.2 Routing.** The routing in mobile Ad-Hoc networks is very challenging due to the frequent updates for changes in topologies, and active routes may be disconnected as mobile nodes move from one place to another, **Misra, et al. 2009.**

**2.3 Transport Protocol:** In mobile Ad-Hoc networks, the frequent changes of the network topology and the shared nature of the multi-hop wireless channel pose a significant challenge for the transport protocols that are used over the network protocol such as Internet protocol (IP), **Misra, et al. 2009.**

**2.4 Application** A mobile Ad-Hoc network consisting of mobile nodes is self-organized and decentralized and communicates among mobile nodes using multi-hop wireless links. Each mobile node is autonomous and can have random movement patterns, **Misra, et al. 2009.**

### **3. HIERARCHICAL FUZZY SYSTEMS**

Since the upper layers of a hierarchical architecture generally deal with low-resolution, imprecise, and incomplete information, more intelligence (or knowledge-based action) would be needed in the associated decision-making process. Yet the performance of the overall system may be acceptable. The characteristic of an intelligent system are task description, knowledge representation, and consequently some intelligence will be needed for interpretation and processing of this information in order to make inferences (and control actions), **Sivanandam et al. 2007.**

### 3.1 Evaluation of QoS Using Hierarchal Fuzzy System (QoSHFS)

The evaluation of QoS for any protocol that depends on applications used, and these are divided into two type:

#### A. Evaluation of QoS Real time Application

To clarify the design process, there are two types of parameters effect, positive parameters (+ve) and negative parameters (-ve). According to this proportionality, QoS is a result of, **Valbonne 2007:**

1. +ve QoS: This calculation of QoS is affected only when parameters have a positive effect on the QoS, which are throughput and packet delivery ratio. When these two parameters decrease, the protocol QoS support will decrease too, **Zaghar and AL Wahab, 2013.**
2. -ve QoS: This calculation of QoS is affected by parameters that have negative effect on the protocol QoS. End-to-end delay (latency) and jitter will belong to this branch of QoS. Decreasing these two parameters will increase protocols QoS, **Zaghar and AL Wahab, 2013.**

In the network design, the increment of +ve QoS is done by increasing the throughput and PDR (Packet Delivery Ratio) and reduction of the -ve QoS is done by reducing the Latency and Jitter. **Fig. 1** illustrates the QoS calculation, **Zaghar and AL Wahab, 2013.**

#### B. Evaluation of QoS Non Real time Application

Each type of applications is very sensitive to a certain set of parameters. The most effect parameters in the QoS in the Email application are (throughput and latency) as shown in **Fig. 2.**



## 4. NEURAL NETWORKS

An Artificial Neural Network (ANN) is an information-processing paradigm that is inspired by the way of biological nervous systems, such as the brain, process information. The key element of this paradigm is the novel structure of the information processing system. An ANN are configure for a specific application, such as pattern recognition or data classification, through a learning process. Learning in biological systems involves adjustments to the synaptic connections that exist between the neurons. This is true for (ANNs) as well, **Karray and de Silva, 2004**.

### 4.1 Neural Network Architecture

Neural networks Architecture can be viewed as weighted directed graphs in which artificial neurons are nodes and direct edges (with weights) are connections between neuron inputs as shown in **Fig. 3**.

The following characteristics of neural networks emphasize their pattern recognition capabilities, making them particularly attractive for solving complex, and data rich problems, **Fakhreddine et al, 2004**:

1. They can be learned from examples and adapted to new situations.
  2. They can be generalize from examples (i.e. can provide correct solutions from data similar to but not exactly like training data).
  3. They can construct solution quickly with no reliance on domain knowledge.
  4. They can approximate any complex multivariate function and form a classification decision from the recognition of the discriminating patterns.
  5. They are computationally efficient (i.e. they have the speed to operate in real time).
  6. They can implicitly account for the relative importance of input sources,
- Karray and de Silva, 2004**.



## 4.2 Artificial Neuron Structure

The human nervous system, built from cells called neurons is of staggering complexity. An estimated ( $10^{11}$ ) interconnections over transmission paths are there and that may range for a meter or more.

Each neuron shares any characteristics with the other cells in the body, but has unique capabilities to receive, process, and transmit electrochemical signals over neural pathways that comprise. The Biological neuron consists of three main components: cell body, dendrite and axon.

Dendrites extend from the cell body to other neurons where they receive signals at a connection point called a synapse. On the receiving side of the synapse, these inputs are conducted to the cell body, where they are summed up. Some inputs tend to excite the cell causing a reduction in the potential across the cell membrane.

The artificial neuron was designed to mimic the first order characteristics of the biological neuron. In essence, a set of inputs is applied, each representing the output of another neuron. Each input is multiplied by a corresponding weight, analogous to a synaptic strength, and all of the weighted inputs are then summed to determine the activation level of the neuron. If this activation exceeds a certain threshold, the unit produces an output response.

This functionality is captured in the artificial neuron known as the threshold logic unit. Here a set of input labeled  $X_0, X_1, \dots, X_n$  is applied from the input space to artificial neuron. These inputs, collectively referred as the input vector “X”, correspond to the signal into the synapses of biological neuron. Each signal is multiplied by an associated weight  $W_0, W_1, \dots, W_n$ , before it is applied to the summation block. The activation function is given by **Equation 1, Karray and de Silva, 2004.**

$$a = W_0 X_0 + W_1 X_1 + \dots + W_n X_n + \theta \quad \dots 1$$

This may be represented more compactly as

$$a = \sum_{i=0}^n X_i W_i + \theta \quad \dots 2$$

Where  $\theta$  the base of the weight

The output  $y$  is then given by  $y = f(a)$ ,

where  $f$  is an activation function used and defined as

$$y = \begin{cases} 1 & \text{if } a \geq \beta \\ 0 & \text{if } a < \beta \end{cases} \quad \dots 3$$

The threshold  $S$  will often be zero. The activation function is sometimes called a step-function. Some more non-linear activation functions were also tried by the researchers like sigmoid, Gaussian, etc. and the neuron responses for different activation functions with the MATLAB program, **Liua, et al. 2007**.

The number of input layers have four neurons (area, number of nodes, ratio of RTA and ratio of NRTA) and there are three hidden layers.

## 5. DESIGN AND EVALUATION

The network are designed using Op-Net Modular V14.5 under specification given in **Table 1**, and the area is changed as following values (100\*100, 200\*200, 400\*400, 800\*800 and 1000\*1000) m<sup>2</sup>. Different numbers of nodes are taken in all scenarios, after all scenarios are done we calculate the QoS for all protocols and used it to leaned Neural network to estimate the Best protocol as shown in **Fig. 4**.

### 5.1 Evaluation and Analysis of QoSHFS

During the evaluation of FIS from the QoSHFS, the first calculations of voice QoS are between the throughput and PDR under the first level of +ve QoS part. The second calculations of voice QoS are between jitter and latency under the same level but





in -ve QoS part. The result from the two parts will be used in the calculation of the final QoS and will be multiplied by the ratio of real time application (depending on the requirements).

Another evaluation of fuzzy is QoS of E-Mail calculated between throughput and latency parameters, which are multiplied by the ratio of non-real time application.

Finally adding the results from the fuzzy voice to results of E-mail under constrain environment, which will be the results of QoS, **Zaghar and AL Wahab, 2013**.

## 5.2 Neural Network.

1. There are 180 simulations designed using Op-Net modular 14.5 by (AODV, DSR, OLSR and TORA) protocols and evaluated the QoS for it using fuzzy interface system.
2. Through **Equation 4**, **Xia, et al. 2012**, and trial and error we concluded the number of hidden layers which is 4 as shown in **Fig. 5**.

$$n \leq 4\sqrt{m(k+1)} \quad \dots 4$$

where

(m) is input layer nodes, (K) the output layer nodes

3. The 180 QoS evaluated from **step 1** in the **Table 2-A,2-B,2-C,2-D,2-E**, will be used to learn neural till 5000 iteration and the best validation 12331 as shown in **Fig. 6** and **Fig. 7**.
4. The input are four elements (area, number of nodes, ratio of R.T.A and ratio of N.R.T.A), the second layer is hidden layer and it contains 20 neurons and the third layer contains 10 neurons and fourth is contains 20 neurons and last
5. Training the network depends on the results from the simulation (QoS) and making the error ratio ( $10^{-7}$ ). This will learn the neural network to get high accuracy digit to estimate the best protocol of the area. This topic describes



two different styles of training. The incremental training in which the weights and biases of the network are updated each time an input is presented to the network. The second style is the batch training in which the weights and biases are only updated after all the inputs are presented. The batch training methods are generally more efficient in the MATLAB 2012A environment, and they are emphasized in the Neural Network Toolbox software, but there are some applications where incremental training can be useful, so that paradigm is implemented as well.

6. Validation the network. Now the network is ready to be used.

After neural network design, one can be sure from accuracy of the results through the input data approximation of data learning.

Test No.	1			Results			
Area	No. Of Nodes	Ratio Of Real Time Application	Ratio of Non-Real Time Application	AODV	DSR	OLSR	TORA
15000 m <sup>2</sup>	50	0.5	0.5	0.9963	0.9945	0.9994	0.9934

From **test 1** the area 15000 m<sup>2</sup> is (122\*122) which is close to the area (100\*100) and result matches the learning data. The best protocol is OLSR.

Test No.	2			Results			
Area	No. Of Nodes	Ratio Of Real Time Application	Ratio of Non-Real Time Application	AODV	DSR	OLSR	TORA
25000 m <sup>2</sup>	45	0.5	05	0.9993	0.9947	0.9925	0.9905

Test No.	3			Results			
Area	No. Of Nodes	Ratio Of Real Time Application	Ratio of Non-Real Time Application	AODV	DSR	OLSR	TORA
50000 m <sup>2</sup>	60	0.5	0.5	0.3311	0.1383	0.5401	0.0158



From **test 2**, increasing the area and decreasing the number of nodes the QoS remains constant and the best of routing protocol for this specification is (AODV).

Test No.	4			Results			
Area	No. Of Nodes	Ratio Of Real Time Application	Ratio of Non-Real Time Application	AODV	DSR	OLSR	TORA
750000 m <sup>2</sup>	40	0.7	0.3	0.7585	0.7200	0.8586	0.4922

In **test 3**, the best protocol is OLSR but it needs to be improved; by adding node server to serve other nodes as shown in **Fig. 8** and making some of nodes static (to reduce the update of table driven in reactive protocol) or increasing the ratio of real time application to improve the QoS.

After adding 6 nodes server and making 25 nodes static the QoS will be improved to (0.6421).

Test No.	5			Results			
Area	No. Of Nodes	Ratio Of Real Time Application	Ratio of Non-Real Time Application	AODV	DSR	OLSR	TORA
300000 m <sup>2</sup>	60	0.5	0.5	0.9968	0.9991	0.9939	0.9902

Test No.	6			Results			
Area	No. Of Nodes	Ratio Of Real Time Application	Ratio of Non-Real Time Application	AODV	DSR	OLSR	TORA
500000 m <sup>2</sup>	48	0.3	0.7	0.9911	0.4838	0.2472	0.1561

Through previous tests and the results showed it was possible to expect the best protocol for any region and the number of nodes application used, which in turn will determine the best protocol, which helps to achieve the best QoS to the network. There



are some of rules to improve QoS through mixing between the two protocols (AODV & DSR) as compared with reference **Bandyopadhyay, 2006**, or distribute some of nodes server to help other nodes by flooding.

## 6.CONCLUSION

This paper presented a research work on QoS technologies for multimedia applications in next generation networks. We used Fuzzy Neural technique to implement this work. The Fuzzy technique evaluated QoS for all protocols by identifying different number of nodes using several areas. The most important parameters in the QoS are: throughput, PDR, Latency, and Jitter. The values of the QoS evaluation were compared with the results of implementing other protocols for the same design. The Neural technique was implemented and tested to identify the best protocol. The Ad-hoc network had used two types of applications: Real time and Non real time applications in the MANET. Finally, the neural technique used all QoS results obtained by Fuzzy technique to learn ANN. The results showed that the proposed approach enhanced performance and it was the best protocol depending on the QoS factor of the medium radio.

## REFERENCES:

- Bandyopadhyay S., Roy S. and Ueda T., 2006, “*Enhancing the Performance of Ad Hoc Wireless Networks with Smart Antennas*”, Published in 2006 by, Auerbach Publications, Taylor & Francis Group, 6000 Broken Sound Parkway NW, Suite 300, Boca Raton, FL 33487-2742.
- Hallani H. and Shahrestani S. A., 2008, “*Fuzzy Trust Approach for Wireless Ad-hoc Networks*”, Communications of the IBIMA, vol.1, pp.212–218,
- Jasani H., 2011, “*Quality of Service Evaluations of On Demand Mobile Ad-Hoc Routing Protocols*”, Department of Computer Science, Northern Kentucky

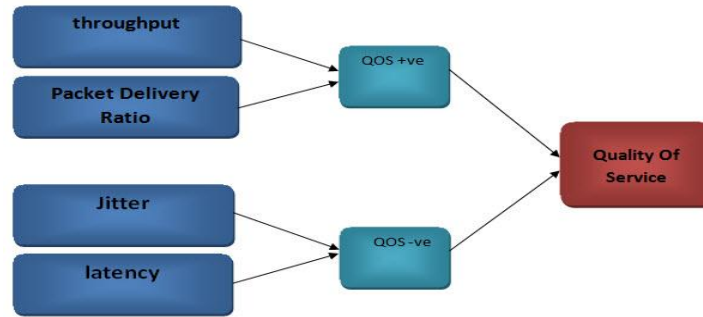


University, Highland Heights, KY, USA, 41099, jasanih1@nku.edu, 978-0-7695-4496-0/11 © 2011 IEEE, DOI 10.1109/NGMAST.31

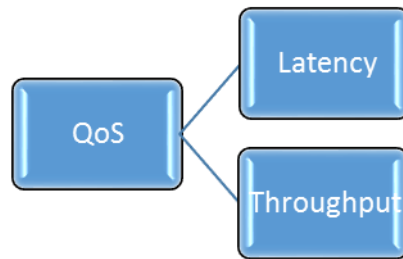
- Karray F. O. and de Silva C., 2004, “*Soft Computing and Intelligent Systems Design*”, Pearson Education Limited, Edinburgh Gate, Harlow, Essex CM20 2JE, England.
- Lewis F. L., 2007, “*Wireless Ad Hoc and Sensor Networks*”, A Thesis in Applied Control Engineering, University of Texas at Arlington, Fort Worth, Texas.
- Liua B., Zhangb X., Xiea S., and Maa H., 2011, “*Variable Weights Decision-Making and Its Fuzzy Inference Implementation*”, School of information science and technology, Tsinghua University, Beijing, China, 100084,b. School of electronics and information engineering, Beijing University of Aeronautics and, Astronautics, Beijing, China, 100084,liu-b03@mails.tsinghua.edu.cn.
- Misra S., 2009, “*Guide to Wireless Ad-Hoc Networks*”, School of Information Technology, Indian Institute of Technology, Kharagpur, India.
- Odom W., 2010, “*CCIE Routing and Switching Exam Certification Guide*”, Third Edition, , CCIE No. 1624, Rus Healy, CCIE No. 15025, Contributing author: Naren Mehta, CCIE No. 9797.
- OPNETWORK 2002, “*Introduction to Using OPNET Modeler*”.
- Reddy T. B., Karthigeyan I., Manoj B. S., Murthy C. S. R., 2004, “*Quality of service provisioning in ad hoc wireless networks a survey of issues and solutions*”, Department of Computer Science and Engineering, Indian Institute of Technology, Madras 600036, India, Received 15 February; accepted 14 April 2004, Available online 5 June.
- Roy R. R., 2011, “*Handbook of Mobile Ad-Hoc Networks for Mobility Models*”, United States Army Research, Development and Engineering Command,



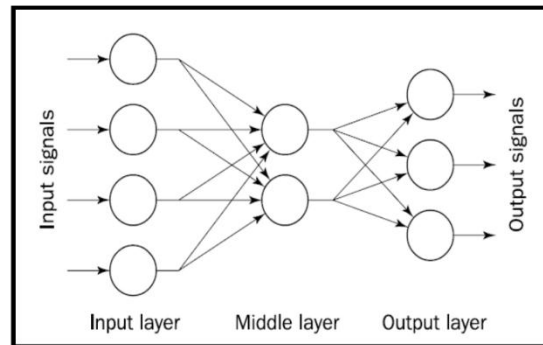
- (RDECOM), Myer Center 2700, Fort Monmouth, NJ 07703, USA, rroy3@optonline.net.
- Shen C., and Rajagopalan S., 2007, “*Protocol-independent multicast packet delivery improvement service for mobile Ad hoc networks*”, Science Direct, Ad Hoc Networks, vol.5, pp.210–227.
  - Sivanandam S. N., 2010, “*Introduction to Fuzzy Logic using MATLAB*”, Dr. Professor and Head, Department of Computer, Science and Engineering, PSG College of Technology, Coimbatore 641 004, Tamil Nadu, India, E-mail: snsivanandam@yahoo.co.in.
  - Valbonne S. A. , “*3GPP support office address*”, 650 Route des Lucioles — FRANCE, Tel.: +33 4 92 94 42 00 Fax: +33 4 93 65 47 16, Internet, <http://www.3gpp.org>.
  - Xia C., Yang Z. and Li H., 2012, “*Electric Load Forecasting Using Virtual Instrument Based on Dynamic Recurrent Elman Neural Network*”, College of Electrical Engineering and Renewable Energy, China Three Gorges, University Yichang, Hubei 443002 China
  - Zaghar D. R. and AL Wahab T. A., 2013, “*Simplified the QoS Factor for the Ad-Hoc Network Using Fuzzy Technique*”, Computer & Software Engineering Department, College of Engineering, Almustansiriyah University, Baghdad, Iraq, Email: DRZ\_RAW@yahoo.com, [Thoalfqar\\_almashaikhy@yahoo.com](mailto:Thoalfqar_almashaikhy@yahoo.com)



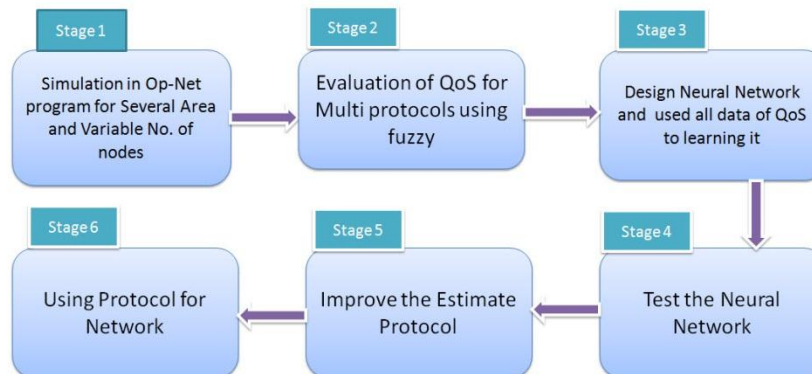
**Figure 1.** Evaluating the QoS of Real Time application.



**Figure 2.** Evaluating the QoS of Non-Real Time application.

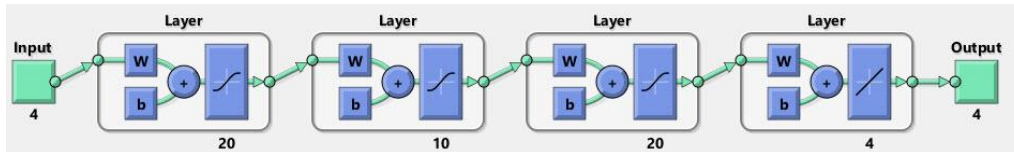
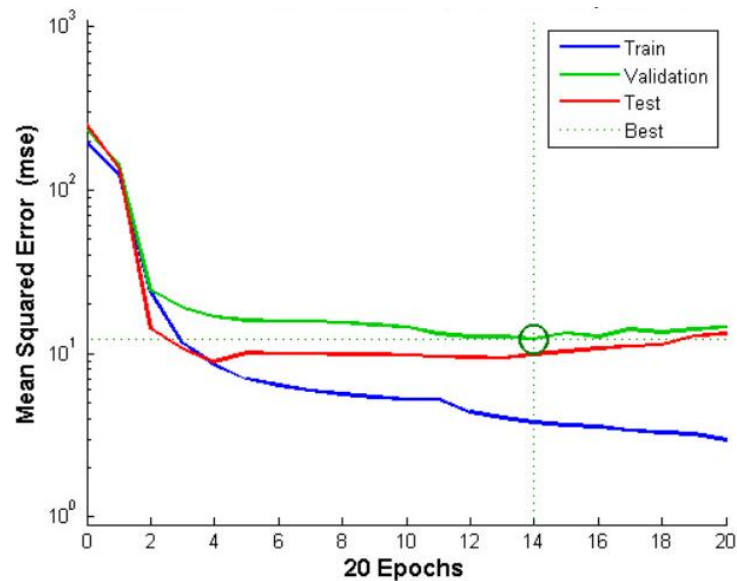
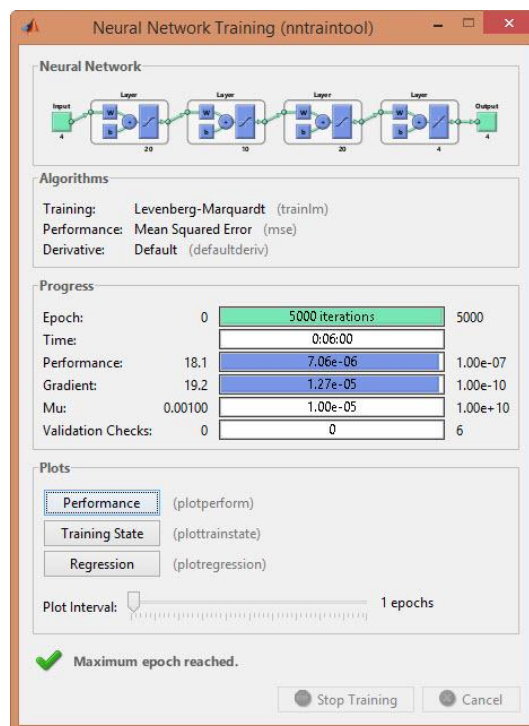


**Figure 3.** Artificial neuron structure (perceptron model).



**Figure 4.** System design.



**Figure 5.** Neural network.**Figure 6.** Best Validation is 12331 at epoch 14.**Figure 7.** Training Neural network after training.

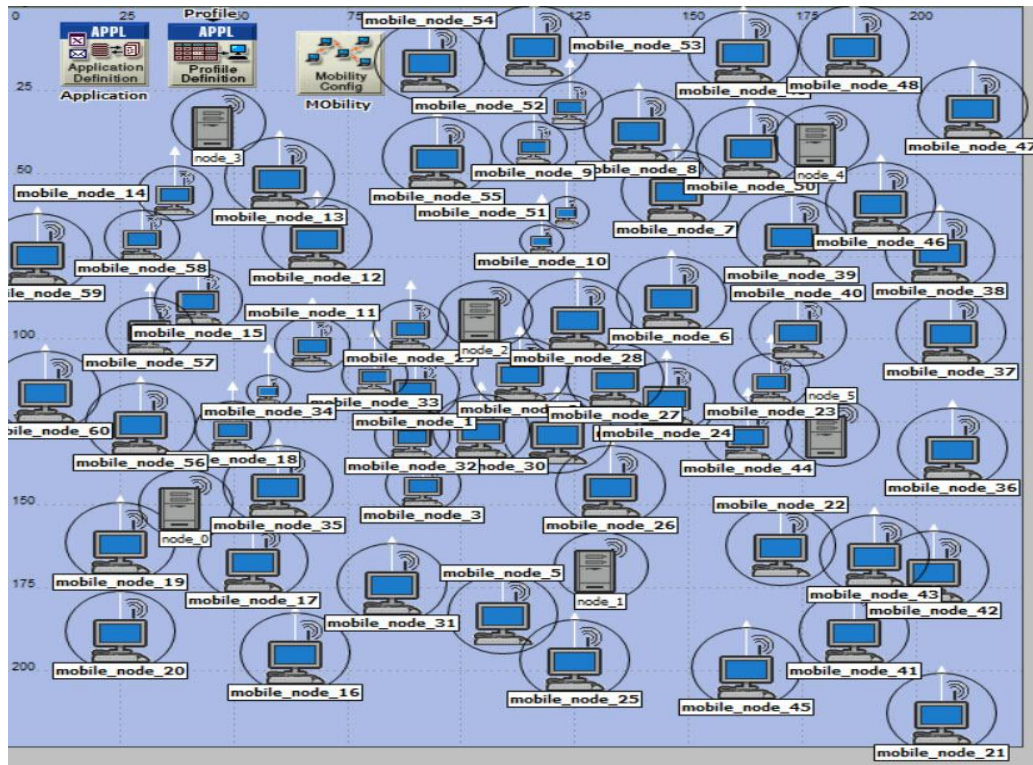


**Figure 8.** Improve the routing protocol OLSR.

**Table 1.** Specification of Design

Simulation Specification	Value
Mobility Model	Random Way Point (RWP)
Node Speed	2.7 m/sec
Areas	100*100 - 200*200 - 400*400 - 800*800 - 1000*1000
Number of Nodes	10,20,40 and 80
Simulation time	1100 sec
Packet Reception Power Threshold	-85 dB
Transmission Power	0.006w or 7.781 dBm
Mac Layer Type	802.11g (12MB)

**Table 2-A.** QoS of simulation on area (100\*100) m<sup>2</sup>.

Area	No. of nodes	Ratio of	QoS of protocols			
		voice used	AODV	DSR	OLSR	TORA
100*100	10	0.1	0.84391	0.84391	0.84391	0.84391
100*100	10	0.2	0.85421	0.85422	0.85422	0.85422
100*100	10	0.3	0.86453	0.86453	0.86453	0.86453
100*100	10	0.4	0.8748	0.87484	0.87484	0.87484
100*100	10	0.5	0.8852	0.88515	0.88515	0.88515
100*100	10	0.6	0.8955	0.89546	0.89546	0.89546
100*100	10	0.7	0.9058	0.90577	0.90577	0.90577
100*100	10	0.8	0.9161	0.91608	0.91608	0.91608
100*100	10	0.9	0.9264	0.92639	0.90639	0.92639
100*100	20	0.1	0.8692273	0.84391	0.84391	0.84391
100*100	20	0.2	0.8798466	0.85422	0.85422	0.85422
100*100	20	0.3	0.8904659	0.86453	0.86453	0.86453
100*100	20	0.4	0.9010852	0.87484	0.87484	0.87484
100*100	20	0.5	0.9117045	0.88515	0.88515	0.88515
100*100	20	0.6	0.9223238	0.89546	0.89546	0.89546
100*100	20	0.7	0.9329431	0.90577	0.90577	0.90577
100*100	20	0.8	0.9435624	0.91608	0.91608	0.91608
100*100	20	0.9	0.9541817	0.92639	0.92639	0.92639
100*100	40	0.1	0.7795	0.78024	0.17427	0.48
100*100	40	0.2	0.7262	0.72688	0.18824	0.46
100*100	40	0.3	0.673	0.62016	0.20221	0.44
100*100	40	0.4	0.6197	0.62016	0.21618	0.42
100*100	40	0.5	0.5664	0.5668	0.23015	0.4
100*100	40	0.6	0.5131	0.51344	0.24412	0.38
100*100	40	0.7	0.4598	0.46008	0.25809	0.36
100*100	40	0.8	0.4066	0.40672	0.27206	0.34
100*100	40	0.9	0.3533	0.35336	0.28603	0.32
100*100	80	0.1	0.7795	0.70155	0.350775	0.78006
100*100	80	0.2	0.7262	0.65358	0.32679	0.72672
100*100	80	0.3	0.673	0.6057	0.30285	0.67338
100*100	80	0.4	0.6197	0.55773	0.278865	0.62004
100*100	80	0.5	0.5664	0.50976	0.25488	0.5667
100*100	80	0.6	0.5131	0.46179	0.230895	0.51336
100*100	80	0.7	0.4598	0.41382	0.20691	0.46002
100*100	80	0.8	0.4066	0.36594	0.18297	0.40668
100*100	80	0.9	0.3533	0.31797	0.158985	0.35334

**Table 2-B.** QoS of simulation on area (200\*200) m<sup>2</sup>.

Area	No. of nodes	Ratio of	QoS of protocols			
		voice used	AODV	DSR	OLSR	TORA
200*200	10	0.1	0.84391	0.84391	0.84391	0.84391
200*200	10	0.2	0.85422	0.85422	0.85422	0.85422
200*200	10	0.3	0.86453	0.86453	0.86453	0.86453
200*200	10	0.4	0.87484	0.87484	0.87484	0.87484
200*200	10	0.5	0.88515	0.88515	0.88515	0.88515
200*200	10	0.6	0.89546	0.89546	0.89546	0.89546
200*200	10	0.7	0.90577	0.90577	0.90577	0.90577
200*200	10	0.8	0.91608	0.91608	0.91608	0.91608
200*200	10	0.9	0.92639	0.92639	0.92639	0.92639
200*200	20	0.1	0.58048	0.78024	0.84391	0.19036
200*200	20	0.2	0.62006	0.72688	0.85422	0.22042
200*200	20	0.3	0.65964	0.67352	0.86453	0.25048
200*200	20	0.4	0.69922	0.62016	0.88515	0.28054
200*200	20	0.5	0.7388	0.5668	0.89546	0.3106
200*200	20	0.6	0.77838	0.51344	0.90577	0.34066
200*200	20	0.7	0.81796	0.46008	0.91608	0.37072
200*200	20	0.8	0.85754	0.40672	0.92639	0.40078
200*200	20	0.9	0.89712	0.35336	0.92639	0.43084
200*200	40	0.1	0.78024	0.78024	0.546168	0.17427
200*200	40	0.2	0.72688	0.72688	0.508816	0.18824
200*200	40	0.3	0.67352	0.67352	0.471464	0.20221
200*200	40	0.4	0.62016	0.62016	0.434112	0.21618
200*200	40	0.5	0.5668	0.5668	0.39676	0.23015
200*200	40	0.6	0.51344	0.51344	0.359408	0.24412
200*200	40	0.7	0.46008	0.46008	0.322056	0.25809
200*200	40	0.8	0.40672	0.40672	0.284704	0.27206
200*200	40	0.9	0.35336	0.35336	0.247352	0.28603
200*200	80	0.1	0.78024	0.7334256	0.468144	0.78024
200*200	80	0.2	0.72688	0.6832672	0.3052896	0.72688
200*200	80	0.3	0.67352	0.6331088	0.2828784	0.67352
200*200	80	0.4	0.62016	0.5829504	0.2604672	0.62016
200*200	80	0.5	0.5668	0.532792	0.238056	0.5668
200*200	80	0.6	0.51344	0.4826336	0.2156448	0.51344
200*200	80	0.7	0.46008	0.4324752	0.1932336	0.46008
200*200	80	0.8	0.40672	0.3823168	0.1708224	0.40672
200*200	80	0.9	0.35336	0.3321584	0.1484112	0.35336

**Table 2-C. QoS of simulation on area (400\*400) m<sup>2</sup>.**

Area	No. of nodes	Ratio of	QoS of protocols			
		voice used	AODV	DSR	OLSR	TORA
400*400	10	0.1	0.83104	0.84391	0.84391	0.84391
400*400	10	0.2	0.84278	0.85422	0.85422	0.85422
400*400	10	0.3	0.85452	0.86453	0.86453	0.86453
400*400	10	0.4	0.86626	0.87484	0.87484	0.87484
400*400	10	0.5	0.878	0.88515	0.88515	0.88515
400*400	10	0.6	0.88974	0.89546	0.89546	0.89546
400*400	10	0.7	0.90148	0.90577	0.90577	0.90577
400*400	10	0.8	0.91322	0.91608	0.91608	0.91608
400*400	10	0.9	0.92496	0.92639	0.92639	0.92639
400*400	20	0.1	0.84391	0.82024	0.84391	0.80242
400*400	20	0.2	0.85422	0.80688	0.85422	0.79104
400*400	20	0.3	0.86453	0.79352	0.86453	0.77966
400*400	20	0.4	0.87484	0.78016	0.87484	0.76828
400*400	20	0.5	0.88515	0.7668	0.88515	0.7569
400*400	20	0.6	0.89546	0.75344	0.89546	0.74552
400*400	20	0.7	0.90577	0.74008	0.90577	0.73414
400*400	20	0.8	0.91608	0.72672	0.91608	0.72276
400*400	20	0.9	0.92639	0.71336	0.92639	0.71138
400*400	40	0.1	0.78024	0.78024	0.48	0.48
400*400	40	0.2	0.72688	0.72688	0.46	0.46
400*400	40	0.3	0.67352	0.67352	0.44	0.44
400*400	40	0.4	0.62016	0.62016	0.42	0.42
400*400	40	0.5	0.5668	0.5668	0.4	0.4
400*400	40	0.6	0.51344	0.51344	0.38	0.38
400*400	40	0.7	0.46008	0.46008	0.36	0.36
400*400	40	0.8	0.40672	0.40672	0.34	0.34
400*400	40	0.9	0.35336	0.35336	0.32	0.32
400*400	80	0.1	0.78024	0.75024	0.450144	0.78024
400*400	80	0.2	0.72688	0.73688	0.442128	0.72688
400*400	80	0.3	0.67352	0.70352	0.422112	0.67352
400*400	80	0.4	0.62016	0.68016	0.408096	0.62016
400*400	80	0.5	0.5668	0.6668	0.40008	0.5668
400*400	80	0.6	0.51344	0.63344	0.380064	0.51344
400*400	80	0.7	0.46008	0.61008	0.366048	0.46008
400*400	80	0.8	0.40672	0.59672	0.358032	0.40672
400*400	80	0.9	0.35336	0.57336	0.344016	0.35336

**Table 2-D.** QoS of simulation on area (800\*800) m<sup>2</sup>.

Area	No. of nodes	Ratio of	QoS of protocols			
		voice used	AODV	DSR	OLSR	TORA
800*800	10	0.1	0.80074	0.23794	0.23794	0.20413
800*800	10	0.2	0.76788	0.31558	0.34558	0.24796
800*800	10	0.3	0.73502	0.39322	0.37322	0.29179
800*800	10	0.4	0.70216	0.47086	0.47086	0.33562
800*800	10	0.5	0.6693	0.5485	0.5485	0.37945
800*800	10	0.6	0.63644	0.62614	0.62614	0.42328
800*800	10	0.7	0.60358	0.70378	0.70378	0.46711
800*800	10	0.8	0.57072	0.78142	0.78142	0.51094
800*800	10	0.9	0.53786	0.85906	0.85906	0.55477
800*800	20	0.1	0.819252	0.78024	0.78266	0.76494
800*800	20	0.2	0.763224	0.72688	0.79502	0.71328
800*800	20	0.3	0.707196	0.67352	0.75738	0.66162
800*800	20	0.4	0.651168	0.62016	0.73974	0.60996
800*800	20	0.5	0.59514	0.5668	0.70721	0.5583
800*800	20	0.6	0.539112	0.51344	0.68446	0.50664
800*800	20	0.7	0.483084	0.46008	0.66682	0.45498
800*800	20	0.8	0.427056	0.40672	0.65918	0.40332
800*800	20	0.9	0.371028	0.35336	0.62154	0.35166
800*800	40	0.1	0.78024	0.78024	0.68024	0.17427
800*800	40	0.2	0.72688	0.72688	0.63688	0.18824
800*800	40	0.3	0.67352	0.67352	0.60352	0.20221
800*800	40	0.4	0.62016	0.62016	0.57016	0.21618
800*800	40	0.5	0.5668	0.5668	0.5668	0.23015
800*800	40	0.6	0.51344	0.51344	0.51344	0.24412
800*800	40	0.7	0.46008	0.46008	0.46008	0.25809
800*800	40	0.8	0.40672	0.40672	0.40672	0.27206
800*800	40	0.9	0.35336	0.35336	0.35336	0.28603
800*800	80	0.1	0.78006	0.77688	0.17427	0.24796
800*800	80	0.2	0.72672	0.75352	0.18824	0.29179
800*800	80	0.3	0.67338	0.73016	0.20221	0.33562
800*800	80	0.4	0.62004	0.6968	0.21618	0.37945
800*800	80	0.5	0.5667	0.67344	0.23015	0.36796
800*800	80	0.6	0.51336	0.56008	0.24412	0.34008
800*800	80	0.7	0.46002	0.55672	0.25809	0.33672
800*800	80	0.8	0.40668	0.52336	0.27206	0.32336
800*800	80	0.9	0.35334	0.50603	0.28603	0.30231

**Table 2-E** QoS of simulation on area (1000\*1000) m<sup>2</sup>.

Area	No. of nodes	Ratio of	QoS of protocols			
		voice used	AODV	DSR	OLSR	TORA
1000*1000	10	0.1	0.71296	0.84391	0.84391	0.84391
1000*1000	10	0.2	0.73782	0.85422	0.85422	0.85422
1000*1000	10	0.3	0.73782	0.86453	0.86453	0.86453
1000*1000	10	0.4	0.78754	0.87484	0.87484	0.87484
1000*1000	10	0.5	0.8124	0.88515	0.88515	0.88515
1000*1000	10	0.6	0.83726	0.89546	0.89546	0.89546
1000*1000	10	0.7	0.86212	0.90577	0.90577	0.90577
1000*1000	10	0.8	0.88698	0.91608	0.92639	0.91608
1000*1000	10	0.9	0.91184	0.92639	0.92639	0.92639
1000*1000	20	0.1	0.40957	0.4341442	0.84391	0.19488
1000*1000	20	0.2	0.46814	0.4962284	0.85422	0.22946
1000*1000	20	0.3	0.52671	0.5583126	0.86453	0.26404
1000*1000	20	0.4	0.58528	0.6203968	0.87484	0.29862
1000*1000	20	0.5	0.64385	0.682481	0.88515	0.3332
1000*1000	20	0.6	0.70242	0.7445652	0.89546	0.40236
1000*1000	20	0.7	0.76099	0.8066494	0.90577	0.40236
1000*1000	20	0.8	0.81956	0.8687336	0.91608	0.43694
1000*1000	20	0.9	0.87813	0.9308178	0.92639	0.47152
1000*1000	40	0.1	0.78024	0.80074	0.17427	0.48
1000*1000	40	0.2	0.72688	0.76788	0.18824	0.46
1000*1000	40	0.3	0.67352	0.73502	0.20221	0.44
1000*1000	40	0.4	0.62016	0.70216	0.21618	0.42
1000*1000	40	0.5	0.5668	0.6693	0.23015	0.4
1000*1000	40	0.6	0.51344	0.63644	0.24412	0.38
1000*1000	40	0.7	0.46008	0.60358	0.25809	0.36
1000*1000	40	0.8	0.40672	0.57072	0.27206	0.34
1000*1000	40	0.9	0.35336	0.53786	0.28603	0.32
1000*1000	80	0.1	0.78006	0.702054	0.3159243	0.78006
1000*1000	80	0.2	0.72672	0.654048	0.2943216	0.72672
1000*1000	80	0.3	0.67338	0.606042	0.2727189	0.67338
1000*1000	80	0.4	0.62004	0.558036	0.2511162	0.62004
1000*1000	80	0.5	0.5667	0.51003	0.2295135	0.5667
1000*1000	80	0.6	0.51336	0.462024	0.2079108	0.51336
1000*1000	80	0.7	0.46002	0.414018	0.1863081	0.46002
1000*1000	80	0.8	0.40668	0.366012	0.1647054	0.40668
1000*1000	80	0.9	0.35334	0.318006	0.1431027	0.35334





## An Adaptive Multi-Objective Particle Swarm Optimization Algorithm for Multi-Robot Path Planning

Dr. Nizar Hadi Abbas

Department of Electrical Engineering

College of Engineering - University of Baghdad

E-mail: [drnizaralmsaodi@gmail.com](mailto:drnizaralmsaodi@gmail.com)

Jaafer Ahmed Abdulsahab

Department of Electrical Engineering

College of Engineering - University of Baghdad

E-mail: [jaafer.almadhhachi@gmail.com](mailto:jaafer.almadhhachi@gmail.com)

### ABSTRACT

This paper discusses an optimal path planning algorithm based on an Adaptive Multi-Objective Particle Swarm Optimization Algorithm (AMOPSO) for two case studies. First case, single robot wants to reach a goal in the static environment that contain two obstacles and two danger source. The second one, is improving the ability for five robots to reach the shortest way. The proposed algorithm solves the optimization problems for the first case by finding the minimum distance from initial to goal position and also ensuring that the generated path has a maximum distance from the danger zones. And for the second case, finding the shortest path for every robot and without any collision between them with the shortest time. In order to evaluate the proposed algorithm in term of finding the best solution, six benchmark test functions are used to make a comparison between AMOPSO and the standard MOPSO. The results show that the AMOPSO has a better ability to get away from local optimums with a quickest convergence than the MOPSO. The simulation results using Matlab 2014a, indicate that this methodology is extremely valuable for every robot in multi-robot framework to discover its own particular proper path from the start to the destination position with minimum distance and time.

**Key words:** multi-robot system, path planning, multi-objective approaches, adaptive multi-objective particle swarm optimization, danger zones.

### تطوير خوارزمية اسراب الطيور متعددة الوظائف لتخطيط المسار لأكثر من روبوت

جعفر احمد عبد الصاحب

قسم الهندسة الكهربائية

كلية الهندسة، جامعة بغداد

د. نزار هادي عباس

قسم الهندسة الكهربائية

كلية الهندسة، جامعة بغداد

### الخلاصة

في هذا البحث تم عرض افضل مسار على اساس خوارزمية اسراب الطيور متعددة الوظائف المعدلة لدراسة حالتين . في الحالة الاولى ، تم تطبيق وتطبيق لتوليد افضل مسار ممكن للروبوت المتحرك في بيئة ثابتة مع تجنب التصادم مع العوائق و مصادر الخطر التي قد تكون موجودة في البيئة والثانية ، لتحسين قدرة البحث لنظام يحتوي على عدد من الروبوتات للحصول على اقصر مسار. الخوارزمية المقترحة تحل المشاكل بطريقة الامثلية عن طريق تقليل دالة الهدف والحصول على المسارات الامثل وبدون تصادم كذلك تقلل من طول الطريق الذي يجب اتباعه بواسطة الروبوت وايضاً تضمن ان المسارات المتولدة على مسافة امنة من مصادر الخطر. بعض دوال الاختبار تم استخدامها للمقارنة بين جودة الخوارزمية المطورة مع

الخوارزمية الاصلية من ناحية الوصول الى افضل الحلول. النتائج اظهرت ان الخوارزمية المطورة تمتلك قدرة افضل للخروج من الاملية المحلية والحصول على تقارب اسرع من الخوارزمية الاصلية. نتائج المحاكاة ونتائج التحقق تبين بأن هذه المنهجية هي قيمة للغاية لكل روبوت في إطار منظومة متعددة الروبوتات لاكتشاف الطريق الصحيح الخاص به من موقع البداية الى الهدف مع الحصول على الحد الأدنى من المسافة المقطوعة والزمن.

**الكلمات الرئيسية:** نظام متعدد الروبوت، تخطيط المسار، طرق الوظائف المتعددة ، خوارزمية اسراب الطيور متعددة الوظائف ، مناطق الخطر.

## 1. INTRODUCTION

The Multi Robot System (MRS) can be described as a group of robots working in the same environment. However, robotic systems may range from simple sensors, acquiring and processing data, to complex human like machines, able to interact with the environment in fairly complex ways. MRS has been widely applied to rescue, industrial, exploration of outer space areas, due to its characteristics of reliability, robustness, and economy. Path planning has been known as one of the main problems in the MRS. The objective was to choose the optimum path without collision among them in the specified arena, **Li, et al., 2009**.

One of the most important tasks in the moving of mobile robots in static (fixed) environments in the existence of multi-obstacles was to arrive the goal as fast as possible using an optimal trajectory. Sometimes, the environments that the robots are working on may be included danger zones (sensitive areas), so it must be considered in the robot path planning (RPP) algorithms. In addition to generating the shortest path, the RPP algorithms also generate trajectories at safe spaces from the danger zones in the arena, **Gong, et al., 2011**.

A MOPSO algorithm is utilized in, **Zhang, et al., 2013**, to generate trajectories for mobile robots that are working on the environments that the robots are working on and may be included danger sources. R. Kala introduced a co-evolutionary genetic programming algorithm to produce a comprehensive, optimal path for multi-robots in map of the maze, where every robot searching for the shortest path in addition to that, each robot avoids the collision with other robots. The results show that this method can find the best paths for whatever number of mobile robots in various arenas and scenarios, **Kala, 2012**. **Kaluder, et al., 2011**, showed a modified Asano's algorithm which is performed to locate the visibility polygons and graphs. According to the result, a cubical complexity of the algorithm is shown, based on reflection point numbers.

The methods that are used for solving RPP can be separated into two methods: traditional and intelligent, the first method contains visibility graphs, configuration space (C-Space) and artificial potential field., **Jaillet, et al., 2010**, addressed path planning issue to consider the cost function defined over the C-Space. The proposed design computes minimum cost paths that follow the valleys and saddle points of the C-Space cost map. According to the results this method is very effective. The second method is a group of obstacles and points in the Euclidean plane and it was applied to find the Euclidean shortest paths between a group of point (polygonal point). The artificial intelligent path planning includes Ant Colony Optimization (ACO), Particle Swarm Optimization (PSO), Genetic Algorithm (GA) and so on. **Chung and Xu, 2010**, suggested a generalized three dimensional (3D) path planning technique for robots using GA with an adaptive evolution process. According to nearest neighbor, the authors presented a new operator, named it a Bind-NN that is randomly separated and reconnect an elitist chromosome. According to the results the efficiency and search effectiveness has a better improvement.

**Chakraborty, et al., 2008**, presented an alternative method for a co-operative multiple RPP problem using parallel differential evolution algorithms. According to the experimental results this method is very useful for each robot in multi-robot systems for searching and finding the shortest path to target.

In this paper, two case studies based on an Adaptive Multi-Objective Particle Swarm Optimization Algorithm (AMOPSO) for solving RPP problem are presented the first one for single robot and the second for multi-robot. In the first case, the AMOPSO algorithm generates optimal paths by maximizing the distance between the generated paths and the danger zones that exist in the arena and also minimizing the length of the path that needs by the mobile robot to reach the target. In the second case, the AMOPSO algorithm improves the ability for multiple robot system to reach the shortest way.

The rest of this paper is organized as follows: section 2 describes a problem formulation; Section 3 describes the theoretical background; Section 4 describes the proposed AMOPSO algorithm and the simulation results and discussion are presented in section 5. Finally, section 6 gives the research conclusions.

## 2. PROBLEM FORMULATION

### 2.1 Single Robot with Danger Zones

The multiple objective optimization algorithm is considered as AMOPSO algorithm, which depends on two objectives to find the optimal paths for single mobile robots in fixed environments that contain a number of obstacles and danger source.

PSO algorithm using a number of the population  $P$  of particles that are taking as a random position in the work space. Every particle has a velocity (randomized) assigned to which they have changed its position in the work space.

Let  $(R)$  be the robot that is used in a known environment in the task of finding the optimal path with existing of danger zones and multi-obstacles. A population of particles ( $P$ ) contains a number of particles ( $N$ ), are participating in the production of optimal path for the robot  $R$ .

The static environment includes a group of obstacles  $\{O_k \mid k = 1 \dots p\}$  and group of danger zones  $\{DZ_k \mid k = 1 \dots r\}$  that are known in advance. As described in, **Gong, et al., 2011**, the danger zone can be found in the environment when the robot is moving to reach the target.

The first objective in this case is to reach the maximum distance among each particle and the danger zones. This means, at each iteration the AMOPSO algorithm attempt to find the maximum Euclidean distance between the particle positions and every point for danger zones. To achieve that, the following objective function is used:

$$fI_i(t) = \frac{1}{\sum_{j=1}^r \sqrt{(X_{DZj} - X_i(t))^2 + (Y_{DZj} - Y_i(t))^2}}, i = 1 \dots N, \quad (1)$$

where  $(X_{DZj}, Y_{DZj})$  are axis for the danger zone's position. When the AMOPSO algorithm reaches the maximum number of iterations, then it eliminated agent's trajectories which have any collision points with any points of danger zones.

The second objective is to find the minimum distance that is needed by the robot from the start position  $(X_i(t), Y_i(t))$  to the goal point  $(X_f, Y_f)$ . The objective function which is used to



reach the minimum Euclidean distance between the agent current location and the goal is formulated as,

$$f2_i(t) = \sqrt{(X_i(t) - X_f)^2 + (Y_i(t) - Y_f)^2}, i = 1 \dots N. \quad (2)$$

Eq. (1) and Eq. (2) are brought together into a single objective function:

$$f_i(t) = f1_i(t) + f2_i(t) \quad (3)$$

Therefore, every iteration finds the maximum distance between the path points and the danger zones points in the arena and also obtain the minimum distance that is needed by the mobile robot.

## 2.2 Multi-Robot System with Shortest Way

There are three principles used to organize the robot movement in order to reach the goal position without collision with obstacles or other robot in the arena, these principles are:

- 1) At first, the robot identifies the next position so as to align itself to a goal.
- 2) This alignment may cause a collision with another robot. This may be happening in the case of more than one robot try to take the same position. Also the collision may be happening with obstacles that found in the next position. To avoid such collision, the robot has to turn left or right by changing its position by increasing x-axis and y-axis with threshold.
- 3) Finally, if the robot can align itself to the goal without any collision with other robot or obstacles, it will move to next position.

The objective is to minimize the distance that is needed for each robot from the start position to its goal with minimum time. The objective function that is used to minimize the Euclidian distance between the agent current position and the goal point is formulated as:

$$f_i(t) = \sqrt{(X_i(t) - X_f)^2 + (Y_i(t) - Y_f)^2}, i = 1 \dots N. \quad (4)$$

where,  $(X_i(t), Y_i(t))$  is initial position and  $(X_f, Y_f)$  is goal point.

## 3. THEORETICAL BACKGROUND

### 3.1 Path Planning

The field of robot path planning (RPP) was begun in 1960's. The RPP problem is a very defying challenging in the field of robotics. The main objective is to find a collision free path from an initial position to a destination position. Robot Navigation (RN) problem has to be concerned with three main matters: accuracy, safety and efficiency. The accuracy and safety issues deal with finding a collision-free path and following the exactly addressed path. Efficiency means that the algorithm searching the shortest distance with acceptable time by not letting the robot to stop and turn many times or take needless steps, which results in squandering of time and energy consumption. **Ehlert, 1999.**

Depending on the environment where the robot located in; RPP can be classified into two types:

- 1) RPP in static environment: if there are fixed obstacles in the arena.
- 2) RPP in dynamic environment: if the arena has both fixed and moving obstacles.

Each of these two types could be further subdivided into a sub-group:

- 1) Global Path Planning (GPP): a total information about fixed obstacles and a path of moving obstacles are known in advance; thus, the GPP can be planned before the robot starts to move (offline).
- 2) Local Path Planning (LPP): a total information about the environment is not obtainable in advance. So, while it moves through the environment the mobile robot obtains information through sensors (online), **Miao, 2009**.

### 3.2 Optimization Technique

#### 3.2.1 Standard PSO Algorithm

Particle Swarm Optimization (PSO) algorithm was invented by Kennedy and Eberhart in 1995 is an evolutionary algorithm inspired by the motion of the fish school or bird flocks in nature. It is used in optimizing the continuous nonlinear functions. PSO uses a population of particles (agents) that are moving in the work space and at each iteration a particle memorized the coordinates of the position in the work space associated with better fitness value achieved so far. PSO also stores the position of the best value from the whole particles, **Kennedy and Eberhart, 1995**.

A position vector  $X_i(t)$  and velocity vector  $V_i(t)$  for every particle in the population is, **Rao, 2009**:

$$V_i(t) = (V_i^X(t), V_i^Y(t)), i=1...N, \quad (5)$$

$$X_i(t) = (X_i^X(t), X_i^Y(t)), i=1...N. \quad (6)$$

where the super-scripts X & Y highlight the vector components in the 2-D work space where the robot is moving. Every agent maintains the best own positions that are reached in the best position vector  $P_{i, best}(t)$ :

$$P_{i, best}(t) = (P_i^X(t), P_i^Y(t)), i=1...N. \quad (7)$$

The best positions of the whole population are maintained in the vector  $P_{g, best}(t)$ :

$$P_{g, best}(t) = (P_g^X(t), P_g^Y(t)), i=1...N. \quad (8)$$

The updating velocity, which is used by the particle in the moving in search space can be found according to:

$$V_i^X(t+1) = w(t) V_i^X(t) + c1 r1 [P_i^X(t) - X_i^X(t)] + c2 r2 [P_g^X(t) - X_i^X(t)], i=1...N. \quad (9)$$

$$V_i^Y(t+1) = w(t) V_i^Y(t) + c1 r1 [P_i^Y(t) - X_i^Y(t)] + c2 r2 [P_g^Y(t) - X_i^Y(t)], i=1...N. \quad (10)$$

where  $r1$  and  $r$  are uniformly distributed random variables in the range of  $[0,1]$ ,  $0.4 \leq w(t) \leq 0.9$  is the inertia weight,  $c1$  and  $c2$  are the weighting factors of the stochastic accelerations pulling the agents towards their final positions and it rang is  $[0,4]$ . The next particle position in the search space is obtained using the following equations:

$$X_i(t+1) = X_i(t) + V_i^X(t+1). \quad (11)$$

$$Y_i(t+1) = Y_i(t) + V_i^Y(t+1). \quad (12)$$

Pseudocode that shows the steps of the standard PSO algorithm works illustrated in **Fig. 1**.

### 3.2.2 MOPSO Algorithm

Mostly, a single condition used by researchers to generate an optimal path, such as the time required by a mobile robot to reach the target or minimum path length. But, in practice, several conditions must be meets to make the path feasible, such as safety, energy consumption, smoothness, etc.

An optimal path for single criterion does not mean that all the other criteria are satisfied, **Fujimura, 1996**, As an example, an energy consumption dose not desired at the expense of shortest path along the path.

So, in multi-objective PSO (MOPSO) algorithm the target is to find a set of different solutions by modifying the original scheme. Three main concepts must be considered when extending PSO to MOPSO. These concepts are **Dehuri, et al., 2008**:

- How to choose the leaders from particles with a view to give priority to non-dominated solutions over those that are dominated?
- How to keep a non-dominated solution that be found within the search process with a view to give a report solution that is non-dominated with respect to all the past agents and not only with respect to the current one?
- How to save the diversity in the swarm with a view to avoid convergence for a single local solution?

Pseudocode that shows the procedure of the standard MOPSO algorithm works presented in **Fig. 2**. Italics are used in **Fig. 2** to clarify the difference process between MOPSO and PSO algorithms.

### 3.2.3 Multi-objective approaches

When the optimization problem contains more than one objective function, the mission of finding one optimal solutions or more is known as multiple objective optimization. The common methods that are used to deal with multiple objective optimization are: weighted sum and pareto front

#### 1. Weighted Sum Approach

The weighted sum method combines all multiple objective functions into one scalar, composite objective function using the weighted sum, **Yang, 2014**.

$$f(x) = \sum_{m=1}^M W_m f_m(x). \quad (13)$$

The important matter in specifying the weighting coefficient,  $W = (W_1, W_2, \dots, W_m)$  because the strongly solution depends on the selection of  $W$ . Obviously, these weights have been positive, satisfying  $\sum_{m=1}^M W_m = 1$ ,  $W_m \in [0,1]$ .

## 2. Pareto Dominance and Pareto Optimality

In a pareto set, a solution back to the pareto set, if there is no other solution can improve at least one objective without degrading on any other one from the objective. In the context of Multi-Objective Optimization (MOO), formally, a decision vector  $\vec{u} \in \Omega$  is said to pareto dominate vector  $\vec{v} \in \Omega$ , in a minimization context, if and only if:

111111

$$\forall i \in \{1, K, N\} f_i(\vec{u}) \leq f_i(\vec{v}),$$

$$\text{and } \exists j \in \{1, K, N\}, f_j(\vec{u}) < f_j(\vec{v}). \quad (14)$$

In the context of Multi-Objective Optimization MOO, Pareto dominance is used to compare and rank decision vectors:  $\vec{u}$  dominating  $\vec{v}$  in the Pareto sense means that  $\vec{F}(\vec{u})$  is either the same or better than  $\vec{F}(\vec{v})$  for all objectives, and there is at least one objective function for which  $\vec{F}(\vec{u})$  is strictly better than  $\vec{F}(\vec{v})$  Yang, 2014.

## 4. PROPOSED AMOPSO ALGORITHM

In this paper, an adaptive approach is proposed to adjust the particles velocity and position to overcome the slow convergence problem that emerged in Standard PSO (SPSO) algorithm.

Thus, in the APSO, the particle position is updated such that the highly fitted particle moves slowly when compared to the lowly fitted particle. Therefore, in order to achieve the promising updating, the following particles' parameters should be adapted according to their objective function values, Humadi, et al., 2013:

1. The adaptive inertia weight factor (AIWF)  $w_i^t$ , is proposed to find out a compromised AIWF that satisfies both exploration (global search) and exploitation (local search). The AIWF is determined as in Eqs. (15 & 16).
2. The adaptive acceleration coefficients (AACs)  $c_{1,i}^t$  and  $c_{2,i}^t$  they are used to award the efficient particle that has high fitness and punishes the not competent one. These AACs are formulated as in Eqs. (17, 18, 19, 20, 21 & 22).
3. The adaptive random numbers (ARNs)  $r_{1,i}^t$  and  $r_{2,i}^t$ , are proposed to increase the movement impact on the third term (swarm) and decrease the movement influence on the second term (individual) of Eqs. (9) and (10). These ARNs are written as in Eqs. (23&24).

$$W_i = (W_{max} - W_{min}) * (e^{-\left(\frac{\text{Max}(Pbest_i)}{Gbest}\right)^2} * \log_{Tmax}(T_i + 1)) + W_{min}. \quad (15)$$

$$W_i = (W_{max} - W_{min}) * L * \log_{Tmax}(T_i + 1) + W_{min}. \quad (16)$$





$C_1$  decrease from 1.5 ~ 0.5,  $C_2$  increase from 1.5 ~ 2.5

$$C_1 = Z + L * \frac{Ti}{T_{max}} \quad (17)$$

$$C_2 = Z + L * \frac{Ti}{T_{max}}. \quad (18)$$

$C_1$  decrease from 1.5 ~ 0.5,  $C_2$  decrease from 1.5 ~ 0.5

$$C_1 = Z - L * \frac{Ti}{T_{max}}. \quad (19)$$

$$C_2 = Z - L * \frac{Ti}{T_{max}} \quad (20)$$

$C_1$  decrease from 1.5 ~ 0.5,  $C_2$  increase from 1.5 ~ 2.5

$$C_1 = Z - L * \frac{Ti}{T_{max}}. \quad (21)$$

$$C_2 = Z + L * \frac{Ti}{T_{max}}. \quad (22)$$

$$r_1 = rand_1 * L * \frac{Ti}{T_{max}}. \quad (23)$$

$$r_2 = rand_2 * L * \frac{Ti}{T_{max}}. \quad (24)$$

where,  $W_i$  must be between (0.4 and 0.9)

- 0.4 when the first part of the Eqs. (15 & 16) equal to zero
- 0.9 when the  $(e^{- (\frac{Max(Pbest_i)}{Gbest})^2} * \log_{T_{max}}(T_i + 1))$  equal to one
- 0.9 when the  $L * \log_{T_{max}}(T_i + 1)$  equal to one
- 0.4 ~ 0.9 when  $(e^{- (\frac{Max(Pbest_i)}{Gbest})^2} * \log_{T_{max}}(T_i + 1))$  not equal to zero or one
- 0.4 ~ 0.9 when  $L * \log_{T_{max}}(T_i + 1)$  not equal to zero or one

$Z = \text{Constant} = 1.5$

$T_i = \text{Current iteration}$

$T_{max} = \text{Maximum number of iterations}$

$L$  must be in this range  $0 \leq L \leq 1$

- $M = \frac{1}{N} * \sum_{i=1}^n Pbest_i$
- $V^2 = \frac{1}{N-1} * \sum_{i=1}^n (Pbest_i - M)^2$
- $Y = \frac{Pbest_i - M}{V}$
- $L = e^{-|Y|}$

$\text{rand}_1$  &  $\text{rand}_2$  = random number between (0 ~ 1)

So, in this paper four AMOPSO cases are simulated, these cases are listed in **Table 1**.

## 5. SIMULATION RESULTS AND DISCUSSION

### 5.1 Simulation Parameter Settings

The following parameters of the AMOPSO path planning algorithm have been used in the experiment:  $N = 8$ , maximum number of iterations  $t_{\max}=120$ , initial velocities  $v_x^i = \text{random}$  and  $v_y^i = \text{random}$ , acceleration constants  $0.5 \leq c_1 \leq 2.5$  and  $0.5 \leq c_2 \leq 2.5$  and inertia weight  $w_{\min} \leq w \leq w_{\max}$ ,  $w_{\min} = 0.4$  and  $w_{\max} = 0.9$ .

The Matlab2014a programming language used to implement the simulation code for path planning and executing on the system with 2.60GHz CPU and 2.0G RAM.

### 5.2 Benchmark Test Functions

Several unimodal and multimodal benchmark functions have been adopted from, **Vesterstrom and Thomsen, 2004**. The list of the test functions and some of their characteristics can be seen in **Table 2** and **Table 3**. In the **Table 2**, the “Range” column gives the defined range of the parameter and the “dim” column shows the number of dimensions used for each function and in the **Table 3** “Min. & Av.” column, the first value represents the minimum of optimal solution and the second one represents the average of optimal solution that obtained over 100 runs are given. Functions  $f1 \sim f3$  are unimodal and  $f4 \sim f6$  multimodal.

The function  $f1$  is the Sphere function:

$$f1(x) = \sum_{i=1}^D x_i^2. \quad (25)$$

The function  $f2$  is the Quadric function:

$$f2(x) = \sum_{i=1}^D (\sum_{j=1}^D x_j^2)^2. \quad (26)$$

The function  $f3$  is the Quadric Noise function:

$$f3(x) = \sum_{i=1}^D ix_i^4 + \text{random}(0,1). \quad (27)$$

The function  $f4$  is the Rastrigin function:

$$f4(x) = \sum_{i=1}^D [x_i^2 - 10 \cos(2\pi x_i) + 10]. \quad (28)$$

The function  $f5$  is the Ackley function:

$$f5(x) = -20 \exp\left(-0.2 \sqrt{\frac{1}{D} \sum_{i=1}^D x_i^2}\right) - \exp\left(\frac{1}{D \cos \sum_{i=1}^D (2\pi x_i)}\right) + 20 + e. \quad (29)$$

The function  $f6$  is the Griewank function:

$$f6(x) = 1/4000 \sum_{i=1}^D x_i^2 - \prod_{i=1}^D \cos(x_i/\sqrt{i}) + 1. \quad (30)$$

The initialization equation for  $x$  in the range of search space:

$$x = (b - a) * \text{random}(0,1) + a. \quad (31)$$

where  $a$  is the maximum limit in the search space and  $b$  is the minimum limit in the search space.

In SPSO,  $c_1=c_2=2$ ,  $r_1=\text{random}(0,1)$ ,  $r_2=\text{random}(0,1)$ ,  $w_{\min}=0.4$  and  $w_{\max}=0.9$ , the inertia weight equation, **Rao, 2009**:

$$w(i) = w_{\max} - \left( \frac{w_{\max} - w_{\min}}{i_{\max}} \right) * i \quad (32)$$

### 5.3 Simulation Results and Discussion

#### 5.3.1 Case study 1: environment with 2 obstacles and 2 danger zones

In this section, the environment used for the planning is a 11\*11 meter, all obstacle positions are listed in **Table 4** and result in **Table 5**. Starting point is (0,0) and target point is (10,10). The experiment has achieved a feasible solution; the best trajectory achieved by AMOPSO1 is illustrated in **Fig. 3**, best trajectory achieved by AMOPSO2 is shown in **Fig. 4**, best trajectory achieved by AMOPSO3 is depicted in **Fig. 5**. While the best trajectory achieved by AMOPSO4 is shown in **Fig. 6**. A best distance achieved by Hybrid PSO-GSA in, Purcaru, et al., 2013, is illustrated in **Fig. 7**. By comparing the results achieved in **Figs. 3, 4, 5, 6** and **Fig. 7** the AMOPSO1, AMOPSO2, AMOPSO3 and AMOPSO4 has a maximum distance from the danger zone and minimum length to reach the target than Hybrid PSO-GSA, according to this if multi robot used in the arena the AMOPSO give better results than Hybrid PSO-GSA. The results obtained from Pareto are better than the results obtained from weighted sum. In pareto, the average of maximum distance from danger zone is 40.04 and the average for minimum path is 14.72 while in weighted sum, the average of maximum distance from danger zone is 35.1 and the average for minimum path is 14.44.

#### 5.3.2 Case study 2: Multi-robot in environment with 5 obstacles

In this section, the environment used for the planning is a 10\*10 meters, all results are listed in **Table 6**. The experiment has achieved a feasible solution; the global path was achieved by AMOPSO is illustrated in **Fig. 8**, In the graph, the start point of robot 1 is [0,0] and the stop point is [10, 10], the start point of robot 2 is [2.5, 0] and the stop point is [2.5, 10], the start point of robot 3 is [7.5, 0] and the stop point is [2.5, 10], the start point of robot 4 is [0, 2.5] and the stop point is [7.5, 10], the start point of robot 5 is [0, 7.5] and the stop point is [10,0]. Best distances achieved by Immune Ant Colony Optimization Network Algorithm in, **Hao, and Xu, 2014**, are listed in **Table 7**. By comparing the results achieved in **Tables 6** and **7** the AMOPSO1 has a minimum time to reach the target than Immune Ant Colony Optimization Network Algorithm and pareto reach the target in 44.8 times less than weighted sum and 562 times less than Immune Ant Colony Optimization Network Algorithm.

## 6. CONCLUSION

In this paper, two case studies for path planning model based on AMOPSO is developed to enhance the performance of the multi-robot path planning. In the first case, the algorithm generates an optimal collision free trajectory in static environments that can contain known multiple obstacles and multiple danger zones and the second case improve the ability of multiple robot system to reach the shortest way. The algorithm achieved by Matlab 2014a and has been applied on two maps, first map, including two obstacles and two danger zones and the second including different barriers. The result of first case shows that the AMOPSO generates an



optimal path by maximizing the distance between the generated paths and the danger zones that exist in the environment and also minimizing the length of the path that needs by the mobile robot to reach the target, these results are better than the results achieved by Hybrid PSO-GSA. And the result for the second one shows that AMOPSO could be suit for a multi-robot system to find the shortest path and without collision between them. These results show that the AMOPSO has shortest time compared with time achieved by Immune Ant Colony Optimization Network Algorithm.

## REFERENCES

- Chakraborty, J., Konar, A., Chakraborty and U. K. and Jain, L. C., 2008, *Distributed Cooperative Multi-robot Path Planning using Differential Evolution*, In Proceeding of IEEE World Congress on Computational Intelligence, Hong Kong, pp.718-725.
- Chung, W. K., and Xu, Y., 2010, *A Generalized 3-D Path Planning Method for Robots Using Genetic Algorithm with an Adaptive Evolution Process*, In Proceeding of 8<sup>th</sup> World Congress on Intelligent Control and Automation, Jinan, China, pp.1354-1360.
- Dehuri, S., Ghosh, A., and Cho, S-B., 2008, *Particle Swarm Optimised Polynomial Neural Network for Classification: A Multi-Objective View*, International Journal of Intelligent Defence Support Systems, vol. 1, no. 3, pp.225-253.
- Ehlert, P. A. M., 1999, *The Use of Artificial Intelligence Robots*, Report on research project, Delft University of Technology, Netherlands.
- Fujimura, K., 1996, *Path Planning with Multiple Objectives*, IEEE Robotics and Automation Magazine, vol. 3, no.1, pp. 33-38.
- Gong, D. W., Zhang, J. H., and Zhang, Y., 2011, *Multi-Objective Particle Swarm Optimization for Robot Path Planning in Environment with Danger Sources*, Journal of Computers, vol. 6, no. 8, pp. 1554–1561.
- Hao, W., and XU, X., 2014, *Immune Ant Colony Optimization Network Algorithm for Multi-Robot Path Planning*, In Proceedings of the 5<sup>th</sup> IEEE International Conference on Software Engineering and Service Science (ICSESS), Beijing, China, pp. 1118-1121.
- Humadi, R. A., Abbas, N. H., and Hammadi, W., 2013, *PID Parameters Optimization Using Adaptive PSO Algorithm for a DCSM Position Control*, International Journal of Electrical Engineering and Technology, vol. 4, Issue 4, pp. 1-13.
- Jaillet, L., Cortés, J., and Siméon, T., 2010, *Sampling-based Path Planning on Configuration-Space Costmaps*, IEEE Transactions on Robotics, vol. 26, no. 4, pp.635-646.
- Kala, R., 2012, *Multi-robot Path Planning Using Co-evolutionary Genetic Programming*, Expert Systems with Applications, vol.39, no. 3, pp.3817-3831.



- Kaluder, H., Brezak, M., and Petrovic, I., 2011, *A Visibility Graph based Method for Path Planning in Dynamic Environments*, In Proceeding of 34<sup>th</sup> International Convention on MIPRO, Opatija, Croatia, pp.717-721.
- Kennedy, J., and Eberhart, R. C., 1995, *Particle Swarm Optimization*, In Proceedings of IEEE International Conference Neural Networks, NJ, USA, pp. 1942–1948.
- Li, H., Yang, S. X., and Seto, M. L., 2009, *Neural Network based Path Planning for a Multirobot System with Moving Obstacles*, In IEEE Transactions on Systems, Man, and Cybernetics, Part C: Applications and Reviews, vol. 39, no. 4, pp. 410-419.
- Miao, H., 2009, *Robot Path Planning in Dynamic Environments Using a Simulated Annealing Based Approach*, Master thesis, Queensland University of Technology, Queensland, Australia.
- Purcaru, C., Precup, R.-E., Iercan, D., Fedorovici, L.O., and David, R.-C., 2013, *Hybrid PSO-GSA Robot Path Planning Algorithm in Static Environments with Danger Zones*, In Proceedings of the 17<sup>th</sup> International Conference on System Theory, Control and Computing, Sinaia, Romania, pp. 434-439.
- Rao, S. S., 2009, *“Engineering Optimization: Theory and Practice”*, 4<sup>th</sup> Edition, Wiley.
- Vesterstrom, J., and Thomsen, R., 2004, *A Comparative Study of Differential Evolution, Particle Swarm Optimization, and Evolutionary Algorithms on Numerical Benchmark Problems*, IEEE Congress on Evolutionary Computation, Portland, USA, vol.2, pp. 1980-1987.
- Yang, X., 2014, *Nature-Inspired Optimization Algorithms*, 1<sup>st</sup> Edition, Elsevier.
- Zhang, Y., Gong, D.-W., and Zhang, J.-H., 2013, *Robot Path Planning in Uncertain Environment Using Multi-Objective Particle Swarm Optimization*, Neurocomput., vol. 103, pp. 172–185.



```
Begin
  for each particle in the swarm
    Initialize its position & velocity randomly
  end for
do
  for each particle in the swarm
    Evaluate the fitness function
    if the objective fitness value is better than the personal best objective fitness value
      ( $P_{best}$ ) in history, current fitness value set as the new personal best ( $P_{best}$ )
    end if
  end for
  From all the particles or neighbourhood, choose the particle with best fitness value as
  the  $G_{best}$ 
  for each particle in the swarm
    Update the particle velocity according to Eqs. 9 & 10
    Update the particle position according to Eqs. 11 & 12
  end for
until stopping criteria is satisfied
end begin
```

**Figure 1.** Pseudocode of the standard PSO algorithm.

```
Begin
  for each particle in the swarm
    Initialize particles position & velocity randomly
  end for
  Initialize External Archive (EA) (initially EA empty)
  Quality (leader)
do
  for each particle in the swarm
    select a particle (leader) from EA
    Evaluate the fitness function
    if the objective fitness value is better than the personal best objective fitness value
      ( $P_{best}$ ) in history then
        current fitness value of the objective function is set as the new  $P_{best}$ 
      end if
    Update the particle velocity according to Eqs. 9 & 10
    Update the particle position according to Eqs. 11 & 12
  end for
  Update leader in EA
  Quality (leader)
until stopping criteria is satisfied
  report the results of EA
end begin
```

**Figure 2.** Pseudocode of the standard MOPSO algorithm.

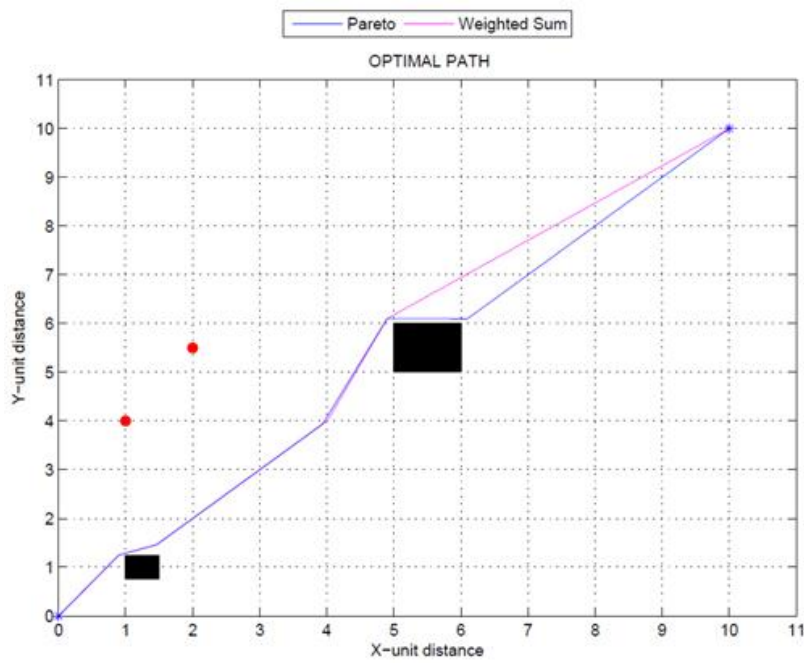


**Figure 3.** Best results achieved by AMOPSO1.

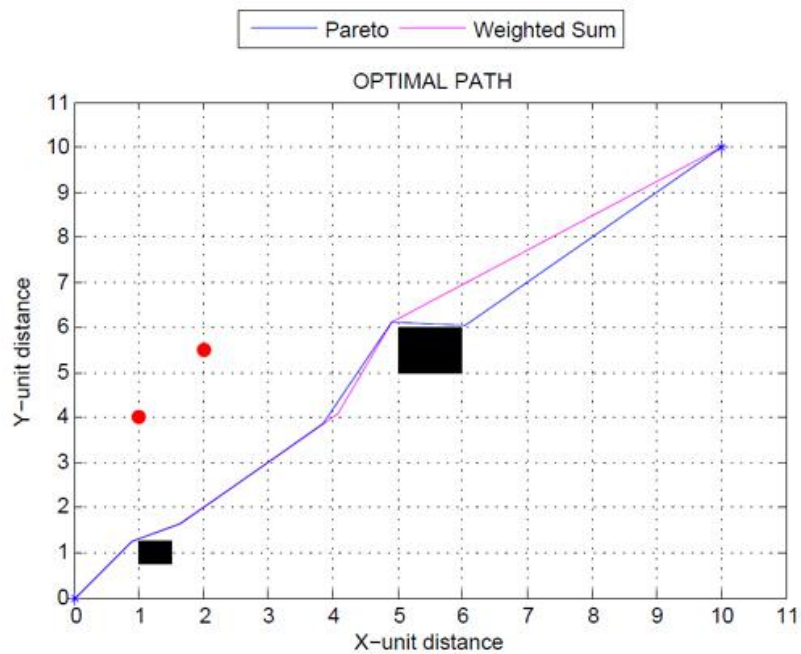


**Figure 4.** Best results achieved by AMOPSO2.



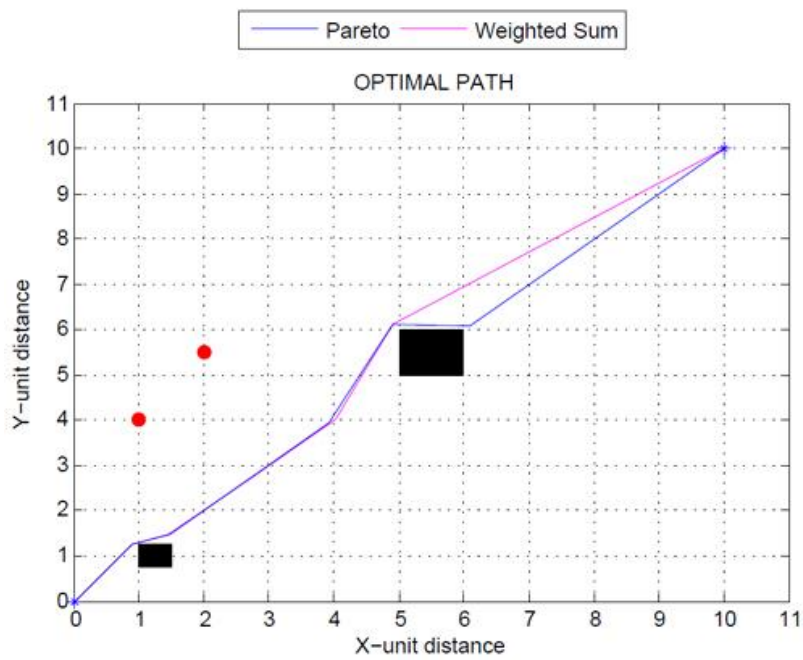


**Figure 5.** Best results achieved by AMOPSO3.

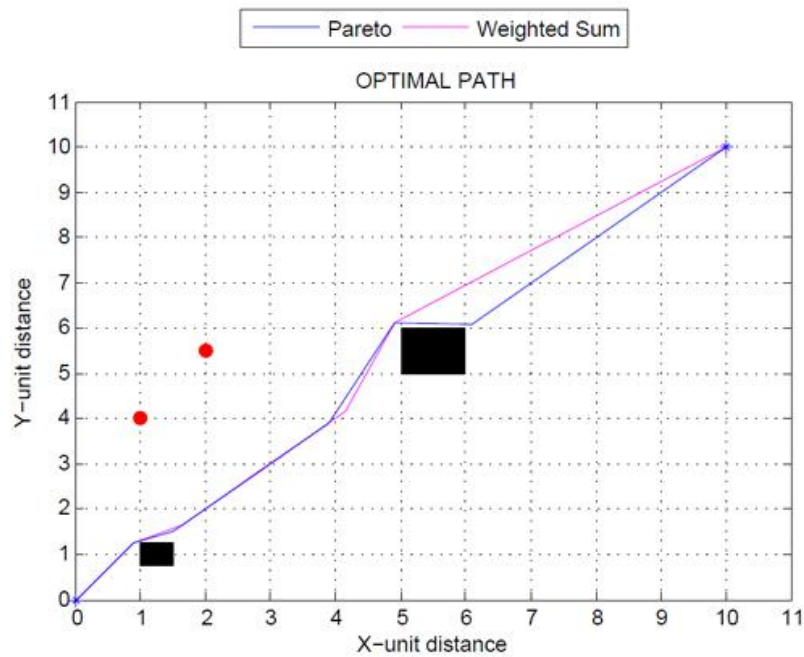


**Figure 6.** Best results achieved by AMOPSO4.

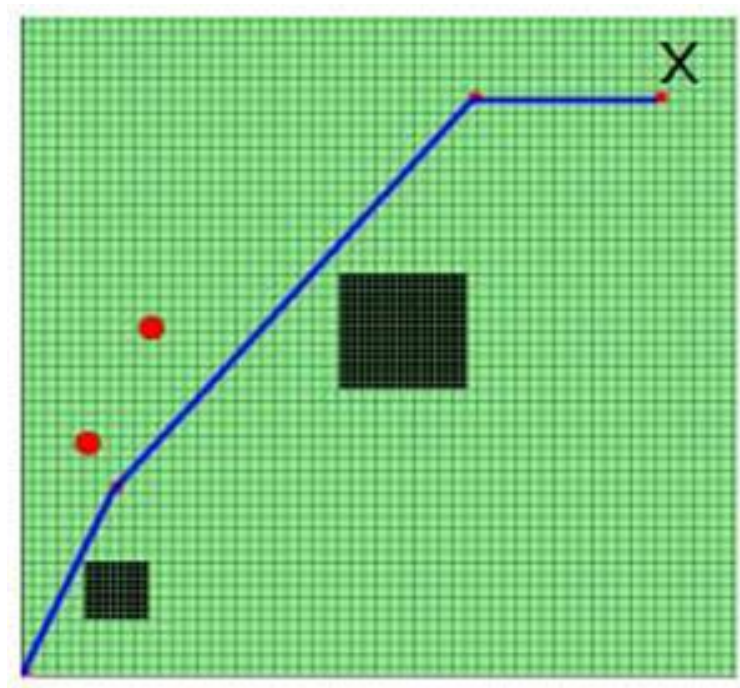


**Figure 7.** Best results achieved by Hybrid PSO-GSA, **Purcaru, et al., 2013.**

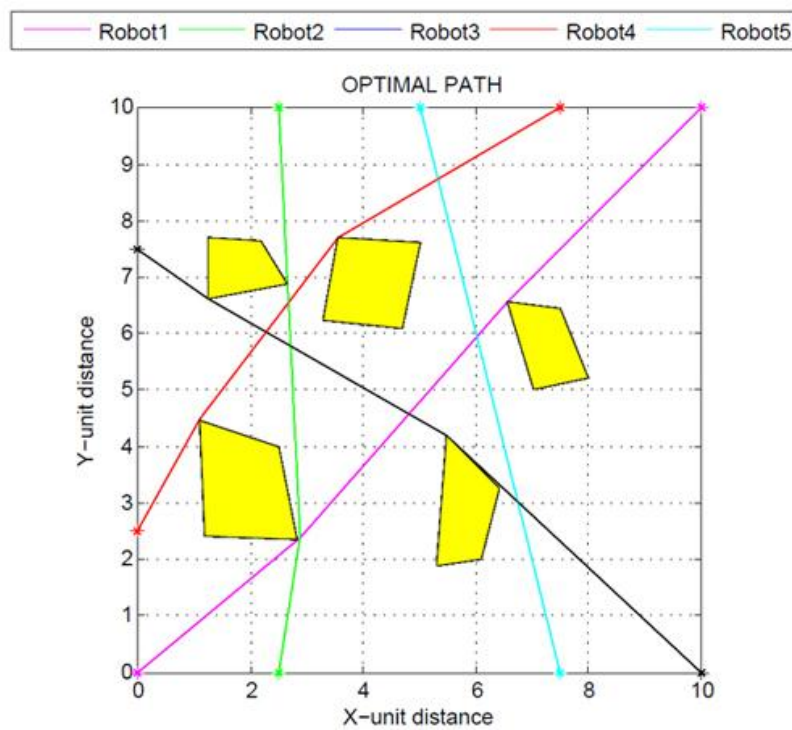


**Figure 8.** Best results achieved for case study 2.

**Table1.** AMOPSO cases

Name	W Equation	C1 & C2 Equation	r1 & r2 Equation
AMOPSO1	15	17 & 18	23 & 24
AMOPSO2	15	19 & 20	23 & 24
AMOPSO3	16	19 & 20	23 & 24
AMOPSO4	16	21 & 22	23 & 24

**Table 2.** Different benchmark functions on the SPSO and AMOPSO have been tested.

Benchmark fun.	Dim	Range
f1	30	$[-100,100]^D$
f2	30	$[-100,100]^D$
f3	30	$[-1.28,1.28]^D$
f4	30	$[-5.12,5.12]^D$
f5	30	$[-32,32]^D$
f6	30	$[-600,600]^D$

**Table 3.** Results for benchmark functions based on the SPSO and AMOPSO1, AMOPSO2, AMOPSO3 and AMOPSO4 algorithms.

f	SPSO	AMOPSO1	AMOPSO2	AMOPSO3	AMOPSO4
	Min. & Av.	Min. & Av.	Min. & Av.	Min. & Av.	Min. & Av.
f1	0.16239 0.26797	0.020316 0.020322	0.022755 0.02276	0.020315 0.020318	0.021744 0.021748
f2	0.61426 0.71556	0.063806 0.063186	0.066616 0.066639	0.060719 0.060745	0.06022 0.060259
f3	0.20384 8.4377	0.07885 0.087416	0.065096 0.070362	0.072637 0.081607	0.031205 0.048147
f4	0.16376 2.1796	0.044989 0.080379	0.078139 0.09372	0.020808 0.02131	0.019634 0.021526
f5	0.21717 0.30033	0.018962 0.019161	0.020767 0.020981	0.021648 0.02187	0.021819 0.022042
f6	0.20413 0.36459	0.027966 0.028254	0.027475 0.0281	0.028591 0.028887	0.028807 0.029154

**Table 4.** Coordinates of obstacles and danger zone for the case study 1.

Obstacles	Center Position
1	1,2,1
2	5,5,5,5
Danger zone	Position
1	1,4
2	2,5,5

**Table 5.** Result for case study 1.

Algorithm	Max. distance from danger zone		Min. distance from start to target position	
	Pareto	Weighted Sum	Pareto	Weighted Sum
AMOPSO1	46.251	39.963	14.725	14.437
AMOPSO2	38.472	33.893	14.72	14.431
AMOPSO3	37.867	33.38	14.729	14.439
AMOPSO4	37.576	33.165	14.724	14.436

**Table 6.** Result for case study 2.

Robot number	Min. distance from start to target position		Time	
	Pareto	Weighted Sum	Pareto	Weighted Sum
Robot 1	14.7	14.7	0.0011602	0.051955
Robot 2	10.041	10.041		
Robot 3	10.308	10.308		
Robot 4	10.889	10.889		
Robot 5	12.571	12.571		

**Table 7.** Result for Immune Ant Colony Optimization Network Algorithm, Hao, and Xu, 2014.

Robot number	Min. distance from start to target position	Time
Robot 1	14.1728	0.6525
Robot 2	10.0423	
Robot 3	10.3078	
Robot 4	10.9045	
Robot 5	12.5720	



## Buckling Analysis of Edge Cracked Sandwich Plate

Rasha Mohammed Hussein

Assistant lecturer

College of Engineering- University of Technology

Email: [mechanicalflower99@yahoo.com](mailto:mechanicalflower99@yahoo.com)

### ABSTRACT

This work presents mainly the buckling load of sandwich plates with or without crack for different cases. The buckling loads are analyzed experimentally and numerically by using ANSYS 15. The experimental investigation was to fabricate the cracked sandwich plate from stainless steel and PVC to find mechanical properties of stainless steel and PVC such as young modulus. The buckling load for different aspect ratio, crack length, cracked location and plate without crack found. The experimental results were compared with that found from ANSYS program. Present of crack is decreased the buckling load and that depends on crack size, crack location and aspect ratio.

**Keywords:** sandwich plate, buckling load, cracked plate

### تحليل الانبعاج للصفائح الشطيرية الحاوية على شق

م.م. رشا محمد حسين

مدرس مساعد

قسم هندسة الميكانيكية \ الجامعة التكنولوجية

### الخلاصة

هذه الدراسة ركزت بشكل رئيسي على تحليل حمل الانبعاج للصفائح الشطيرية بوجود ابو بدون شق لمختلف الحالات . وقد تم تحليل حمل الانبعاج عمليا وعدديا بواسطة برنامج الانسز (ANSYS 15). في الجانب العملي تم تصنيع الصفائح الشطيرية ذات الشقوق من مادة ستينلس ستيل stainless steel ومادة PVC وقد تم ايجاد معامل المرونة لكل منها وايجاد حمل الانبعاج للصفائح الشطيرية لحالات مختلفة من نسبة الطول للعرض وطول شق وموقع الشق للصفائح الحاوية على شق وشفيفة غير حاوية على شق ومقارنة النتائج العملية مع برنامج الانسز (ANSYS). ان وجود الشقوق يقلل من حمل الانبعاج بالاعتماد على حجم الشق وموقعه ونسبة الطول للعرض.

**الكلمات الرئيسية:** صفائح الشطيرية، حمل الانبعاج، صفائح حاوية على شق.



## 1. INTRODUCTION

Sandwich structures occupy a large proportion of composite materials design. They were very light weight and high flexural rigidity, excellent thermal isolation characters but the risk of buckling is greater than for classical structures. **Daniel, et.al, 2003**.

The transition of the plate from the stable state of equilibrium to the unstable one is referred to as buckling or structural instability. The smallest value of the load producing buckling is called the buckling load. According to this formulation, the critical load is the smallest load at which both the flat equilibrium configuration of the plate and slightly deflected configuration are possible. **Ventsel, and Krauthammer, 2001**. The behavior of plates are affected by presence of defects such as cracks due to corrosion, chemical attack, fatigue, impact and imperfections.

Many research had studied buckling analysis of plate. **Kumar, et al., 2004**, investigated plates behavior with various type of crack, like edge crack and central crack under different types of loading. They calculated buckling loads using hierarchical trigonometric functions. **Hiraman, et al., 2004**, studied quasi-static buckling tests were performed on natural fibre sandwich composites without delamination, with single delamination and with two delamination were prepared. From the results obtained it is evident that natural fibre structures without delamination displayed the highest load approximately 90% higher than the samples with delamination.

**Nathera, 2011**, investigated buckling phenomenon of cracked plates under compression load numerically using ANSYS by calculating the effect of crack length and crack location (i.e. cracks parameters) as well as the direction of load parallel or perpendicular to the crack faces. It is found from the results which are shown graphically in figures that the crack parameters and loading direction have significant effects on the critical buckling load (i.e. increased or decreased) of compressed cracked plate. **Ole, et al., 2012** described the development of a semi-analytic buckling model for steel-elastomer sandwich plate using the Rayleigh-Ritz method. All combinations of in-plane tensile, compressive and shear loads are measured. The model has been implemented in a FORTRAN program and the results have been compared with these obtain from the finite element program ABAQUS. **Nathera, and Saddam, 2012**, In this work, the buckling behavior for edge cracked plates with compression loading is studied numerically using ANSYS considering the effect of the crack parameter (i.e. size, location and orientation), aspect ratio of plate and boundary conditions. The results are shown that the crack parameters, aspect ratio of plate and boundary condition are efficient factors on the buckling load coefficient.

**Hatem, and Nawal, 2014**, studied the effect of using two skins material on the strength of sandwich plates with the effect circular hole when the mechanical loads are applied. Theoretically, numerically by ANSYS and experimentally are done for many cases of sandwich plates. The sandwich plates under bending or buckling load determine experimentally. The results showed that the stress concentration that occur in in hole weaken the strength of sandwich plate is depending on the size of hole and the face materials. **Shariati, et.al., 2014**, the buckling and post-buckling behaviors of cracked stainless-steel plates under uniform axial compression load were investigated experimental and numerical and parameter effects such as length of crack, crack angle, position of crack, plate imperfection, load band, and thickness of plate on the critical buckling load were analyzed. In the experimental work, mechanical



properties and plastic behavior of plates made from stainless steel were determined for the numerical study. Results are shown the considerable effects of the above parameters on the critical buckling load.

The present work focuses on how to evaluate buckling load for sandwich plate with crack experimentally and numerically. Mechanical properties for stainless steel and PVC are determined experimentally. Compression test done to find critical buckling load for different cases.

Also Finite element coded by ANSYS15.0 used to find it. According to author's knowledge about the published papers on the buckling field, there is no report on the buckling analysis of edge cracked sandwich plate.

## 2. NUMERICAL ANALYSIS

### 2.1 Element Selection and Modeling

Finite element method has been employed to analyze buckling load (critical loads at which a plate becomes unstable). The model was developed in ANSYS 15.0 using the element called shell281 as shown in **Fig.1** which is suitable for analyzing thin plate to moderately thick plate. The element has eight nodes at each node there were six degrees of freedom: translations in the global coordinate  $x$  is directed along the width of the plate, while the global  $y$  coordinate is directed along the length and the global  $z$  direction corresponds to the thickness direction, and rotations about the  $x$ ,  $y$ , and  $z$  axes. It may be used for modeling that has layered applications such as composite shells. It includes the effects of transverse shear deformation. The accuracy in modeling composite shells is governed by the first order shear deformation theory. The shell section allows for layered shell definition, options are available for specifying the thickness, material, orientation through the thickness of the layers.

There were four steps for the eigenvalue buckling in ANSYS 15.0:

1. Build up the model: it includes defining element type (shell 281), material properties (young modulus and poisson ratio of steel and aluminum) and models.
2. Solution (static analysis): includes made boundary conditions, applying loads and the analysis solve.
3. Eigen buckling analysis: from eigenvalue buckling analysis can be found the theoretical buckling strength of the plate.
4. Postprocessor: these steps includes listing result such as buckling loads and viewing mode shape of buckling , it can be plot the deformed and un-deformed shape of laminated plate.

### 2.2 Mesh Convergence

A convergence study was performed to determine the appropriate finite element mesh to be used in the buckling analysis of sandwich plate model. Meshes were developed, with increasing numbers of elements in the  $x$  and  $y$  directions and the buckling load for each of these models is shown in **Fig. 2**.



When increasing the degree of freedom from (576) to (2046) the difference in buckling load is only a (0.036%). No difference observed between D.O.F. (2046) and D.O.F. (4416). The buckling load for each of these models is shown in **Table 1**. This indicates that D.O.F. (2046) is capable of performing the analysis within a reasonable degree of accuracy.

### 2.3 Verification Case Studies

In the present study, Series of preselected cases are modeled to verify the accuracy of the method of analysis. The results of **Nathera, and Saddam, 2012** are compared to numerical solution (ANSYS).see **Table 2** from these results, it is obvious that the methods of solution gives better results for numerical solution.

## 3. EXPERIMENTAL WORK

In the present work, three- purposes were investigated. First, to outline the general steps to manufacture models are then used to evaluate the young modulus of steel and PVC alone. Second, design and fabricate the sandwich plate from stainless steel and PVC and made different cases of crack. Third, the buckling test can be done to calculate the critical buckling load of sandwich plate for simply free boundary conditions with or without crack.

### 3.1 Tensile Test

Test specimens were cut from the plates using cutting tool CNC machine shown in **Fig. 3**. The two samples one made of steel and the second made of PVC are divided according to dimensions, as set by ASTM-E8 as in **Fig. 4**. The specimen's tensile test is mounted vertically in a servo-hydraulic testing machine, and hydraulically pulled with stroke control with large steel grips, tensile machine shown in **fig. 5** Maximum capacity (50KN). The results (the young modulus) are listed in **Table 3**.

### 3.2 Manufacturing the Sandwich Plate

A sandwich structure results from the assembly by bonding-or welding-of two thin facings or skins on a lighter core that is used to keep the two skins separated. The facing materials are from stainless steel, and the core materials is from PVC it is as light as possible. One can denote couples of compatible materials to form the sandwich. The difference between the skins (faces) and the core in the mechanical properties is closed by the range of the ratio of Young modulus of faces to the Young modulus of core **Daniel, et.al, 2003**

$$10 \leq \frac{E_f}{E_c} \leq 100 \quad (1)$$

To determine the ratio in **Eq. (1)**, stainless steel alloy is selected to be the constitutional materials of faces while PVC is represented the core. To obtain the mechanical properties of each constitution materials, tensile test is done. The faces and core are cut, a small cut has been added to the each specimens using suitable cutting tool, as shown **Fig. 6**. The ferton power tools,



with (330 W) power and (10000-32000 r.p.m) has been used to create cracks in the plates. The crack width equal to thickness of cutter disc ( $d=2\text{mm}$ ). Then, bonded the two stainless steel faces with PVC core by cyanoacrylate adhesive shown in **Fig. 7** and press them until the adhesive material dried.

### 3.3 Buckling Test:

The specimen was loaded in axial compression (vertical direction) using tensile test machine of (200 kN) capacity shown in **Fig. 8** The specimen was simply supported at two ends and kept free at the other two ends. The specimen was loaded slowly until buckling. Simply supported boundary conditions were simulated along the top and bottom edges. For axial loading, the test specimen was placed between two extremely stiff machine heads of which the lower one was fixed during the test, whereas the upper head was moved downwards by servo hydraulic cylinder. The sandwich plate was loaded at constant cross-head speed of (3 mm/min) .The experimental set up as shown in **Fig. 9**.

## 4. RESULTS AND DISCUSSION

### 4.1 Aspect Ratio

**Fig.10** for S-F-S-F sandwich plates with central 5mm edge crack show that the buckling load decreases when  $a/b$  increase with high percentage reaches to 37. 45% when the aspect ratio increase from 1 to 2. 32.64% On the other hand when  $a/b$  varies from 1 to 1.5, and 1.5 to 2, the decreasing of buckling load 6.85% and 32.64% respectively. The difference between ANSYS program and experimental result is 3.4%, 4.9%, 2.5% for aspect ratio 1, 1.5 and 2 respectively.

### 4.2 Crack Location

It is shown from **Fig.11** that the buckling load for S-F-S-F sandwich plate with 5mm edge crack decreases when crack location change from  $a/4$  to  $a/2$  (i.e, 55mm to 110mm) with small percentage 0.4% . It can be also observed that the buckling load is increase with small percentage when crack location varies from  $a/2$  to  $3a/4$  (i.e., 110mm to 165mm) reach to (0.13%). The buckling load for the cases  $a/4$  and  $3a/4$  is approximately equal. These result show that the buckling load is effected with crack location with very small percentage.

### 4.3 Crack Size

It is shown from **Fig.12** that the buckling load for S-F-S-F sandwich plate with central edge crack decreases when crack size increase change from 5mm to 10mm with small percentage 1.3% . It can be also observed that the buckling load is decrease with small percentage when crack size varies from 10mm to 15mm reach to (1.9%). The buckling load when they were no crack is the large value and it decreases by 4.4% when adding 5mm central edge crack see **Table 4**.



## 5. CONCLUSION

In the present work, the buckling behavior of the edge cracked sandwich plate made from stainless steel and PVC has been considered. The effect of some parameters such as aspect ratio, crack location and crack length for S-F-S-F supported boundary conditions on the critical buckling load of compressed cracked plates have been investigated experimentally and numerically using Finite Element Method (ANSYS Package). It is shown from the computed results that:

1. The buckling load is very sensitive to aspect ratio change. When the aspect ratio increases the critical buckling load decreases. And maximum buckling load occurs in square plate.
- 2- Small crack have a little effect on the critical buckling load and it becomes higher for larger crack and the buckling load became lower and more dangerous more than the case that is no crack.
- 3- The crack location is the most an effective parameters on the buckling load.

## REFERENCES

- Daniel gay, Soung V. Hoa, Stephen W. Tsai, 2003, *Composite Materials: Design and Applications*, New York.
- Dr. Hatem Rahem Wasmi, Nawal Falkhous Eshaut, 2014, *Study the Effect of Face Sheets Material on Strength of Sandwich Plates with Circular Hole*, Journal of Engineering, Number 6 Volume 20 June – 2014.
- Dr. Nathera Abdual Hassan Saleh, Saddam Kallsan Kuess, 2012, *Studying a Buckling Behavior for Edge Cracked Plates Under Compression*, Eng. And technology journal, vol.30, No.1.
- Hiranman, S., Kanny, K.1 and Ramsaroop, A., 2004, *buckling response of natural fibre sandwich plates*, Proceedings of the 2nd Biennial International Composites Africa ,ISBN Number: 1-920-01720-8.
- Kumar Satish Y.V., Paik J.K., *Buckling analysis of cracked plate using hierarchical trigonometric functions* ,Thin-Walled Structures 42(2004) 687-700.
- Nathera Abdual Hassan Saleh, 2011, *Influence of Crack Parameters and Loading Direction on Buckling Behavior of Cracked Plates Under Compression*, Basrah Journal for Engineering Science.



- Ole J. Hareide, Lars Brubak, Eivind Steen and Jostein Hellesland, 2012, *Approximate buckling model for steel-elastomer sandwich plates*, Proceedings of the 25th Nordic Seminar on Computational Mechanics.
- Sarath Babu C. , Kant T., 2000, *refined higher order finite element models for thermal buckling of laminated composite and sandwich plates*, Journal of Thermal Stresses, 0149-5739.
- Shariati M., Majd Sabeti A. M. and Gharooni H., *A numerical and experimental study on buckling and post-buckling of cracked plates under axial compression load*, journal of computational and applied research in mechanical engineering , vol.4., no.1,2014, issn:2228-7922.
- *Theory, Analysis, and Element Manuals*, ANSYS 15 Program.
- Ventsel E. and Krauthammer T.,2001, *Thin plates and shells-theory, analysis and applications*, New York.

## NOMENCLATURE

$a, b$ = Dimension of plate in  $x$  and  $y$  coordinate, m.

$E$ = Elastic Young modulus, GPa.

$E_f, E_c$ = Elastic Young modulus for face and core, GPa.

$t$ = Thickness, m.

$N_{xx}, N_{yy}, N_{xy}$ = The resultant of in-plane force per unit length, N/m

D.O.F. = Degree of freedom, dimensionless.

S-F-S-F= simply free simply free

$\nu$ = Poison ratio, m/m.

$k$ = Buckling coefficient, dimensionless,

$C$ = Crack size, m.

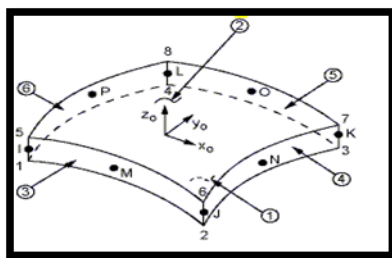


**Figure 1.** Shell281 Geometry [ANSYS 15.0 Program]

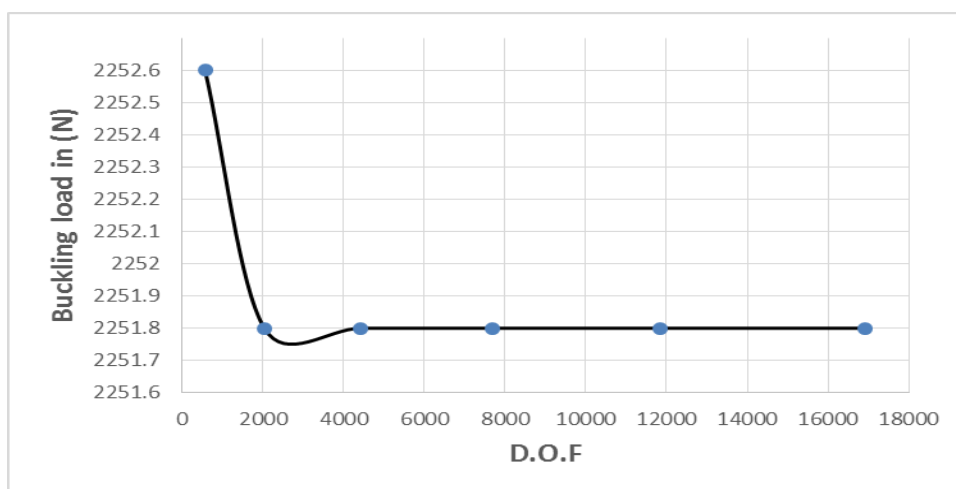


**Figure 2.** Convergence study of Buckling load versus D.O.F. for S-F-S-F plate without crack

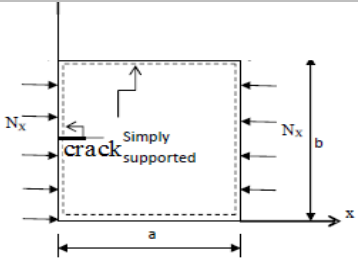
**Table 1.** Buckling load convergence study for S-F-S-F plate without crack

No. of element	No. of node	D.O.F	Buckling load (N)
25	96	576	2252.6
100	341	2046	2251.8
225	736	4416	2251.8
400	1281	7686	2251.8
625	1976	11856	2251.8
900	2821	16926	2251.8



**Figure 3.** Cutting tool CNC machine

**Table 2.** Buckling coefficient  $k = \frac{12b^2(1-\nu^2)N_x}{\pi^2 Et^3}$  of simply supported edge cracked plate

c/a	Nathera, 2012	Present [ANSYS15.0]	 <p><math>E=200\text{GPa}</math> , <math>t=10\text{mm}</math>, <math>\nu=0.3</math>, <math>a/b=1</math></p>
0.1	4	3.823	
0.2	3.98	3.754	
0.3	3.96	3.687	
0.4	3.9	3.613	
0.5	3.69	3.5	

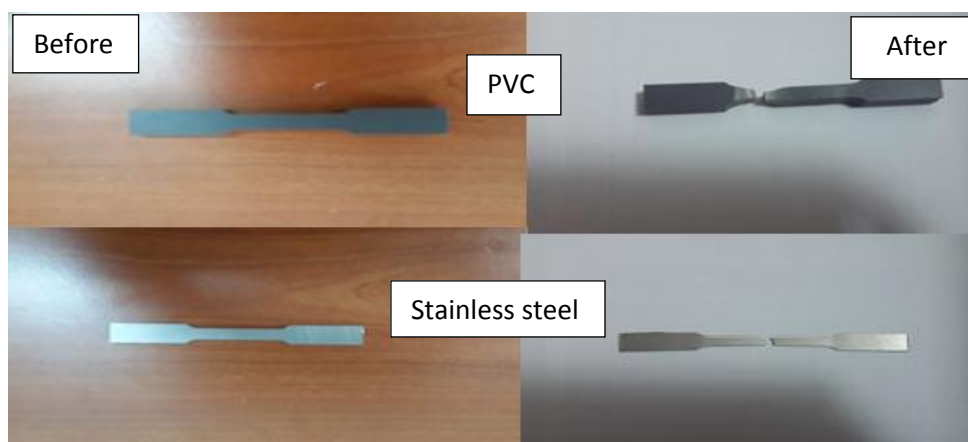


**Figure 4.** Samples of tensile test one made of steel and the second made of PVC.



**Figure 5.** Tensile test machine



**Figure 6.** The ferton power tools

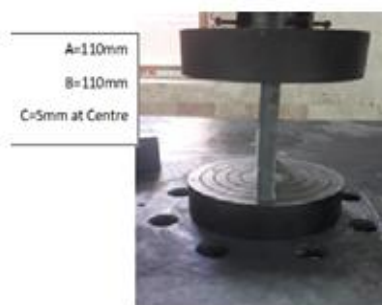




**Figure 7.** Cyanoacrylate adhesive



**Figure 8.** Buckling test machine



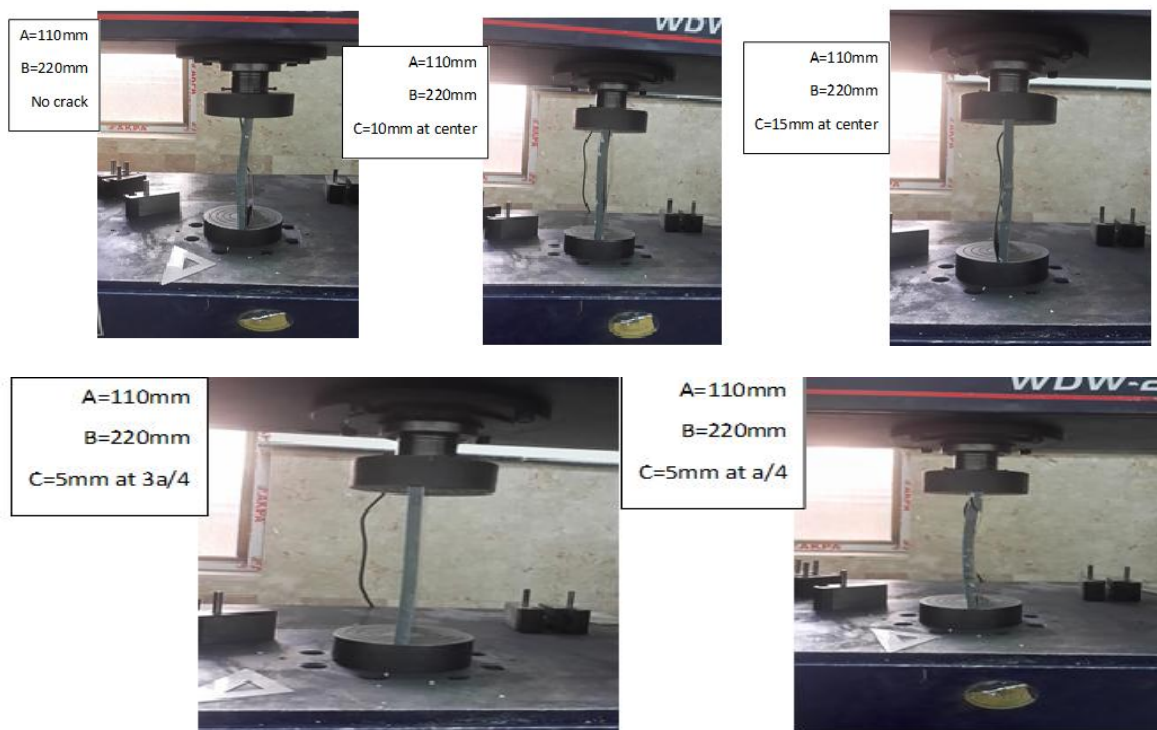


**Figure 9.**The experimental set up

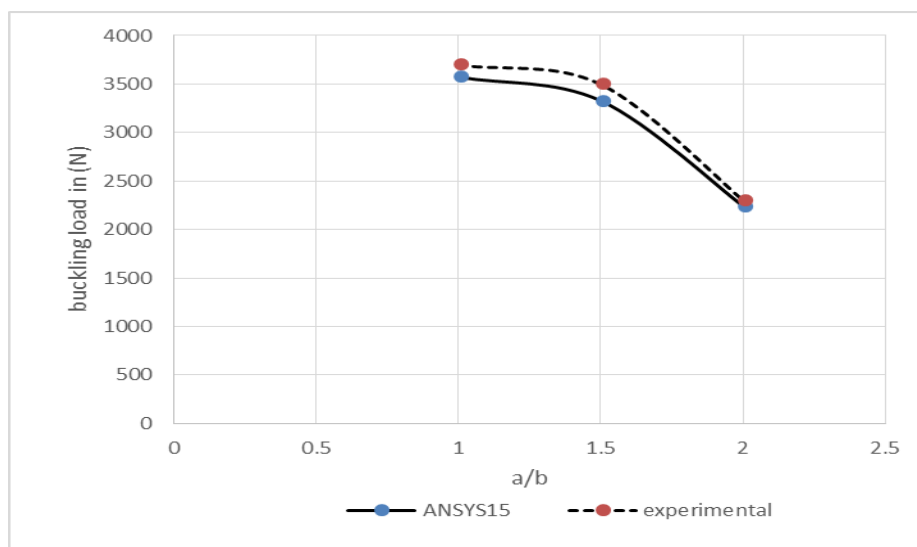


**Figure 10.** Effect of aspect ratio on buckling load for S-F-S-F sandwich plate with (5mm) central edge crack

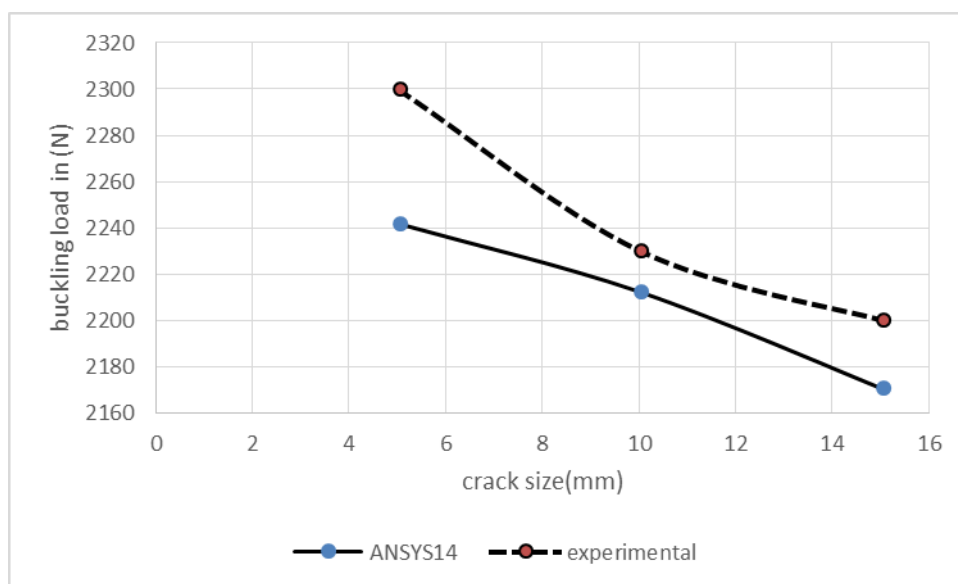


**Figure 11.** Effect of crack size on buckling load for S-F-S-F sandwich plate with central edge crack and  $a=110\text{mm}$ ,  $b=220\text{mm}$

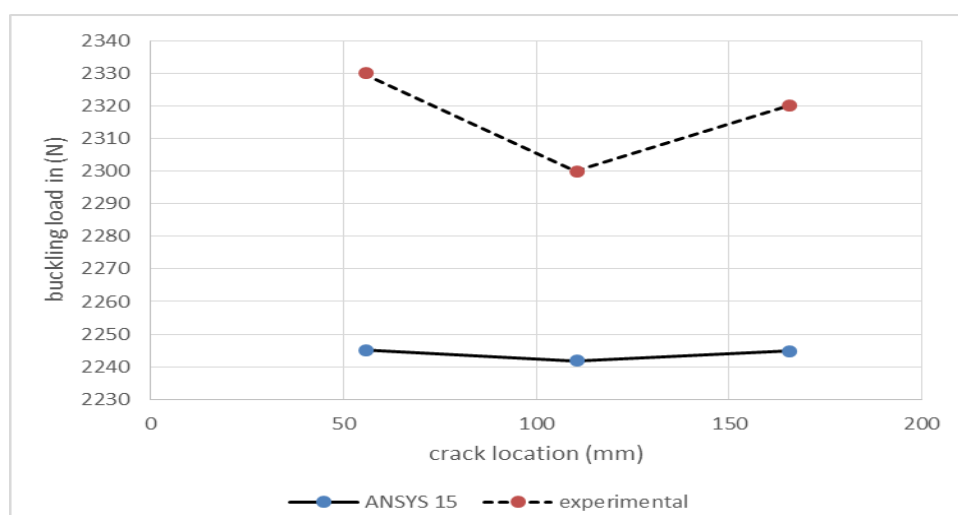


**Figure 12.** Effect of crack location on buckling load for S-F-S-F sandwich plate with (5mm) edge crack and  $a=110\text{mm}$ ,  $b=220\text{mm}$

**Table 4.** Buckling load of S-F-S-F sandwich plate without crack and different central crack size

a=110mm, b=220mm

No. of element	Buckling load (N) experimentally	Buckling load (N) in ANSYS15.0	Error%
no crack	2500	2251.8	9.93
5	2300	2241.9	2.53
10	2230	2212.4	0.79
15	2200	2170.7	1.3

## دور البيئة المعلوماتية في بناء المدينة الذكية

محسن جبار عودة  
ماجستير هندسة معمارية  
أمانة بغداد

بهجت رشاد شاهين  
أستاذ متمرس  
كلية الهندسة/جامعة بغداد  
قسم هندسة العمارة

### الخلاصة

يتناول البحث مفهوم المدينة الذكية، كونه أحدث توجهات التصميم الحضري، بإستثمار قدرات الذكاء الإنساني، و الذكاء الإصطناعي للنهوض بواقع المدينة. يوصف مفهوم المدينة الذكية بأنه أحد أهم تجليات الثورة المعلوماتية، مع نهاية القرن العشرين، و مطلع القرن الحادي والعشرين، و يعزو البحث ظهور المفهوم الى: قصور الأساليب، و الطرق التقليدية في إنشاء و تطوير المدن، فضلاً عن الزيادة الكبيرة في عدد سكان المدن و الحواضر العالمية. و لذلك إعتد نهج المدينة الذكية، المباديء و الأساليب المبتكرة التي تعزز أداء و كفاءة المدينة على المستويات الخدمية، و الصحية، و الإقتصادية، و الإجتماعية، و البيئية.

تشير الدراسات العالمية، الى ندرة الإسهامات الحضرية، في مجال المدينة الذكية، لذلك فقد برزت الحاجة لدراسة المفردات و العناصر و الحلول المبتكرة التي تطبق في المدن العالمية، و من ثم دور المعلوماتية بتحقيق هدف مبادرة المدينة الذكية. و عليه تتمثل مشكلة البحث بـ: وجود فجوة معرفية حول تأثير البيئة المعلوماتية، لقيام مبادرة المدينة الذكية. يتبنى البحث الفرضية الآتية: يؤدي الفكر المعلوماتي متعدد التخصصات، دوراً جوهرياً في تحقيق مبادرة المدينة الذكية.

لمعالجة المشكلة البحثية، يهتم البحث بتعريف مفهوم المدينة الذكية، و توفير القاعدة المعرفية، و دراسة مقاربات المدينة الذكية، فضلاً عن البيئة الحضرية الذكية و بنية المدينة الذكية و أهم عناصرها و شبكاتها الذكية، ليستخلص أهم مفردات و مؤشرات و مقومات إنشاء المدينة الذكية، و من ثم تطبيقها على الحالات الدراسية معتمداً المنهج الوصفي التحليلي، وصولاً الى أهم مقومات قيام المدينة الذكية في العراق.

خلص البحث الى تأكيد دور الفكر المعلوماتي، ممثلاً بالمؤسسات البحثية العالمية، و شركات المعلوماتية متعددة الجنسيات، لتحقيق المدينة الذكية، بإعتماد مباديء: الشراكة، و التعددية، و إستدامة ذكاء المدينة، و عليه تعد المدينة الذكية: خلاصة الفكر و المعرفة الإنسانية.

**الكلمات الرئيسية:** المعلوماتية، المدينة الذكية، المدينة المعلوماتية، البيئة الذكية، الشبكات الذكية.



## The Role of Informational Environment in Building Smart City

**Bahjat Rashad Shahin**

Professor

Engineering College-Baghdad University

E-mail: bahjatsha@yahoo.com

**Muhsin Jabbar Awda**

Master Degree in Architecture

Baghdad Mayoralty

E-mail: muhsinjabbar@yahoo.com

### ABSTRACT

The research addresses smart city concept as it is the latest urban design trends, by the investment of the capabilities of human, and artificial intelligence for the sake of the advancement of the city. The concept of a smart city is described as one of the most important manifestations of the information revolution, with the end of the twentieth, and the beginning of twenty – first century, The research attributes the emergence of the concept to: deficiencies of means, and traditional methods in building and development of cities, as well as The significant increase in the number of city and global metropolises dwellers. So, smart city approach has been adopted, along with innovative principles and methods which consolidate the performance and efficiency of the city at services, health, economic, social, and environmental levels. Global studies indicate, to the urban contributions scarcity, in the area of smart city, so the need of vocabularies, elements, and innovative solutions studies have emerged and then the role of information's in achieving the aim of smart city initiatives.

**The research problem is:** The acknowledge gap about the impact of the informational environment, to establish smart city initiative. **The research adopts the hypothesis:** A multi-disciplinary informational thought plays an essential role in achieving smart city initiative.

To address the research problem, the research starts with the definition of the concept of smart city, to provide the knowledge platform, then addresses the smart city approaches, as well as, smart urban environment, smart city structure, key elements and smart networks, to concludes key vocabulary, indicators and constituents of smart city establishment, Then applied to the case studies with analytical descriptive approach, to conclude the key constituents to establish smart city in Iraq.

The research concluded to confirm the role of the informational thought, represented by global research institutions, and multinational Informational companies, at the level of thought and application, to achieve Smart City, with depending on principles of partnership, pluralism, and sustaining of city smartness, so the smart city is: the conclusion of thought and human knowledge.

**Key Words:** Informatics, Smart city, Informational city, Smart Environment, Smart Grids.

**المقدمة:**

يعد مفهوم المدن الذكية أحد تجليات العولمة والحضرية المتحررة الجديدة التي تجسدها المعلوماتية و التكنولوجيا الحديثة المقترنة بتطور الذكاء الاصطناعي إذ جاءت نتيجة ملحة لتطوير المدن بشكل متزامن مع التطور السريع في الحقول المعرفية الأخرى. توصف المدينة الذكية بأنها ظاهرة حضرية معاصرة و أحد أهم تجليات المعلوماتية، ظهرت مع أواخر القرن العشرين و بدايات القرن الحادي و العشرين. قلما تناولها الباحثون، بشكل شامل لكل مفرداتها، مقوماتها و سبل تنفيذها، لاسيما خلال السنوات الأخيرة من القرن الحالي (الحادي و العشرين). تفرض الزيادة في عدد سكان الأرض حاجة ملحة لإعادة التفكير و إيجاد طرق جديدة أكثر ذكاءا و إبداعا، لتفادي الكوارث المتوقعة و إيجاد فرص لحياة أفضل في المدن الحاضرة، سيما و إن العالم يندفع بسرعة متزايدة لم يسبق لها مثيل نحو مستقبل إستثنائي، و بدون رؤى واضحة. يشكل التحضر على المستوى العالمي و نشوء المجتمعات الذكية، حقيقة كشفت قصور الأساليب التقليدية و قيودها الحضرية و الإجتماعية. تتضمن الدراسة الحالية: دور المعلوماتية في إنشاء و تطور المدينة الذكية و مقارباتها الفكرية، بأستخدام الوسائل والآليات المعاصرة، إذ يتناول البحث الجانب الفكري و التطبيقي، فضلاً عن مقومات المدن الذكية، التي أصبحت احد التوجهات الاساسية التي إنتشرت في أرجاء العالم، لما توفره من تبادل للمعارف و الافكار، و أدوات لانجاز الاعمال و توفير الخدمات بكل سهولة و يسر.

**تعريف، و توصيف المدينة الذكية:**

يعتمد تعريف المدينة الذكية، على تخصصات علمية مختلفة، لذلك فقد عكس وجهات نظر حاجات مختلفة. يعتمد التعريف على الطروحات النظرية، التعاريف والمفاهيم الأساسية للمدن الذكية. تم إعتداد مصطلح المدينة الذكية من قبل الحكومات المختلفة، المنظمات الإستشارية و الفرق البحثية. بالرغم من إستخدام المصطلح بشكل واسع، فإن معناه لا يزال غير واضح، لتتويع الرؤى و الأهداف التي تتشدها المدن وراء تبنيها المفهوم.

تؤكد طروحات (R. Hall's)<sup>(1)</sup>، و (Hartley)، المتخصصة بحقل المعلوماتية، الإتصالات و الحوسبة على البعد التكنولوجي، إذ ترى بأن المدينة الذكية: هي المدينة التي ترصد (monitors) و تكامل (integrate) بناها التحتية الأساسية. يعد نظام المراقبة الذاتية (self-monitoring) و الإستجابة الذاتية (self-response)؛ من أهم آليات المدينة الذكية وتعمل على ربط كل من البنية الفيزيائية (المادية) الأساسية؛ البنية الإرتكازية لتكنولوجيا المعلومات؛ البنية التحتية الإجتماعية و البنية التحتية للأعمال، للإستفادة من قيم الذكاء الجمعي للمدينة (Hartley, 2005)<sup>(2)</sup>.

يصف (Caragliu)<sup>(3)</sup> المدينة الذكية (Caragliu, 2009): بأنها المدينة التي تدعم النمو الإقتصادي المستدام و الإرتقاء بنمط الحياة، من خلال الإدارة الحكيمة للموارد الطبيعية، فضلاً عن إعتداد الحكم القائم على المشاركة. إذ يتوقع أن تسهم المدن الذكية بتحسين نوعية نمط حياة مواطنيها بشكل جذري، فضلاً عن تشجيع رجال الأعمال على الإستثمار لإرساء دعائم البيئة الحضرية المستدامة (Vasseur & Dunkels, 2010). و يؤكد على إن المدينة الذكية تدعم الابتكار المفتوح (open innovation) (Paskaleva, 2011).

<sup>(1)</sup> Robert E. Hall : إستاذ في جامعة ستانفورد، كاليفورنيا، الولايات المتحدة، متخصص في الإقتصاد المعرفي، و عضو الأكاديمية الوطنية الأمريكية للفنون و العلوم، ساهم في التأسيس لمفهوم المدينة الذكية من خلال البحث العلمي. للمزيد من المعلومات: REHall@stanford.edu  
<sup>(2)</sup> Jean Hartley : أستاذة التحليل المؤسسي، و الإدارة العامة، في (Warwick Business School)، المملكة المتحدة، تركز في دراساتها على: أساليب الإدارة و الابتكار في الخدمات الحضرية العامة المتعلقة بالمدينة الذكية، للمزيد من المعلومات:

<http://www.open.ac.uk/people/jfh248#tab1>

<sup>(3)</sup> الباحث الدكتور (Andrea Caragliu): الأستاذ المساعد في كلية العمارة و البيئة المبنية، و هندسة البناء، ميلانو - إيطاليا. متخصص في مجال الإقتصاد الحضري و الأقليمي في (Politecnico di Milano)، و باحث زائر في الإقتصاد الحضري و الأقليمي - جامعة (VU) أمستردام، و للمزيد من المعلومات: andrea.caragliu@polimi.it



يصف كل من: (Vasseur)<sup>(4)</sup> و (Dunkles)<sup>(5)</sup> المدينة الذكية (Vasseur & Dunkles, 2010)؛ بكونها المدينة التي تستقطب أفضل و ألمع المتميزين و الموهوبين من مختلف أنحاء العالم (Bloomberg, 2011)، يؤكد هذا، حقيقة أن المدن التي تحوي الجامعات و المؤسسات التعليمية المتطورة، تنمو أسرع من تلك التي تمتلك مستوى تعليمي أقل، ذلك إن المدن التي تحوي المهارات، تتميز بالإنتاجية العالية على المستوى الإقتصادي، فضلاً عن كونها أكثر قدرة على التكيف مع الصدمات الإقتصادية (Glaeser & saiz, 2003).

يعرف كل من (Nam)، و(Pardo) مفهوم المدينة الذكية ؛ بوصفها بؤرة للإبتكار الحضري، إذ ينبغي أن تُفهم المدينة الذكية على إنها قدرة فكرية مؤكدة (certain intellectual ability)، تعالج العديد من الجوانب الإجتماعية – التقنية، و الإجتماعية – الإقتصادية التنموية للإبتكار (Nam & Pardo, 2011).

**تعريف المدينة الذكية:**

يعرف البحث المدينة الذكية، بأنها: المدينة التي تعتمد الذكاء الإنساني و الذكاء الإصطناعي، بإعتماد المعلوماتية أساساً لإيجاد و تطبيق الحلول للمشكلات الحضرية. تحاكي المدينة الذكية الكائن الحي من حيث شبكات الإتصالات الرقمية (الأعصاب The nerves)؛ قيم الذكاء المنتشر – في كل مكان – (العقول Brains)؛ المتحسسات و البطاقات (sensors and tags)، التي تمثل الأعضاء الحسية (the sensory organs) و البرمجيات (المعرفة و الكفاءة المعرفية – الإدراكية)، و تعتمد المعلوماتية في إدارة الأنظمة الحضرية.

**مقاربات المدينة الذكية:**

تمثل المدن الذكية: أحدث فصل في تاريخ التجديد الحضري، مع إطلالة القرن الحادي و العشرين. إن المستوى غير المسبوق من التحضر العالمي و ما يترتب عليه من نمو في حجم و عدد المدن في أنحاء العالم، يقدم كل من الفرص و التحديات. لمواجهة هذه التحديات، تنتهج إدارات المدينة طرقاً جديدة لتبدأ بالشروع بمبادرة المدينة الذكية (Ojo, et al, 2014, p: 1).

يمكن تحديد أهم المقاربات المعلوماتية لمفهوم المدينة الذكية بما يأتي:

#### المعلوماتية (Informatics):

تعني إستخدام الحوسبة الإلكترونية؛ و الربط من خلال الشبكات و تتكامل تكنولوجيا المعلومات و تكنولوجيا المواد خلال الأنظمة الحسية (Sensor Systems) و تعتمد بشكل خاص على أساس تكنولوجيا الذكاء الإصطناعي. تعمل المعلوماتية على نقل المعطيات رقمياً لنشر المعرفة و الثقافة متجاوزة الحدود الدولية (<https://ar.wikipedia.org>).

#### المدينة المعلوماتية (Informatics City):

هي المدينة التي تتميز بتكوين المجتمع المعلوماتي خلال فضاءات المعلومات الحضرية، هدفها تحقيق أسلوب جديد لتوفير الخدمات بعيداً عن الطرق التقليدية، إذ تمتلك كل الأبنية و الوسائل محتوى معلوماتي واسع النطاق (عودة، 2007، ص: 66).

#### المدينة الإلكترونية (Electronic City):

هي المدينة التي تقدم الخدمات و المعلومات إلكترونياً و بكل شفافية و مساواة و بسرعة متناهية و دقة عالية في أي وقت و من أي مكان من خلال قطاعاتها و أجهزتها الخدمية المختلفة بإستخدام تكنولوجيا المعلومات و الإتصالات، و النظم

<sup>(4)</sup> الدكتور فسيور (Jean-Philippe Vasseur) أحد مهندسي مؤسسة (Cisco)، عمل في بنية بروتوكول الإنترنت (IP). في مجال هندسة المرور (Traffic Engineering)، و إسترداد الشبكات (Network Recovery)، و شبكات الإستشعار (Sensor Networks). شارك في تأليف المراجع المتخصصة في شبكة الأشياء الذكية (Smart Object Networks).

<sup>(5)</sup> الدكتور (Adam Dunkels): أحد علماء المعهد السويدي لعلوم الكمبيوتر، في مجال برمجة و تكنولوجيا الشبكات و الإتصالات، و شبكات المتحسسات اللاسلكية عبر الإنترنت، هو الذي أنشأ (Thingsquare): البرنامج الذي يرتبط الأشياء و المنتجات مع الهاتف الذكي. و هو مصمم نظام التشغيل مفتوح المصدر (Contiki). للمزيد من المعلومات على الرابط: [https://en.wikipedia.org/wiki/Adam\\_Dunkels](https://en.wikipedia.org/wiki/Adam_Dunkels)

المعلوماتية الذكية، إذ يتم إختصار الكثير من الحلقات الروتينية في إنجاز الأعمال، و تقديم الخدمات المختلفة لمواطنيها (Komninos, 2015)، (Paskaleva, 2014).

#### المدينة الرقمية ( Digital City ):

تشير المدينة الرقمية الى: المدينة التي تجمع البنية التحتية للاتصالات ذات النطاق العريض (Broad Band)، و البنية التحتية للحوسبة الموجهة المعتمدة على معايير الصناعة المفتوحة، و الخدمات المبتكرة لتلبية حاجات الحكومات و موظفيها، و مواطنيها، و الأعمال. هدفها أيجاد بيئة المعلوماتية، و التعاون، و التشغيل المتداخل، و تنمية خبرات السكان في أي مكان من المدينة، من خلال التقنيات الرقمية (Yovanof & Hazapis, 2009, P: 445- 463)، و تربط تلك الشبكات كلاً من: المنظمات، و المجموعات الاجتماعية، و مؤسسات المدينة (Anthropoulos & Fitsilis, 2010, p: 360-372).

#### المدينة الافتراضية (Virtual City):

تعتمد المدينة الافتراضية تطبيق وظائف المدينة في الفضاء الافتراضي (CyberSpace)، ويشمل مفهوم المدينة الذكية (Smart City) مفهوم المدينة الهجينة (Streitz, 2009)، الذي يتألف من الواقع المادي الملموس، و السكان الحقيقيين، و موازي للمدينة الافتراضية، لما يناظرها من الكيانات الواقعية و الناس.

أن تجمع الاتصالات و الشبكات في كل مكان (Ubiquitous)، يعزز البنية التحتية لتكنولوجيا المعلومات (IT) بالقابليات؛ مراكز البيانات و التشغيل المتبادل. و لا يزال المكان يمتلك تأثيراً كبيراً في التمثيل الافتراضي لعدد كبير من المدن.

#### المدينة كلية الوجود (موجودة في كل مكان) ( Ubiquitous City ):

تمثل المدينة كلية الوجود امتداداً للمدينة الرقمية، من حيث الوصلية (Accessibility) و البنية التحتية المنتشرة في كل مكان من المدينة (Anthropoulos & Fitsilis, 2010, p: 360-372)، إذ تجعل من الحوسبة و المعلوماتية متوفرة في كل العناصر الحضرية؛ الأبنية؛ البنية التحتية و الفضاءات المفتوحة (Lee et al, 2008, p: 148-169). هدفها أيجاد بيئة عمرانية، تتميز بالخدمات، في أي مكان، و في اي وقت (بشكل فوري real time)، و من خلال أية أجهزة معلوماتية متوفرة. بينما يتم إنشاء العناصر الحضرية في المدينة الافتراضية، من خلال التصور البصري في الفضاء الافتراضي، فإن المدينة كلية الوجود يتم إنشاؤها بواسطة رقائق الحاسوب (Computer Chips) و المتحسسات (Sensors) التي يتم دمجها و صهرها ضمن بنية عناصر البيئة الحضرية و تصبح جزءاً لا يتجزء منها.

#### مدينة المعلومات ( An Information City ):

تشير مدينة المعلومات ( I-City ) الى البيئات الرقمية التي تجمع المعلومات من المجتمعات المحلية، تقوم بتوزيعها على عامة المجتمع، عن طريق شبكات الانترنت المنتشرة في المدينة (Sproull & Patterson, 2004, p: 3-37)، (Widmayer, 1999, p: 40-46). في هذه المدينة، حيث العديد من الساكنين المعلوماتيين ، القادرين على العيش و العمل على شبكة الأنترنت. تعد المدينة المعلوماتية مركزاً حضرياً يدعم التجارة، الخدمات الاجتماعية و المدنية، التفاعلات الاجتماعية بين الناس و المؤسسات التجارية و الحكومية.

#### المدينة الذكية ( Intelligent City ):

إنبتق مفهوم المدينة الذكية من وجود العناصر المشتركة لكل من: مجتمع المعرفة، و المدينة الرقمية. توصف المدينة الذكية؛ بأنها المدينة التي تمتلك كل من البنية التحتية المعلوماتية (Infostructure) لتكنولوجيا المعلومات، و أحدث تقنيات تكنولوجيا الاتصالات (Telecommunications)، لتحويل نمط الحياة و العمل في إطار المنطقة، بطرق مبدعة و ذكية، بدلا من الطرق التقليدية - التدرجية (Malek, 2009). يمكن التمييز بين المدينة الرقمية و المدينة الذكية، إذ تمتلك (المدينة الذكية)

القدرة لدعم التعلم، و التطور التكنولوجي، و فعل الابتكار، و بهذا المعنى؛ فأن كل مدينة رقمية هي ليست بالضرورة مدينة ذكية، لكن كل مدينة ذكية تمتلك مكونات رقمية. إذ ان كل من المفهومين يختلف، من حيث الربط بين المدينة الواقعية و المدينة الافتراضية. تتضمن المدينة الرقمية كل وظائف المدينة التقليدية مثل؛ العمل، و السكن، و النقل، و الترفيه و البيئة. أما المدينة الذكية (Intelligent City)، فتتضمن وظائف كل من؛ البحث، و نقل التكنولوجيا، و تطوير الإنتاج، و الابتكار التكنولوجي (Komninos & Seferdzi, 2009).

### الأهداف العامة لمبادرات المدينة الذكية (Objectives of Smart City Initiatives):

تهدف مبادرات المدينة الذكية بشكل عام الى (Ojo, et al, 2014, p: 8):

- التقليل (الحد من) نسبة إنبعاث غاز ثاني أوكسيد الكربون في الجو (غازات الدفيئة).
- تحقيق الكفاءة في إستهلاك الطاقة (ترشيد أستهلاك الطاقة).
- الإستفادة من رفع مستوى تكنولوجيا المعلومات، و الإتصالات لتطوير الصناعات المتخصصة بالوسائط المتعددة (multimedia)، و المعرفة.
- تحقيق أفضل نوعية بيئة، بما يحقق نمط الحياة المناسبة للسكان.
- تطوير، و توسيع المناطق الخضراء داخل المدينة.
- تنمية، و تطوير البنى الإرتكازية المتقدمة (المتطورة state-of-the art) للمعلوماتية، و وضعها في متناول الجميع.
- تحقيق النمو الإقتصادي، و بما يوازي جودة نمط الحياة.
- تنمية المجتمعات المستدامة.
- ضمان الانسجام الإجتماعي بين المجموعات المختلفة للسكان.
- تطوير المدينة، بوصفها مختبراً حياً لتشجيع الإستدامة.

### المقومات العامة للمدينة الذكية:

تعد المدينة الذكية مفهوماً شمولياً، من حيث إستيعاب كل جوانب الحياة الإجتماعية، و الإقتصادية، و الثقافية. إذ تشجع المدينة الذكية الإبداع، و الابتكار المفتوح، و المشاركة، و التقييم المستمر، و التجديد عبر التفاعل بين المواطنين. تتطلب المدينة الذكية الدعم الفاعل لعموم المجتمع، ممثلاً بالحكومة المحلية، و المواطنين، و القطاع الخاص، و المنظمات، و الجامعات، و بالتالي التحليل الدقيق، و تحديد الرؤية، و الإستراتيجية، فضلاً عن توشي الدقة في تنفيذ خطة العمل، و تتمثل أهم مقومات النجاح الأساسية لبرامج المدينة الذكية، بكل من (Ojo, et al, 2014, p: 10):

#### 1. القيادة و الإرادة السياسية و المجتمعية:

تعد الحاجة المجتمعية، و الإيمان بضرورة التغيير، بشكل عام، المحرك الرئيس للمبادرات القائمة؛ للإرتقاء في ظروف المدينة في عصر المعلوماتية، و المعرفة وإصلاح الأوضاع الراهنة الصعبة، و التي يمكن ترجمتها الى إرادة سياسية، و بدعم من الحكومة و القيادة المحلية (كاريللو، 2011، ص: 36).

#### 2. الرؤية الإستراتيجية و اعتماد نهج حكومي متكامل و شامل:

يعتمد نجاح التحول على وضوح الرؤى الإستراتيجية، و الشمولية، و العمق (Nam and Pardo, 2011). فالمدن المتميزة تستهدف القليل من القطاعات، و في ذات الوقت تضع خططاً هادفة لكل قطاع، فضلاً عن السعي لتحقيق التوازن بين

المصالح، و الموارد المتاحة، و القدرة التنافسية على المستوى الإقليمي؛ فضلاً عن وضع نظام جودة التعليم العالي، و إيجاد نمط الحياة المناسب، من خلال توفير الخدمات (كاريللو، 2011، ص: 36).

### 3. الدعم المالي و الإستثمار:

يعد الدعم المالي و الإستثمار النوعي: حجر الزاوية، و أحد أهم مقومات نجاح مبادرة المدينة الذكية، إذ ينبغي تأمين التمويل المناسب قبل الشروع بتنفيذ إجراءات الخطة الإستراتيجية. و يمكن التسويق من جذب الإستثمارات الخارجية المطلوبة للتمويل، و يحصل الدعم المالي من قبل الموارد العامة و الخاصة، فضلاً عن تطبيق الخطط الضريبية المناسبة لجذب التمويل على المستوى الوطني و العالمي (السيد نصار، 2008).

### 4. تعزيز بناء الشراكات التعاونية مع الجهات المعنية:

يعد بناء الشراكات التعاونية أمراً أساسياً لنجاح مبادرة المدينة الذكية، تأخذ الشراكات أشكال المؤسسات التقنية، مراكز و معاهد بحثية، وأحات تكنولوجية و الجامعات و غيرها. و تشارك في تصميم و تنفيذ المشاريع، فضلاً عن إجراءات البحوث العلمية بغية التعاون، تبادل المعرفة، جذب و إستبقاء (توطين) العاملين في مجال المعرفة، إستدامة التنمية الإقتصادية و تسويق مفهوم المدينة الذكية (Engles, 2003).

### 5. عالمية المدينة و تعددية الأعراق:

تبنى المدن الذكية الناجحة على التنوع، و يفضل الموهوبون والمبدعون العيش في المدن التي تتصف بالتنوع، التسامح و الإنفتاح الفكري، مما يحفز تبادل الأفكار و التطبيقات المعلوماتية و يشجع على تدفق المعرفة. تدعم المدن الذكية وجهات النظر، الثقافات و الخبرات المختلفة لمواطنيها، بما يسهم و طرح الأفكار الجديدة التي تدعم الابتكار (Florida, 2002).

### 6. موقع المدينة على شبكة الإنترنت:

يؤدي الموقع المؤثر للمدينة على شبكة الإنترنت دوراً أساسياً في الإستجابة لحاجات المواطنين، من خلال توفير المعلومة، فضلاً عن تفاعل المجتمع، و تمثل نوعية الموقع تعبيراً عن الإبداع و سر جاذبية المدينة، و يتصف الموقع الناجح بكونه نافذة واحدة مبسطة و سهلة الوصول و الإستخدام، فضلاً عن تحديث المعلومات و تتميز بالجذب البصري، تلبية معايير المستخدم وتوفير خدمات الحكومة الإلكترونية، بما يسهل إنجاز أعمال و حاجات المواطن بكل سهولة و يسر، لتوفير الوقت، الجهد و المال (كاريللو، 2011، ص: 38).

### البيئة الحضرية الذكية:

أسهم التطور المتسارع في تكنولوجيا المعلومات و الإتصالات، بإحداث التغير الكبير في حياة الإنسان، تسخير البيئة، و توفير وسائل الراحة و الملاءمة و الأمن، فضلاً عن متطلبات الحياة العصرية (فريحات، 2003، ص: 1). تتألف البيئة من مكونين أساسيين: الإنسان، كل إمكانات البيئة، و الموجودات الحضرية الموضوعية. يتحدد سلوك الفرد من خلال تفاعله، و تأثيره في البيئة الحضرية (الكناني، 2005، ص: 9). يرى (Walters) بأن الأماكن الذكية هي تلك التي تجمع بين العالم المادي و العالم الافتراضي، من خلال إنتشار الوسائل المعلوماتية، الإتصالاتية، سويةً في ذات المكان، إذ تقدم التكنولوجيا أبعاداً جديدة في البيئة، من حيث تغير أنماط العمل، الحياة و الترفيه (Walters, 2011). عليه يتمحور العالم اليوم بأسره حول الشبكة المعلوماتية و الإتصالاتية و يتجه نحو تكوين علاقات حضرية جديدة، تعتمد أساساً على المعلومات و الإتصالات (العلوان، 2012، ص: 79). فالبيئة الحضرية الذكية، تتميز بقدرتها على إيجاد حالة التوافق بين البيئات الحضرية التقليدية و البنى الحضرية الذكية، فالبعد المادي لازال مؤثراً في المدينة الذكية، التي تمتلك القوة على تركيز الذكاء المكاني، الغني بوسائل

المعلوماتية، في بؤر جاذبة للموهوبين و المبدعين، فضلاً عن توفير بيانات التفاعل الإجتماعي ، وجهاً لوجه، بين مختلف أوساط مجتمع المدينة.

#### بنية المدينة الذكية:

بإعتماد محاكاة تكوين الكائن العضوي، يكمن ذكاء المدن الجديد في التكامل بين شبكات الإتصالات الرقمية (الأعصاب The nerves)؛ الذكاء المضمن و المنتشر - في كل مكان - (العقول Brains)؛ المتحسسات و البطاقات (sensors and tags) التي تمثل الأعضاء الحسية (the sensory organs) و البرامج (المعرفة و الكفاءة المعرفية - الإدراكية). تتكامل كل هذه المكونات مع الأنظمة الحضرية الأخرى، تتمحور أساساً حول الإنسان، بوصفه رابطاً لهذه العناصر ، مكونة شبكة واسعة من الإتصالات المباشرة للنظم المعلوماتية في الأبنية؛ الأجهزة المنزلية؛ الآلات الإنتاجية؛ محطات المعالجة؛ نظم النقل و شبكات تجهيز الكهرباء و الطاقة الأخرى؛ شبكات إمدادات تجهيز المياه؛ شبكات التخلص من النفايات (waste removal networks)؛ أنظمة الأمن؛ السلامة العامة و أنظمة ادارة كل النشاطات الإنسانية (Mitchell, 2007, p:1-5).

#### العناصر الحضرية للمدينة الذكية:

يمكن تحديد أهم العناصر الحضرية التي تميز المدينة الذكية، سواءاً كانت تقليدية إتخذت صفة الذكاء من خلال التضمين الرقمي الذكي، أو تلك التي ظهرت مع ظهور مفهوم الذكاء الإصطناعي و المدينة الذكية، بما يأتي:

مبنى العمليات المركزي:

بما يماثل الكيان الحي، فقد ظهرت البنى الجديدة في المدينة الذكية، كمبنى المعالج المركزي، الذي يقوم بالعمليات التنظيمية الأساسية بإستقبال البيانات و المعلومات، فضلاً عن إتخاذ القرار المناسب، بإعتماد الحواسيب المركزية ، إذ يمثل العقل المدبر في المدينة، يعمل على أساس نظام من الأنظمة (System of Systems)، عن طريق جمع معلومات كل أنظمة المدينة كنظام المرور، النقل، نظام الخدمات الصحية، شبكة المياه و شبكة الطاقة، رصد حركة سلوك المشاة و نظام الأمن... الخ، ليتم إتخاذ القرار من قبل النظام الرئيس بالتوافق مع المعلومات لبقية الأنظمة، و من ثم تحرير الإستجابة الفورية على وفق المعطيات الخاصة بكل مدينة. يؤشر مبنى العمليات المركزي، عنصر الذكاء الأهم في المدينة، الذي يمثل الدقة، التنظيم، و الترابط بين عموم العناصر الحضرية ، ذلك لإعتماده البيانات و المعلومات التي يتم الحصول عليها من البيئة الحضرية، بواسطة المتحسسات و المشغلات المضمنة في البيئة، المرتبطة عن طريق الأعصاب و الألياف البصرية. تشكل عناصر الربط ؛ البنية الأرتكازية الحضرية، أسفل مستوى سطح الأرض، عن طريق القنوات ،المخصصة لتمديد الكابلات، و الألياف البصرية' و العقد الذكية، تحت الشوارع و تحت الأبنية.

#### الأبنية الذكية (Smart Buildings):

يتم إعتماد المناهج التي تحد من إستهلاك الطاقة الناضبة، و تتراوح من الأنظمة الذكية الى التصميم الذكي. تطبق هذه المناهج في الأبنية، سيما مع سهولة إقتناء العديد من الأجهزة الكهربائية. تشكل أتمتة المباني أحد الطرق الذكية لخفض إستهلاك الطاقة، إذ تعمل التطبيقات الذكية على تقليل شدة إضاءة وسائل الإنارة ، و إطفاء و تشغيل أجهزة التكييف بشكل أوتوماتيكي، وفقاً لحاجة الشاغل، بما يتوافق مع البيئة الداخلية للمبنى. تشكل الوسائل المعلوماتية و العدادات الذكية قلب عملية إستشعار الطاقة المنزلية، إذ يتم التفاعل البيئي من خلال الإتصال بين الوسائل المعلوماتية، مثل متحسسات إستهلاك الطاقة، و العدادات الذكية لتقديم تقرير مفصل و دقيق لإستهلاك الطاقة الناضبة، فضلاً عن التنبؤ الدقيق بالطلب حول الطاقة (Hancke et al, 2013, p: 406).

### الشبكات الذكية (Smart Grids):

#### شبكة توزيع المياه (Water Distribution Grid):

يتضمن الرصد في شبكة توزيع المياه الذكية، مراقبة محتوى خزانات جمع المياه، فضلاً عن كشف التسرب و مراقبة نوعية الماء في نقاط محددة على طول نظام التوزيع، حيث يتم مراقبة خطوط انابيب توزيع المياه، من خلال نشر عدد كبير من أجهزة الاستشعار (sensors) حول خط الأنابيب، بغية توفير المراقبة المستمرة، الشكل (1). يتم تحليل البيانات و المعلومات التي يتم جمعها عن بعد. و تعمل أجهزة المعالجة عندما يتم الكشف عن الحالات غير الاعتيادية. تقوم الشبكة بأعمال الإصلاح الذاتي من خلال المشغلات (actuators). لا تتطلب قرارات المشغلات التدخل البشري، إذ يتم جمع البيانات و المعلومات عن طريق وسائل الاستشعار، و يتم تحليلها و تصنيفها، و من ثم إتخاذ القرار الذكي، من حيث الصيانة و معالجة الخلل بواسطة المشغلات (Metje, 2012, Pp: 315–320).

#### شبكة توزيع الطاقة الكهربائية (Electricity Distribution Grid):

يعد النظام ثنائي الاتجاه (bi-directional system)، أحد الحلول الأساسية لخطط تحسين شبكة التوزيع التقليدية، بمعنى إن مرور التيار سيكون من محطات التجهيز الى المستهلك و العكس صحيح. عليه يمكن زيادة كفاءة استخدام الطاقة ، بحيث يمكن للطاقة الكهربائية أن تتدفق (تتجه) راجعة من المستهلك الى المصدر، ليتم تخزينها لإستخدامها عند إنخفاض الطلب. تعرف هذه الأنظمة مجتمعةً بكل عناصرها و حلقاتها: بالشبكات أو الأنظمة الذكية (Smart Systems).

يتميز مفهوم التوليد المتوزع (Distributed Generation)، بوجود عدة نقاط توليد الطاقة الكهربائية ، عند مناطق إستهلاك الطاقة. يمكن هذا المنهج من الإستجابة الفورية، الأكثر ذكاءً، للطلب على الطاقة. تقدم الشبكات الذكية العديد من المزايا؛ مثل الرصد و المراقبة الذاتية (Gungor et al, 2010, Pp: 3557–3564). يعد التحسس (الإستشعار) أحد أهم التطبيقات المعلوماتية لمراقبة خطوط نقل الطاقة. إن الغرض الرئيس من هذه التدابير و استخدام هذه المتحسسات، لغرض الرصد الدقيق، بالتالي ضمان الأداء الأفضل و زيادة كفاءة الشبكة. (Moghe et al, 2012, Pp: 653–663).

#### شبكة النقل (Transportation Grid):

تستثمر أنظمة المرور الذكية، التقنية المعلوماتية، لجمع بيانات المرور، فضلاً عن تنظيم التنقل. تساعد البيانات مراكز إدارة المرور، بتحليل و إتخاذ القرارات بهدف إدارة شبكات الطرق، و تطبيق رسوم المرور في الطرق و تنظيم خدمات النقل العام. يمكن لهذه البيانات من تزويد المسافرين بمعلومات الرحلة. يقلل هذا النهج من هدر الوقت، ترشيد إستهلاك الوقود، تقليل إنبعاث غاز ثاني أكسيد الكربون، فضلاً عن تعزيز مستوى السلامة العامة (Schaefer et al, 2011, p: 1–3).

#### المواقف الذكية: المركبات و الدراجات الهوائية:

تشجع المدينة الذكية على استخدام الدراجات الهوائية، إنشاء مواقف السيارات و الدراجات الهوائية المبتكرة، ضمن اعتماد مبادئ التصميم الحضري: التضام؛ التقارب؛ الوصلية، فضلاً عن الحاجة لتوسيع المناطق الخضراء و المناطق الترفيهية في المدينة. تعمل المواقف الذكية على إيجاد الفضاءات الشاغرة في مواقف السيارات، و أقرب موقف للمركبات، إذ تستخدم الأنظمة الجديدة أنواع المتحسسات (فوق الصوتية ultrasonic) للكشف عن المواقف الشاغرة؛ المشغولة؛ المحجوزة، فضلاً عن مواقف سيارات ذوي الإحتياجات الخاصة (Kianpisheh, et al, 2012, p: 51–58).

#### المنصة تحت الأرض (Underground Platform):

تمثل المنصة تحت الأرض: بالفضاءات تحت الأرض، التي تمتلك القدرة على تخفيف حدة المشكلات الحضرية، عند إستغلالها، فضلاً عن توفير الفضاءات و المساحات لنمو و تطور المدن (Kaliampakos and Benardos, 2013, ).



(p:1). يمكن أن توفر الفضاءات تحت الأرض كل من (Ronka et al, 1998): المرافق الحكومية العامة، و وسائل الربط بين مترو الأنفاق؛ فضاءات المرور و وسائل النقل العام (mass transit)، و الطرق الرئيسية، و مواقف السيارات؛ ومرافق الصيانة الفنية، لمرافق جمع النفايات و الصرف الصحي و معالجة المياه؛ مرافق توليد الطاقة؛ مرافق خطوط الأنابيب و الكابلات؛ المرافق و المنشآت الصناعية؛ المخازن و المستودعات؛ معالجة الضوضاء و الغبار؛ مرافق الدفاع و الاتصالات السلكية و اللاسلكية. (Ronka et al. 1998, p: 39-49).

يهدف استخدام تحت الأرض: توفير الفضاءات فوق مستوى سطح الأرض، اللازمة لفعاليات الترفيه، النشاطات الاجتماعية و توسيع الفضاءات الخضراء (الحدايق و المتنزهات)؛ توفير فضاءات السكن؛ المحافظة على المساحات الحساسة من التدخل، كالمراكز التاريخية و المواقع الأثرية، فضلاً عن الحد من رحلات السفر الطويلة و إختصار الوقت و الحد من إستهلاك الطاقة (Kaliampakos and Benardos, 2013, p: 2).

يتم نقل البضائع، و المواد تحت مستوى سطح الأرض (Underground Freight Transportation – UFT)، سيما في المناطق ذات الكثافة السكانية العالية (Pielage, 2001, Pp: 762-767)، بإستخدام مركبات الشحن المؤتمتة غير المأهولة (unmanned automated cargo vehicles/cargo capsules)، التي تتحرك في أنفاق تحت الأرض، أو خطوط الأنابيب، الشكل (2) (Vance and Mills, 1994). تمثل مرافق الأنفاق البنى التحتية الأساسية للمدن، لعدد كبير من الخدمات الحضرية، مثل خطوط النقل، أنابيب التدفئة و التبريد، أنظمة تجهيز الماء و الكهرباء، فضلاً عن روابط كابلات نقل البيانات المعلوماتية و إرتباطاتها مع مركز البيانات و بقية عناصر المدينة.

#### الحالات الدراسية:

يهدف البحث: دراسة المدن الذكية على المستوى العالمي، سيما تلك التي يتم الترويج لها على إنها الآبقون الجديد للمدن الذكية الرائدة، عن طريق تطبيق نتائج الفكر المعلوماتي، لتحقيق الأهداف السامية بفعل إضفاء صفة المدن الذكية عليها، رغم إنها إبتدأت مدناً مستدامة، ثم ركبت الموجة الجديدة، بتشجيع و دعم من المؤسسات الرائدة في مجال التصميم، و التنفيذ، و تجهيز وسائل الذكاء الإصطناعي، و بناء مراكز العمليات التي تدير مرافق و شبكات، و خدمات المدينة، و ربطها سوية من خلال المعدات الصلبة (Hardware) و البرمجيات (Software)، و أجهزة التحسس التي يتم نشرها بالآلاف في كل عنصر من المدينة. تتضمن العينة البحثية المتمثلة بأهم مدينتين على المستوى العالمي، و هما مدينة (Songdo) في كوريا الجنوبية أولاً، و من ثم مدينة (مصدر) الواعدة في دولة الإمارات العربية المتحدة ثانياً، لإستخلاص أهم المقومات و التطبيقات الذكية، التي يمكن أن تطبق على المستوى العراقي، بعد عرض نتائج و إستنتاجات دراسة هذه المدن .

اتخذ البحث في استقاء المعلومات، عن المدن الذكية في هذه الدراسة، من المصادر العالمية المنشورة على صفحات الأنترنت و الأدبيات المختلفة، كالكتب، و البحوث المنشورة، فضلاً عن الصفحات الخاصة بهذه المدن على الشبكة العالمية، التي توفر المعلومات و البيانات بهدف الترويج لإمكانية إعتماها كأ نموذج أولي للمدن الذكية، و إعادة تسويقها و تنفيذها على المستوى العالمي. يعتمد البحث أسلوب الدراسة الوصفية التحليلية (Analytical Descriptive Method) للعينات البحثية، في تحقيق هدف البحث والتوصل إلى النتيجة النهائية، من خلال التطبيق الشمولي للمفردات و المؤشرات النظرية. يعتمد البحث وصف و تحليل أداء العناصر التي إقترنت مع مفهوم المدينة الذكية، فضلاً عن المؤشرات التي تؤكد كفاءة و ديمومة الأداء، بما يتفق مع مبادئ المدينة الذكية، لتحقيق النتائج المتوخاة من إعتماها كأهداف أساسية من وراء تنفيذ مبادرة المدينة الذكية ، بالتالي تحقيق فرضية البحث: يؤدي الفكر المعلوماتي متعدد التخصصات، دوراً جوهرياً في تحقيق مبادرة المدينة الذكية.



يمثل الجدول (1) أهم المؤشرات و المقومات التي سيتم تطبيقها على مدينة (سونغدو) في كوريا الجنوبية، و مدينة (مصدر) في الإمارات العربية المتحدة، للوصول الى تحديد أهم مقومات بناء المدينة الذكية في العراق.

الجدول (1): مؤشرات ، و مقومات مبادرة المدينة الذكية، التي سيتم تطبيقها على الحالات الدراسية.

1	مؤشرات مقومات موقع المدينة الذكية: من حيث طرق النقل، و توفر المياه، و طبيعة التربة
2	مؤشرات إستلهاج الموروث الحضاري : المحلي و العالمي، و التجارب التي أثبتت نجاحها
3	مؤشرات الإرادة و التشريعات الحكومية: بهدف جذب الشركات المعلوماتية، و شركات التمويل
4	مؤشرات المشاركة الدولية: تتمثل بأهم مؤسسات المعلوماتية، و التصميم، و التمويل
5	مؤشرات المنصة التحتية : إستغلال تحت الأرض لتوفير الخدمات المعلوماتية
6	مؤشرات الفضاءات العامة و المساحات الخضراء : لأغراض الترفيه و توفير الفضاءات الإجتماعية
7	مؤشرات ذكاء المدينة
8	مؤشرات الترابط و الإتصال و إحساس و إدراك المدينة

#### دراسة مدينة (Songdo) - كوريا الجنوبية:

لا تزال مبادرة مدينة (Songdo Smart City) الذكية بحاجة للتغذية الإسترجاعية و التعديل على وفق مستجدات التطور في وسائل ذكاء المدينة، رغم كونها الأنموذج الأول لمبادرة المدينة الذكية، التي يتم التأسيس لها من الصفر ( start from scratch)، على مستوى العالم، الشكل (3). لقد تم الحصول على البيانات و المعلومات من الصفحة الرسمية لمدينة (سونغدو) على الإنترنت : (www.songdo.com)، فضلاً عن البحوث و المقالات المنشورة في الإنترنت للتحقق من تطبيق المؤشرات ، و الخاصة بمقومات، و مؤشرات البيئة الحضرية للمدينة الذكية على مدينة (Songdo)، و على وفق ما يأتي:

- 1- **موقع المدينة:** تحقق مقوم الموقع في قيام المدينة الذكية، إذ تقع المدينة على شبكة الطرق الرئيسية، و القرب من مطار إنشيون الدولي (Incheon International Airport)، ترتبط المدينة بشبكة المترو و السكك الحديدية السريعة.
- 2- **الإستلهاج من التجارب العالمية:** تستلهم مدينة (سونغدو) من معظم التجارب و الرموز العالمية للمدن المشهورة، تسعى المدينة لتحقيق النجاح، بما يظاهي نجاحات تلك التجارب. تتمثل هذه التجارب بكل الحديقة المركزية لمدينة (نيويورك)، و (دار سيدني أوبرا) في مدينة (سيدني)، و شوارع مدينة (باريس) المشجرة.
- 3- **الإرادة ، و التشريعات الحكومية:** تحققت بتشريع القوانين و القرارات، التي أقدمت عليها حكومة كوريا الجنوبية بهدف جذب الشركات العالمية، لإكتساب الخبرات و إستدامة ذكاء المدينة. من أهمها تخفيض ضريبة الدخل للأفراد و الشركات بنسبة (17%)، فضلاً عن حق تملك الأجانب للأراضي الكورية.
- 4- **المشاركة الدولية:** تحققت من خلال التسهيلات التي قدمتها الحكومة الكورية، للمؤسسات و الشركات الدولية المشاركة في المشروع، المتمثلة في (Gale International)، كشركة منفذة رئيسية، (Kohen Pederson Fox) كمصمم معماري، (POSCO) كمشارك محلي، (Cisco) في مجال تكنولوجيا المعلومات و الاتصالات، و (U Life Songdo)

في مجال تأسيس مركز عمليات المدينة، مما ساعد في تعزيز ثقة المجتمع، من خلال مشاركة الشركات العالمية الرائدة بتقديم أحدث الأفكار و التكنولوجيا.

**5- الفضاءات تحت الأرض:** تستخدم كأماكن لوقوف السيارات في المستوى تحت الأرض لعموم الأبنية، فضلاً عن إمداد خدمات جمع النفايات بطريقة الشفط الهوائي (Pneumatic system)، لتساعد على توفير الفضاءات الإضافية فوق مستوى سطح الأرض على شكل مساحات خضراء و الحد من حركة مركبات جمع النفايات، و بالتالي الحد من انبعاثات غاز ثاني أكسيد الكربون و توفير بيئة صحية تدعم التفاعل الاجتماعي.

**6- توفير المناطق الترفيهية، و المساحات الخضراء:** تتمثل في الحديقة المركزية (Central Park)، التي تمثل قلب المدينة النابض بالحياة، تتميز بتعدد الأنشطة، كبيئة إنسانية تشجع على التفاعل الاجتماعي، تبادل الأفكار و إختلاط الثقافات المحلية و العالمية . تشكل المساحات الخضراء، بما فيها ملعب الغولف و المساحات المنتشرة في عموم المدينة، نسبة (40%) من مساحة المشروع، تماشياً مع مؤشرات المدينة الذكية.

**7- ذكاء المدينة:** تحقق من خلال مركز العمليات، العقد و المتحسسات الذكية، التي تنتشر في كل جزء أو عنصر من المدينة. يمثل مركز العمليات (الدماغ) و عقل المدينة المفكر لإرتباطه بالأقسام القائمة على إدارة المدينة، يشتمل على كل البيانات و المعلومات المتعلقة بالمدينة و مواطنيها. بارتباط مركز العمليات مع العناصر الحضرية، تتمكن المدينة من إدراك البيئة الحضرية، فضلاً عن الاستجابة الفورية لكل حدث ممكن، بإحداث التغييرات المطلوبة على وفق البرامج المعدة سلفاً.

**8- الترابط و الإتصال:** تم ربط كل عناصر المدينة بشبكة من الألياف البصرية، و الكابلات الممتدة تحت الشوارع و فضاءات المدينة، لتتجه نحو مركز عمليات المدينة الرئيس، الذي يعمل على مراقبة حركة المرور و أنشطة المدينة، لتلافي حدوث أية مخاطر يمكن أن تهدد حياة السكان ، فضلاً عن إمكانية التحكم و السيطرة على الأنظمة الذكية، عن بعد من قبل السكان، لتوفير البيئات التي تتلاءم و تطلعاتهم.

يتضح مما سبق بحثه و التحقق منه تطبيقياً، إن مدينة (سونغدو)، تعد أنموذج للمدينة الذكية على المستوى العالمي ، و هي بطبيعة الحال تحتاج للتجديد المستمر، و التغذية الإستراتيجية، بعد الإشغال، من قبل السكان و الباحثين في مجال المدينة الذكية، بوصفها توجهاً لمفهوم جديد في مجال التصميم الحضري، و يمكن للمدن الأخرى إقتفاء أثرها، مع الإحتفاظ بثقافة المجتمع و موروته الحضاري، بل و توظيف تطبيقات المدينة الذكية بما ينسجم و تقاليد المجتمع المحلي و التوجه سويةً نحو العالمية، و الإسهام في ردف هذا التوجه بأفكار و إبتكارات جديدة، فالمدينة الذكية لا تتوقف عن حد معين، إذ تعني إستدامة الإبتكار و التجديد المستمر.

نتيجة إختبار فرضية البحث: يتضح من تطبيق مؤشرات الإطار النظري، بأن مدينة (سونغدو) قد حققت فرضية البحث، المتعلقة بالدور الكبير لفكر المعلوماتية، الذي يؤدي الى تحقيق المدينة الذكية، و المتمثل بالمؤسسات العالمية المساهمة، فضلاً عن الباحثين في مؤسسات البحث العلمي.

**دراسة مدينة (مصدر) - دولة الإمارات العربية المتحدة:**

تشكل دراسة مبادرة مدينة (مصدر) الذكية، الشكل (4)، أهمية كبيرة، و ذلك لقربها من العراق ، فضلاً عن التشابه الكبير مع البيئة العراقية، و مصادر التمويل، و التقارب على مستوى القيم و العادات. لقد شرعت حكومة أبوظبي بإعداد متطلبات إنشاء المدينة، كمدينة خضراء مستدامة خالية من انبعاثات غاز ثاني أكسيد الكربون، فضلاً عن توفير سبل جذب الشركات الرائدة

في مجال تكنولوجيا الطاقة النظيفة. تميزت مدينة (مصدر)، بتحقيق مجموعة من المقومات، التي تضعها في تصنيف المدن الذكية، و هي كلاً مما يأتي :

1. **موقع المدينة:** يتحقق مقوم الموقع، بكون المدينة تقع على شبكة الطرق الرئيسية، و القرب من (مطار أبو ظبي)، و بما يحقق الوصلية العالية، سيما و إن المدينة تشكل حلقة الوصل المحورية لأسواق الشرق الأوسط و آسيا.

2. **الإستلهاام من التجارب المحلية:** إعتد المصمم (فoster و مشاركوه Foster and Partners): إستلهاام مباديء المدينة العربية التقليدية التي تتسم بالصروح، و الفضاء الإجتماعي المركزي، فضلاً عن المساحات الخضراء. إستلهاام التصميم من المدن العربية: قلعة مدينة (حلب) في سوريا؛ و مدينة (فاس) في المغرب؛ و الأبراج السكنية لمدينة (شيبام) في اليمن. أكد (نورمان فوستر): بأن هذه المستوطنات، تتسم بالإستدامة، و الإكتفاء الذاتي، من خلال توظيف الرياح العالية لأغراض التبريد، إذ تحتوي على العناصر الحضرية المرتفعة (أبراج الرياح)، لسحب الهواء الى المستويات الدنيا.

3. **الإرادة و التشريعات الحكومية:** تقدم مدينة (مصدر) العديد من المزايا، بهدف جذب الشركات العالمية للإستثمار في مبادرة المدينة الذكية، فضلاً عن الإشتراك في وضع المخططات و التصاميم، و من ثم عمليات التنفيذ. لقد وضعت دولة الإمارات العربية المتحدة / إمارة أبو ظبي، مجموعة من التشريعات التي تسمح للأجانب حق التملك الكامل للأراضي الإماراتية، و إعفاء الشركات و الأفراد من الضرائب، و القيود، و الرسوم الجمركية بالكامل ، فضلاً عن توفير بيئة أعمال مريحة، و تقديم التسهيلات في الحصول على التأشيرات، و توفير الأطر القانونية لحماية الملكية الفكرية.

4. **المشاركة الدولية:** تهدف مبادرة مدينة مصدر، أساساً في إيجاد قطاع إقتصادي جديد في (أبوظبي) يركز على مصادر الطاقة النظيفة و تطويرها، عن طريق جذب الشركات العالمية للإستثمار ، و من خلال تخصيص الأموال لصندوق دعم التكنولوجيا النظيفة. لقد تم جذب الشركات العالمية العاملة في مجال الطاقة المتجددة و التكنولوجيا النظيفة، فضلاً عن المؤسسات المصرفية الممولة لمشاريع الطاقة الشمسية و طاقة الرياح، و الشركات الرائدة في مجال الإلكترونيات و الهندسة. تتمثل هذه الشركات، فضلاً عن الشركة المصممة للمشروع (نورمان فوستر و مشاركوه)، فهناك العديد من الشركات العالمية، منها؛ (Consensus Business Group) و (Credit Suisse) و (Siemens AG).

5. **المساحات الخضراء و المناطق الترفيهية:** توفر المناطق الخضراء البيئات الترفيهية لسكان مدينة (مصدر)، فضلاً عما تمثله من مناطق التفاعل الإجتماعي عند مناطق التجمع الحضرية العامة و الفضاءات شبه العامة. تم توقيع المناطق و المتنزهات الخضراء بإمتداد حافة المدينة الجنوبية الشرقية حتى حافتها الشمالية الغربية، و تمثل المتنفس الرئيس للمدينة، و حواجز لعزل المدينة عن البيئة الصحراوية المحيطة، فضلاً عن كونها تشكل حدوداً خارجية، لمنع تمدد المدينة خارج حدودها بشكل غير مخطط.

6. **إستغلال الفضاء تحت الأرض:** تتسم مدينة (مصدر) بميزة فريدة من نوعها، من خلال رفع مستوى عموم المدينة سبعة أمتار فوق مستوى سطح الأرض الطبيعية، إذ تستغل الطبقة التحتية لتوفير فضاءات خدمات، و شبكات الاتصالات، و أنابيب المياه، و شبكات الصرف الصحي، و توفير مساحات الطرق المغطاة لسيارات النقل الشخصي و محطات نقل الركاب، و بدأ يتم توفير مساحات إضافية فوق مستوى سطح الأرض، تستغل كمناطق خضراء، و مساحات للأبنية الإضافية، كطريقة ذكية لتوفير تلك المساحات فوق مستوى سطح الأرض.

7. **الترابط و الإتصال:** يتحقق الترابط و الإتصال في مدينة (مصدر)، من خلال التقارب، فضلاً عن الربط بالشبكات التي تمتد خلال المنصة التحتية. توفر المسالك لمرور الأعصاب، لتربط كل أجزاء المدينة و تقرب المسافات، فضلاً عن وجود أنواع وسائل النقل، من سيارات النقل الشخصي، الى السكك الحديدية، ثم نظام مترو الأنفاق. ترتبط المدينة من خلال شوارع

المشاة المسقفة، مما يوفر بيئة مقاربة، و متصلة تشجع على المشي، و الحد من إستخدام السيارات، و بالتالي الحد من إنبعاث غاز ثاني أكسيد الكاربون، و الحفاظ على نظافة البيئة.

**8. ذكاء المدينة:** يتحقق ذكاء مدينة (مصدر)، من خلال إستخدام الوسائل و التقنيات المتطورة. تستخدم الشبكات الذكية، و العدادات، و المتحسسات في عموم مناطق المدينة، و تتراوح من تعيين مناطق تسرب و أعطال شبكات المياه، حتى توجيه سيارات النقل الشخصي بدون سائق بواسطة الكمبيوتر، فضلاً عن العقد الذكية في نظام جمع النفايات بطريقة الشفط بالهواء المضغوط. تقوم أنظمة جمع المياه تحت الأرض بجمع المياه الفائضة عن عملية السقي، ليتم إستخدامها مرة أخرى. لقد تم نصب الأجهزة الذكية في بنى المدينة لغرض الإستخدام الكفوء للطاقة، إذ تستخدم هذه الأجهزة القليل من الطاقة و يتم ربطها مع نظام إدارة طاقة البيوت لمراقبة إستهلاك الطاقة و ضبط الأجهزة المنزلية تبعاً لذلك.

يتضح مما سبق طرحه، بأن مدينة (مصدر) المقترحة، و التي قد تم تنفيذ بعض من أجزائها ، تحقق مؤشرات المدينة الذكية، بحسب المعطيات المذكورة آنفاً. عليه تحقق مدينة (مصدر) فرضية البحث.

#### مقومات المدينة الذكية في العراق:

خلص البحث لمقومات آفاق مستقبل المدينة الذكية، الواعدة لتجاوز حالات القصور التي تعاني منها معظم المدن العراقية، على مستوى الإدارة و الخدمات، و مواكبة أحدث التطورات العلمية في تكنولوجيا المعلومات، و الإتصالات، و نتائجها الحضرية: ظهور مفهوم المدينة الذكية.

لم يشهد العراق تجربة المدينة الذكية، و لكنه يمتلك من المقومات الأساسية لقيامها، سيما و إنه يمر بظروف تحتم إعتداد أسس و مبادئ المدينة الذكية، بوصفها توجهاً صاعداً يوفر الحلول المبتكرة للمشكلات الحضرية المعقدة، التي يصعب معالجتها بالطرق التقليدية، فضلاً عن رسم خارطة الطريق للنهوض بالواقع و تحديد المراحل الزمنية لبلوغ الهدف. تتمثل بمقومات الموقع: إذ يتميز العراق، و مدنه بالموقع المتميز الذي يربط البلدان الإقليمية، و يشكل حلقة الوصل لشبكة المواصلات الرئيسية بين آسيا، و أوروبا، و الشرق الأوسط، فضلاً عن إمتلاكه نهري دجلة و الفرات، و المسطحات المائية، و البحيرات التي ترتبط بالنهرين، و التربة الخصبة لوادي الرافدين، و الموارد النفطية، و المعادن، و يتميز على المستوى العالمي بالمواقع الأثرية، و التاريخية، و الدينية. أما مناخ العراق فيتميز بكونه مشمس على الأغلب، و هذا ما يدعم إستغلال الطاقة الشمسية لتوليد الطاقة الكهربائية، سيما و إن العراق يمتلك مصانع إنتاج الواح الطاقة الشمسية، فضلاً عن وجود البحوث المستمرة، لإنتاج هذه الألواح بمواصفات عالية تتلائم و البيئة العراقية. يمثل أتمتة الأبنية العامة، و السكنية، و التجارية، من أهم مؤشرات المدينة الذكية، عليه يشكل أهمية كبيرة في إيجاد حلول للمشكلات المعاصرة التي تعاني منها المدينة العراقية، بهدف مراقبة كل عنصر من عناصر البيئة الحضرية، بالتالي تحقيق الأمن، و منع حصول المشكلات الحضرية قبل وقوعها. و كذا الحال بالنسبة لإستخدام نظام جمع النفايات الذكي تحت و فوق الأرض.

إن العراق بحاجة ماسة لتنفيذ المدينة الذكية، سواء تلك التي تنشأ من الأساس (الصفري) (start from scratch)، أو التدرجية، بأستخدام التطبيقات الذكية، على المدن التقليدية القائمة، ذلك لأنها تقدم حلولاً للمشكلات الحضرية المستعصية، التي يشهدها العراق في الوقت الراهن، و تلك التي يتوقع حصولها في المستقبل.

#### الإستنتاجات: خلص البحث الى مجموعة من الإستنتاجات، من أهمها ما يأتي:

**1.** تحاكي المدينة الذكية، الكائن الحي بما يمتلكه من قدرة على التفكير و التحسس، ممثلاً بالعقل و الذكاء الإصطناعي في المدينة الذكية؛ و الأعصاب (شبكات الإتصالات الرقمية)؛ الأعضاء الحسية (المتحسسات و العقد و البطاقات الذكية)، فضلاً عن المعرفة و الكفاءة ممثلة بالبرمجيات، المعلومات و البيانات التي يتم تخزينها في الأنظمة الذكية. ترتبط جميع هذه

العناصر بوساطة الإنسان، بالأنظمة الحضرية القائمة في جميع مرافق، و عناصر، و بنى المدينة؛ الأبنية؛ و الأجهزة المنزلية ؛ و الشبكات؛ و خدمات المدينة.

2. يمثل مفهوم المدينة الذكية أحدث نتاجات التصميم الحضري، إذ يمثل خلاصة الذكاء و الفكر الإنساني في التعامل مع البيئة الحضرية، على مر التاريخ بما يحمله من رموز و ملامح عمرانية تعكس تطور المجتمع الإنساني، فضلاً عن الأيديولوجيا التي يؤمن بها، و الأنظمة التي تستجيب للحاجات، الإنسانية، الاجتماعية، السياسية و الاقتصادية ، تنعكس هذه القيم على فضاءات و شبكات الطرق و نمط النسيج الحضري.

3. تتميز المدينة الذكية بقدرتها على التشغيل المتبادل، لكل المرافق الحكومية المرتبطة بالشبكة ، حيث يمكن الإتصال من أي مكان ، و في أي وقت لمعالجة العمليات على المستوى الداخلي؛ الخارجي للحكومة و المواطنين، إذ تسخر المدينة الذكية البنية التحتية المعلوماتية، لتحويل الحياة و العمل بطرق مبدعة و ذكية، معتمدة في ذلك إستثمار مكوناتها الرقمية. توصف المدينة الذكية بأنها: أفضل الحلول التي يقدمها صناع القرار و المشاركة الجماهيرية للحد من البيروقراطيات في إدارة المدينة.

4. أسهم الفكر المعلوماتي ، ممثلاً بالمؤسسات البحثية العالمية و الشركات من مختلف الجنسيات، الرائدة في مجال المعلوماتية، بوصفها فكرياً أساسياً، و نتائجها المادية الملموسة؛ بتحقيق و بلوغ هدف المدينة الذكية، من خلال اعتماد مباديء؛ الشراكة ؛ و التعددية؛ سواء في التصميم ، أو التنفيذ ، الإستغلال، و من ثم إستدامة الذكاء نهجاً و فكرياً.

5. لقيام المدينة الذكية العراقية، ينبغي أولاً؛ تشريع القوانين و التسهيلات الحكومية، فضلاً عن توفير الجانب الأمني، إذ تعتمد بؤر الابتكار، أو البيئات الذكية على توفر مجموعة من المقومات، في مقدمتها البيانات الآمنة، و الخالية من الجريمة، و تعتمد مبدأ التسامح و التعددية الإثنية و العرقية، و التنوع على مختلف المستويات: البيئة، و النقل ، و الطاقة، و الإقتصاد، فضلاً عن التنوع على مستوى الجنسيات المشاركة في التخطيط، و التصميم، و تنفيذ مبادرة المدينة الذكية.

6. يمتلك العراق القدرات، و الموارد البشرية الخلاقة، و الجامعات و المراكز البحثية، التي تؤهله للقيام بمبادرة المدينة الذكية، فضلاً عن مقومات الموقع، إذ تقع أغلب المدن العراقية على الطرق الرئيسية، و على نهري دجلة و الفرات. توفر الأنهار المياه لإنشاء البحيرات، و القنوات المائية، التي تقلل من أحمال درجات الحرارة، بالتالي تقليل إستهلاك الطاقة.

7. تعد مبادرة المدينة الذكية، ضرورة ملحة بالنسبة للعراق، لما توفره من قدرات إستثنائية، في وضع الحلول للمشكلات الحضرية المتفاقمة، فضلاً عن الحلول غير المألوفة، و الابتكارات، و لا سيما في الجانب الأمني، من خلال نتاجات المعلوماتية.

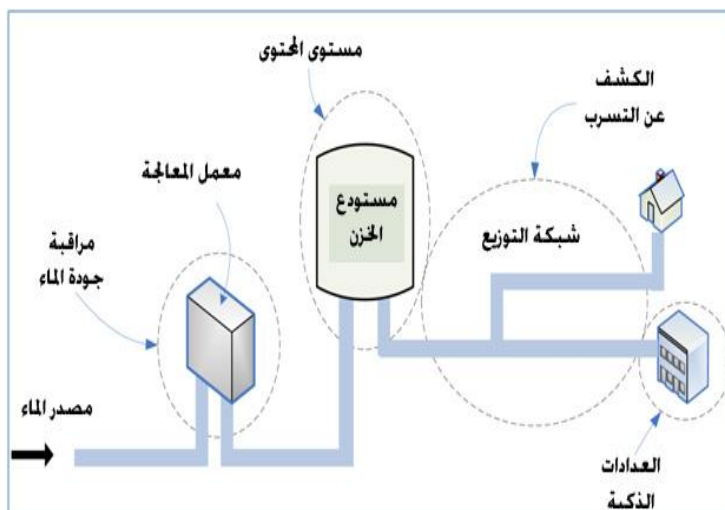
الأشكال التوضيحية:

الشكل (1):

شبكة توزيع الماء الذكية:

تتميز مراحل شبكات التوزيع بالأتمتة و التحكم الذاتي، فضلاً عن الصيانة و المعالجة الذاتية. المصدر:

(Hancke et al, 2013, p: 403)







الشكل (2): يوضح إستغلال تحت الأرض، إذ يتم تمرير الخدمات و نقل البضائع بطرق نقل مختلفة، تتراوح بين القطارات الى إستخدام الأنابيب و ضغط الهواء. توفر هذه الإجراءات المساحات لإنشاء المرافق الترفيهية فوق مستوى سطح الأرض. المصدر:

[http://www.cargocap.de/files/cargocap\\_download/CargoCap\\_Kreuzung\\_2011-01.jpg](http://www.cargocap.de/files/cargocap_download/CargoCap_Kreuzung_2011-01.jpg)



الشكل (3): مدينة (سونغدو)، كوريا الجنوبية: منظور جوي من الجهة الشمالية، يوضح كافة أجزاء المدينة، التي تقدم فكرة جديدة في تصميم المدن الذكية، إذ تعد الأنموذج الأول للمدينة الذكية، على المستوى العالمي.

المصدر : <http://inhabitat.com/songdo-ibd-south-koreas-new-eco-city/songdo-ecocity-3>





الشكل (4) مدينة (مصدر)، الإمارات العربية المتحدة: منظور جوي لمدينة مصدر المقترح يوضح شكل المدينة العام و يتضح مراعاة البيئة و إحاطة المدينة بالحزام الأخضر و الجدران حسب المبادئ التصميمية للمدينة العربية التقليدية.  
المصدر: <http://www.wired.co.uk/magazine/archive/2013/12/features/reality-hits-masdar>

#### المصادر العربية:

- السيد نصار، وليد محمد عبد الوهاب، (تكامل المشروعات الحضرية الذكية مع البيئة العمرانية المحيطة)، أطروحة دكتوراه مقدمة الى قسم التخطيط العمراني / كلية الهندسة في جامعة عين شمس، القاهرة، مصر، 2008.
- عامر شاكر خضير، (أثر العولمة في تغير إدراك الصورة الذهنية للفضاءات الحضرية: دراسة لشوارع تجارية منتخبة من مدينة بغداد)، أطروحة دكتوراه مقدمة الى المعهد العالي للتخطيط الحضري و الأقليمي، جامعة بغداد، 2005.
- العلوان، هدى عبد الصاحب و بلسم علوان شلال، (دور الاتصال و التواصل في مدن التوابع المعلوماتية)، بحث منشور في مجلة الهندسة العدد (4) لسنة 2012.
- فريحات، حيدر، (تخطيط المدينة الإلكترونية: دراسة تحليلية)، ورقة عمل مقدمة الى ندوة "الحكومة الإلكترونية: الواقع و التحديات"، التي عقدها المعهد العربي لإنماء المدن، بالتعاون مع بلدية مسقط / عمان، 2003.
- كاريللو، فرانسيسكو جافير، (مدن المعرفة: المداخل، الخبرات و الرؤى)، ترجمة خالد علي يوسف، مجلة عالم المعرفة، العدد (381) لسنة 2011.
- محسن جبار عودة، (المشهد الحضري لمركز المدينة و التوجهات الفكرية المعاصرة)، رسالة ماجستير مقدمة الى قسم الهندسة المعمارية في الجامعة التكنولوجية، 2007.

#### المصادر الأجنبية:

- Anthopoulos, L., & Fitsilis, P. "From online to ubiquitous cities: The technical transformation of virtual communities". In A. B. Sideridis & C. Z. Patrikakis (Eds.), *Next*





*Generation Society: Technological and Legal Issues (Proceedings of the Third International Conference, e- Democracy, Athens, Greece, Sep 23–25, 2009)*, Vol. 26. Berlin, Germany: Springer. 2010.

<http://www.springerlink.com/content/g644776482968k36/fulltext.pdf>.

- Bloomberg, M. R. "The Best and the Brightest – New York City's bid to attract science talent could serve as a model for other cities". *Scientific American*, 305(3), 11. (2011).
- Caragliu, A., Del Bo, C., & Nijkamp, P. "Smart cities in Europe". In *Proceedings of the 3rd Central European Conference in Regional Science* (Košice, Slovak Republic, Oct 7–9). (2009). [http://www.cers.tuke.sk/cers2009/PDF/01\\_03\\_Nijkamp.pdf](http://www.cers.tuke.sk/cers2009/PDF/01_03_Nijkamp.pdf).
- Durmisevic, S., "The future of the underground space". *Cities*, 16(4), 1999.
- Engels, R. "The Berlin Strategy: Develop our strengths – manage our weaknesses", *Presentation to the Value of Cities International Conference, Deputy Managing Director, IHK Berlin*. (2003).
- Florida, R.L. "The Rise of the Creative Class: and How it's Transforming Work, Leisure, Community and Everyday Life". New York, 2002.
- Glaeser, E. L., & Saiz, A. "The Rise of the Skilled City". *Social Science Research*. (No. No 25). (2003) Cambridge, Massachusetts.
- Gungor, V.; Lu, B.; Hancke, G.P. "Opportunities and Challenges of Wireless Sensor Networks in Smart Grid". *IEEE Trans. Ind. Electr.* 57, **2010**.
- Hancke, Gerhard P. and Silva, Bruno de Carvalho. "The Role of Advanced Sensing in Smart Cities", *Journal of Sensors*, Vol. (13), 2013.
- Hartley, J. "Innovation in governance and public services: Past and present". *Public Money & Management*, 25(1) (2005).
- Kaliampakos, Dimitrios, and Benardos, Andreas, "Underground Solutions for Urban Waste Management: Status and Perspectives", *National Technical University of Athens Lab. of Mining and Environmental Technology, the International Solid Waste Association*. 2013.
- Kianpisheh, Amin; Mustaffa, Norlia; Limtrairut, Pakapan and Keikhosrokiani, Pantea. "Smart Parking System (SPS) Architecture Using Ultrasonic Detector", *International Journal of Software Engineering and Its Applications*, Vol. 6, No. 3, July, 2012. [http://www.sersc.org/journals/IJSEIA/vol6\\_no3\\_2012/7.pdf](http://www.sersc.org/journals/IJSEIA/vol6_no3_2012/7.pdf)
- Komninou, Nicos. "The Age of Intelligent Cities", Routledge, Taylor and Francis Group, New York, 2015.



- Lee, S., Yigitcanlar, T., Han, J., & Leem, Y. "Ubiquitous urban infrastructure: Infrastructure planning and development in Korea". *Innovation: Management, Policy & Practice*, 10(2-3), (2008).
- Malek, J. A. "Informative global community development index of informative smart city". In *Proceedings of the 8th WSEAS International Conference on Education and Educational Technology* (Genova, Italy, Oct 17-19). 2009.
- Metje, N.; Chapman, D.; Walton, R.; Sadeghioon, A.; Ward, M. :Real time condition of buried water pipes". *Tunneling Undergr. Space Technol.* 28, **2012**.
- Mitchell, William J., "Intelligent cities". *UOC Papers. Iss. 5*.(2007). <http://www.uoc.edu/uocpapers/5/dt/eng/mitchell.pdf>.
- Moghe, R.; Lambert, F.; Divan, D. "A novel low-cost smart current sensor for utility conductors". *IEEE Trans. Smart Grid*, 3, **2012**.
- Nam, Taewoo and Pardo, Teresa A., "Smart City as Urban Innovation Focusing on Management, Policy, and Context", 2011.
- Ojo, Adegboyega; Curry, Edward and Janowski, Tomasz. "Designing Smart City Initiative", *Twenty Second European Conference on Information Systems*, Tel Aviv 2014.
- Paskaleva, Krassimira Antonova, "The Smart City: A nexus for open Innovation?" *Journal of Intelligent Buildings International* Vol. 3 (2011), Taylor & Francis Group.
- Paskaleva, Krassimira, "E- Governance as an enabler of the Smart City", Routledge, Taylor and Francis, London. 2014.
- Pielage, J-B., "Underground Freight Transportation. A new development for automated freight transportation systems in the Netherlands". *Proc. Intelligent Transportation Systems* 2001.
- Ronka, K., Ritola, J., Rauhala, K., "Underground Space in Land-Use Planning". *Tunnelling and Underground Space Technology*, Vol. 13, No 1, 1998.
- Sproull, L., & Patterson, J. F. "Making information cities livable". *Communications of the ACM*, 47(2), (2004).
- Streitz, N. "Ambient intelligence landscapes for realizing the cities of the future: Introduction and overview". In *Proceedings of the 3rd European Conference on Ambient Intelligence* (Salzburg, Austria, Nov 18-21). (2009). <http://www.smart-future.net/14.html>.
- Vance, L. Mills, M., "Tube Freight Transportation". *Public roads*, Vol. 58, No. 2. 1994.



- Vasseur, J.-P., & Dunkels, A. "Smart Cities and Urban Networks". In *Interconnecting Smart Objects with IP – The Next Internet*. Morgan Kaufmann. Elsevier Inc, USA. (2010).
- Walters, David, "Smart Cities: Smart Places, Smart Democracy: Form based codes, Electronic governance and the role of Place in making Smart Cities", 2011.
- Widmayer, P. "Building digital metropolis: Chicago's future networks. IT Professional", 1(4), (1999).
- Yovanof, G. S., & Hazapis, G. N. "An architectural framework and enabling wireless technologies for digital cities & intelligent urban environments". *Wireless Personal Communications*, 49(3), (2009).  
<http://www.springerlink.com/content/g1v63025217mt8x0/>.

• مصادر الإنترنت:

- Komninos, N., & Sefertzi, E. "Intelligent cities: R&D off shoring, Web 2.0 product development and globalization of innovation systems". Paper presented at the Second Knowledge Cities Summit. 2009. Available at <http://www.urenio.org/wpcontent/uploads/2008/11/Intelligent-Cities-Shenzhen-2009-https://ar.wikipedia.org>.
- Schaefer, Steffen; Harrison, Colin; Lamba, Naveen; Srikanthm Vishwanath, "Smarter Cities Series: Understanding the IBM Approach to Traffic Management". 2011.  
<http://www.redbooks.ibm.com/redpapers/pdfs/redp4737.pdf>.

## دراسة تحسين ذوبانية الالياف السليلوزية

الدكتور المهندس عاصم حسن محمد حسن

مدرس

معهد تكنولوجيا/ الجامعة التقنية الوسطى

### الخلاصة

في هذه الدراسة تركّز عملنا على تحسين زيادة ذوبانية الياف السليلوز في محلول هيدروكسيد الصوديوم بتركيز تتراوح بين ( 4- 12 % ) هذا من ناحية ومن ناحية اخرى في محلول هيدروكسيد الصوديوم واليوريا بتركيز ( 6% NaOH + 4% يوريا ) تحت درجات حرارة منخفضة ( -15 ، - 20 ) درجة مئوية . معتمدين بالدرجة الاساس في هذا البحث على مبدأ تقليل درجة البلمرة (Degree of polymerization) لزغب القطن ( Cotton Linter ) والذي يمثل في تجاربنا ورق الترشيع رقم 1- ( Whatman filter paper, Grade 1 ) ، بعض النماذج سوف نستخدم فيها معالجة اولية ( Pretreatment ) لزغب القطن بطريقة كيميائية تحاكي طريقة تحليل المواد السليلوزية التي تستخدمها الفطريات التي تنمو على الاشجار ، هذه الطريقة تتضمن استخدام مواد كيميائية تشمل بيروكسيد الهيدروجين ( $H_2O_2$ ) حامض الاوكسالك ( $C_2H_2O_4$ ) و كبريتات الحديدوزالثائية ( $FeSO_4$ ) ليكون لنا تفاعل يعرف بكاشف فينتون ( Fenton's reagent ) ينتج من هذا التفاعل جذور حرة تساعد على تحليل الياف السليلوز . وكانت النتائج كما يلي : بالنسبة الى ذوبانية الياف السليلوز في محلول هيدروكسيد الصوديوم بتركيز هو 8% كانت افضل نسبة اذابة تصل 42% للسليلوز المعالج في كاشف فينتون اما بالنسبة للسليلوز الغير معالج فكانت افضل نسبة ذوبان تصل الى 28% و كانت افضل درجة حرارة لعملية اذابة الياف السليلوز المعالج والغير معالج هي بحدود - 20 درجة مئوية . أما بالنسبة الى ذوبانية الياف السليلوز في محلول هيدروكسيد الصوديوم واليوريا ( NaOH/urea ) والذي كان بتركيز ( 6% NaOH + 4% يوريا ) فكانت نسبة الاذابة تصل اكثر من 60% للسليلوز المعالج في كاشف فينتون و للسليلوز الغير معالج فكانت افضل نسبة ذوبان تصل الى 35% وكانت افضل درجة حرارة لعملية الاذابة هي - 15 درجة مئوية .

الكلمات الرئيسية: الياف السليلوز ، ذوبان الياف السليلوز في محاليل هيدروكسيد الصوديوم ، كاشف فينتون



## Studying the Improvement of the Solubility of Cellulosic Fibers

Dr. Asem Hassan Mohammed

Lecturer

Technology Institute-Middle Technical University

E-mail: asemh2005@yahoo.com

### Abstract

This study focuses for improving the increase the solubility of fiber cellulose in sodium hydroxide solution in concentrations ranging from (4- 12%), from one point of view and from other point of view in (sodium hydroxide and urea) solution concentration (6% NaOH + 4% urea), under low temperature (- 15, - 20 C°), depending on the principle of reducing the degree of polymerization for fiber cellulose, which is represented in our tests cotton linter who its represent (Whatman filter paper, Grade 1), some samples subjected to chemical pretreatment as simulation the method of decomposition of cellulosic materials by white or brown fungi that grow on trees, this method involves the use of chemical materials, including hydrogen peroxide (H<sub>2</sub>O<sub>2</sub>), oxalic acid C<sub>2</sub>H<sub>2</sub>O<sub>4</sub> and ferrous sulfate FeSO<sub>4</sub> to be reaction known (Fenton reaction or Fenton's reagent) which produce free radicals helps the decomposition of cellulose fibers. The results were as follows: The solubility of cellulose fiber in sodium hydroxide solution was up to 42% cellulose and the best sodium hydroxide concentration is 8% for treated samples in Fenton solution and for untreated samples were the best solubility of cellulose fiber up to 28% and the best temperature is -20 C° for both. For the solubility of cellulose fibers in sodium hydroxide and urea solution (6% NaOH + 4% urea) was more than 60% of treated cellulose in Fenton reaction, while for untreated cellulose was the best solubility ratio up to 35% and it was the best temperature - 15 C°

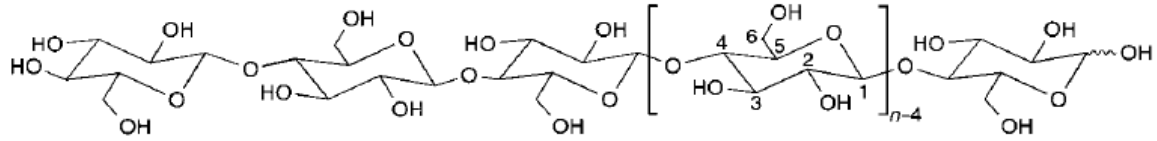
**Keyword:** cellulose fiber, cellulose dissolution, sodium hydroxide solution, Fenton reaction, Fenton's reagent

### المقدمة :

يمكن تعريف المادة السليلوزية كيميائياً على أنها مادة عضوية تحمل الصيغة التالية (C<sub>6</sub>H<sub>10</sub>O<sub>5</sub>) وتعتبر من السكريات المتعددة (polysaccharide) والتي تتألف من سلسلة خطية من وحدات الكلوكوز، تتراوح من مئات إلى الوف تتصل فيما بينها عن طريق الاصرة β(1→4) (Klemm et al. 2005) كما مبين في الشكل -1- .

كما يمكن تعريف وتصنيف المواد السليلوزية فيزيائياً على أنها المواد التي لا يمكن إذابتها حتى في درجات حرارة أقل من درجة حرارة تفككها، وذلك بسبب تركيبها البلوري العالي والناتج من الاواصر الهيدروجينية الموجودة في السليلوز والتي بدورها تمنع ذوبانها في اغلب المذيبات (Ying Wang, 2008) .

المادة السليلوزية هو المركب الأساسي في الخلايا النباتية وبالذات في جدار الخلية النباتية (Gardner et al. 1974) وهو كذلك موجود في جميع أنسجة النباتات ، يعتبر السليلوز من أكثر المركبات الكيميائية وفرة على وجه الأرض وأكثرها رواجاً حيث يشكل قرابة 33% من بنية النباتات و 90% من بنية القطن و 45% في الخشب (Sjostrom, 1993) ويشكل المادة الخام الأساسية في كثير من الصناعات المختلفة مثل صناعة الورق واللدائن والمنسوجات القطنية و الألياف الصناعية مثل الحرير الصناعي و يستخدم كذلك في المتفجرات عالية القدرة (Ying Wang, 2008) .



شكل رقم 1- التركيب البنائي للسليلوز

يعتبر السليلوز من المواد الصعبة التلدين بسبب الصلادة التي يمتلكها والناجمة من الشبكة الكبيرة من الاواصر الهيدروجينية التي توجد بين وحدات الكلوكوز المكونة لمادة السليلوز مكونة ما يعرف بالتبلور (Crystallinity) والسبب الاخر هي درجة البلمرة العالية (Degree of polymerization, DP) .

ان مجموع هذين السببين لها تأثير مهم على عدم ذوبان مادة السليلوز في اغلب المذيبات العضوية وغير العضوية ، ويصنف السليلوز على انه لا من البوليمرات المطاوعة للحرارة (thermoplastic polymer) ولا من المتصلبة حرارياً (thermoset polymer) ، كل هذه الاسباب جعلت منه مادة محدودة الاستعمال ومادة خاملة لاجلب التفاعلات الكيميائية (Ying Wang, 2008) .

وعليه ان عملية تطوير اذابة السليلوز بالتاكيد هي التي سوف تعطي دفعة جديدة لهذه المادة في صناعة الاليف السليلوزية والصناعات الاخرى ذات الصلة بهذه المادة .

سوف يتركز اهتمامنا في هذه المقدمة على اربعة اشياء مهمة هـ : درجة البلمرة ، التبلور ، ذوبانية السليلوز بشكل عام في المحاليل ، ذوبانية السليلوز في المحاليل القاعدية

### • درجة البلمرة

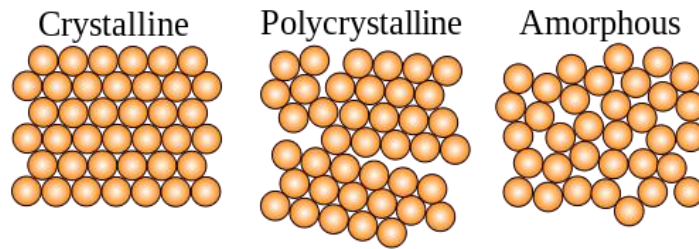
تعرف درجة البلمرة (Degree of polymerization, DP) على انها متوسط عدد الوحدات المتكررة في سلاسل جزئية البوليمر (McNaught and Wilkinson, 1997) ، وتعتبر درجة البلمرة مقياس للوزن الجزيئي الذي قد يصل الى عشرات الالاف ، ويمكن التعبير عن درجة البلمرة بالقانون التالي :

$$DP = \frac{\text{Total MW of the polymer}}{\text{MW of the repeating unit}} \equiv X_n = \frac{M_n}{M_0}$$

حيث ان  $M_n$  معدل الوزن الجزيئي للبوليمر ،  $M_0$  الوزن الجزيئي للمونومر . كثير من خواص السليلوز تعتمد على درجة البلمرة للسليلوز والتي تمثل عدد وحدات الكلوكوز المكونة للسليلوز ، والتي تختلف باختلاف مصدر السليلوز المتكون ، فمثلا ان عجينة الخشب لها درجة بلمرة ما بين 300 – 1700 وحيدة كلوكوز ، اما بالنسبة الى الياف القطن واليااف النباتات الاخرى مضافا اليها الياف السليلوز المكونة لجدار بعض انواع البكتريا فتكون ما بين 800 – 10000 وحدة ( Klemm et al.2005 ) .

### • التبلور (Crystallinity)

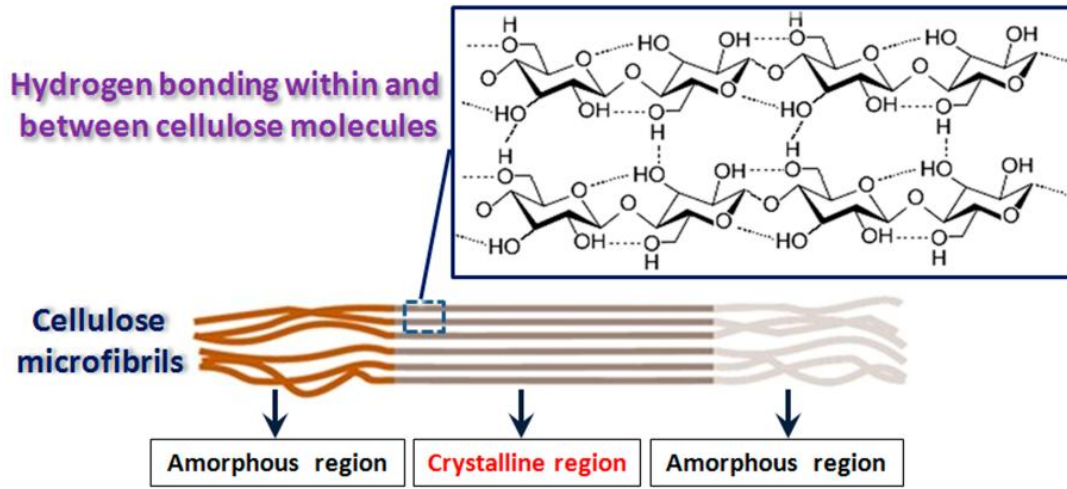
التبلور او البلورة هي عملية تشكيل طبيعية او صناعية للجزيئات بشكل منظم وباسلوب معين للمادة الصلبة ، وللتبلور تأثير كبير على الصلادة والكثافة والانتشار والشفافية ، كثير من المواد السيراميكية والبوليمرات تتركب جزئيا بحيث يحتوي هذا التركيب على خليط الجزء الاكبر منه يكون متبلور ( Crystalline ) والجزء الاخر يكون منطقة غير متبلورة ( Amorphous ) بمعنى انها غير مرتبة بالشكل الذي تترتب به جزيئات المنطقة المتبلورة (Peng et al. 2011) كما موضح في الشكل التوضيحي رقم 2 -



الشكل -2- البناء البلوري للمواد

ان سبب التبلور في السليلوز يعزى الى البناء الجزيئي لمادة السليلوز والتي تكون نتيجة للاواصر الهيدروجينية الموجودة بين جزيئات الكلوكوز المؤلفة للسليلوز ، هناك نوعين من الاواصر الهيدروجينية ، اواصر هيدروجينية موجودة بين الجزيئات المتجاورة في نفس السلسلة واواصر هيدروجينية تكون بين السلاسل المتجاورة ، عن طريق هذين النوعين من الاواصر يتكون عندنا ما يعرف بالبناء البلوري للسليلوز ( D. Klemm et al.2005 ) كما موضح في الشكل التوضيحي رقم 3- .



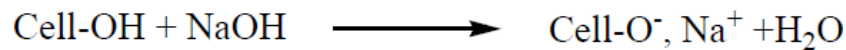


الشكل -3- البناء البلوري للسليولوز

### • ذوبانية السليولوز (Cellulose Dissolution)

ان عملية ذوبان السليولوز (Cellulose Dissolution) تختلف عن عملية تحلل الالياف السليولوزية (Cellulose Hydrolysis) . نقصد بعملية التحلل (Hydrolysis) هو عملية كسر للجزئية العملاقة اما من المنتصف او من نهايات السلسلة البوليمرية للسليولوز للحصول على جزئية ذات وزن جزيئي اصغر وحتى يمكن الحصول جزئية ثنائية الكلوكوز (cellubiose) والكلوكوز (glucose) كجزئية احادية (Ladisch, 1982) و (Maximino and Adell, 2000) . اما بالنسبة الى عملية ذوبان السليولوز فنقصد به عملية تكسير للاواصر الهيدروجينية الموجودة في بوليمر السليولوز سواء كانت بين جزيئات الكلوكوز الموجودة في نفس السلسلة او الاواصر الهيدروجينية الموجودة بين سلاسل المتجاورة لالياف السليولوز . ببساطة ان عملية ذوبان السليولوز هي عملية مشابهة لانصهار المادة الصلبة (solid melting) . وقد تحتاج عملية ذوبان السليولوز الى عملية تحلل كمعالجة اولية (pretreatment) وخاصة للجزئيات التي تمتلك درجة بلورة عالية (Ying Wang, 2008) .

فمثلا عند انتاج الحرير الصناعي بطريقة الفسكوز يتم معاملة الياف السليولوز مع محلول هيدروكسيد الصوديوم بتركيز 17 - 20 % وعند درجة حرارة الغرفة لعدة ساعات تتحول بعدها الياف السليولوز الى الياف سليولوز - قاعدي (Cellulose-Alkaline) كما في المعادلة التالية :



بعدها تنتفخ الياف السليولوز وتكون اكثر فاعلية تجاه العمليات الكيميائية. بعد ازالة هيدروكسيد الصوديوم الزائد بالعصر تقطع الياف السليولوز الى قطع صغيرة ويبقى لفترة من الزمن تستمر لمدة يومين في مرحلة تسمى مرحلة التعتيق (Aged stage) وتكون

تحت درجة حرارة مسيطر عليها للحصول على درجة البلمرة المطلوبة وللزوجة الملائمة لسائل الفسكوز المتكون لاحقا، بعدها تتفاعل هذه الالياف المعتقة مع ثنائي كبريتيد الكاربون ( $C_2S$ ) مكون ما يعرف بزئذات السليلوز (cellulose xanthate) الذي تكون قابل للذوبان في محلول هيدروكسيد الصوديوم بتركيز 6% مكونا سائل كثيف القوام يعرف الفسكوز والذي يصنع منه الياف الحرير الصناعي (Ying Wang, 2008) ، ان من محددات هذه الطريقة هي السمية العالية المرافقة للانتاج والناجمة عن تولد غاز كبريتيد الهيدروجين ( $H_2S$ ) الناتج من استخدام مادة ثنائي كبريتيد الكاربون ( $C_2S$ ) والتي تكون بدورها مادة سامة ايضا ، ان اهم مايميز هذه الطريقة هو امكانيتها في استخدام الياف السليلوز الناتجة من الخشب على عكس الطرق الاخرى التي تحتاج الى الياف سليلوزية نقية خالية من اللكنين الموجود في مادة الخشب (Ying Wang, 2008) . وعلى الرغم من استخدام هذه الطريقة صناعيا الا ان المخاطر الكيميائية المرافقة لهذه العملية جعل الباحثون يستمرون في البحث عن طرق جديدة لاذابة السليلوز بصورة اكثر ملائمة للبيئة وقل كلفة ، في السنوات الاخيرة اعتبر استخدام المحاليل القاعدية كخيار بديل جيد لدى الباحثون .

ايضا يوجد الكثير من المذيبات التي تستخدم لاذابة الاليف السليلوزية والتي تتضمن مذيبات عضوية وغير عضوية . فمثلا يستخدم حامض الكبريتيك بصورة واسعة لتحليل الياف السليلوز الى اطوال اصغر وخاصة لتحليل السليلوز الى وحداته من الكلوكوز

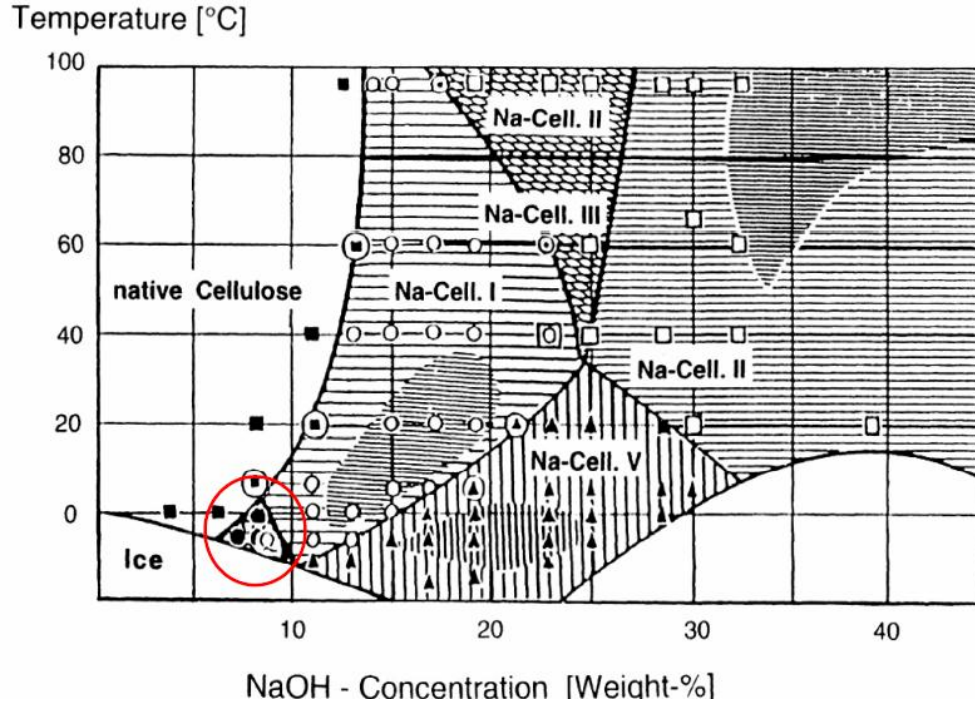
### • ذوبان السليلوز في المحاليل القاعدية (Cellulose Dissolution in Alkali Solution)

نالت عملية اذابة السليلوز في المحاليل القاعدية وخاصة في محلول هيدروكسيد الصوديوم اهمية كبيرة من قبل الباحثين وذلك بسبب التغير البنوي (structural change) الذي يحدثه هيدروكسيد الصوديوم على بنية السليلوز حيث سوف تتغير البنية البلورية للسليلوز القاعدي (Na-cell) من الطور الاول الى اطوار اخرى مختلفة مكونا معقدات بنيوية مختلفة من السليلوز-الصوديوم (Na-cellulose). بعض الباحثين فسروا ما يحدث خلال عملية الالكنة (alkalization) حيث يقوم هيدروكسيد الصوديوم بتمزيق الاواصر الموجودة في الياف السليلوز (I) مما يؤدي الى انتفاخ السليلوز ومن ثم سوف تتحرك جزيئات السليلوز الى اطوار اخرى كما موضح في الشكل-4 الذي يمثل مخطط الاطوار (Sobue et al. 1936) .

ايضا لاحظ الباحثون في نفس الشكل توجد منطقة مثثلة الشكل صغيرة والتي يرمز لها (Q) في مخطط الطور والتي تكون عند تركيز 6 - 10 % هيدروكسيد الصوديوم ودرجة حرارة من 4 الى 10 درجة مئوية ، عند هذه المنطقة سيكون انتفاخ السلسلوز عالي ويوجد ايضا ذوبان مباشر لاليف السليلوز الذي تمتلك درجة بلمرة واطنة الى متوسطة ، وان نسبة الاذابة كانت مساوية تقريبا لتركيز هيدروكسيد الصوديوم اي ما بين 6 - 10 % من السليلوز الاصلي (Aravindanath et al. 1986) كما مبين في الشكل -4.

لكي يحدث هذا الانتقال بين الاطوار يجب ان تحتوي الياف السليلوز الاصلي على المناطق الرخوة او الغير متبلورة (amorphous region) التي تم الاشارة اليها سابقا كي يبدأ التحول مبتدا من هذه المنطقة الغير متبلورة (Aravindanath)

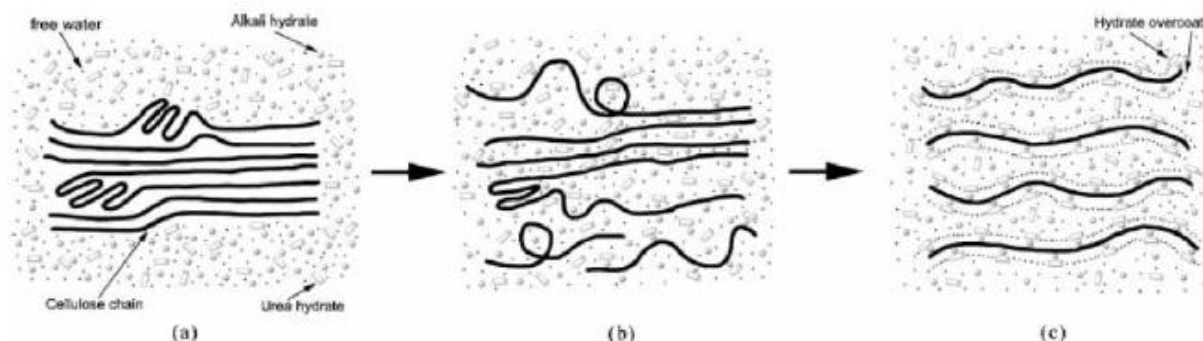
(et al. 1986) ، بعض الباحثين فسروا ما يحدث خلال عملية الالكنة (alkalization) حيث يقوم هيدروكسيد الصوديوم بتمزيق الاواصر الموجودة في الياف السليلوز ( I ) مما يؤدي الى انتفاخ السليلوز ومن ثم سوف تتحرك جزيئات السليلوز الى الاطوار الاخرى (Ying Wang, 2008) .



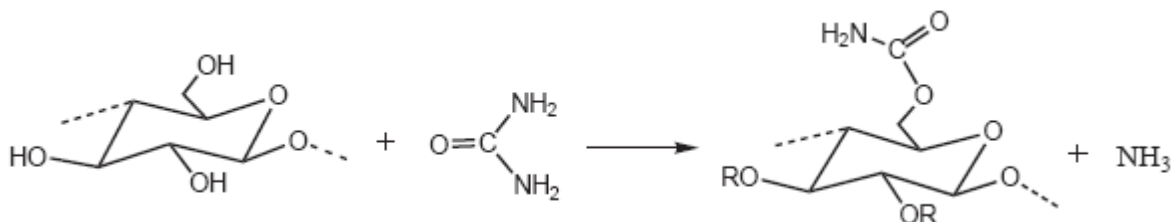
الشكل -4- مخطط الطور لالياف السليلوز مع هيدروكسيد الصوديوم (Sobue et al. 1936) .

ان عملية الازابة هذه تكون جيدة في درجات حرارة منخفضة تكون عملية الازابة بالمجمل تكون باعثة للحرارة ، تؤخذ هذه العملية بنظر الاعتبار على انها عملية متعددة المراحل ، والتي تتضمن : - اولاً: حصول ذوبان (melting) في المنطقة البلورية للسليلوز تسمى هذه مرحلة الانصهار (fusion) ثم انتقال المنطقة الغير متبلورة (amorphous) الى الحالة المرنة (elastic state) وتسمى هذه مرحلة الانتقالية (transition) ، ثانياً: تحول جزء من جزيئات السليلوز الغروية الى جزيئات لها القابلية على الذوبان وتسمى مرحلة التداخل (interaction) ، ثالثاً: واخيراً ذوبان الاخير وانتشاره في المذيب وتسمى مرحلة المزج (mixing) (Ramos, 2005) .

اما بالنسبة الى عمل اليوريا مع محلول هيدروكسيد الصوديوم فتعمل على تكوين غطاء مع جزيئات الماء يحيط بجزيئات هيدروكسيد الصوديوم ويعمل على منح واستقبال اواصر الهيدروجين بين المذيب ويعمل على اعادة الترابط بين جزيئات السليلوز كما موضح في الشكل -5- وهناك رأي ثان يقول ان اليوريا تتفاعل مع السليلوز لينتج الكاربامات في خطوة مشابهة لما قد يحدث في عملية الزنتنة كما موضح في الشكل -6- (D. Klemm et al. 2005) .



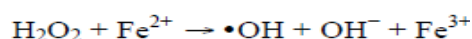
الشكل 5- مخطط عملية الاذابة ( Cai and Zhang, 2005 ) .



الشكل 6- مخطط تكوين الكربامات (D.Klemm et al. 2005 )

### • المعالجة الكيميائية بواسطة كاشف فنتون ( Fenton's reagent ) .

يتضح مما سبق ان لدرجة البلمرة دور مهم في عملية الاذابة ، وفي صناعة الحرير الصناعي بطريقة الفسكوز يتم تقليل درجة البلمرة باستخدام محلول هيدروكسيد الصوديوم بتركيز 20% في مرحلتى التفتيح والتعتيق اما في بحثنا هذا فسوف نستخدم محلول كيميائي يعرف بكاشف فنتون ( Fenton's reagent ) يتكون من بيروكسيد الهيدروجين وايون الحديد وحامض الاوكسالك. في هذا الكاشف يقوم ايون الحديدوز ( $Fe^{+2}$ ) بتحفيز تحلل بيروكسيد الهيدروجين المخفف لتشكيل جذور الهيدروكسيد كما في التفاعل التالي :

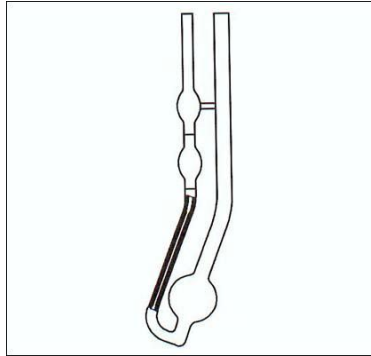


يجري هذا التفاعل في محلول منظم يتكون من حامض الاوكسالك واوكسالات الصوديوم عند مقياس حمضية 4.2 - 5 , PH , حيث وجد لحامض الاوكسالك تاثير لا يابس به على تقليل درجة بلمرة الياف القطن السليلوزية على ان يكون ضمن مقياس الحمضية

المشار اليه سابقا. تتم هذه العملية باخذ نماذج من ورق الترشيح رقم -1- الذي يمثل الياف السليلوز الذي يتفاعل مع كاشف فينتون بوزن 0.2 غرام من الياف السليلوز مع 10 مل من محلول فنتون وبالتراكيز التالية :  $80\text{mM H}_2\text{O}_2$  ،  $0.5\text{mM}$  ،  $10\text{mM sodium oxalate}$  ،  $10\text{mM oxalic acid}$  ،  $\text{FeSO}_4$  ، وللحصول على مقياس الحامضية المطلوب  $\text{PH} = 4.67$  يتم الخلط بين حامض الاوكسالك و اوكسالات الصوديوم وفق النسبة الحجمية التالية : (1:13) ، توضع النماذج في انابيب بلاستيكية سعة 30 مل على هزاز دوار ولمدة 24 ساعة بعدها تغسل النماذج جيدا بالماء الخالي من الايونات ويترك بعدها ليجف في درجة حرارة 50 درجة مئوية ولمدة 8 ساعات (Anne et al. 2011) ثم يذاب السليلوز المعالج مع  $0.5\text{M}$  من (cupriethylenediamine (CED) ثم تقاس لزوجة المحاليل المتكونة بواسطة انبوبة فينسكي لقياس اللزوجة وباستخدام العلاقة التالية :

$$1/n_{sp} = t_0/(t - t_0).$$

حيث ان  $(1/n_{sp})$  هو مقلوب اللزوجة النوعية و  $t$  هو الوقت التدفق و  $t_0$  هو القيمة القياسية لانبوبة قياس اللزوجة بعدها تحول اللزوجة النوعية الى درجة البلمرة حسب (Cowling, 1960) . الشكل -7- يوضح انبوبة ( Cannon-Fenske viscometer )



شكل-7- انبوبة فينسكي لقياس اللزوجة

#### • اهداف البحث :

ان الهدف الرئيسي من بحثنا هو تطوير استخدام محاليل هيدروكسيد لاصوديوم ضمن مدى معين من التراكيز وفي درجات حرارة منخفضة في اذابة الياف السليلوز المتمثلة في زغب القطن والذي يمتلك درجة البلمرة ما بين 2200 - 2600 وايجاد ما يلي :

- 1- ايجاد افضل تركيز لمحاليل هيدروكسيد الصوديوم ما بين 4% الى 12% وهو المدى المقبول لاذابة الالياف السليلوزية في درجات حرارة 15- 20 درجة مئوية .

2- اجراء مقارنة لعملية اذابة السليلوز بين افضل تركيز لمحلول هيدروكسيد الصوديوم و محلول هيدروكسيد الصوديوم واليوريا سويا بتركيز ثابت وهو ( 6 هيدروكسيد الصوديوم + 4% يوريا ) .

3- اجراء معالجة لالياف السليلوز باستخدام ما يعرف بكاشف فنتون لتقليل درجة البلمرة ومن ثم تحسين اذابة السليلوز في محلول هيدروكسيد الصوديوم و محلول هيدروكسيد الصوديوم واليوريا سويا .

## الجانب العملي

### الاجهزة والمواد المستعملة

- 1- ورق ترشيح رقم 1- ( Whatman filter paper, Grade 1 ) التي تتالف من مواد نقية من الياف السليلوز ، تم استخدامه كمصدر لالياف السليلوز المستعملة في التجارب والذي يتالف من زغب القطن المقاسة درجة بلمرته بالطريقة المشار اليها سابقا في هذا البحث والتي كانت بحدود 2200 - 2600 .
- 2- محلول هيدروكسيد الصوديوم بتركيز 38% ( معمل الحرير الصناعي سدة الهندية )
- 3- ماء مقطر
- 4- انابيب اختبار
- 5- ثلاثة ( فريز ) ( Vestel )
- 6- محرار
- 7- جهاز طرد مركزي
- 8- حامض الهيدروكلوريك
- 9- محلول فينتون كيميائي وبالتراكيز التالية : 80mM H<sub>2</sub>O<sub>2</sub> ( Applichem GmbH ) ، ( 0.5mM FeSO<sub>4</sub> ، 10mM sodium oxalate ، 10mMoxalic acid ، ( Merck ) لاجراء المعالجة الاولى

### طريقة العمل

- 1- تحضير محاليل هيدروكسيد الصوديوم بتركيز 4% ، 6% ، 8% و 12% . عن طريق تخفيف محلول هيدروكسيد الصوديوم الاصلي ( 38% ) الموجود في المختبر كمصدر لمحاليل هيدروكسيد الصوديوم باستخدام قانون التخفيف .
- 2- اجراء معالجة اولية لبعض النماذج باستخدام كاشف فنتون وبالتراكيز المشار اليها سابقا لدراسة تاثير المعالجة الاولى على ذوبان السليلوز في محاليل هيدروكسيد الصوديوم .

3- تتكون نماذج التجارب من 10 غم من محلول هيدروكسيد لاصوديوم و 0.25 غم من السليلوز ويوضعان في ابوبة اختبار واخذت هذه بالاعتماد على المصادر السابقة ( Ying Wang, 2008 ) .

4- تترك النماذج بعد التحضير لمدة ساعة بعدها توضع في حاوية بلاستيكية تحتوي على ايثيل كلايكول بتركيز 38% والباقي ماء وتوضع هذه الحاوية مع النماذج لمدة 24 ساعة داخل فريز التلجة .

5- اخراج النماذج من الفريز وتركها فترة لاتقل عن ساعة من الزمن في درجة حرارة الغرفة لاذابة النماذج، تؤخذ بعدها النماذج الى جهاز الطرد المركزي وبسرعة 2500 دورة في الدقيقة لفصل الالياف المذابة عن الغير المذابة .

6- فصل الجزء المذاب و اخراج الجزء الغير المذاب من الالياف من انابيب الاختبار وغسلها بالماء غسلا جيدا بعدها تجفف ويقاس وزنها ويقارن مع الوزن الاصلي (0.25غم ) ومن ثم ايجاد نسبة السليلوز المذاب .

## الحسابات :

### 1.التخفيف

كمية NaOH قبل التخفيف = كمية NaOH بعد التخفيف

تركيز هيدروكسيد الصوديوم x وزن المزيج ( H<sub>2</sub>O + NaOH ) = تركيز هيدروكسيد الصوديوم x وزن المزيج ( H<sub>2</sub>O + NaOH )

### 2.حساب كمية السليلوز المذاب

$$\text{نسبة السليلوز المذاب ( الذوبانية )} = \frac{\text{كمية السليلوز قبل الاذابة} - \text{كمية السليلوز بعد لاذابة}}{\text{كمية السليلوز قبل الاذابة}} \times 100\%$$



## النتائج والمناقشة

في بداية تجاربنا تم تحديد افضل تركيز لمحلول هيدروكسيد الصوديوم والذي كانت التراكيز فيه ما بين 4% الى 12 % لدرجات الحرارة -15 و -20 درجة مئوية، تم اختيار هذين الدرجتين بالاعتماد على المصادر السابقة التي تعاملت مع الموضوع ( Ying Wang, 2008 ) ومن ثم قياس نسبة اذابة السليولوز في المحلول وتم اختيار نموذجين لكل تركيز ونوعين مختلفين من النماذج احدهما معالج مع كاشف فنتون ذات تراكيز معلومة ومشار اليها سابقا" ولمدة 24 ساعة وفي درجة حرارة الغرفة واخر غير معالج ولمحاولتين لضمان دقة النتائج ، انظر الشكل -8-، كانت درجة البلمرة ( DP ) للنماذج المعالجة بحدود 400 - 450 بعد قياسها بالطريقة المشار اليها سابقا" وكانت النتائج كالتالي

جدول-3- التجربة الاولى المحاولة الاولى كانت تحت درجة حرارة -15 ± 2 درجة مئوية

التسلسل	تركيز هيدروكسيد الصوديوم	4%	6%	8%	12%
1	نسبة اذابة السليولوز (نموذج معالج -1)	10%	21%	30%	16%
2	نسبة اذابة السليولوز (نموذج معالج -2)	12%	20%	31%	14%
3	نسبة اذابة السليولوز (نموذج غير معالج -1)	5%	15%	23%	10%
4	نسبة اذابة السليولوز (نموذج غير معالج -2)	4%	15%	23%	9%

جدول-4- التجربة الاولى المحاولة الثانية كانت تحت درجة حرارة -15 ± 2 درجة مئوية

التسلسل	تركيز هيدروكسيد الصوديوم	4%	6%	8%	12%
1	نسبة اذابة السليولوز (نموذج معالج -1)	10%	23%	31%	16%
2	نسبة اذابة السليولوز (نموذج معالج -2)	11%	22%	31%	14%
3	نسبة اذابة السليولوز (نموذج غير معالج -1)	6%	15%	24%	10%
4	نسبة اذابة السليولوز (نموذج غير معالج -2)	4%	16%	24%	10%

جدول-5- التجربة الثانية المحاولة الاولى كانت تحت درجة حرارة -20 ± 2 درجة مئوية

التسلسل	تركيز هيدروكسيد الصوديوم	4%	6%	8%	12%
1	نسبة اذابة السليولوز (نموذج معالج -1)	12%	25%	41%	17%
2	نسبة اذابة السليولوز (نموذج معالج -2)	13%	27%	42%	18%
3	نسبة اذابة السليولوز (نموذج غير معالج -1)	7%	16%	28%	10%
4	نسبة اذابة السليولوز (نموذج غير معالج -2)	8%	17%	29%	10%

جدول 6- التجربة الثانية المحاولة الثانية كانت تحت درجة حرارة  $20 \pm 2$  درجة مئوية

التسلسل	تركيز هيدروكسيد الصوديوم	%4	%6	%8	%12
1	نسبة اذابة السليلوز (نموذج معالج -1 )	%13	%26	%42	%17
2	نسبة اذابة السليلوز (نموذج معالج -2 )	%13	%27	%42	%17
3	نسبة اذابة السليلوز (نموذج غير معالج -1 )	%7	%17	%28	%10
4	نسبة اذابة السليلوز (نموذج غير معالج -2 )	%8	%17	%29	%10

نلاحظ من هذه الجداول ان النتائج بالنسبة الى التجربة الاولى والتي كانت تحت  $15^{\circ}\text{C}$  وللمحاولتين كانت متقاربة واحسن نسبة اذابة كانت في تركيز 8% والتي كانت بحدود 31% . اما بالنسبة للتجربة الثانية والتي كانت تحت درجة حرارة  $20^{\circ}\text{C}$  فالنتائج كانت متقاربة ايضا للمحاولتين و احسن نسبة اذابة كانت في تركيز 8% والتي كانت بحدود 42% . علما ان النتائج المسجلة سابقا حصلت على افضل اذابة بتركيز مابين 6-8 % وأفضل اذابة كانت هي 28 % وكانت بدون معالجة كيميائية ( Ying Wang, 2008 ) . انظر الشكل 8-

بعد ذلك اجرينا تجارب باضافة يوريا الى محلول هيدروكسيد الصوديوم لزيادة فعالية الاذابة وبتركيز ثابت وهو ( 6% هيدروكسيد الصوديوم + 4% يوريا ) اخذ هذا التركيز على دراسة سابقة ( Ying Wang, 2008 ) ، وبنفس درجات الحرارة  $15^{\circ}\text{C}$  و  $20^{\circ}\text{C}$  ، وكما موضح في الجداول التالية:

جدول 7- التجربة الاولى المحاولة الاولى كانت تحت درجة حرارة  $15 \pm 2$  درجة مئوية

التسلسل	تركيز المحلول	( 6% هيدروكسيد الصوديوم + 4% يوريا )
1	نسبة اذابة السليلوز (نموذج معالج 1 )	%62
2	نسبة اذابة السليلوز (نموذج معالج 2 )	%61
3	نسبة اذابة السليلوز (نموذج غير معالج 1 )	%35
4	نسبة اذابة السليلوز (نموذج غير معالج 2 )	%34

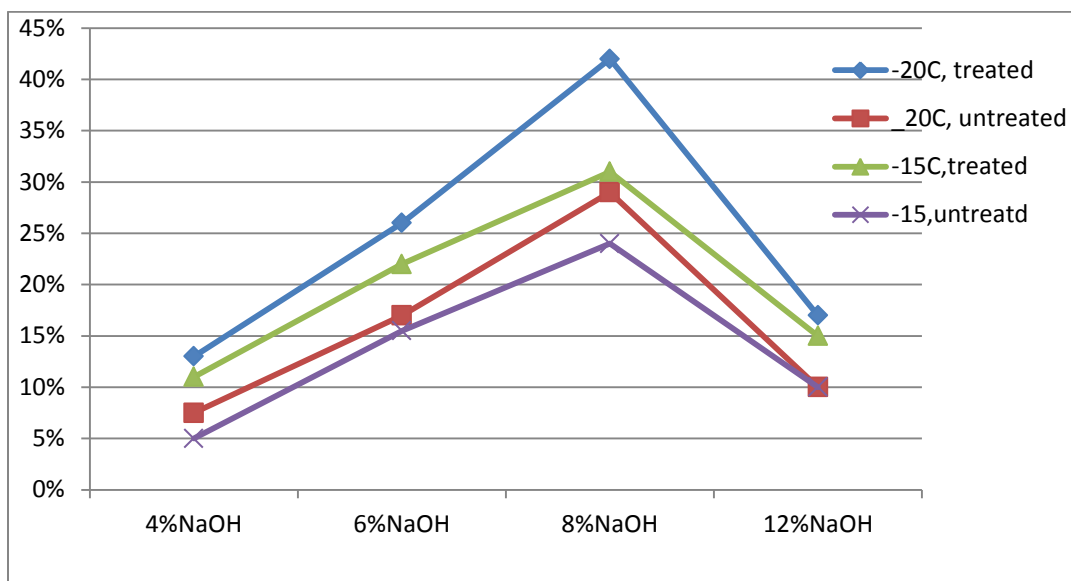
جدول-8- التجربة الاولى المحاولة الاولى كانت تحت درجة حرارة  $-20 \pm 2$  درجة مئوية

التسلسل	تركيز المحلول	( 6% هيدروكسيد الصوديوم + 4% يوريا )
1	نسبة اذابة السليلوز (نموذج معالج 1 )	35%
2	نسبة اذابة السليلوز (نموذج معالج 2 )	36%
3	نسبة اذابة السليلوز (نموذج غير معالج 1 )	28%
4	نسبة اذابة السليلوز (نموذج غير معالج 2 )	29%

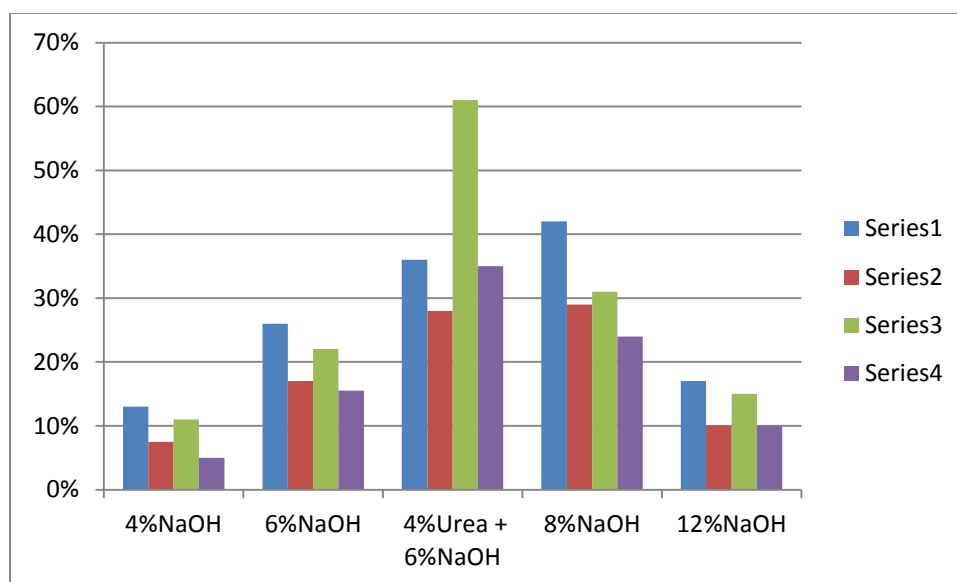
يمثل الجدول -7- معدل النتائج لمحاولتين من التجارب وكذلك الحال بالنسبة للجدول -8- . نلاحظ من هذين الجدولين ان نسبة الاذابة في محلول هيدروكسيد الصوديوم واليوريا وللنماذج المعالجة مع كاشف فينتون كانت افضل من بين الجميع وكانت عند درجة الحرارة -15 درجة مئوية الافضل حيث كانت نسبة الاذابة اكثر من 60 % ، بينما كانت نسبة الاذابة 36% للنماذج المعالجة مع كاشف فينتون والتي اجريت في درجة حرارة -20 درجة مئوية . انظر الشكل -9- ، ويمكن تفسير ذلك ان عملية الاذابة هي عملية ثرموديناميكية و خير من يمثل هذه العملية الثرموديناميكية هي طاقة كبس الحرة ( Gibbs free energy ) وحسب العلاقة التالية :

$$\Delta G = \Delta H - T \cdot \Delta S$$

فمثلا عند درجة حرارة -15 م<sup>0</sup> تكون طاقة كبس الحرة لعملية كسر التبلور ( decrystallization ) تساوي 79 kJ/mol بينما لدرجة حرارة -20 م<sup>0</sup> كانت طاقة كبس الحرة 80.55 kJ/mol وكلما كانت طاقة كبس الحرة اقل كانت عملية الاذابة افضل ، كذلك ترتبط طاقة كبس الحرة بمعدل التفاعل ( Reaction rate ) والذي سوف يكون اعلى عند -15 م<sup>0</sup> ( Ying Wang, 2008 ) . ان زيادة نسبة اذابة الياف السليلوز في محلول هيدروكسيد الصوديوم وكذلك في محلول هيدروكسيد الصوديوم واليوريا يعزى الى عملية المعالجة في كاشف فينتون والتي ادت الى تقليل درجة البلمرة والتي كان لها دورا مؤثرا في زيادة اذابة الياف السليلوز . الاشكال التالية توضح عملية الاذابة والتي تبدا من اختيار افضل تركيز لمحلول هيدروكسيد الصوديوم وتنتهي بافضل اذابة لالياف السليلوز المعالج و الغير معالج ،



الشكل 8- ذوبانية السليلوز في محاليل هيدروكسيد الصوديوم لدرجتي الحرارة -15 و -20 درجة مئوية



الشكل 9- ذوبانية السليلوز في محلول هيدروكسيد الصوديوم و هيدروكسيد الصوديوم واليوريا ( 4% urea + 6% NaOH ) للتراكيز المستخدمة في التجربة

## الاستنتاجات

هذه الدراسة بينت بوضوح تأثير المحلول فينتون الكيميائي المستعمل في المعالجة الأولية والذي ادى بدوره الى تقليل درجة البلمرة للسليولوز بالإضافة الى تأكيدها على تأثير درجة البلمرة على ذوبانية الالياف السليولوزية في محلول هيدروكسيد الصوديوم وكذلك تأثير اضافة اليوريا الى محلول هيدروكسيد الصوديوم . و للحصول على افضل اذابة هناك العديد من المتغيرات التي يجب اخذها بنظر الاعتبار منها درجة الحرارة ، تركيز محلول هيدروكسيد الصوديوم و وقت المعالجة في تفاعل فينتون وكذلك ايضا وقت اذابة الياف السليولوز في محلول هيدروكسيد الصوديوم .

## التوصيات

- لكي يكون هناك فهم اعمق لعملية لاذابة الياف السليولوز في محلول هيدروكسيد الصوديوم هناك بعض الاشياء التي يجب ان تفسر بصورة جيدة منها
- 1- ايجاد موديل رياضي يربط بين وقت المعالجة مع تفاعل فينتون ودرجة البلمرة
- 2- دراسة تأثير بعض الاضافات وتركيزها على محلول هيدروكسيد الصوديوم لزيادة نسبة ذوبانية السليولوز كاليوريا مثلا
- 3- دراسة ميكانيكية التفاعل ( عملية الاذابة الياف السليولوز ) لغرض ايجاد موديل رياضي للعملية ياخذ درجة البلمرة بنظر الاعتبار .
- 4- لكي يكون البحث اكثر رصانة اوصي بفحص ال XRD لفحص البلورية والحجم البلوري

## REFERENCES

- Anne Christine Steenkjær Hastrup ., Caitlin Howell., Bo Jensen., Frederick Green., 2011, *Non-enzymatic depolymerization of Cotton Cellulose by Fungal Mimicking Metabolites*, International Biodeterioration & Biodegradation ( 65 ) 553-559.
- Aravindanath, S., Bhama Iyer, P., and Sreenivasan, S., 1986, *Further Evidenc for The presence of Ccellulose I and II In The Same Cross Section of Partially Mercerized Cotton Fibers*, Textile Research Journal, vol. 56, no. 3, pp. 211- 212.
- Cai, J. and Zhang, L., 2005, *Rapid Dissolution of Cellulose in LiOH/urea and NaOH/urea Aqueous Solutions*, Macromolecular Bioscience, vol. 5, no. 6, pp. 539-548.
- Cowling, E.B., 1960, *Method for Chemical Analysis of Decayed Wood*. Forest Service, U.S. Department of Agriculture, Madison, Wisconsin, USA, 2177, pp. 1e24.
- Gardner, K. H. and Blackwell, J., 1974, *The structure of Native Cellulose*, Biopolymers, vol. 13, no. 10, pp. 1975-2001.
- Klemm, D., H.-P. Fink et al., 2005 , *Cellulose: Fascinating Biopolymer and Sustainable Raw*



*Material.*, *Angew, Chem. Int. Ed.*, 44, 3358 – 3393.

- Ladisch, C. M., Chiasson, C. M., and Tsao, G. T., 1982 , *Acid and Enzymatic Hydrolysis of Pretreated Cellulosic Materials as An Analytical Tool*, in *Textile Research Journal*, vol. 52, (Purdue Univ, West Lafayette, Indiana, USA), pp. 423-433.
- Peng, B. L., Dhar, N., Liu, H. L. and Tam, K. C., 2011, *Chemistry and Applications of Nanocrystalline Cellulose and Its Derivatives: A nanotechnology perspective*. The Canadian Journal of Chemical Engineering **89** (5): 1191–1206.
- Maximino, M. G. and Adell, A. M., 2000, *Acid Hydrolytic Treatment of Cotton Linters*, *Cellulose Chemistry and Technology*, vol. 34, no. 3-4, pp. 229-240.
- McNaught, A. D. , and A. Wilkinson, 1997, in *Compendium of Chemical Terminology* (IUPAC Gold Book),
- Sjostrom, E., 1993, *Wood Chemistry. Fundamentals and Applications*. Second edition ed., San Diego: Academic press. 292.
- Ramos, L. A., Assaf, J. M., ElSeoud, O. A., and Frollini, E., 2005, *Inuence of The Supramolecular Structure and Physicochemical Properties of Cellulose on Its Dissolution in a Lithium Chloride N,N-Dimethylacetamide Solvent System*, *Biomacromolecules*, vol. 6, no. 5, pp . 2638-2647.
- Smook, G. A., *Handbook for Pulp & Paper Technologists*. TAPPI, 1989.
- Sobue, H., Kiessig, H., and Hess, K., 1939, *The Cellulose-Sodium Hydroxidewater System as A Function of The Temperature.*, *Z. Physik. Chem. B*, vol. 43, pp. 309-328.
- Ying Wang, 2008, *Cellulose Fiber Dissolution In Sodium Hhdroxide Solution At Low Temperature* . PhD Thesis , Georgia Institute of Technology December

## دراسة خصائص متراكبات سليكات الصوديوم كحاجز وقائي يفصل بين بطانة أبراج

### التصفية النفطية والابخرة الكيميائية للنفط الخام

سجى اباد كاظم

[saja.alabassi@yahoo.com](mailto:saja.alabassi@yahoo.com)

ماجستير علم المواد

قسم العلوم التطبيقية- الجامعة التكنولوجية

أ. رولا عبد الخضر عباس

استاذ

قسم العلوم التطبيقية- الجامعة التكنولوجية

د. سلام حسين علي

استاذ مساعد

قسم العلوم التطبيقية- الجامعة التكنولوجية

### الخلاصة

تم دراسة الصلادة السطحية، مقاومة البلى، قوة الالتصاقية، مقاومة التآكل الكهروكيميائية والموصلية الحرارية لطلاءات مكونة من سليكات الصوديوم المقواة بمسحوق الكرافيت المايكروي مرة والكاربون النانوي مرة اخرى وينسب وزنية تتراوح بين (1-5%) بغية تغطية وحماية ابراج تكرير النفط. لقد اظهرت نتائج المقارنة بأن الطلاءات المتراكبة المدعمة بالكاربون النانوي تتفوق في مقاومتها للغرز، البلى الميكانيكي و الالتصاقية وخصوصاً عند النسبة 5% و 1% على طلاءات متراكبة الكرافيت المايكروي، كما خلص البحث الى نتائج واضحة هو انه يمكن تأخير تقادم الفولاذ المقاوم للصدأ 304 للتآكل بسبب الابخرة النفطية باستعمال الطلاءات المتراكبة حسب نوع التدعيم وهذا يتوافق مع النتائج الحقلية عند وضع النماذج المحضرة في اعلى برج التقطير.

كلمات رئيسية: سليكات الصوديوم، المواد المتراكبة، ابراج التصفية النفطية، مسحوق الكاربون، المواد النانوية، التآكل الكهروكيميائي، الصلادة، البلى الميكانيكي، متانة الالتصاق، الموصلية الحرارية.

### Study the Properties of Sodium Silicate Composite as a Barrier Separating Between the Internal Oil Distillation Towers and Chemical Fumes of Crude Oil

#### ABSTRACT

The study of surface hardness, wear resistance, adhesion strength, electrochemical corrosion resistance and thermal conductivity of coatings composed from sodium silicate was prepared using graphite micro-size particles and carbon nano particles as fillers respectively of concentration of (1-5%), for the purpose of covering and protecting the oil distillation towers. The results showed that the sodium silicate coating reinforced with carbon nano-powder has higher resistance to stitches, mechanical wear, adhesive and thermal conductivity than graphite/sodium silicate composite especially when the ratio 5% and 1%, the electrochemical corrosion test confirmed that the coating process of stainless steel 304 lead to increasing the corrosion resistance, where the reinforcing of sodium silicate lead to a significant improvement in the corrosion resistance, the corrosion resistance behavior change depending on the type of reinforcement material, this is consistent with the field test results.



## 1- المقدمة:

يعرف التآكل (Corrosion) بأنه تلف جزئي أو كلي يحدث للمعدن أو السبيكة من حيث المظهر أو الاداء بسبب التفاعل الذي يحدث بين المعدن أو السبيكة مع الاجواء المحيطة به سواء كانت غازية أو سائلة، وهناك عوامل كيميائية وفيزيائية كثيرة تؤثر على معدلات التآكل مثل تركيز الاملاح والغازات المذابة والحرارة وغيرها (الكيلاني، 2008). التآكل ظاهرة نراها في حياتنا اليومية، فمثلاً طبقات وترسبات ذات لون اصفر على الارض النحاسية كذلك ظهور طبقات على نوافذ وابواب المنازل المصنوعة من فلز الحديد، كل هذه الظواهر هي في الحقيقة نتيجة تأكسد (أي تأكل) الفلز أو السبيكة بسبب تعرضه للظروف المحيطة. ويعد التآكل احدى المشاكل التي تتعرض لها وتعاني منها الكثير من المنشآت البترولية كخطوط نقل البترول والغاز والخزانات وابراج التقطير كما يحدث في الكثير من القطاعات الاخرى الهامة كقطاعات الصناعة والنقل البحري. وذلك لان التآكل يحدث تلف شديد في هذه المنشآت مما ينتج عنه تكاليف ضخمة تتمثل في فواقد الانتاج وبالتالي قلة الكفاءة بالإضافة الى تكاليف تطبيق اساليب مقاومة التآكل. ولاشك في ان البيئة لها دور كبير في تنشيط التآكل اذا كانت تحمل عناصر مساعدة للتآكل. فمياه البحر مثلاً فيها اكثر من سبعين عنصراً اهمها ايونات كلوريد الصوديوم والكالسيوم وايضاً الكبريتات، وهي تشكل اكثر من 99% بالوزن من الاملاح الذائبة. كذلك التربة المذابة فيها املاح ومواد عضوية مختلفة تحتوي على انواع كثيرة من البكتريا. كذلك المياه الطبيعية (مياه الانهار ومياه الابار ومياه تحت طبقات الارض وغيرها). تحمل معها املاح الكربونات والبيكربونات، كذلك الهواء قد يحمل معه ذرات مختلفة من الغبار واملاح الصوديوم وغاز ثنائي اكسيد الكاربون والرطوبة واخيراً مختلف المواد الحمضية بأنواعها هي بيئات نموذجية للتآكل (Schweizer, 1996). يرى العلماء ان السبب الأساسي لتآكل المعادن واختلاف معدلات التآكل بين معدن وآخر، يعود إلى منشأ هذه المعادن وخواصها ومكوناتها، معظم المعادن، وخاصة المعادن غير الثمينة مثل الحديد والزنك، لا تتواجد في الطبيعة كمعدن نقي ولكن على شكل مركبات كيميائية مثل الأكاسيد والكربونات والكبريتات والتي تسمى عادة بخامات هذه المعادن، وعند استخلاص المعادن النقية من هذه الخامات لابد من بذل مقدار من الطاقة، وبذلك فإن المعدن النقي سوف يكون مجبراً على التواجد في حالة تختلف عن الحالة التي كان عليها في الطبيعة، لذا فإنه يميل إلى ترك هذه الحالة الجديدة المفروضة عليه والعودة إلى الحالة الأصلية أي إلى الخام، هذا في اطار عملية تسمى بالتآكل (Corrosion) (الخرجي وآخرون، 2010). لهذا السبب تمكن العديد من العلماء والباحثين من تحضير طلاءات من مواد متراكبة ذات مواصفات هندسية دقيقة والتي تمتاز بالكفاءة العالية تبعاً لنوع المادة الاساس ومادة التسليح والتكنولوجيا المستخدمة بشكل تعمل على منع أو تقليل التلف الذي يصيب الفلزات وسبائكها وجاءت بحوثهم لتسليط الضوء قدر المستطاع على اهمية هذه المواد وخواصها الميكانيكية والكيميائية والحرارية. ففي عام 2013 قام الباحث (AL-Atia) باستخدام محاليل جيلاتينية في ترسيب طبقة طلاء سيراميكية نانوية على سطح الفولاذ المقاوم للصدأ بغية تطوير خصائصه البيولوجية زيادة مقاومته للتآكل والبلى. حيث قام بترسيب طبقة طلاء مفردة من الالومينا على نماذج من اربعة محاليل جيلاتينية حضرت بإذابة ايزدبروكسايد الالمنيوم في الماء بتركيز مختلفة من الالومينا. حيث بينت النتائج امكانية الحصول على خصائص حماية واضحة تسهل المقارنة بين انواع الطلاء الرقيق المترسب على اسطح الفولاذ المقاوم للصدأ بطريقة المحلول الجيلاتيني (Al-Atia, 2013). في عام 2013 قامت الباحثة (Huda) وآخرون بتحويل و معالجة راتنج الايبوكسي مع بعض المواد المضافة والحشوات مثل السليكا المتطايرة حيث يتراوح قطر الدقائق ما بين (65-55) نانوميتر، دقائق اوكسيد الحديد بمعدل قطر 0.4 مايكرومتر، ملدن، دقائق كاربونات الكالسيوم بمعدل قطر

0.65 مايكرومتر لغرض الحصول على مادة متراكبة راتنجية . ولقد أظهرت النتائج المختبرية ان المادة المركبة ذات قوة صدمة و قوة صلادة عالية اضافة الى امكانياتها على مقاومة انحلالها في الماء، المادة المركبة الجديدة تم تطبيقها لاجراض طلاء الاسطح والقطع المعدنية المستخدمة في صناعة الزوارق والقطع البحرية لغرض حمايتها من التآكل , كذلك استخداماتها بما يتلاءم مع بعض التطبيقات التي تدخل في طلاء الناقلات والانابيب النفطية (AL- Pana, et al, 2013). استخدم الباحث (Fadhil) وآخرون في عام 2014 تقنية الرش الحراري لغرض طلاء نماذج من سبائك الفولاذ منخفض السبائكية والتي تستخدم في برج حفر الابار النفطية والغازية استخدم نوعين من المواد السيراميكية كمادة طلاء لمجموعتين من نماذج الفولاذ منخفض السبائكية حيث كانت الاولى زركونيا والثانية الالومينا كذلك استخدم مسحوق متراكب من النيكل -الألمنيوم كمادة رابطته. تم دراسة الصلادة وممانعة الالتصاق لطبقات الطلاء بالإضافة الى معدل البلى للمجموعتين ومقارنتها مع النماذج غير المطلية أظهرت النتائج زيادة في الخواص الميكانيكية ونقصان بقيم معدل البلى للنماذج المطلية مقارنة مع النماذج غير المطلية (Fadhil, 2014). اما الدراسة الحالية فهي تهدف الى تقليل من الآثار السلبية الناتجة عن تراكم الابخرة والغازات الحامضية والقاعدية المتدفقة بكميات كبيرة من المكونات النفطية في مادة ابراج التكرير باستخدام طلاءات من مواد متراكبة ذات اساس سيراميكي نوع سليكات الصوديوم (الزجاج المائي) المدعمة بالكرافيت المايكرومي مرة والكاربون الاسود النانوي مرة اخرى كاسلوب لزيادة مقاومة مادة البرج (سبيكة الفولاذ المقاوم للصدأ 304) للتآكل وبذلك اطالة العمر التشغيلي لهذا البرج. كما تهدف هذه الدراسة الى معرفة مدى الانحراف الحاصل في بعض الخصائص الميكانيكية والكيميائية والحرارية للطلاءات السيراميكية المحضرة بفعل تغير نسبة مواد التدعيم الوزنية ما بين (5-1%) لتحديد افضل نسبة تسبب تضاول قدرة هذه الابخرة الحمضية والقلوية على تآكل مادة البرج ومن جانب ثاني خصائص ميكانيكية وحرارية جيدة وعلى وجه التحديد مقاومة البلى والصلادة السطحية ومعامل التوصيل الحراري وقوة الالتصاقية فكلما كانت مادة الطلاء ذات قوة التصاق وصلادة عالية كلما ساعد ذلك في عزل مادة البرج عن الابخرة النفطية.

### معلومات توصيفية نظرية :

#### **1-2 الفولاذ المقاوم للصدأ Stainless Steel**

سبائك الفولاذ المقاوم للصدأ يمكن ان تعرف بأنها السبائك الحاوية على اكثر من 12% من Cr. لان نسبة 12% من الكروم تمثل ادنى قيمة لازمه لمنح سبائك الفولاذ مقاوميه كافيه للتآكل بواسطه تكوين طبقة الاوكسيد الخامدة (Passive Oxide Film) على السطح (علم المواد الهندسية، تر، الخزرجي وآخرون 2010) (Kutz, 2002). وسبائك الفولاذ المقاوم للصدأ يمكن ان تصنف الى ثلاث مجاميع رئيسيه (الخزرجي وآخرون 2010).

(1) صنف الفريت (Ferrite Grad، 2) صنف المارتنسايت (Martensite Grad، 3) صنف الاوستنايت (Austenite Grad).

#### **2-2 الفولاذ المقاوم للصدأ 304**

وهو الصلب الاوستنايتي ذو التركيب الكيميائي موضح في الجدول رقم (1) (Totten and Howes, 2002). ان وجود نسبة 18% من الكروم في هذه السبيكة يجعلها اكثر مقاومه للأكسدة والتآكل. وكذلك وجود نسبة 8% من النيكل يجعلها مقاومه للتآكل الناجم من المواد الكيميائية (Murray, 1997).

### 3-2 التآكل الكهروكيميائي للمعادن (Electro- Chemical Corrosion of Metal)

ينشأ هذا النوع من التآكل نتيجة ظهور التيار الكهربائي بسبب التفاعل بين المعدن والالكترونيات المحيطة به. تتفصل الايونات الموجبة عن سطح تلامس المعدن وتنتقل الى الوسط المجاور الذي يسمى بالالكتروليت ،. حيث يسمى فرق الجهد المتكون عند سطح تلامس المعدن مع الالكتروليت بالجهد القطبي وهو الدال على مدى ميل المعدن للذوبان، اذ المعادن ذات الجهد الموجب تكون قابليتها للتآكل قليلة اما المعادن ذات الجهد السالب تكون اكثر قابلية للتآكل (الخرجي واخرون، 2010).

#### 4-2 طرق تجنب التآكل:

لا يمكن من الناحية العملية منع التآكل منعاً تاماً الا باحتياطات وتحت ظروف قاسية لا يسهل ايجادها. الا انه يمكن تحسين مقاومة الفلزات والسبائك للتآكل بوسائل عديدة، وبالتالي يمكن حماية المنشآت الصناعية وإطالة عمرها، وهذه بعض الطرق الهامة المتبعة (Schweizer, 1996):

- 1) اختيار التصميم المناسب
- 2) تعديل نوعية المعدن
- 3) تعديل وتغيير وسط التآكل
- 4) التغليف المعدني
- 5) الحماية الكاثودية
- 6) التغطية Coating

#### 5-2 التغطية Coating

الغرض من التغطية هو تكوين غشاء مكون من مادة عازلة للكهرباء على سطح المعدن المراد حمايته عن الوسط الالكتروليتي الملاصق له والمحيط به وكذلك اعتراض الدائرة (الانودية- الكاثودية) عن طريق ذلك الغشاء ذو المقاومة الكهربائية العالية وبالتالي يضمحل بل يكاد يتلاشى تيار التآكل ، عموماً يجب التأكد هنا من الخصائص التالية لمواد التغطية بأن تكون : جيدة التلاصق، تقاوم اجهادات التربة، لها مقاومة ضد الماء، لها مقاومة كهربائية عالية. كما ان طرق التغطية بالتغليف انواع منها:

- التغطية بشرائط البلاستيك: تستعمل لتغطية المواسير المدفونة تحت الارض وتستعمل عادة شرائط بلاستيك مصنوعة من البولي اثلين عالٍ ومنخفض الكثافة، وكذلك شرائط قطران الفحم.
- التغطية بالدهانات: يوجد نوعان: الاغطية العضوية (البويات المانعة للتآكل) وزجاج السيراميك (الاجطية الغير معدنية الغير عضوية)(الكيلاني، 2008).

#### 6-2 طلاء السيراميك Ceramic coating

استعملات السيراميك عديده حيث يستعمل لحمايه الاجزاء المصنوعة من المعادن ومواد البناء الاخرى من التآكل، ومن تأثر درجات الحرارة العالية وكذلك الحك والسوفان العالي مثل النوزلات Nozzles والمشاعل Burners وأيضاً الاجزاء التي تتعرض للزجاج والمعادن الذوابة حيث تزيد مقاومة هذه الاجزاء للحك عند جريان هذه المواد ولدرجات الحرارة العالية التي تتعرض لها. ان عملية الطلاء بالمواد السيراميكية تتم بعدة طرق ومنها طريقه الغمس او التغطيس Dipping ، التريذ بالبلازما Plasma spraying، السول جيل Sol-Gel، عمليه الترسيب الفيزيائي للبخر او الترسيب الكيميائي للبخر. حيث ان الاجزاء التي تتم طلاءها بالسيراميك هي الفولاذ ومواد البناء والمواد غيرالفلزية(الكيلاني، 2008).

## 7-2 المواد المتراكبة ( Composite Materials )

المتراكبات بصورة عامة هي عبارة عن مزج مادتين أو أكثر للحصول على مادة جديدة ذات خواص تختلف عن خواص المواد الداخلة في تكوينها في كونها احسن جودة ومميزة فيزيائياً وكيميائياً ولذلك فهي تصنف حسب نوعية المادة الاساس (الطور المضيف Matrix) الى متراكبات (بوليميرية ، معدنية، سيراميكية) وحسب نوعية المادة المدعمة (طور التقوية) (Reinforcement) الى متراكبات مدعمة (بالألياف، بالحشوات، بالقشور، بالدقائق) مرة أخرى (Broutman and Krock, 1978).

## 8-2 التقوية بالدقائق (particulate Reinforcement).

تختلف المتراكبات المدعمة بالدقائق عن تلك المدعمة بالألياف أو القشور في توزيع المضافات، إذ إن توزيع الدقائق يكون عشوائياً أكثر مما هو منتظم، لذلك فإن المتراكبات الدقائقية تمتلك خواصاً موحدة متماثلة في جميع الاتجاهات (Isotropic). ويمكن اجمال أنواع المتراكبات الدقائقية كما يلي:

### 1) المواد المتراكبة المدعمة بالتشتيت (Dispersion Composites)

في هذا النوع من التدعيم يكون معدل قطر الدقائق اقل من  $(0.1 \mu m)$ ، والتي تعمل على تقوية مادة الاساس عن طريق اعاقه حركة الانخلاعات خلال عملية التشوه اللدن، ويستخدم هذا النوع من المواد المتراكبة في صناعة المكابس واذرع التوصيل.

### 2) المواد المتراكبة المدعمة بالدقائق (Particulate Composites)

في هذا النوع من التدعيم يكون معدل قطر الدقائق اكبر من  $(1 \mu m)$ ، ويستخدم هذا النوع من المواد المتراكبة في صناعة رؤوس اقلام القطع (Caiiister, 2003).

## 3- الجزء العملي:

### 1-3 المواد المستعملة:

#### أ- المادة الاساس Matrix Material

المادة الاساس المستعملة في العمل الحالي هي سليكات الصوديوم (Sodium Silicate) الزجاج المائي المنتجة محلياً من مخلفات الزجاج للشركة العامه لصناعه الزجاج والسيراميك، اللزوجه Viscosity عند درجه حراره  $(30^{\circ}C)$  هي 1.426 سنتي بوايز، نسبة ال  $NaO_2$  هي 13.92 %، نسبة ال  $SiO_2$  هي 29.5%

#### ب- مواد التدعيم (التقوية) Reinforcement Material

استعمل نوعان من مواد التدعيم لتقوية سليكات الصوديوم وهي:

##### 1- مسحوق النانو كاربون Carbon Nano Pawder

بحجم حبيبي  $< 50 \text{ nm}$  امريكي المنشاء ، اسود اللون عديم الرائحة.

##### 2- مسحوق الكرافيت Graphite Powder

بمعدل قطر دقائق  $< 38 \mu m$  وهو شكل من اشكال الكاربون المتأصلة.

## 2-3 تحضير النماذج:

تضمنت عملية تحضير النماذج ثلاثة مراحل وهي:

أ- تقطيع سبيكة الفولاذ المقاوم للصدأ 304 بمكائن خاصة بأبعاد تناسب اجهزة الفحص المستخدمة، ثم تنضيف العينات بواسطة جهاز الصقل باستخدام اوراق الصنفرة بحجم 50P المصنوعة من اوكسيد الالمنيوم لمدة 5Min

- ب- تهيئة سليكات الصوديوم  
لجعل سائل سليكات الصوديوم ذو لزوجة مناسبة يسهل عملية خلطه بمواد التدعيم بشكل متجانس بتسخينه الى درجة حرارة ( $100^{\circ}\text{C}$ ) في بيكر بواسطة جهاز (Hotplate Stirrer) سرعه 5 دوره/الدقيقة لمدة ساعه واحده.
- ج- تضاف دقائق الكرافيت بنسب مختلفه تتراوح (5-1%) الى سليكات الصوديوم المعد وفق الخطوة (أ) ولمدة (25) دقيقة مع بقاء سرعة جهاز (Hotplate Stirrer) (5 دوره/الدقيقة) وبدرجة حرارة ( $50^{\circ}\text{C}$ ) .
- ونعود الى تكرار الخطوات السابقة ولكن مع اضافة الكربون النانوي وبنفس النسب مع استمرار عملية الخلط لمدة (15) دقيقة.
- د- تطلى عينات الفولاذ المقاوم للصدأ باستخدام قالب قاعدته بلاستيكية تثبت عليه قطعه الفولاذ وتحاط من جهاته الاربعه بمادة زجاجية.

### 3-3 الاجهزة المستخدمة:

- 1- مجهر القوة الذرية تم اجراء الفحص باستخدام جهاز (Scanning probe microscopy (CSPM- (5000)).
  - 2- جهاز روكويل لقياس صلادة الفولاذ المقاوم الصدأ 304 وجهاز Shor-D لقياس الصلادة السطحية لطلاءات الزجاج السيراميكي ومتراكباته ذو المنشأ ايطالي.
  - 3- جهاز مقاومة البلى (Wear) العراقي المنشأ بتسليط حمل مقداره (0.5 kg) وسرعة دوران 500 دورة/ الدقيقة ولمدة (1Min) وينصف قطر انزلاقي مقداره (7cm).
  - 4- جهاز قوة الالتصاقية ذو المنشأ الياباني.
  - 5- جهاز قياس سمك النماذج (Posi Tectir) ذو المنشأ امريكي.
  - 6- جهاز قياس التآكل الكهروكيميائي بطريقة تأكل ذو المنشأ الالمانى.
- بعد تحضير المتراكبات اجريت الفحوصات التالية:
- (1) فحص مجهر القوة الذرية. (2) اختبار الصلادة السطحية. (3) اختبار معدل البلى . (4) اختبار قوة الالتصاقية .
  - (5) اختبار التآكل الكهروكيميائي. (6) اختبار الموصلية الحرارية.
- ان من الجدير بالذكر ان جميع الفحوصات السابقة الذكر تأخذ النتائج مباشرة من الجهاز الفاحص الا ان مقاومة البلى يتم الحصول عليها باحتساب معدل البلى من القانون التالي (Wiely and Sons 1965):

$$\text{Wear rate} = \Delta W / S_D \text{ (gm/cm)} \quad (1)$$

علماً أن:  $\Delta W$  - الفرق بالكتلة للعينة قبل وبعد الاختبار (gm).

$$\Delta W = w_1 - w_2 \quad (2)$$

$S_D$  : - مسافة الانزلاق (cm) وتحسب من العلاقة:

$$S_D = 2\pi r n t \quad (3)$$

علماً أن:-

$r$  :- نصف قطر الانزلاق (cm).  $n$  :- عدد دورات القرص (دورة/دقيقة).  $t$  :- مدة الاختبار (دقيقة).

### 3-4 اختبار حقلي (ميداني):

ان الاختبارات الحقلية يمكن اعتبارها مقياسا لكفاءة المواد المحضرة ، تم اجراء اختبارات لمقاومة الطلاءات المتراكبة المحضرة للتآكل الكيميائي بشكل يحاكي الواقع في وزارة النفط/ مركز البحث والتطوير النفطي.

### 4- النتائج والمناقشة:

#### 4-1 فحص مجهر القوة الذرية (AFM) Atomic Force Microscope

يوفر مجهر القوة الذرية معلومات حول بنية السطح ويتبين من الاشكال (1) و (2) مورفولوجيا Morphology السطح والتي يظهر فيها سطح طبقة مادة الطلاء المكونة من سليكات الصوديوم المدعمة بالكرافيت مرة، والكربون النانوي مرة اخرى، بأشكال غير منتظمة والتي تتوزع بشكل عشوائي على السطح بأكمله. حيث اظهرت نتائج الاختبار ان مربع متوسط الجذر والخشونة Root Mean Square (RMS) Roughness لسطح مادة الطلاء المكونة من سليكات الصوديوم المدعمة بالكرافيت مرة والكربون النانوي مرة اخرى تزداد مع زيادة نسب التدعيم من (1-5%) كما موضح في الجدول (2) .

#### 4-2 اختبار الصلادة السطحية Hardness Test

لوحظ من الجدول (3) ان قيم الصلادة تبدأ بالانخفاض بعد الطلاء بسليكات الصوديوم مقارنةً بسبيكة الفولاذ المقاوم للصدأ 304 ثم ترتفع تدريجياً بعد تغليفها بطلاءات من متراكبات سليكات الصوديوم ارتفاعاً يصل الى ادنى قيمة له عند نسبة التدعيم 1% بمقدار (66.75NO.) بالنسبة لمتراكبات سليكات الصوديوم المدعمة بمسحوق الكرافيت بينما تصل قيمة الصلادة الى (82.36 NO.) عند نفس النسبة الوزنية باستبدال مسحوق الكرافيت بالكربون النانوي. مما يؤكد التأثير الايجابي لعملية التدعيم بهذا النوع من الدقائق وذلك لما تمتلكه من الخصائص على سد وتقليل الفجوات والفراغات المتكونة اثناء عملية القولية مما يزيد في معامل المرونة للمادة ويزيدها صلادة علاوة على ذلك اعاقا امتداد الشروخ وهذا الميل يعني زيادة المساحة السطحية للشروخ، ومع ذلك فأن زيادة المساحة غير كافٍ لتقدير الارتفاع الحاصل في المتانة (هناك محمد، 2015). والشكل (3) يشير الى تفوق مضافات التدعيم نوع النانو كربون على الكرافيت المايكرو بمقدار (15.61NO.) بالمقارنة مع طلاء سليكات الصوديوم عند نسبه 1% فتتحسن صلاده سليكات الصوديوم، وذلك لان الخصائص الميكانيكية للمواد تتحسن عند استخدام الدقائق ذات الحجم الصغير جداً اقل من 50 مايكرون اذ ان الدقائق الصغيرة اثناء عملية التصنيع تكون سهلة التغلغل الى داخل المادة الاساس المتمثلة بسليكات الصوديوم والى داخل الفراغات البينية والمسامات والتي تتكون اثناء عملية التحضير المتراكب، والذي يؤدي بدوره الى زيادة مساحة التماس ما بين مكونات المادة المتراكبة المحضرة ومن ثم زيادة الترابط فيما بينهما وبشكل متكامل مما يعطي قيم اكثر ايجابية في زيادة مقاومتها للصلادة نتيجة زيادة مقاومتها للتشوه اللدن (اريج رياض وآخرون 2011) . ومع زيادة النسبة الوزنية لمضافات التدعيم ما بين (1-5%) ادت هذه الزيادة الى حصول ارتفاع في قيم صلادة سليكات الصوديوم وصولاً الى نسبه 4% بالنسبة لسليكات الصوديوم المدعة بمسحوق الكرافيت المايكرو، بينما يستمر الارتفاع في قيم الصلادة لسليكات الصوديوم المدعمة بالكربون النانوي الى نسبه تدعيم 5%. ولا شك ان السبب في زيادة قيم الصلادة للنماذج المحضرة بإضافة الكرافيت الى سليكات الصوديوم الى اعلى

قيمه لها عند 4% حيث بلغت (79.8 NO.) هو ان دقائق التدعيم تؤدي الى اعاقه حركه الانخلاعات وحدوث التقوية وامكانية الدقائق على مشاركته طور الاساس في تحمل القوى والاجهادات المسلطة عليها وهذا يتفق مع ما جاء به الباحث (Higgins, 1973). وعلى الرغم من الدور الايجابي للتدعيم في تحسين صلادة المتراكبات المحضرة الا ان الاستمرار بزيادة النسبة المئوية للكرافيت الى 5% يسبب في هبوط صلادة سليكات الصوديوم الى (75.6 NO.) وذلك بسبب ما تخلقه من تركيز للإجهادات غير المرغوب بها حولها، بدرجة تقود الى تكوين فجوات Cavities والتي تظهر بمظهر التشققات cracks وبالتالي نقصان متانه المتراكب ونقصان في معامل مرونتها، وهذا التفسير استناداً ما جاء به (Pand and Sharma, 1973) و (Abdul Saheb, 2011) ومن ثم يكون سبباً لنقصان صلادة المادة المتراكبة. وفي دراسة للباحث (Subhranshu and Smurtisih, 2008) ذكر ان اضافة الكاربون النانوي يغير الحجم الحبيبي للمادة الناتجة وبالتالي فأن قيم الصلادة تتغير حيث ان التغيرات الحاصلة في المادة الناتجة كبيره وتؤثر على الخواص الميكانيكية للمتراكب الناتج وعليه فأن وجود مسحوق الكاربون النانوي في جسم السيراميكي (سليكات الصوديوم) يعمل على رفع الصلادة نتيجة لزيادة المقاومة للتشوه اللدن والذي امتد الى نسبة 5%، حسب زيادة التداخل والتراص والذي يعرض حركه جزيئات سليكات الصوديوم الى الانخفاض، الامر الذي يؤدي الى زيادة المقاومة للخدش (Scratching) والقطع والتشوه اللدن (Nassier, 2013).

#### 3-4 اختبار معدل البلى Wear Rate

يوضح الجدول (4) زيادة معدل البلى لمادة سليكات الصوديوم غير المدعمة على سبيكة الفولاذ المقاوم للصدأ 304 غير المطلية بسليكات الصوديوم بمقدار ( $8 \text{ gm/cm}^3 * 10^{-8}$ ) في حين ينخفض معدل البلى عند طلاء السبيكة بهذه المادة اللاصقة المدعمة بالكرافيت عن السبيكة بدون طلاء بحوالي ( $8 \text{ gm/cm}^3 * 10^{-8}$ ) عند التدعيم بأفضل نسبة من الكرافيت ويستمر معدل البلى بالانخفاض اكثر بعد طلاء السبيكة بسليكات الصوديوم المدعمة بلكاربون النانوي عن السبيكة من دون تدعيم يقدر بحوالي ( $8 \text{ gm/cm}^3 * 10^{-8}$ ) عند التدعيم بأفضل نسبة من الكاربون النانوي. ويعزى سبب ذلك الى ان عملية الطلاء بسليكات الصوديوم فقط يصاحبها زياده شديده في التشوه اللدن وتكسر في الطبقات تحت السطحية (Subsurface- Layers) وعند تدعيمها بدقائق الكرافيت المايكرو والكاربون النانوي تعمل المادة الدقائقية كعوائق لتشوية المادة الاساس (سليكات الصوديوم) في اثناء التحميل بسبب صلابتها العاليه خصوصاً وانها تؤدي الى زياده جساءه الجسم السيراميكي ومتانته علاوة على تحسين معامل تمدده الحراري (Subhranshu and Smurtisih, 2008).

الا ان الشكل (4) يشير الى تفوق مضافات التدعيم نوع نانو كاربون على الكرافيت المايكرو بمقدار ( $8 \text{ gm/cm}^3 * 10^{-8}$ ) عند النسبه 1% مثلاً في تحسين مقاومه البلى لسليكات الصوديوم، نظراً لقدرة الدقائق النانويه بحجمها الصغير على خفض معدل البلى والذي نستنتج منه بأن مقاومة البلى ترتبط بشكل مباشر بمتانة وتماسك المتراكب بعلاقه طردية وكلما تحسن ارتباط او تماسك الكتل المتراكبه كلما انخفض معدل البلى او فقدان المادة، اذ ان اضافة الدقائق النانوية والتوزيع المنتظم لتلك الدقائق يقلل المسافة بين الجسيمات او الجزيئات وبالتالي تزداد مقاومة المادة للبلى والخدش لان المادة اصبحت اكثر تراص (Gautam, 2015).

كما نلاحظ من المنحنيات المعروضة بالشكل (4) انخفاض معدل البلى لسليكات الصوديوم المدعمة بدقائق الكرافيت بزيادة نسبة المواد المضافة حيث بلغت اعلى قيمة لمقاومة البلى ( $8 \text{ gm/cm}^3 * 10^{-8}$ ) عند النسبه الوزنيه 4% وذلك لان حبيبات الكرافيت لها قدرة عالية على ان تعمل كمزيت (Antifriction Material) تحت ظروف التشغيل الجافة حيث لا تملك ايه قيمة لمعامل الاحتكاك أي يكون معامل الاحتكاك قريباً للصفر وفي هذه الحالة قد



نتوقع ان تكون درجه حرارة السطح المحتك واطئة نسبياً اذ قورنت بدرجة حرارة السطوح المعدنية اوالسيراميكية ببعضها، علاوة على ذلك ان حبيبات الكرافيت تملك قدرة عالية على تبريد نفسها وبذلك تساهم في تقليل معدل البلى (سعد حميد واخرون 2009) (اسراء عبد القادر وياقر، 2009). ولكن من المؤكد ايضاً ارتفاع النسبة الوزنية اعلى من 5% يؤدي الى ضعف مقاومة البلى وذلك لان هذه الاثار تمت بصلة مباشرة مع المتانة والتماسك الميكانيكي للمركب كما هو مذكور سابقاً. بينما في نطاق سليكات الصوديوم المضاف لها دقائق الكاربون النانوي تزداد مقاومة البلى مع زياده النسبة المئوية حيث بلغت اعلى قيمه لها حوالي  $(0.5 \times 10^{-8} \text{ gm/cm})$  ضمن النسبة 5% للأسباب السابقة الذكر.

#### 4-4 اختبار قوة الالتصاق Adhesive Test

بصورة عامة يحدث الفشل في المادة اللاصقة سليكات الصوديوم غير المدعمة الخاضعة لفحص السحب اومتانته اللصق بتحطيم الارتباطات والقوى المسؤلة عن ميكانيكية الالتصاق وفيها مايلي:

قوى فاندروالز (Vander Wall) والتي تكون اكثر فعالية بين اللواصق (Adhesive) والمادة الملصوقة (Substrate)، وقوى الترابط الكيميائي (Chemical Bonding) والتي تعطي نوع من التقوية للالتصاق والذي يتحقق عندما تمتلك المادة المتأثرة (Substrate) مجاميع كيميائية (Chemical Groups) تتفاعل مع اللاصق (Adhesive)، وقوى التشابك الميكانيكي (Mechanical Inter Locking) (رولا عبد الخضر، 2007).

الا ان لطبيعة المواد اللاصقة والمادة المتأثرة (الملصوقة) تأثير كبير على القوى السابقة الذكر، فمع اضافة حبيبات الكرافيت المايكرو مرة والكاربون النانوي مرة اخرى الى المادة اللاصقة (سليكات الصوديوم) تزداد متانته الالتصاق كما هو موضح في الجدول (5). لما تمتلك هذه الدقائق من خصائص سابقة الذكر. علاوة على ذلك لخشونة المادة تأثير كبير على متانة اللصق للمقطع مربوط حيث تختلف النعومة المثالية للربط باختلاف المادة ونوعها وطريقه تصنيعه (Buz, 1993). اذ بينت النتائج المستحصلة من مجهر القوة الذرية كما هو مبين في الجدول (2) ان خشونة مادة الطلاء (سليكات الصوديوم) تزداد مع زيادة نسب التدعيم، لذلك تزداد متانة اللصق لمادة سليكات الصوديوم المدعمة بالكرافيت مع زيادة نسب التدعيم من (5-1%) لتصل الى اعلى قيمة لها (3.45Mpa) عند النسبة 5% كما هو موضح في الشكل (3). حيث تهشمت المادة الصمغية المستخدمة في الفحص (لاصق الجهاز) ولم تتفصل طبقة الطلاء عن سطح السبيكة برغم من تكرار الاختبار عدة مرات وهذا يدل على جودة اللصق لجميع العينات (صالح كريم 2010). وبعد ان تبين الدور الايجابي لخشونة سطح الطلاء في زيادة قوة الالتصاق وهذا ما تميزت به سليكات الصوديوم المدعمة بدقائق الكرافيت المايكرو. الا ان متراكبات سليكات الصوديوم المدعمة بمسحوق النانو كاربون تظهر عكس ذلك، حيث تزداد خشونة المادة مع زيادة نسب التدعيم لكن متانته اللصق تزداد مع زيادة نعومة طبقة الطلاء حيث كانت اعلى قيمة لمتانة اللصق (4Mpa) عند النسبة 1% كما هو موضح في الشكل (5). ان سبب زياده متانته اللصق مع زيادة النعومة يرجع الى ان مواضع سليكات الصوديوم المدعمة بالكاربون النانوي عند السطح تكون بمثابة مخازن لمادة لاصق جهاز مقياس قوة اللصق وتزداد ازاله المادة المركبة من السطح ليحل محلها لاصق الجهاز الذي ادى الى زياده في قوة اللصق مع زياده النعومه وهذا يتفق مع (صالح كريم 2010).

#### 4-5 اختبار مقاومة التآكل الكهروكيميائي Electrochemical corrosion

اوضحت النتائج المستحصلة من هذا الاختبار جدول تغير كثافة التيار لكل نوع من انواع الطلاءات المحضرة مقارنة مع السبيكة المراد تغليفها بهذه الطلاءات، وهذا يعني ان كثافة التيار هو مقياس لمقاومة التآكل الكهروكيميائي علاوة على جهد التآكل (السالبية). وتشير المعلومات العملية المستحصلة من الجدول (6) أن كثافة التيار لمادة الطلاء نوع سليكات الصوديوم وصلت الى  $(5.77 \text{ nA/cm}^2)$ ، وهذا يدل على تحسن مقاومة التآكل

بشكل كبير جداً مقارنةً مع السبيكة من دون طلاء، ويعود ذلك الى تكوين جلاتين السيلكا نتيجة سلسلة من التفاعلات بين حامض الهيدروكلوريك وسليكات الصوديوم وتكون طبقة او قشرة تعمل مع مرور الزمن على حماية السطح من الخارج (العبيدي، 2009)، فضلاً عن تكون املاح الصوديوم كنتيجة للتفاعل حامض الهيدروكلوريك مع مكونات السيلكا لتكوين طبقة قلووية (Thomas, 1999). كما ان عملية الطلاء بسليكات الصوديوم المدعمة بدقائق الكرافيت المايكروبي بنسب تدعيم من 1% الى 5% قد اعطت افضل النتائج، اذ اظهرت تحسن ملحوظ في مقاومة السبيكة للتآكل مقارنةً مع السبيكة من دون طلاء وايضاً مع السبيكة المطلية بمادة سليكات الصوديوم وحدها او من دون تدعيم وهذا يمثل زيادة في تحمل السبيكة واطالة عمرها التشغيلي وبطريقة اقتصادية وذلك لان سليكات الصوديوم والكرافيت مواد رخيصة الثمن ، اذ ينخفض التيار مع زيادة نسب التدعيم حتى يصل الى اقل قيمه له ( $1.06 \text{ nA/cm}^2$ ) عند نسبه تدعيم 3% وجهد التيار ( $-94.1 \text{ mv}$ ) كما موضح في الشكل (6). ان انخفاض كثافة التيار لمادة الطلاء هذه بالمقارنة مع الفولاذ غير المطلي بحوالي ( $868.55 \text{ nA/cm}^2$ ) يدل على المقاومة العالية لطبقة الطلاء وذلك لان الكرافيت يمتاز بمقاومة جيدة للتآكل في الاوساط الحامضية والمركبات العضويه وغير العضويه لذلك فوجوده ادى الى تحسن في مقاومة المادة للتآكل، ويمكن اعتبار التآكل الكهروكيميائي الحاصل في طبقة الطلاء شرح من خلال تشكيل اكاسيد الكاربون على السطح في مواقع منفصلة (Iken and Basseguy, 2007). كما ان جهد التآكل للفولاذ غيرالمطلي اكثر سالبية (أي بمعنى اقل جهد تآكل) من الفولاذ المطلي بسليكات الصوديوم المدعمه بلكرافيت الفرق حوالي ( $47.2 \text{ mv}$ ) وهذا يعني ان وجود دقائق الكرافيت تجعل طبقة الطلاء اكثر نبلاً لضمان افضل حماية للخصائص (عبد الواحد كاظم وآخرون، 2010). اما عملية الطلاء بمادة سليكات الصوديوم المدعمة بدقائق الكاربون النانوي اظهرت تحسن بمقاومه التآكل مقارنةً مع سبيكة الفولاذ المقاوم للصدأ 304، ولكنها اعطت انخفاضاً في مقاومتها للتآكل مقارنةً مع السبيكة المطلية بسليكات الصوديوم من دون تدعيم، حيث تقل كثافته التيار مع زياده نسب التدعيم حتى وصل الى اقل قيمه لها ( $10.60 \text{ nA/cm}^2$ ) عند نسبه تدعيم 5% اذ انخفضت كثافته التيار بحوالي ( $859.55 \text{ nA/cm}^2$ ) بالمقارنة مع الفولاذ المقاوم للصدأ كما هو موضح في الشكل (6)، وذلك لان الكاربون يتأكسد ويكون ثنائي اوكسيد الكاربون عند تسليط فولتية اعلى من القيمة القياسية ( $0.207 \text{ v}$ ) (Sayyid et al 2015)، حيث ان وجود اوكسيد الكاربون تكون طبقة عازلة تمنع ذوبان المعدن واتحاده بالاكسجين وبالتالي توقف التفاعل او تقلله (Yu Liu, 2006). وكذلك ان جهد التآكل للفولاذ غير المطلي بطبقة الحماية يكون اكثر سالبية من الفولاذ المطلي بسليكات الصوديوم المدعمة بلكاربون النانوي الفرق حوالي ( $106.2 \text{ mv}$ ) وهذا يعني ان وجود دقائق الكاربون تجعل طبقة الطلاء اكثر نبلاً لضمان افضل حماية للخصائص (عبد الواحد كاظم وآخرون 2010).

#### 4-6 اختبار الموصلية الحرارية Thermal Conductivity

ظهرت النتائج المستحصلة ان طلاء سبيكة الفولاذ المقاوم للصدأ 304 بمادة سليكات الصوديوم ادى الى خفض التوصيلية الحرارية بمقدار ( $13.47 \text{ W/m.k}$ ) وانخفضت اكثر بعد تقوية طلاءات السليكات الصوديوم بمسحوق الكرافيت مرة والكاربون النانوي مرة اخرى، فقيمة (k) لسليكات الصوديوم غير المدعمة بالمسحوق تقدر ( $1.13 \text{ W/m.k}$ ) عند درجة حرارة الغرفة ( $23^\circ\text{C}$ ) في حين قيمتها لطلاء سليكات الصوديوم المدعمة بمسحوق الكرافيت ( $0.1909 \text{ W/m.k}$ ) و ( $0.09135 \text{ W/m.k}$ ) لمسحوق النانو كاربون عند النسبة 1% وكما مبين في الجدول (7) وذلك يعود الى حقيقة ان هذه المساحيق ذات تركيب مسامي وعالية عندما تحتوي الطلاءات المحضرة على فراغات هوائية فأنها تصبح ذات موصلية اقل لأن اسواء انواع الموصلات الحراريه هي الغازات (هناء محمد،

(2005). ومن الملاحظ من الشكل (7) ان طلاء سليكات الصوديوم المدعمة بمسحوق الكرافيت تتفوق في توصيلها الحراري على الطلاء المدعم بالنانو كاربون والتي تزداد مع زيادة النسبة الوزنية من 1% الى 5% بمقدار  $(0.9291 \text{ W/m.k})$ ، ويرجع ذلك الى مقاومة الكرافيت العاليه للصدمة الحرارية وارتفاع الموصلية الحرارية الذي ينجم عن ذلك زيادة متانتها بارتفاع درجات الحرارة مع ثباته النسبي مقارنة بمسحوق اسود الكاربون النانوي (Lee et al,2015).

ومن الطبيعي ان زيادة نسبة المواد المدعمة لطلاء سليكات الصوديوم سواء كان بمسحوق الكرافيت او الكاربون النانوي يعمل على زيادة الموصلية الحرارية فمثلاً زيادة نسبة الكاربون النانوي من 1% الى 5% يؤدي الى رفع الموصلية الحرارية لطلاء سليكات الصوديوم بمقدار  $(0.7956 \text{ W/m.k})$  من خلال زيادة الجزيئات المساهمة في تشكيل السلاسل والتجمعات الذي يميل الى تكوينها اسود الكاربون حيث مع زيادة نسبة الكاربون النانوي فأن الجزيئات تلامس بعضها البعض اذ تكون المسافة بين الجزيئات بضع او عدة نانومترا وبذلك فأن التركيب العالي لاسود الكاربون النانوي يبدء في تكوين سلسلة كاربونية موصلة (Carbon Conductive Chains) وبالتالي يعطي قيم توصيل حراري عالي (Abdul Razak et al,2009) (Hamza et al,2013).

## 5- الاستنتاجات:

ان هذه الدراسة اظهرت بأن هناك العديد من الخصائص التي تبين امكانية استخدام متراكبات سليكات الصوديوم كحاجز وقائي يفصل بين بطانة ابراج التصفية والابخرة الكيميائية للنفط الخام وعليه يمكن تمييز اربع استنتاجات وكالاتي تشير الى ما يلي:

1- تساهم مواد التدعيم الماكرويه وكذلك النانويه في زياده صلابه سليكات الصوديوم ومقاومتها للبلل التي تزداد بزيادة نسب التدعيم .

2- تسبب خشونة طبقة الطلاء في حدوث زيادة قوة التصاق هذه الطبقة على سطح بطانة ابراج تكرير البترول.

3- تتسارع مقاومة التآكل الكهروكيميائية لبطانة برج التصفية النفطية في التحسن مع كافة انواع الطلاءات المنجزة الا ان طلاء سليكات الصوديوم المدعم بـ 3% من مسحوق الكرافيت يعد ترتيبه الاول بين الطلاءات في مقاومة التآكل الكهروكيميائي.

4- تدعيم سليكات الصوديوم بالكرافيت المايكروي والكاربون النانوي ادى الى خفض التوصيلية الحرارية التي تزداد مع زياده نسب التدعيم.

**\*شكر وتقدير:** اتقدم بالشكر والامتنان الى جميع منتسبي مركز البحث والتطوير النفطي لجهودهم ودعمهم الكبير واخص بالذكر الاستاذ صلاح مهدي علي.

## 6- المصادر:

- 1- Abdul Saheb, D., "Aluminum Silicon Carbide and Aluminum Graphite Particulate Composites", Arppn Journal of Engineering and Applied Sciences", Vol.6, No.10, PP.45, 2011.
- 2- Abdul Razak, A. A., Salah, N. J. and W. Abdul Kazem, "Electrical and Thermal Properties of Epoxy Resin Filled With Carbon Black", Eng.&Tech. Journal, Vol.27, No.11, PP.(2223-2224), 2009.



- 3– Al –Atia, M. H. J., " Comprehensive Electrochemical Evaluation of Protective Coatings Properties by Sol–Gel Route for Stainless Steel Corrosion", Journal of Engineering and Technology, Vol 31,No.4,PP(71–72),2013.
- 4– Al Pana, H. A., Fakry, N. A. and Hussain. N.A, "Composite Resin Coating for The Protection of Surfaces and Metals", Iraqi Journal of Science, Vol. 54,.No .1, PP110,2013.
- 5– Broutman, L. J. and Krock, R. H., "Composite Materials", Mechanics of Composite Materials, Volume 2,1974.
- 6– Buz, K. T., "Recent advances in bonding to gold, amalgam and porcelain", Journal of Clin. Orthod, No. 27, PP (661–665), 1993.
- 7– Callister, W. D., "Materials Science and Engineering An Introduction", Sixth Edition, John Wiley and Sons, Inc., 2003.
- 8– Chyad, F. A., Hamood, A. F. and Faiq, L. S., " Effect of Thermally Sprayed Ceramic Coating on Properties of Low Alloy Steel", Journal of Engineering and Technology, Vol 32,Part A No.10,PP2568,2014.
- 9– Gautam,R. and kar, K.K., "The Effects of Nano– Sized Carbon Black Content and The Particale Size on The Properties of Carbon /Phenolic Composite Bipolar Plates", Journal of Multidisciplinary Engineering Science and Technology (JMEST), Vol.2, No.2, PP.(195–196),2015.
- 10– Hamza, M. S., Majeed, A. H. and Kareem, H. R., " Enhancing Thermal and Water Absorption Properties of Unsaturated Polyester and Epoxy by Nano carbon Black Powder ", Eng. &Tech. Journal, Vol.31,Part(A), No.12, PP.(2314–2315), 2013.
- 11– Higgins, R. A., "Engineering Metallurgy, London,1973.
- 12– Iken, H., Basseguy, R. and Guenbour, b. A. and Bachir, A. B.," Classic and local analysis of corrosion behavior of graphite and stainless steels in polluted phosphoric acid", Electro chemical Act 52 (2007).
- 13– Kutz, M., "Handbook of Materials Selection", John Wiley & Sons, 2002.
- 14– Lee, S. M., Su Kang, D. and Roh, J. S.," Bulk graphite materials and manufacturing process", Carbon Letters Vol. 16, No. 3,Pp 135, 2015.
- 15– Murray, G., "Handbook of Materials Selection for Engineering Applications", CRC Press,1997.
- 16– Nassier, A.H.N, "Studying The Effect of Nano carbon black on Mechanical Properties of Unsaturated Polyester Resin", "The Iraqi Journal for Mechanical and Material Engineering", Vol.13, No.4, PP.789, 2013.

- 17- Pand, J. and Sharma, D., "Fracture toughness of Short Glass Fiber and Glass Particles hybrid", Fiber and Technology, Vol.21, No.4 ,PP.(307-317) 2011.
- 18- Sayyid, F. F., Ali, A. M. and Tawfek, W. A, " Evaluation of Corrosion Resistance of Medium Carbon Steel Using Different Protection Methods ", Journal of Engineering and Technology, Vol 30, No.7, PP158, 2012.
- 19-Schweitzer, P. A, "Corrosion Engineering Handbook", Second Edition – 3 Volume Set, CRC Press,1996.
- 20- Subharnashu, S. S. and Smurutisikha, B., "Carbon Nanotube Ceramic Matrix Composites", Journal of Minerals & Materials Characterization &Engineering, Vol.7, Na.4,PP(366-367),2008.
- 21- Thomas, H., "Acid Resistant Cement Composition", U.S. patent No.5989330, 1999.
- 22- Totten, G. and Howes, M., " handbook of residual stress deformation of steel",Asm International, 2002.
- 23- Wiely, O. J. S., "fraction and wear of materials" Inc, New York (1965).
- 24- Yu Liu," Chemistry of Novel Nano Scale Carbon Materials: Nano Diamond and Carbon Nano-Onions",ProQuest Information and Learning Company, 2006.
- 25- الخزرجي، قحطان خلف، الشريف، عبد الجواد محمد، " التآكل "، مطبعة دار دجلة، الطبعة الاولى، 2010.
- 26 ترجمة: الخزرجي، قحطان خلف، الساعدي، عباس خماس الساعدي، صباح خماس، "علم المواد الهندسية"، مطبعة دار دجلة، الطبعة الاولى، 2010.
- 27- اريج رياض سعد ، سه وينج نور الدين، "دراسة الخصائص الميكانيكية لمترابكات البولي اثلين المدعم بدقائق مسحوق الصدف"، " مجله الهندسة والتكنولوجيا المجلد. 29 ، العدد.15، الصفحة. 611 ، 2011.
- 28- اسراء عبد القادر، مريم عبد العظيم باقر، " تأثير اضافته دقائق الكرافيت على مقاومه البلى ومعامل الاحتكاك لسبيكة البراص الفا"، مجلة الهندسة والتكنولوجيا المجلد. 27، العدد.9، الصفحة.23، 2009.
- 29- العبيدي، وليد يونس، "تحضير ماده رابطة مقاومة للحوامض اللاعضوية باستخدام صخور الكوارتزيت العراقي"، مجلة علوم الرافدين، المجلد 20، العدد 4، الصفحة 107، 2009.
- 30- الكيلاني، احمد رشيد محمد، " وقاية المعادن من التآكل"، مطبعة شركه الاديب ، عمان، 2008.
- 31- رولا عبد الخضر عباس، " تحضير مادة لاصقة مدعمة بدقائق الكرافيت ودراسة خواصها الميكانيكية والكهربائية والحرارية"، مجلة ام سلمة للعلوم، مجلد 4، العدد 20، 2007.
- 32- سعد حميد نجم ، عمار جبار بدر، اسيل هادي حمزه، "تأثير نسبه الكرافيت على مقاومة البلى لسبيكة النيوم\_ سليكون"، مجله القادسية للعلوم والهندسة، مجلد.2، العدد.2، رقم الصفحة. 75، 2009.
- 33- صالح كريم وحيد، " تأثير خشونة السطح على قوة ربط نحاس عالي التوصيل باستخدام الايبوكسي " مجلة ديالى للعلوم الهندسية - عدد خاص الصفحة. (35-36)، 2010.

- 34- عبد الواحد كاظم راجح، السلطاني، كاظم فنطيل، احمد فاضل حمزة، "حماية الالمنيوم من التآكل باستخدام مثبت عضوي جديد"، مجلة جامعة بابل، العلوم الصرفة والتطبيقية ، العدد.2، المجلد 18، الصفحة.795، 2010.
- 35- هناء محمد علي مجيد، "دراسة السلوك الميكانيكي والحراري لمادة متراكبة من الصوف الصخري"، رسالة ماجستير، قسم العلوم تطبيقية-الجامعة التكنولوجية، 2005.

**جدول(1) يوضح التركيب الكيميائي لسبيكة الفولاذ المقاوم للصدأ 304.**

Grade%	C	Mn	Si	P	S	Cr	Mo	Ni	N
304	-	-	-	-	-	17.5	-	8.0	-
	0.7	0.2	0.75	0.045	0.030	19.5		10.5	0.10
304L	-	-	-	-	-	17.5	-	8.0	-
	0.30	0.2	0.75	0.045	0.030	19.5		12.0	0.10
304H	0.04	-	-	-	-	18.0	-	8.0	-
	0.10	0.2	0.75	0.045	0.030	20.0		10.5	

جدول (2) مربع متوسط جذر الخشونة لسليكات الصوديوم المدعمة بالكرافيت المايكروي مرة، والكربون النانوي مرة أخرى.

نوع المادة	Root Mean Square(nm)	Roughness(nm)
$\text{Na}_2\text{SiO}_3+1\%\text{G.Powder}$	1.98	1.72
$\text{Na}_2\text{SiO}_3+2\%\text{G.Powder}$	2.36	2
$\text{Na}_2\text{SiO}_3+3\%\text{G.Powder}$	2.8	2.43
$\text{Na}_2\text{SiO}_3+4\%\text{G.Powder}$	3.55	3.08
$\text{Na}_2\text{SiO}_3+5\%\text{G.Powder}$	6.83	5.96
$\text{Na}_2\text{SiO}_3+1\%\text{C.Nano}$	2.11	1.89
$\text{Na}_2\text{SiO}_3+2\%\text{C.Nano}$	2.21	1.9
$\text{Na}_2\text{SiO}_3+3\%\text{C.Nano}$	2.32	2.07
$\text{Na}_2\text{SiO}_3+4\%\text{C.Nano}$	3	2.63
$\text{Na}_2\text{SiO}_3+5\%\text{C.Nano}$	3.3	2.93

جدول (3) قيم صلادة شور D لمادة سليكات الصوديوم المدعمة بالكرافيت مرة والكربون النانوي مرة أخرى عند النسب الامثل ومقارنتها مع صلادة روكويل لسبيكة الفولاذ المقاوم للصدأ 304.

نوع الفحص نوع المادة	الصلادة السطحية
Stainless steel 304 Rockwell Hardness(MPa)	80
$\text{Na}_2\text{SiO}_3$ Shore D Hardness(NO.)	44
$\text{Na}_2\text{SiO}_3+5\%\text{C.Nano}$ Shore D Hardness(NO.)	90.96
$\text{Na}_2\text{SiO}_3+4\%\text{G.Powder}$ Shore D Hardness(NO.)	79.8

جدول (4) قيم معدل البلى للفولاذ المقاوم للصدأ 304 ولسليكات الصوديوم، ولمتراكبات سليكات الصوديوم المدعمة بالكرافيت المايكروي مرة والكربون النانوي مرة أخرى عند النسب الامثل.

نوع الفحص نوع المادة	معدل البلى $10^{-8} \text{ (wear rate) (gm/cm)}$
Stainless Steel 304	11.368
$\text{Na}_2\text{SiO}_3$	72
$\text{Na}_2\text{SiO}_3+5\%\text{C.Nano}$	0.5184
$\text{Na}_2\text{SiO}_3+4\%\text{G.Powder}$	0.9045



جدول (5) قيم متانة اللصق لسليكات الصوديوم، ولمتراكبات سليكات الصوديوم المدعمة بالكرافيت الماكروي مرة والكاربون النانوي مرة أخرى عند النسب الأمثل.

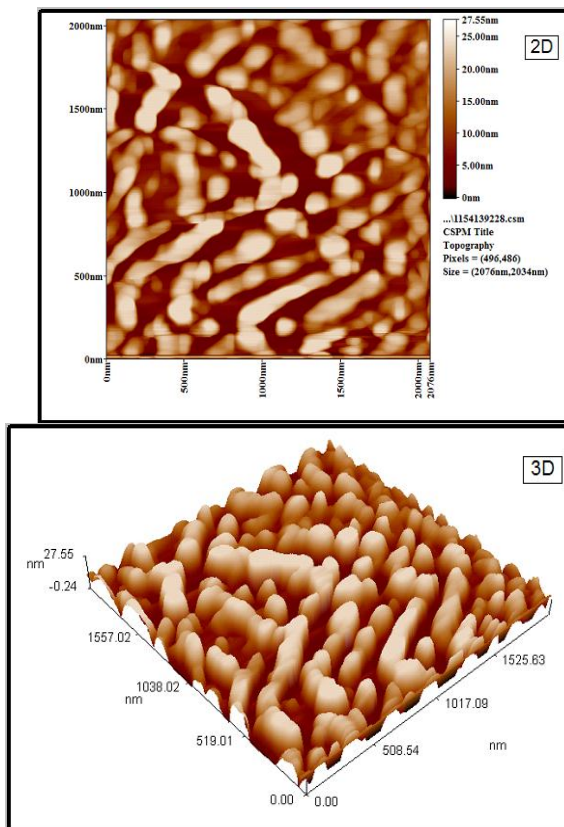
نوع المادة	نوع الفحص	قوة الالتصاقية (MPa)
Stainless steel 304		–
Na <sub>2</sub> SiO <sub>3</sub>		1.938
Na <sub>2</sub> SiO <sub>3</sub> +1%C.Nano		4
Na <sub>2</sub> SiO <sub>3</sub> + 5%G.Powder		3.45

جدول (6) قيم كثافة تيار التآكل الأدنى (معدل التآكل الأقل) لمتراكبه سليكات الصوديوم المدعمة بالكرافيت مره والكاربون مره عند النسب الأفضل، ومقارنتها مع الفولاذ من دون طلاء وطلاء سليكات الصوديوم بصورة منفردة.

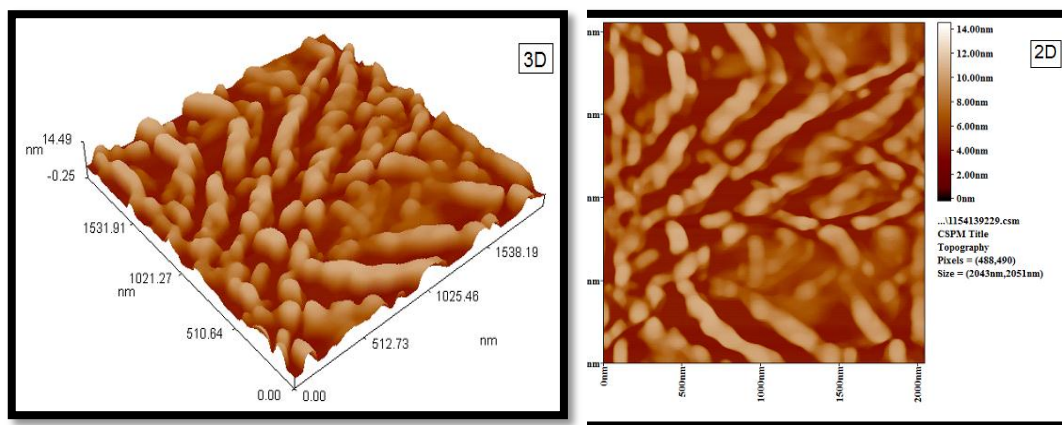
نوع المادة	نوع الفحص	كثافة تيار التآكل (nA/cm <sup>2</sup> )	جهد التيار (mv)
Stainless steel 304		869.55	– 141.3
Na <sub>2</sub> SiO <sub>3</sub>		5.77	–102
Na <sub>2</sub> SiO <sub>3</sub> +5%C.Nano		10.60	–35.1
Na <sub>2</sub> SiO <sub>3</sub> +3% G.Powder		1.06	– 94.1

جدول (7) تعيين التوصيلية الحرارية لسليكات الصوديوم وسليكات الصوديوم المدعمة بالكرافيت المايكروي مرة والكاربون النانوي مرة أخرى عند النسب الأمثل، ومقارنتها مع سبيكة الفولاذ المقاوم للصدأ 304.

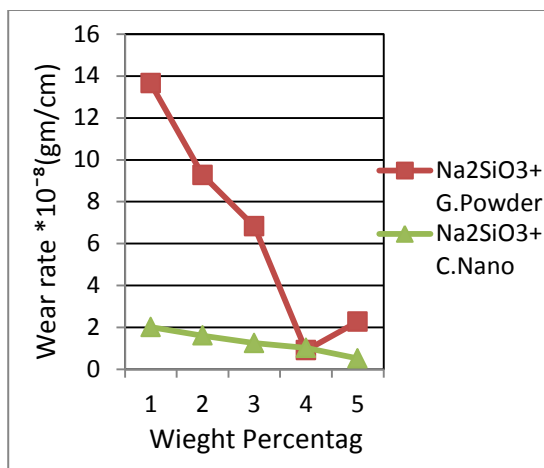
نوع المادة	نوع الفحص	التوصيلية الحرارية (W/m. <sup>0</sup> k)
Stainless steel 304		14.6
Na <sub>2</sub> SiO <sub>3</sub>		1.13
Na <sub>2</sub> SiO <sub>3</sub> +1%C.Nano		0.09135
Na <sub>2</sub> SiO <sub>3</sub> + 1%G.Powder		0.1909



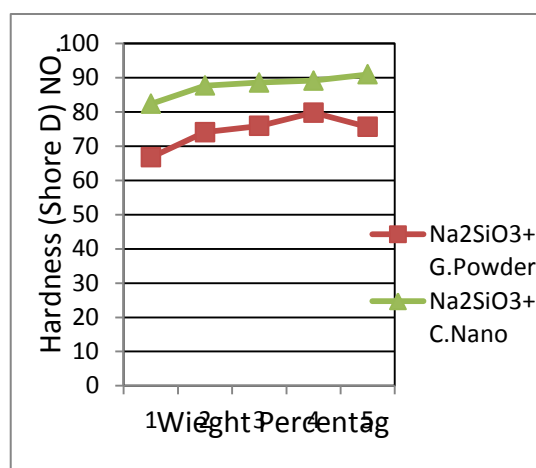
شكل (1) صورة 3D,2D لسليكات الصوديوم المدعمة ب 5% من الكرافيت بواسطة مجهر القوة الذرية .AFM



شكل (2) صورة 3D,2D لسليكات الصوديوم المدعمة ب 1% من الكربون النانوي بواسطة مجهر القوة الذرية .AFM



شكل (4) تغير قيم معدل البلى لسليكات الصوديوم

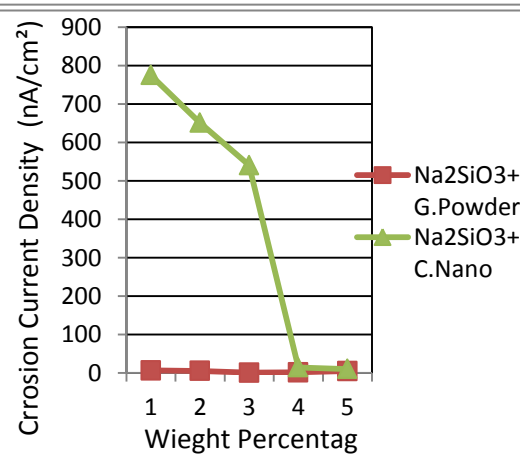
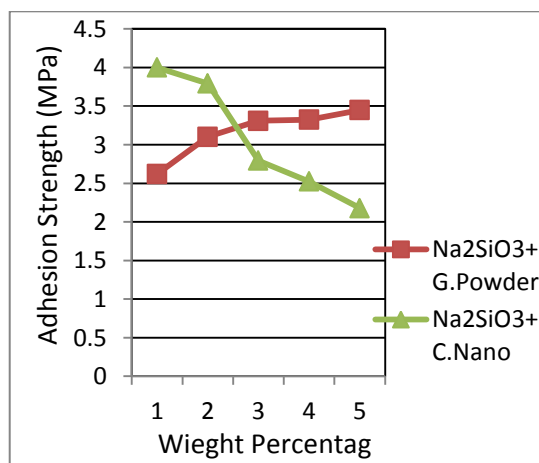


شكل (3) تغير قيم الصلادة لسليكات الصوديوم مع

مع

تغير نسب مسحوق الكرافيت الماكروي مرة ومسحوق الكاربون النانوي مرة اخرى.

تغير نسب مسحوق الكرافيت الماكروي مرة ومسحوق الكاربون النانوي مرة اخرى.

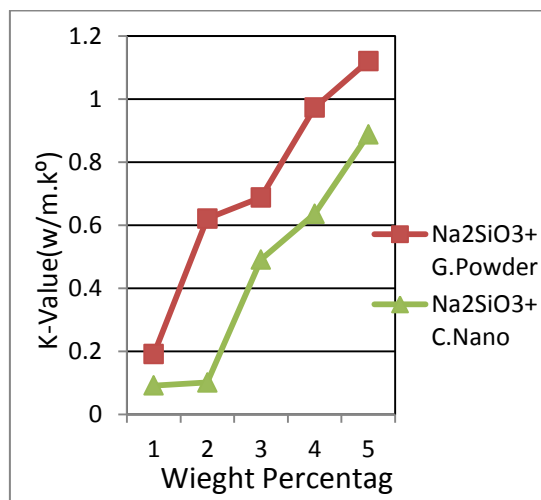


شكل (6) تغير كثافة تيار التآكل لمتراكبة سليكات الصوديوم المدعمة بمسحوق الكرافيت المايكروي مرة

شكل (5) تغير متانة اللصق لسليكات الصوديوم مع تغير نسب مسحوق الكرافيت الماكروي مرة ومسحوق

الكاربون النانوي مرة اخرى.

والكاربون النانوي مرة اخرى.



شكل (7) تغير التوصيلية الحرارية لمتراكبات سليكات الصوديوم المدعمة بالكرافيت المايكروي مرة والكاربون النانوي مرة اخرى.